EPFL

Corticolumbar dynamics during recovery after spinal cord injury

Selin ANIL

École
polytechnique
fédérale
de Lausanne

2020

Thesis abstract

In humans, a severe spinal cord contusion interrupts the vast majority of supraspinal projections to the spinal cord below the lesion. Permanent paralysis results from the chronic failure of these spared projections to engage lumbar circuits producing leg movement. We modeled these injuries in rodents, and showed the immediate access of cortical circuits onto the electrochemically-enabled lumbar spinal cord. Neuroprosthetic rehabilitation leveraged spared motor circuits elements, ultimately leading to the establishment of a cortico-reticulo-spinal relay that mediated the recovery of voluntary control over the legs. Cortical fibers underwent a drastic anatomical remodeling, contacting glutamatergic reticulospinal neurons in the brainstem which, despite lesion variability, consistently retained synaptic connections onto lumbar circuits. This circuit-level reorganization mediated a cortex-dependent recovery of natural locomotor behaviors.

In the aim of refining our understanding of the cortical contribution to the restoration of leg motor control with neuroprosthetic rehabilitation, we established a methodology to translate to rats a technique of endoscopic calcium imaging in freely-moving animals. We increased the stability of the implant, reaching unprecedented chronic degrees of longevity. Using this newly implemented technology, we tracked the activity of single corticolumbar cells during natural walking in intact rats, showing a strong representation of motor behavioral features in the population. We additionally highlighted the stability of locomotion-related classifications of individual neurons, suggesting a segregation of movement-related representations. The contusion was accompanied by important anatomical changes of corticolumbar cell bodies, preventing the longitudinal identification of single neurons across injury. However, population-level analyses highlighted a maintained strong representation of locomotion at late stages after injury and training. We did not find any dynamic change in corticolumbar population activity correlating with the recovery of voluntary leg motor control, which reflected in a stability of the fractions of movement-related neurons. These early results start shedding light on possible mechanisms of functional plasticity accompanying recovery after spinal cord injury, as a peculiar form of motor learning.

Concurrently to the functional reorganization of corticolumbar neurons, we investigated the anatomical plasticity of this specific population with contusion and training. Neuroprosthetic rehabilitation led to a strengthening of collateral connections onto the thoracic spinal segments above the lesion. However, we found no effect of training on the anatomical remodeling throughout the brain and brainstem. Notably, the absence of sprouting of corticolumbar collaterals in the brainstem reticular formation leads us to question the identity of the cortical population involved in the formation of the cortico-reticulo-spinal relay.

Résumé de la thèse

Une contusion à la moelle épinière interrompt la quasi-totalité des projections du cerveau vers la portion spinale située sous la lésion. L'incapacité de cette minorité de projections épargnées à activer les circuits lombaires produisant les mouvements de la jambe se manifeste par une paralysie permanente. Nous avons modélisé ce type de lésion chez le rongeur, et démontré l'accès immédiat des circuits corticaux aux circuits lombaires stimulés par une potentialisation électrochimique. La réhabilitation neuroprosthétique exploite les éléments épargnés des différents circuits moteurs, entraînant à terme l'établissement d'un relai cortico-réticulo-spinal qui sous-tend la récupération du contrôle volontaire des jambes. Les fibres provenant du cortex moteur subissent une importante réorganisation anatomique, formant des contacts synaptiques avec les neurones glutamatergiques dans la formation réticulée du tronc cérébral, qui, malgré la variabilité de la lésion, gardent systématiquement des connexions sur les circuits lombaires. Cette réorganisation des circuits sous-tend une récupération des comportements locomoteurs naturels qui est dépendante du cortex.

Dans le but d'affiner notre compréhension de la contribution du cortex dans la restauration du contrôle des jambes avec la réhabilitation neuroprosthétique, nous avons établi une méthodologie pour transférer au rat une technique d'enregistrement endoscopique d'activité calcique dans l'animal libre de toute contrainte. Nous avons amélioré la stabilité de l'implant, permettant d'atteindre un degré de chronicité sans précédent. À l'aide de cette nouvelle technologie, nous avons traqué l'activité de neurones corticolombaires individuels pendant l'exécution de la marche naturelle chez le rat sain, démontrant une forte représentation du comportement moteur au niveau de la population. Nous avons également mis en évidence la stabilité de la classification des neurones individuels relative à la marche, proposant une ségrégation des représentations liées au mouvement. La contusion est accompagnée de changements anatomiques importants des corps cellulaires corticolombaires, ce qui empêche l'identification longitudinale des neurones individuels transversalement à la lésion. Cependant, l'analyse de la population neuronale met en évidence le maintien d'une solide représentation de la locomotion à un stade chronique après la lésion et l'entraînement. Nous n'avons pas mis en évidence de dynamique notoire dans l'activité de la population au cours de la récupération, ce qui se reflète dans la stabilité des fractions de neurones corrélés au mouvement. Ces résultats préliminaires ouvrent la voie à la compréhension mécanistique de la plasticité fonctionnelle qui accompagne la récupération après une lésion à la moelle épinière, en tant que forme particulière d'apprentissage moteur.

En parallèle de la réorganisation fonctionnelle des neurones corticolombaires, nous avons étudié la plasticité anatomique de cette population spécifique suite à la contusion et avec l'entraînement. La réhabilitation neuproshtétique entraîne un renforcement des connections collatérales sur les

segments spinaux thoraciques situés au-dessus de la lésion. Cependant, nous n'avons pas observé d'effet de l'entraînement sur ce réarrangement anatomique à travers le cerveau et le tronc cérébral. Notamment, l'absence d'augmentation de densité synaptique de collatéraux corticolombaires dans la formation réticulée du tronc cérébral nous pousse à interroger l'identité de la population corticale engagée dans la formation du relai cortico-réticulo-spinal.

Mots-clé: lésion de la moelle épinière, contusion, locomotion, réhabilitation neuroprosthétique, stimulation électrochimique, réorganisation corticolombaire, plasticité fonctionnelle, plasticité anatomique, apprentissage moteur, imagerie calcique chronique chez le rat non-contraint.

Acknowledgements

I would like to thank first Prof. Grégoire Courtine for giving me the chance to perform my thesis in his laboratory. He generously opened the door of his group to me, from the very early day when, as a master student, I asked for a volunteer position in his laboratory. Ever since, he kept showing great enthusiasm, faith and ambition for my scientific achievements. I also thank him for his guidance during this project, and his never-ending visionary ideas and eagerness to revolutionize the world through science. Finally, I admire and am very grateful for his exceptional intuition to bring the right people together. These five years spent alongside remarkably talented, passionate, fascinating and lovely people were a delight.

I would like to also thank my thesis committee, for their precious time reading my manuscript and examining my work.

I further thank my coworker Dr. Quentin Barraud, for the permanent advice and feedback on my work during these years, and of course for his never-ending sense of humor. A huge thank you to Dr. Shiqi Sun and Dr. Luke Urban for the exciting collaboration. This transdisciplinary project would not have been possible without their exceptional skills and working force. Thank you also to Arnaud Bichat, Katia Galan, Simon Borgognon and Matthieu Gautier for their help along my project. I especially thank Dr. Léonie Asboth for everything she has taught me, from technical skills to lab life, for her precious scientific feedback, but above all for the most entertaining time spent sharing my office. Thank you as well to Dr. Kay Bartholdi, for offering his help and being so trustworthy and attentive as a person. And of course, I thank Dr. Jonathan Zapata for his remarkable availability helping me with implementing the Inscopix technology and for his constant support. Finally, thank to you to the lab executive assistants during my thesis: Kim, Pauline and Joelle.

I would like to further thank my students, who have shared a little portion of my path along this project: Celia, Chloé, Angelina, and Lucie. Each of them has been of great help in the realization of this thesis. I hope they have learnt valuable professional and personal skills while working under my supervision, and I wish them all the best for their future.

My sincere thanks to my mentor Prof. Stéphanie Lacour for her time and listening, whose advice has been extremely valuable in the completion of this thesis.

I would like to express my gratefulness to my friends in the lab: Sophie, Jérôme, Sir Nick James, and of course Jean-Baptiste and my twin-in-lab Camille for the fun times and their constant care.

Table of contents

List of figures and tables

I. Background and state-of-the-art

1.1. Introduction to SCI in humans

Overview

Spinal cord injury (SCI) is estimated to 500,000 new cases per year worldwide and leaves most affected individuals with permanent motor and sensory deficits, as well as autonomic dysfunctions. The importance of the impairments depends on several factors, including the type, severity, shape and level of the lesion. In most cases however, the consequences of SCI drastically reduce the quality of life of patients.

Most human SCI are contusions, resulting from sports or car accidents. In the clinics, lesions are commonly classified into motor and sensory complete or incomplete, depending on the remaining functions of the body parts controlled by the spinal circuits located below the level of injury. While cervical lesions result in tetraplegia, a lesion at the thoracic, lumbar or sacral level leads to paraplegia. Depending on the neurological damage, the completeness of the lesion is further characterized according to the ASIA Impairment Scale (American Spinal Injury Association) (Ditunno, Young et al. 1994):

- ASI A: sensory and motor complete
- ASI B: motor complete and sensory incomplete
- ASI C: motor incomplete
- ASI D: motor complete with most muscle scores above 3 below the level of the lesion

Most human injuries are functionally incomplete (McKinley, McNamee et al. 2006). While spontaneous recovery is reported to happen to some extent, it mainly occurs within the 3 first months after injury and remains limited in terms of functional improvement, due to the restrained ability of the central nervous system to repair itself. For ASI C and D patients, recovery is usually more substantial, although more variable. In contrast, very little recovery is observed in motor complete patients, namely ASI A and B (Fawcett, Curt et al. 2006). As a consequence, many deficits remain permanent, and in only half of the cases, supraspinal control of movements below the level of the lesion is regained.

Current SCI management

SCI is to date not curable. Current management consists in a first phase of acute treatment and a second longer phase of rehabilitation. The acute care includes emergency interventions focusing on preventing further damage and trauma, such as surgical decompression and stabilization of the backbone (Ahuja, Wilson et al. 2017). After stabilization of the initial spinal shock, rehabilitation is engaged, which requires an extensive multidisciplinary team involving a physical therapist, occupational therapist, rehabilitation nurse, rehabilitation psychologist, social worker, dietician, recreation therapist and a medical doctor specialized in SCI (Dobkin and Havton 2004). Depending on the initial severity of the lesion, rehabilitation will focus on a various range of goals, from maintaining and strengthening the remaining muscle function to learning how to use assistive devices for everyday life. Despite the tremendous human and financial effort represented by rehabilitation, the functional improvement offered by current therapies remains extremely limited (National.Spinal.Cord.Injury.Statistical.Center 2014).

As such, there is a definite need for a better understanding of the biological mechanisms of action in recovery in order to improve therapeutic strategies in the clinics. For this reason, preclinical research is essential: rodent and non-human primate models of SCI are developed for the investigation of respectively fundamental mechanisms and translational potency.

1.2. Motor control in healthy and injured mammals

The motor-circuit communication matrix

For a powerful and successful development of therapeutic interventions, the investigation of the anatomical bases of functional impairment and recovery after SCI requires *a priori* a strong understanding of motor control mechanisms in healthy mammals. Despite the paramount importance of motor behavior and decades of research, the neurological control of locomotion is still poorly understood, be it in healthy or injured systems. While the motor systems controlling evolutionary primitive functions such as locomotion seem to be highly conserved across species, differences arise with more refined and specialized behaviors, such as grasping or skilled motor learning (Lemon and Griffiths 2005). Evolution has yielded a highly complex and redundant motor system that involves neurological control and feedback centers in the motor cortex, midbrain, brainstem, the spinal cord, the peripheral nervous system and muscles. As a result, a simplistic approach where neural circuits straightforwardly map to precise and univocal behavioral outputs does not comply with biological reality. Emphasizing the tremendous complexity underlying motor control, Arber et al. conceived in 2014 the concept of the "motor-circuit communication matrix" (Pivetta, Esposito et al. 2014) (Fig. 1).
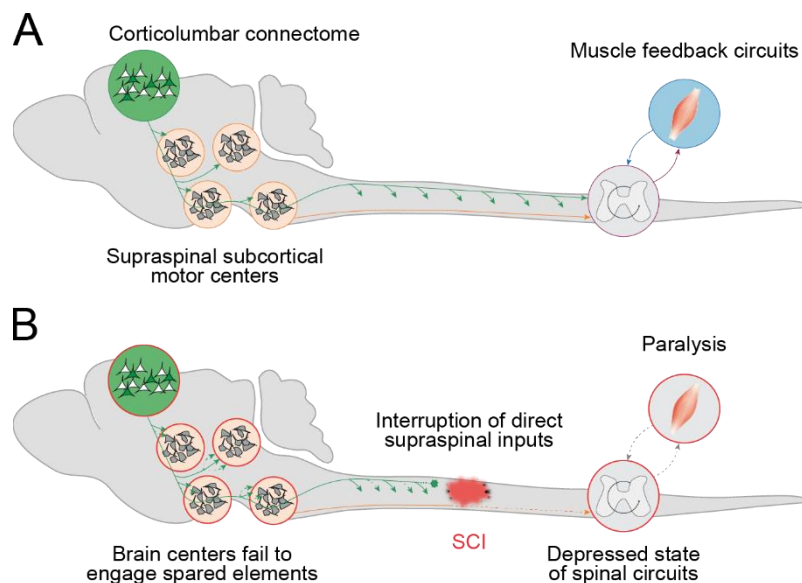
Fig. 1 | The motor-circuit communication matrix.
A. The heathy motor-circuit communication matrix, composed of supraspinal motor circuits, including the corticolumbar neurons and their collateral projections, as well as spinal lumbar circuits controlling leg movement and receiving feedback from the muscles. **B.** Disruption of the motor-circuit communication matrix by a SCI: brain centers fail to engage the lumbar circuits, which remain in a dormant state, leading to muscle and limb paralysis.

Motor control in healthy animals

Movement is the resulting behavioral output of descending motor commands from supraspinal centers and continuous feedback from sensory circuits (Edgerton, Courtine et al. 2008). The interplay of these inputs onto the spinal circuits controlling limb movements in turn determines the activation of motor neurons, and hence specific and timed muscle contractions (Fig. 1A). Concurrently, ascending sensory circuits convey feedback information to the supraspinal centers, allowing a permanent adaptation of descending commands. The main descending pathways involved in the motor-circuit communication matrix are the corticospinal (Lemon and Griffiths 2005, Lemon 2008), rubrospinal (Whishaw, Gorny et al. 1998, Riddle, Edgley et al. 2009), reticulospinal (Schepens and Drew 2004, Riddle, Edgley et al. 2009), the mesencephalic (Ryczko and Dubuc 2013), the vestibulospinal (Basaldella, Takeoka et al. 2015) and pontine reticulospinal tracts (Luccarini, Gahery et al. 1990).

Disruption of the motor-circuit communication matrix after SCI

A SCI suddenly disrupts the highly complex and precise organization of the motor-circuit communication matrix, even in centers remotely located from the injury (Wrigley, Press et al. 2009, Ghosh, Peduzzi et al. 2012, Nardone, Holler et al. 2013). Neuronal death occurs in the grey matter at the level of the injury, as well as damage to passing axons of descending and ascending pathways. The interruption of these axons leads to demyelination and formation of a retraction cone on the side of the cell body, while the part of the axon and all synaptic connections on the other side of the injury are completely lost. As a consequence, the communication between most supraspinal centers and the spinal circuits below the lesion is abolished (Fig. 1B). The spinal circuits below the lesion, albeit functional, remain in a dormant state, due to the lack of neuromodulation originating from the interrupted descending pathways (Harkema 2008, Beauparlant, van den Brand et al. 2013).

Spontaneous recovery after SCI

Yet, even in the case of functionally complete injuries, residual fibers retain connections below the lesion. Some extent of spontaneous recovery can occur thanks to the leveraging of these spared elements of the motor-circuit communication matrix (Courtine, Song et al. 2008, Rosenzweig, Courtine et al. 2010, Friedli, Rosenzweig et al. 2015). Nevertheless, depending on the shape, position and size of the lesion, the nature and extent of these spared elements may vary. Therefore, after a more severe SCI, the remaining supraspinal inputs onto spinal circuits below the injury are not sufficient to elicit movement: the lesion leads to permanent paralysis (Fig. 1B) (van den Brand, Heutschi et al. 2012).

In humans, fMRI yields information about the localization and the extent of the lesion. Combined with electrophysiological measurements, such as motor evoked potentials with transcranial magnetic stimulation, such evaluations can help identifying the spared motor pathways, and hence predict to some extent the degree of functional recovery (Barthelemy, Willerslev-Olsen et al. 2015). Yet, in many cases, large discrepancies are observed between fMRI-based predictions

and actual outcome, emphasizing the lack of a reliable biomarker in humans for a precise anatomical evaluation of spared pathways and prediction of recovery.

1.3. Innovative research strategies to improve recovery

Activity-dependent plasticity and activity-based therapy

Pioneering work from Philippson (Philippson 1905) and Sherrington (Sherrington 1910) in respectively transected dogs and cats established the ability of spinal circuits to generate reflex activity leading to alternated stepping movements in the absence of supraspinal input. Edgerton et al. later demonstrated the training-specificity of motor function recovery: spinalized cats trained for stepping showed greater stepping performance than non-trained animals, while cats trained for standing showed poor performance at stepping (Lovely, Gregor et al. 1986, Lovely, Gregor et al. 1990, de Leon, Hodgson et al. 1998, De Leon, Hodgson et al. 1998). The targeted enhancement of spinal activity during training promotes plastic changes capable of restoring locomotion after a severe SCI.

Leveraging this activity-dependent plasticity thus arose as a judicious strategy to improve rehabilitation outcomes after SCI. Activity-based therapies target at eliciting or strengthening movement of the paralyzed limbs during training. Several approaches have been developed, using weight-bearing systems, lower limb exoskeletons, functional electrical stimulation of muscles or spinal cord neuromodulation techniques (Dobkin and Havton 2004).

Interventions for an immediate improvement of motor function

Concurrently, strategies that aim at enhancing spinal activity upstream of muscle activation are being developed in preclinical as well as clinical research. Continuous electrical epidural stimulation (EES) has been shown to elicit alternated stepping-like movements in individuals with a complete spinal cord injury laying in supine position (Dimitrijevic, Gerasimenko et al. 1998, Minassian, Jilge et al. 2004). As the implantation of an epidural stimulator was originally approved by the US Food and Drug Administration for use in humans as a treatment for pain, the translation of this technique to other functional purposes such as locomotion can be greatly accelerated (Tator, Minassian et al. 2012).

In animal models as well, EES applied at different spinal levels exhibits impressive ability to encourage specific patterns of locomotion (Musienko, van den Brand et al. 2009). These empirical findings enabled to refine the placement of stimulation electrodes onto the dorsal aspect of the spinal cord, in the aim of optimizing the kinematics and muscle activity of the resulting gait pattern. Thus, EES applied at the L2 spinal level promotes leg flexion, while EES at the S1 level promotes leg extension. The combination of tonic stimulation at both sites, combined with the sensory inputs

elicited by passive leg movement on a treadmill, leads to the production of rhythmic stepping patterns.

Only recently the mechanisms underlying the production of such movements have been unraveled. Thanks to a transdisciplinary approach allying computational modelling and preclinical experiments in rats, Capogrosso et al. demonstrated that EES recruits proprioceptive circuits by the direct stimulation of dorsal roots (Moraud, Capogrosso et al. 2016). This, in turn, generates action potentials in the motor neurons involved in the specific spinal level corresponding to the stimulated root, ultimately resulting in muscle contractions. The understanding of these mechanisms enabled the refinement of stimulation protocols, thus improving locomotor performance in paralyzed rats after a spinal contusion thanks to spatiotemporal targeted stimulation patterns (Wenger, Moraud et al. 2016). Ultimately, this strategy has been translated to humans in a recent clinical trial. The timed stimulation of specific dorsal roots in SCI patients reestablished an adaptive control over the paralyzed muscles during overground walking (Wagner, Mignardot et al. 2018).

Another approach to increasing spinal circuit excitability is pharmacological neuromodulation. Volume transmission (Agnati, Guidolin et al. 2010) is a cell signaling pathway acting over time windows ranging from minutes to hours. During locomotion, the fast glutamatergic signals from the brain received by spinal circuits add up onto this slower modulation through volume transmission of monoaminergic neurotransmitters. Thus, the coordinated release of dopamine, serotonin and noradrenalin by supraspinal sources onto spinal circuits is key to the successful execution of locomotion (Jordan, Liu et al. 2008). Following a SCI, the lack of monoaminergic inputs to spinal circuits can be compensated for by the administration of neuromodulators or agonists to their receptors. Thus, agonists of 5-HT_{2A} and $5\text{-HT}_{1A/7}$ receptors mediate the facilitation of treadmill stepping in rodents after SCI (Antri, Mouffle et al. 2003, Landry, Lapointe et al. 2006). The systemic administration of specific monoaminergic agonists enables to further precisely tune gait features in spinal rats, thus opening possibilities to a personalized pharmacological aid for stepping (Musienko, van den Brand et al. 2009, Musienko, van den Brand et al. 2011).

The integration of these two neuromodulation strategies into a single electrochemical neuroprosthesis has become a standardized way to promote locomotion-like movements after SCI. The electrochemical neuroprosthesis thus immediately transforms dormant spinal circuits, completely isolated from supraspinal inputs by a full spinal transection, into highly excitable states (Courtine, Gerasimenko et al. 2009). The timed sensory feedback from the legs on a moving treadmill belt is then a sufficient input for spinal circuits to generate a coordinated stepping pattern.

Long-term effects of neurorehabilitative strategies

After a period of several months of subthreshold lumbosacral EES combined with stand training, four motor complete individuals were reported to have regained the ability to generate voluntary movements (Harkema, Gerasimenko et al. 2011, Angeli, Edgerton et al. 2014). On the preclinical side, Courtine et al. integrated the electrochemical neuroprosthesis, promoting an immediate

enabling effect of locomotion, into a neuroprosthetic rehabilitation protocol involving a motor training program. Thanks to this therapy, otherwise paralyzed rats consistently recovered voluntary control over the legs after a double hemisection (van den Brand, Heutschi et al. 2012). The authors showed that this recovery is contingent to encouraging voluntary descending drives under highly functional spinal states, as treadmill-restricted rehabilitation does not achieve such functional outcomes. Thus, the interplay between supraspinal volitional commands and the spinal circuits rendered highly excitable with electrochemical neuromodulation favors the long-lasting establishment of a new motor-circuit communication matrix.

Translating this therapy to humans, Wagner et al. integrated spatiotemporal EES into a personalized overground rehabilitative training over several months. The participants regained voluntary control over previously paralyzed muscles, without the need for stimulation (Wagner, Mignardot et al. 2018).

These preclinical as well as clinical results suggest that the prolonged spinal cord neuromodulation triggered an anatomical reorganization of motor circuits thanks to activity-dependent plasticity, emphasizing the tremendous potential of targeted neurotechnologies in leveraging activity-dependent plasticity. However, in order to further develop and refine these therapeutic strategies, there is a fundamental need to understand the mechanisms of motor control in the healthy system, as well as the reshaping of the motor-circuit communication matrix after injury.

1.4. Role of the motor cortex in healthy locomotion

Motor maps

The motor cortex is horizontally organized in motor maps, constituting a topographic representation of body movement. This somatotopic classification has historically emerged from results of surface and intracortical microstimulation experiments in mammals (Asanuma and Sakata 1967) and later transcranial magnetic stimulation in humans (Hallett 2007). Further advances have enabled to lay strong anatomical bases to this classification thanks to connectivity studies.

The historical work of Sherrington et al. reversed the previously established idea that the motor cortex is organized in a simple and rigid one-to-one topographic representation (Brown Thomas and Sherrington Charles 1912). Cortical map boundaries are broad and flexible: focal intracortical microstimulations can elicit different movements over time (Kleim, Barbay et al. 1998), specific muscle responses are represented redundantly within motor maps (Li and Waters 1991), and longer stimulation times can recruit extended cortical areas to elicit behaviorally complex movements (Harrison, Ayling et al. 2012). Thus, and most importantly, representations depend not only on the direct output channel from the motor cortex to the spinal cord, but also from intracortical circuits. Despite this complexity, motor mapping still is a simple and commonly

established tool to study the organization of motor cortex and its plasticity following alterations to the motor-circuit communication matrix.

Organization of the MC and CST across species

The motor cortex is further anatomically and functionally organized in layers. Excitatory glutamatergic and inhibitory GABAergic neurons constitute intracortical circuits (Keller 1993, Mao, Kusefoglu et al. 2011), and the output to other motor-involved centers of the central nervous system originates in the population of large pyramidal excitatory neurons located in layer 5 (L5). Kuypers was the first to describe the regions of projection of these corticofugal axons, which broadly connect to subcortical areas, the brainstem and onto spinal circuits (Kuypers and Lawrence 1967, Donoghue and Kitai 1981, Kuypers 1982, Gao and Zheng 2004).

Corticospinal axons originate in the layer 5b of the motor cortex and descend caudally through the internal capsule, the pons and the brainstem. At the level of the pyramids, the corticospinal tract (CST) decussates and follows its course within the white matter of the spinal cord, mostly in the ventral part of the contralateral dorsal funiculus. All along this path, corticospinal axons defasciculate and form collaterals that branch out to contact various brain and spinal cord regions: rubrospinal, tectospinal, vestibulospinal and reticulospinal motor systems, as well as cortical, striatal, thalamic systems, and the spinal gray matter (Armand 1982, Kuypers 1982, Canedo 1997).

Although this general course is shared among all mammals, the finer organization of the CST further varies across species (Kuypers 1982, Courtine, Bunge et al. 2007, Serradj, Agger et al. 2017) (Fig. 2A). In primates, the corticospinal axons project mainly in the contralateral dorsolateral funiculus (88%), with minor components following the ipsilateral dorsolateral (10%), the ispilateral ventral (1%) and the contralateral ventral (0.3%) funiculi (Kuypers, Fleming et al. 1962, Lacroix, Havton et al. 2004). CST fibers terminate widely in the spinal gray matter, mostly on the side contralateral to their cell bodies (88.8%) (Kuypers 1960, Kuypers, Fleming et al. 1962, Lacroix, Havton et al. 2004). However, the spinal projection pattern of CST axons is highly bilateral in primates: significant spinal midline crossing results in the innervation of the ipsilateral gray matter (Rosenzweig, Brock et al. 2009). Importantly, anatomical and electrophysiological evidence show the presence of direct corticomotoneuronal connections to various extents in different species of primates including humans (Lacroix, Havton et al. 2004, Lemon and Griffiths 2005, Lemon 2008). In rats, the CST mainly projects through the ventral aspect of the contralateral dorsal funiculus (> 90%) (Fig. 2D1), while a minority of axons project in the ipsilateral dorsal (1-2%) (Fig. 2D1), ipsilateral ventral (1-2%) (Fig. 2D2) and contralateral dorsolateral funiculi (1%) (Fig. 2D3) (J. Casale, R. Light et al. 1988, Liang, Moret et al. 1991, Brosamle and Schwab 1997, Steward, Zheng et al. 2004, Bareyre, Kerschensteiner et al. 2005). CS axons terminate mostly in the dorsal horn of the spinal cord (Fig. 2D4), where they make synaptic contacts onto premotor circuits (J. Casale, R. Light et al. 1988, Serradj, Agger et al. 2017) (Fig. 2B). Contrary to the primate, there are no evidence of direct corticomotoneuronal synapses in the rodent, and spinal projections remain essentially contralateral (Yang and Lemon 2003, Alstermark, Ogawa et al. 2004).

Illustrating these inter-species variations, the anatomical importance of the CST increases along evolution, which is suggested to support the emergence of fine motor abilities such as precision grip (Courtine, Bunge et al. 2007). Consistent with these anatomical evidence, CST disruption results in increasingly important and permanent motor deficits from rodents to non-human primates and to humans (Lemon and Griffiths 2005, Courtine, Bunge et al. 2007). As a correlate, the motor consequences of SCI (Vilensky 1987) and the importance of the CST in recovery increase along evolutionary species (Friedli, Rosenzweig et al. 2015).
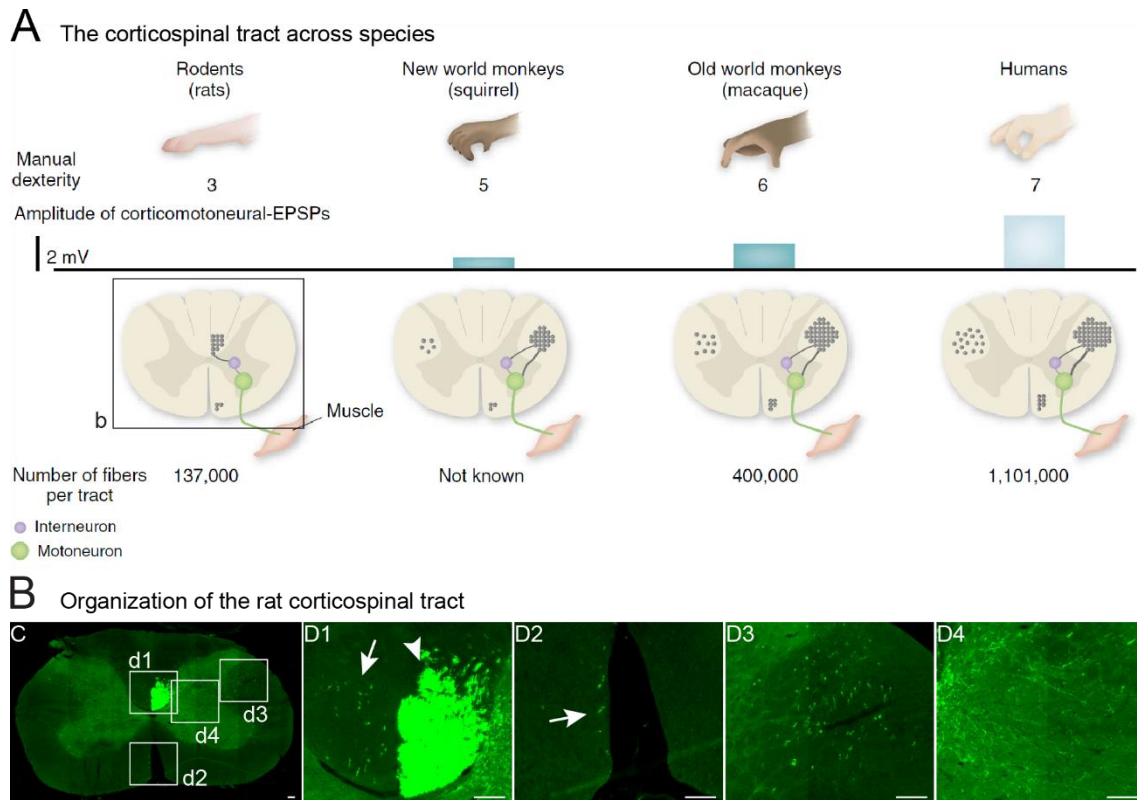
Fig. 2 | Organization of the corticospinal tract
A. Relationship between the development of the corticospinal tract and the emergence of fine motor control abilities. In rodents, there are no direct connections between corticospinal neurons and the cervical motoneurons that innervate forelimb muscles: interneurons relay cortical input to motor neurons. In the evolution of the corticospinal tract in non-human primates and humans, direct corticospinal connections with motoneurons have emerged, together with an increase in the size and number of the corticospinal fibers. Accordingly, the size of the excitatory postsynaptic potential (EPSP) elicited by cortical neurons on motoneurons has increased during primate evolution. Furthermore, most of the corticospinal tract fibers in rodents travel in the dorsal columns. In contrast, the primate corticospinal tract is mostly located in the lateral columns, and a significant proportion of corticospinal fibers (10–20%) descend ipsilaterally. Development of the corticospinal tract correlates with the improvement in the index of dexterity (as quantified in ref. 30), particularly in the ability to perform finger-thumb precision grip. Adapted from (Courtine, Bunge et al. 2007). **B.** Detail of the rat corticospinal tract (CST) organization in A. Scale bars represent 100μm. **C.** Image of a coronal section of the rat spinal cord, corticolumbar axons labelled in green with GFP. **D1-D4.** Higher magnification of the insets in C. **D1.** Arrowhead designates the main CST in the ventral part of the dorsal funiculus contralateral to the cell bodies. Arrow shows the ipsilateral dorsal minor component of the CST. **D2.** Arrow shows the ipsilateral ventral minor component of the CST. **D3.** Contralateral dorsolateral minor component of the CST. **D4.** Termination of corticospinal fibers in the dorsal spinal gray matter.

Role of the motor cortex in motor execution

It is commonly admitted that supraspinal - and *a fortiori* cortical - control of locomotion is more important in higher evolutionary species, such as primates, in contrast to rodents (Fedirchuk, Nielsen et al. 1998, Vilensky and O'Connor 1998). Thus, in primates, the CST significantly contributes to natural locomotion. After a unilateral thoracic CST lesion in monkeys, although substantial yet incomplete recovery occurs in walking, some permanent deficits remain (Courtine, Roy et al. 2005). Similarly, CST interruption at the cervical level causes permanent deficits in dexterous movements, emphasizing the importance of this pathway in skilled motor control as well (Lawrence and Kuypers 1968, Courtine, Roy et al. 2005).

L5 neurons in the rodent MC do encode information about movement (Li, Ko et al. 2017, Heindorf, Arber et al. 2018). However, historical lesion studies, followed more recently by circuit interrogation studies, have enabled to reach the consensus that the motor cortex is not needed for the execution of natural locomotion (Muir and Whishaw 1999, Kawai, Markman et al. 2015). A pyramidotomy (Muir and Whishaw 1999, Siegel, Fink et al. 2015) or a bilateral M1 ablation in mice (Asante, A et al. 2010) leaves natural locomotion largely intact. These results confirm the important role of subcortical circuits in rodent motor control. In contrast, the motor cortex - and *a fortiori* the CST - are necessary for fine adaptive locomotion, as demonstrated by motor cortex ablation experiments and genetic manipulations disrupting CST development (Asante, A et al. 2010, Serradj, Paixao et al. 2014). Indeed, the fine tuning of motor output necessitates sensorimotor integration, mediated by the motor cortex (Heindorf, Arber et al. 2018). Likewise, the CST is necessary for the execution of skilled movements (Weidner, Ner et al. 2001, Lemon and Griffiths 2005): permanent deficits remain in rats after complete unilateral or incomplete bilateral CST transection (Castro 1972, M Piecharka, Kleim et al. 2005).

Thus, while not necessary for the execution of natural locomotion in rodents, the motor cortex is essential for the execution of fine adaptive locomotion as well as skilled movements.

Motor learning

The malleable nature of motor representations is central in the plasticity accompanying motor learning or trauma across species (Pascual-Leone, Nguyet et al. 1995, Nudo, Milliken et al. 1996, Kleim, Barbay et al. 1998). Skilled motor learning is consistently accompanied by an increase in the motor map area corresponding to the engaged body parts in rats (Kleim, Barbay et al. 1998) and humans (Pascual-Leone, Nguyet et al. 1995). .

Contrary to skilled motor learning, skilled repetition of unskilled movements does not result in motor maps plasticity in rats (Kleim, Hogg et al. 2004) and primates (Plautz, Milliken et al. 2000). Although this specific form of learning is impaired by a motor cortex ablation, its execution is not affected if previously learnt (Kawai, Markman et al. 2015). Yet, a permanent ablation leaves space for compensatory subcortical circuit reorganization, and hence possible spontaneous recovery of the learnt task. In contrast, acute disruption of cortical circuits, through injection of the GABA agonist muscimol or transient optogenetic stimulation, does impair the execution of previously learnt sequences of unskilled movements (Guo, Graves et al. 2015, Otchy, Wolff et al. 2015).

All together, these results emphasize the major role of the motor cortex in the initiation, execution and learning of a novel motor task. However, to date, most studies of motor control and learning have focused on the intact animal and tested forelimb function. As a consequence, the understanding of the mechanisms underlying supraspinal motor control of leg movement after injury remains strikingly limited.

1.5. Role of the motor cortex after injury

Plasticity of motor maps after SCI

In humans, motor cortex excitability by transcranial magnetic stimulation is drastically reduced after a SCI, both in terms of threshold and latency to elicit a motor response (Davey, Smith et al. 1998, Smith, Savic et al. 2000, Roy, Zewdie et al. 2011). The injury induces a reduction in motor map areas corresponding to the most impaired body parts, as well as an expansion of motor maps corresponding to zones of partial preservation (Topka, Cohen et al. 1991, Freund, Rothwell et al. 2011). This motor map plasticity is also observed in rodents: contralateral hindlimb motor areas are drastically weakened, abolished, or taken over by trunk and forelimb motor representations after a dorsal CST injury (Fouad, Pedersen et al. 2001, Bareyre, Kerschensteiner et al. 2004) or a full thoracic spinal transection (Oza and Giszter 2014). Consistently, functional recovery of specific muscles and skilled movements after mild injuries is accompanied by the expansion of the corresponding motor representations (Girgis, Merrett et al. 2007, Martinez, Delcour et al. 2010, Hollis, Ishiko et al. 2016).

Thus, the motor cortex integrates the plastic changes throughout the motor-circuit communication matrix, after injury and with recovery.

Role of the MC in movement after recovery

After a unilateral injury, the ipsilesional cortex exhibits the ability to take over the representation of the impaired limb, resulting in a bilateral representation of both limbs, and to support spontaneous recovery (Ghosh, Sydekum et al. 2009, Brown and Martinez 2018). This rearrangement highlights the importance of the motor cortex in recovery. Interestingly, after a chronic unilateral pyramidotomy in rats, the inactivation of the spared motor cortex by injection of the GABA agonist muscimol does not reverse the effects of spontaneous recovery. In contrast, in case of recovery enhanced by electrical stimulation of the spared motor cortex, the motor deficits reappear by injection of muscimol (Carmel, Kimura et al. 2014). These results suggest that different recovery mechanisms might underlie spontaneous vs training-enhanced recovery. In turn, after a more severe injury model such as a double hemisection in rats, the muscimol-mediated transient inactivation of the motor cortex abolishes voluntary hindlimb locomotion, which

had been previously recovered thanks to neurorehabilitation (van den Brand, Heutschi et al. 2012).

Thus, the motor cortex output plays a pivotal role in regaining supraspinal access to the impaired limbs after a severe SCI and training. The reorganization of the motor-circuit communication matrix naturally depends on the spared elements that can be leveraged for the formation of new functional circuits. Thus, the nature, laterality and extent of the lesion are major criteria that will determine the plasticity mechanisms engaged in spontaneous – and *a fortiori* rehabilitation-enhanced – recovery.

1.6. Mechanisms of spontaneous recovery

Plasticity of spared CST components

After a lateral lesion, spared CST axons are known to form collaterals that cross the spinal midline, projecting into the ipsilateral hemicord below the lesion (Brus-Ramer, Carmel et al. 2007, Ghosh, Sydekum et al. 2009). In turn, after a bilateral injury interrupting the main component of the CST, the spared minor CST pathways contribute to spontaneous recovery. The minor ventral components exhibit sprouting into the spinal gray matter onto motoneuron pools below the injury in mice (Bareyre, Kerschensteiner et al. 2005) and rats (Weidner, Ner et al. 2001). However, the functional role of these new connections has not yet been interrogated. Furthermore, after bilateral dorsal column transection in mice, the selective chemogenic silencing of the spared dorsolateral CST reversed the spontaneously recovered motor function (Hilton, Anenberg et al. 2016). Anatomical analysis showed an extensive sprouting of dorsolateral CST fibers below the lesion, exhibiting midline crossing, thus resulting in the innervation of the contralateral gray matter (Steward, Zheng et al. 2004). Thus, in rodents, spontaneous sprouting and midline crossing from spared CST components contribute to the observed motor map plasticity and are strongly suggested to support the partial functional recovery (Weidner, Ner et al. 2001, Bareyre, Kerschensteiner et al. 2004, Ghosh, Haiss et al. 2010).

Similar plastic mechanisms are observed in primates, where extensive sprouting from spared CST elements has been shown to underlie spontaneous recovery after injury (Raineteau and Schwab 2001, Weidner, Ner et al. 2001, Lacroix, Havton et al. 2004). Notably, functional improvement is mediated by the formation of collaterals engaging in midline crossing after a unilateral lesion (Rosenzweig, Courtine et al. 2010).

In humans, a significant degree of spontaneous restoration of motor fucntion is commonly observed after functionally incomplete injuries (Fawcett, Curt et al. 2006). Despite pronounced species divergence, the previous findings in rodents and non-human primates lead to believe that similar mechanisms, involving the sprouting of spared CST elements, support this recovery (Nathan and Smith 1973, Friedli, Rosenzweig et al. 2015).

Formation of propriospinal relays

After spontaneous recovery following a thoracic hemisection in mice, propriospinal projections are increased in the depleted side of the spinal cord above the lesion. These propriospinal axons, crossing the midline, were shown to be essential for the recovery of supraspinal control of stepping after a single and after two temporally and spatially separated hemisections (Courtine, Song et al. 2008). Furthermore, the bilateral ablation of the dorsal CST at the thoracic level in rats induces sprouting of axotomized fibers into the cervical spinal cord (Fouad, Pedersen et al. 2001, Ghosh, Haiss et al. 2010). After a dorsal hemisection, the new projections from hindlimb corticospinal neurons into the cervical gray matter above the lesion form synaptic contacts onto long propriospinal neurons (Bareyre, Kerschensteiner et al. 2004), which in turn retain connections with the lumbar circuits below the lesion. The restoration of cortical input onto lumbar spinal circuits is accompanied by the reestablishment of a hindlimb cortical representation, and correlates with recovery. Thus, intraspinal plasticity is a key mechanism of spontaneous recovery, through the formation of propriospinal relays mediated by the sprouting of supraspinal fibers above injury.

Formation of supraspinal relays

Aside from the corticospinal tract, the other supraspinal descending pathways present a substantial degree of plasticity after injury as well. Chemogenic inactivation experiments demonstrated that after a complete bilateral CST interruption by pyramidotomy, sprouting of rubrospinal projections drive the spontaneous recovery of skilled movement in mice (Siegel, Fink et al. 2015). Consistently, rubrospinal projections have been shown to have a greater importance in the control of skilled locomotion in the absence of CST (Han, Cao et al. 2015). Furthermore, after lesion to both the CST and rubrospinal tract, brainstem circuits take over the supraspinal control of skilled movements in rats (Garcia-Alias, Truong et al. 2015).

In case of moderate lesions, such as a cervical hemisection in rats, spontaneous recovery of natural locomotion is enabled by the formation of detour circuits reconnecting cortical, brainstem and intraspinal projection neurons to denervated circuits below injury. The reticulospinal tract, originating in the brainstem, was shown to underlie the recovery of function thanks to collateral sprouting including spinal crossing below the lesion (Zörner, Bachmann et al. 2014). In turn, the increase of collaterals from these reticulospinal fibers ipsilesionally above the lesion is strongly thought to be accompanied by synaptic contacts onto double midline crossing propriospinal neurons (Filli, Engmann et al. 2014). These result emphasize the redundancy of motor control systems, and the flexibility of both supraspinal and spinal plasticity underlying recovery after a disruption of the motor-circuit communication matrix.

1.7. Strategies to enhance recovery after SCI

Research strategies to enhance neuroplasticity underlying recovery

The understanding of spontaneous plasticity mechanisms contributing to functional improvement after injury can then be leveraged for the design of interventional strategies aiming at enhancing recovery. Experimental approaches include neuroprotection, axonal regeneration, axonal sprouting and rehabilitative training.

Although it had been commonly admitted that the adult central nervous system has a very limited ability to regenerate (Fawcett 2019), recent studies achieved substantial growth of severed axons across a spinal injury site, by manipulating the cellular or molecular environment of the lesion, thus overcoming the historical dogma (Lu, Wang et al. 2012, Anderson, Burda et al. 2016, Anderson, O'Shea et al. 2018, Rosenzweig, Brock et al. 2018). Alternatively, neurotrophic factors such as NT-3 or BDNF have been commonly studied for their role in axonal protection after SCI (Grill, Murai et al. 1997, Weishaupt, Li et al. 2013). Activity-dependent modulation levels of BDNF were shown to play an essential role in the remodeling of spared circuits and the correlated locomotor recovery (Ying, Roy et al. 2008). Attempts to attenuate inhibitory cues thanks to molecular approaches in order to promote axonal regeneration (Lee, Geoffroy et al. 2010) or sprouting (Hollis, Ishiko et al. 2016) have yet yielded limited anatomical results, and no satisfying functional recovery.

In contrast, electrical stimulation of the spared CST elements (Brus-Ramer, Carmel et al. 2007) and of the uninjured motor cortex (Carmel, Kimura et al. 2014) were reported to enhance the functional recovery of skilled reaching movements. Likewise, a treatment with Nogo-A antibody in rats encouraged the sprouting of intact CST collaterals across the spinal midline, and resulted in functional recovery (Wahl, Omlor et al. 2014). Interestingly, another study pointed out that after a cervical dorsal column transection, only the combination of molecular targeting with training yields a significant anatomical sprouting of CST collaterals and subsequent functional recovery in skilled reaching (Hollis, Ishiko et al. 2016), emphasizing the potential of multifaceted approaches.

Neuroprosthetic rehabilitation as a pragmatic strategy to enhance recovery of leg motor control after a severe SCI

While some of the previously described studies demonstrate some extent of functional recovery, most of them carefully target specific and characterized anatomical plastic mechanisms, and use mild to moderate injury models, such as CST-restricted lesions or hemisections (Grill, Murai et al. 1997, Girgis, Merrett et al. 2007, Rosenzweig, Courtine et al. 2010, Carmel, Kimura et al. 2014, Hilton, Anenberg et al. 2016). Despite important anatomical plasticity, very limited recovery is observed after more severe SCI in animal models, raising the question of the adequacy of such mechanistic-oriented strategies in the aim of drastically improving motor function (Duffy, Wang et

al. 2012, Lu, Wang et al. 2012, Danilov and Steward 2015). Furthermore, functional recovery is often studied through the paradigm of forelimb motor control, by testing skilled movement tasks such as reaching and grasping. The differences in motor control for skilled movement vs natural locomotion, as well as the clinical priority for the improvement of walking ability in human patients, emphasize a need to focus on hindlimb motor control.

The pragmatic approach of neuroprosthetic rehabilitation integrates these multiple goals, leveraging activity-dependent plasticity and circuit-wide engagement without targeting a precise molecular or cellular pathway. This neurorehabilitation therapy restored supraspinal control over the paralyzed hindlimbs in rats after a double hemisection, and was accompanied by an extensive neuroplasticity (van den Brand, Heutschi et al. 2012). This anatomical remodeling involved sprouting of spared cortical fibers in various areas of the brainstem and in the spinal cord above the lesion. Furthermore, sprouting collaterals exhibited midline crossing, resulting in the bilateral innervation of the spinal gray matter between both hemisections, and formed synaptic contacts onto propriospinal neurons that retained connections onto the lumbar spinal cord. In turn, propriospinal neurons exhibited anatomical remodeling as well, leading to the strengthening of intraspinal detour circuits around the lesion. These extensive plastic changes throughout various modules of the motor-circuit communication matrix were only observed in animals who had received neuroprosthetic rehabilitation, as opposed to non-trained and treadmill-trained animals. Finally, motor cortex inactivation with the GABA-agonist muscimol reversed the recovered voluntary control over the legs, thus demonstrating the training-mediated reestablishment of a motor-cortex dependent recovery after severe SCI.

II. Synopsis, aim of the thesis & contributions

AIM 1

Despite great advances in the field, the knowledge of the mechanisms underlying recovery after SCI remains limited. A colossal gap still persists between the well-controlled environment of the preclinical laboratory and the bedside. As the mechanisms of neuroplasticity highly depend on the nature of the lesion, and in the aim of ultimate translation to therapeutic strategies for severe paralyzing injuries, future research needs to head towards a preclinical model that mimics best human injuries in terms of nature and severity. To address this issue, we applied the neuroprosthetic rehabilitation protocol to animals with a clinically relevant model of a severe spinal contusion, and investigated the circuit-level plasticity underlying the recovery of voluntary control over the hindlimbs.

The study presented in the first chapter of this thesis was published in the review Nature Neuroscience (Asboth, Friedli et al. 2018). In the scope of the article reported here, my contribution entails the leading, execution and analysis of the experiment of hindlimb motor cortex chemogenic inactivation in rats. This work involves experimental design, surgeries, animal training, behavioral testing, recordings and subsequent analysis, as well as anatomical processing of histological tissues and subsequent analysis.

AIM 2

The role of the motor cortex in motor control and learning, and more importantly in the recovery of motor function after injury, makes it a highly relevant region to study further. Especially, the corticospinal tract is known to underlie some extent of functional recovery after various forms of SCI. Although our lesion model leads to a complete interruption of the CST, the first chapter of this thesis highlighted a specific cortex-dependent mechanism of recovery. As a consequence, we sought to understand the dynamics in corticolumbar neurons activity throughout recovery after contusion.

In order to be able to track the activity of this specific neuronal population across several months, we developed an experimental framework for chronic calcium recordings in freely-moving rats. The technological set-up was adapted from the nVista solution commercially available from the company Inscopix, which was originally designed for calcium recordings in mice over periods extending up to 6 weeks. The translation to rats and the enhancement of the implant stability involved the adaptation and optimization of surgical and recording procedures, presented in the second chapter of this thesis.

With this newly established experimental set-up, and in the aim of understanding the role of corticolumbar neurons in the control of leg movement, we first performed calcium recordings during locomotion in intact animals. We then addressed the question of the functional plasticity of this specific population of neurons in the recovery of leg motor control after lesion. Calcium recordings of the same corticolumbar neurons were thus performed in freely-moving rats throughout a contusion SCI and recovery enabled by neuroprosthetic rehabilitation. I led and designed the study, performed all surgeries, animal training, data collection and processing of calcium recordings. I received support for the computational data analysis of calcium movies, namely cell identification, classification, registration and behavioral decoding. I further performed the final data analysis and interpretation. The early results of this ambitious study are presented in the third chapter of this thesis.

AIM 3

The recovery of leg motor control after a severe SCI is mediated by an extensive neuroplasticity throughout the whole motor-circuit communication matrix. Cortical fibers exhibit a drastic sprouting in various brainstem areas with neuroprosthetic rehabilitation. Furthermore, the well documented ability of the CST for midline crossing and formation of new collaterals after various forms of SCI led us to investigate the anatomical plasticity of the corticolumbar tract after contusion and with neuroprosthetic rehabilitation.

We achieved an exhaustive brain and spinal screening of the corticolumbar connectome in intact, contused untrained and trained rats. We aimed at quantifying the density of synapses in various target regions, in the ultimate goal of revealing anatomical remodeling effects of the contusion and of neuroprosthetic rehabilitation. This study is presented in the fourth chapter of this thesis.

III. Chapter 1

MOTOR CORTEX-DEPENDENT RECOVERY OF NATURAL LOCOMOTION AFTER A CONTUSION SCI

Abstract

Severe spinal cord contusions interrupt nearly all brain projections to lumbar circuits producing leg movement. Failure of these projections to reorganize leads to permanent paralysis. Here we modeled these injuries in rodents. A severe contusion abolished all motor cortex projections below injury. However, the motor cortex immediately regained adaptive control over the paralyzed legs during electrochemical neuromodulation of lumbar circuits. Glutamatergic reticulospinal neurons with residual projections below the injury relayed the cortical command downstream. Gravity-assisted rehabilitation enabled by the neuromodulation therapy reinforced these reticulospinal projections, rerouting cortical information through this pathway. This circuit reorganization mediated a motor cortex-dependent recovery of natural walking and swimming without requiring neuromodulation. Cortico-reticulo-spinal circuit reorganization may also improve recovery in humans.

3.1. Introduction

After a spinal cord injury (SCI), only half of affected individuals regain supraspinal control of movements below the level of the lesion. However, imaging (Petersen, Wilm et al. 2012), electrophysiological (Angeli, Edgerton et al. 2014, Barthelemy, Willerslev-Olsen et al. 2015) and anatomical (Kakulas 1999) evaluations reveal that even the most severe SCIs usually spare regions of white matter. These bridges contain residual fibers from mixed populations of projection neurons that maintain a physical connection with the lumbar spinal cord, where the circuits coordinating leg movements reside. Nevertheless, these residual connections are insufficient to elicit volitional muscle contractions.

Two main reasons have been invoked to explain this failure. First, the interruption of descending pathways suppresses the sources of modulation and excitation that render lumbar spinal circuits functional (Kiehn 2006, Courtine, Gerasimenko et al. 2009). Second, conduction failure in the vicinity of injured regions (James, Bartus et al. 2011) contributes to silencing residual fibers that could contribute to recovery (Bachmann, Matis et al. 2013).

These findings guided the design of therapies that specifically target spared lumbar circuits and projection neurons with residual fibers below injury to improve recovery from SCI (Rossignol, Giroux et al. 2001, Mushahwar, Jacobs et al. 2007, Courtine, Gerasimenko et al. 2009, van den Brand, Heutschi et al. 2012, Angeli, Edgerton et al. 2014, Radhakrishna, Steuer et al. 2017). These interventions act over two time windows. In the short term, monoamine receptor agonists and epidural electrical stimulation are delivered to the lumbar spinal cord to compensate for the interrupted source of modulation and excitation. Electrochemical neuromodulation therapies instantly enables paralyzed rats to execute complex locomotor behaviors. Similarly, electrical stimulation enables individuals with motor complete paralysis to produce isolated leg movements (Angeli, Edgerton et al. 2014). In the long term, rehabilitation enabled by these neuromodulation therapies improves volitional motor performance (Rossignol, Giroux et al. 2001, Carhart, He et al. 2004, Angeli, Edgerton et al. 2014), suggesting a reorganization of residual projections that enhances supraspinal control of spinal circuits (van den Brand, Heutschi et al. 2012). However, both in animal models and humans, movements occur only in the presence of neuromodulation therapies.

The mechanisms enabling motor control when delivering neuromodulation therapies and improvements with rehabilitation remain enigmatic and vividly debated (Slawinska, Rossignol et al. 2012, Wernig 2014). It is therefore critical to address these knowledge gaps to support mechanism-based therapeutic development and apply these findings clinically.

Various investigations have uncovered key mechanisms of recovery from SCI. These studies were primarily conducted in moderate cut models of SCI, which combine two important advantages. First, precise cuts into defined regions interrupt specific pathways, which supports unambiguous conclusions on anatomical reorganization.

Second, multiple spared neural pathways allow a progressive spontaneous recovery of function. These well-controlled conditions demonstrated that the formation of detour circuits reconnecting cortical, brainstem and intraspinal projection neurons to denervated circuits below injury contributes to spontaneous recovery (Bareyre, Kerschensteiner et al. 2004, Ballermann and Fouad 2006, Jankowska and Edgley 2006, Courtine, Song et al. 2008, van den Brand, Heutschi et al. 2012, Takeoka, Vollenweider et al. 2014, Zörner, Bachmann et al. 2014).

Nevertheless, spinal cord damage in humans primarily results from contusions. These injuries induce highly variable pathway interruption and pronounced secondary damage, including cavity formation (Basso, Beattie et al. 1996), inflammatory responses (Silver, Schwab et al. 2014) and demyelination (James, Bartus et al. 2011), that impair residual pathway functionality. Consequently, the mechanisms supporting recovery from contusion remain undefined. Moreover, the capacity of neuromodulation therapies and rehabilitation to restore motor control after severe contusions is unknown.

We tackled these questions in rodent models of severe contusions leading to permanent paralysis. Electrochemical neuromodulation therapies and gravity-assisted rehabilitation enabled rats to regain supraspinal control of locomotion that persisted without neuromodulation, even during unpracticed, natural tasks. Using cell-specific optogenetics, circuit-level inactivation and unbiased whole brain-spinal cord microscopy, we demonstrate that the reorganization of cortico-reticulo-spinal circuits mediated a motor cortex-dependent recovery in these animals.

3.2. Results

Contusion model leading to paralysis

We modeled severe contusions in rats (Fig. 3a) using robotically controlled impacts (255.5 ± 1.3 kdyn) onto T8/T9 segments (Supplementary Fig. 1). This lesion spared 9.75 ± 0.57% of intact cross-sectional tissue (Fig. 3b) and induced highly variable white matter sparing (Supplementary Fig. 2).

One week after injury (the subacute condition), all rats showed flaccid leg paralysis. We reactivated lumbar circuits with agonists to serotonergic and dopaminergic receptors and with epidural electrical stimulation applied to lumbosacral segments. These stimulations instantly restored automated (involuntary) locomotion on a treadmill (Supplementary Fig. 1).

To encourage supraspinal (voluntary) activation of leg movements without confounding contribution of forelimbs, we positioned the rats bipedally in a robotic interface. This gravity-assist allows bipedal locomotion in a safe environment (Dominici, Keller et al. 2012). Early after contusion, all rats failed to initiate locomotion, even with electrochemical neuromodulation.

Neurorehabilitation restores volitional locomotion

Before injury, rats were randomly assigned to untrained and trained groups that followed a comprehensive rehabilitation program (van den Brand, Heutschi et al. 2012) with electrochemical neuromodulation and gravity assist (Supplementary Fig. 1 and Supplementary Table 1) 6 days per week during 9 weeks (Supplementary Fig. 1). After training, all rats regained weight-bearing locomotion during electrochemical neuromodulation (body weight support, 36 ± 4%; Fig. 3b,c). Under electrical neuromodulation only (no chemical modulation), 88% of rats were still able to walk. Without any neuromodulation, 62.5% of rats still progressed forward (Fig. 3d). In contrast, untrained rats showed minimal motor improvement (Fig. 3c,d). Even with electrochemical neuromodulation and 5 consecutive days of habituation, untrained rats were unable to produce locomotion (Fig. 3b–e and Supplementary Fig. 3).

To quantify performance, we applied a principal component (PC) analysis (Takeoka, Vollenweider et al. 2014) to 129 parameters calculated from kinematics, kinetics and muscle activity (Supplementary Table 2). PC1 captured the effects of rehabilitation ($p < 0.0001$; Fig. 3e), while PC2 segregated neuromodulation conditions ($p < 0.0001$; Supplementary Fig. 3). Analysis of parameters correlating with PC1 revealed that trained rats tested under electrochemical neuromodulation produced gait patterns that shared many features with those of intact rats (Supplementary Fig. 3). Parameters clustering on PC2 indicated that the removal of chemical neuromodulation led to decreased muscle activation ($p = 0.0015$) and reduced ground reaction forces. These same parameters were further affected without any neuromodulation (muscle activation: $p < 0.0001$; Fig. 3 and Supplementary Fig. 3). These results show that rehabilitation

enabled by electrochemical neuromodulation restored supraspinal control of locomotion that persisted without neuromodulation.
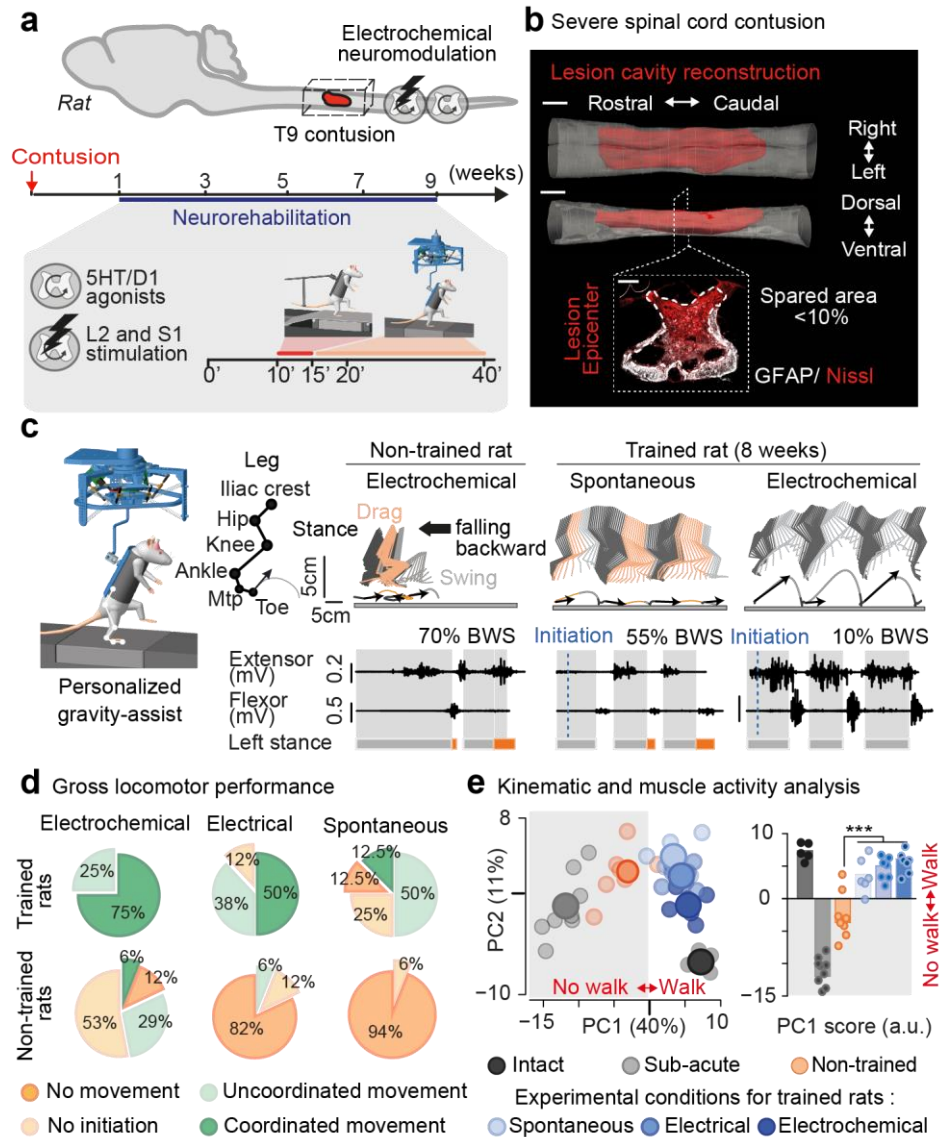
Fig. 3 | Neurorehabilitation restores supraspinal control of leg movements in rats
a, Scheme and timeline summarizing the experiments. **b**, Top and side view of a 3D reconstruction of the lesion cavity. Photograph of a representative coronal section through the contusion epicenter (GFAP, glial fibrillary acidic protein). Scale bars 1 mm for 3D reconstructions, 250 µm for cross-section. **c**, Untrained and trained rats tested during bipedal locomotion with gravity assist, both without and with electrochemical neuromodulation. Stick diagram decompositions of right leg movements; leg endpoint trajectory with acceleration at toe-off; activity of extensor and flexor muscles of the ankle. The gray, white and orange backgrounds correspond to the stance, swing and drag phases of gait, respectively. **d**, Circular plots reporting the gross leg motor performance of untrained and trained rats under the different conditions of neuromodulation. **e**, PC analysis of gait parameters averaged for each rat and condition (small circles). Large circles show the average per group. Bar plot shows the average scores on PC1, which quantify the locomotor performance of untrained rats (9 weeks post-injury, n = 8), trained rats (9 weeks post-injury, n = 7) and subacute rats (1 week post-injury, n = 9) compared to intact rats (n = 5). **p < 0.01, ***p < 0.001. One-way ANOVA followed by Bonferroni's post hoc test.

41

Trained rats transform contextual information into task-specific commands

We then evaluated whether trained rats could execute tasks that required adaptations of limb kinematics. All trained rats were able to climb a staircase when receiving electrochemical neuromodulation (Fig. 4a,b). This task required an increase in step height (Fig. 4b; p = 0.005; 9.6 ± 2.1 mm). Theoretically, paw contacts with staircase may trigger withdrawal reflex responses allowing this adaptation (Slawinska, Rossignol et al. 2012). Video analyses revealed the absence of contact with staircase in 50 ± 7.4% of trials (Fig. 4b).

We next evaluated natural quadrupedal locomotion (Fig. 4c). With electrochemical neuromodulation, all rats displayed weight-bearing locomotion with balance maintenance (Fig.
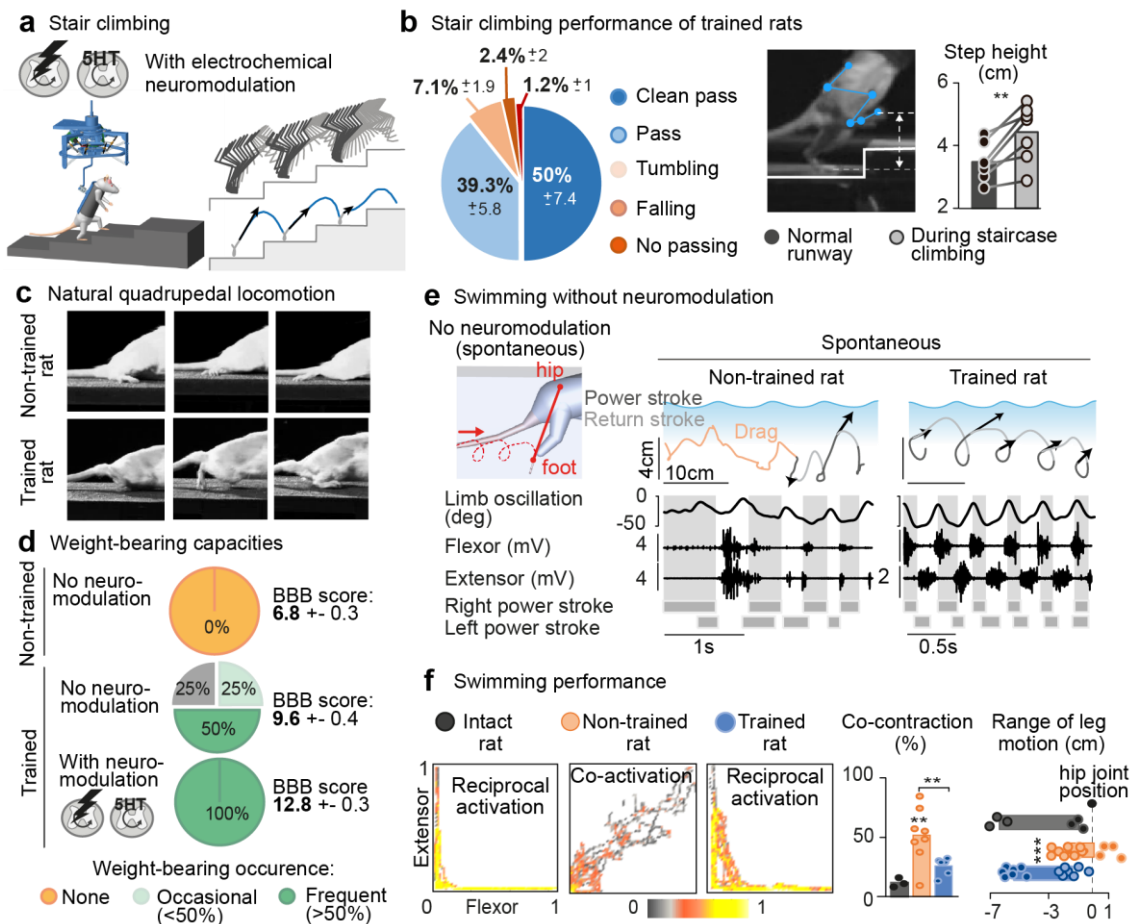
Fig. 4 | Transfer of motor performances to unpracticed tasks
a, Scheme of the staircase climbing task. The trained rats were tested with electrochemical neuromodulation. Stick diagram decomposition of leg movements and endpoint trajectory are shown. **b**, Circular plot reporting the behavioral performance of trained rats during staircase climbing. The bar plot reports the mean step height for each animal (n = 7) during walking along the horizontal runway and for the same animal during staircase climbing. **p < 0.01, two-tailed paired Student's t-test. Static image from the video recordings show the capacity to lift the leg above the stair. **c**, Three sequential snapshots of an untrained and a trained rat walking quadrupedally without electrochemical neuromodulation.
d, Circular plots reporting the percentage of animals with weight-bearing capacity in untrained rats (n = 6) without electrochemical neuromodulation and in trained rats (n = 8) tested both without and with electrochemical neuromodulation. Basso–Beattie–Bresnahan (BBB) score for each group is reported as mean and s.e.m. **e**, Scheme of the swimming task, including the virtual limb representing the connection of the hip to the foot. Contused rats were tested without neuromodulation. Leg kinematics and ankle muscle activity are shown using the same conventions as in Fig. 3f. The density plots display the activity of antagonistic muscles of the ankle throughout a trial, reflecting intralimb coordination. Bar plots report gait parameters measured from kinematic recordings of intact (n = 3), untrained (n = 8) and trained (n = 7) rats. **p < 0.01, ***p < 0.001. One-way ANOVA followed by Bonferroni's post hoc test.

4d). Without neuromodulation, 75% of rats still produced occasional or frequent weight-bearing steps. In contrast, untrained rats showed either no movement or occasional leg flexions likely triggered by sensory feedback.

Finally, we tested their ability to swim across a straight pool of water without neuromodulation (Fig. 4e,f). Untrained rats displayed coactivation of antagonist muscles resembling spasms observed in humans (Fig. 4f). Trained rats instead generated powerful swimming movements (p < 0.001; Fig. 4f) with reciprocal activity of extensor and flexor muscles (p < 0.01; Fig. 4f). These experiments show that trained rats regained the ability to transform contextual information into task-specific motor commands to produce natural behaviors without neuromodulation therapies.

Motor cortex regains control over paralyzed legs during neuromodulation

We next studied the mechanisms underlying motor control during neuromodulation. We first conducted experiments in mice because the association of activation and inactivation methods together with pathway-specific anatomical visualization of the entire brain and spinal cord in transgenic animals allows precise dissection of circuits under well-controlled conditions. Previous studies suggest that motor cortex critically contributes to motor execution after injury (van den Brand, Heutschi et al. 2012, Hilton, Anenberg et al. 2016, Hollis, Ishiko et al. 2016). Consequently, we first evaluated the contribution of motor cortex projection circuits to electrochemically enabled motor control.

To test this hypothesis, we optogenetically manipulated the activity of motor cortex projection circuits in Thy1:ChR2-YFP mice expressing channelrhodopsin-2 (ChR2) in pyramidal neurons (Fig. 5a,b). We conducted retrograde anatomical tracing in intact mice to identify the region containing corticospinal tract neurons projecting to lumbar segments (Supplementary Fig. 4). We then mapped this region to identify the hotspot that induced the maximal amount of contralateral leg movements during optogenetic stimulation (Fig. 5a). We implanted optic fibers bilaterally into the identified hotspot.

The mice then received a contusion that led to leg paralysis (T8–T9, 90 ± 8.8 kdyn; sparing 23.97 ± 1.65%; Supplementary Fig. 4). We positioned the mice bipedally in a robotic interface allowing locomotion (von Zitzewitz, Asboth et al. 2016). All mice failed to initiate locomotion (Fig. 5c). Without neuromodulation, optogenetic stimulation (40 Hz, 5 ms pulse) of motor cortex projection circuits led to rhythmic forelimb movements (5.9 ± 0.85 Hz), but was ineffective at engaging the paralyzed legs. In contrast, when we activated lumbar circuits with serotonergic agonists (van den Brand, Heutschi et al. 2012), optogenetic stimulation instantly triggered weight-bearing locomotion (p < 0.001; Fig. 5c). Locomotion ceased when the laser was turned off (latency: 1.13 ± 0.5 s, Supplementary Fig. 4).

To determine whether motor cortex regained adaptive control over the paralyzed legs, we manipulated the activity of motor cortex projection circuits with optogenetic stimulation increments. Leg muscle activation scaled with laser intensity (p < 0.0001, R2 = 0.69, Fig. 5d,e and Supplementary Fig. 5), which produced linear adaptations of kinematic parameters such as step height (p < 0.0001, R2 = 0.57, slope = 0.46 ± 0.3; Fig. 5e). These experiments show that

neuromodulation therapies instantly enabled motor cortex projection circuits to trigger and modulate locomotor movements of paralyzed legs.
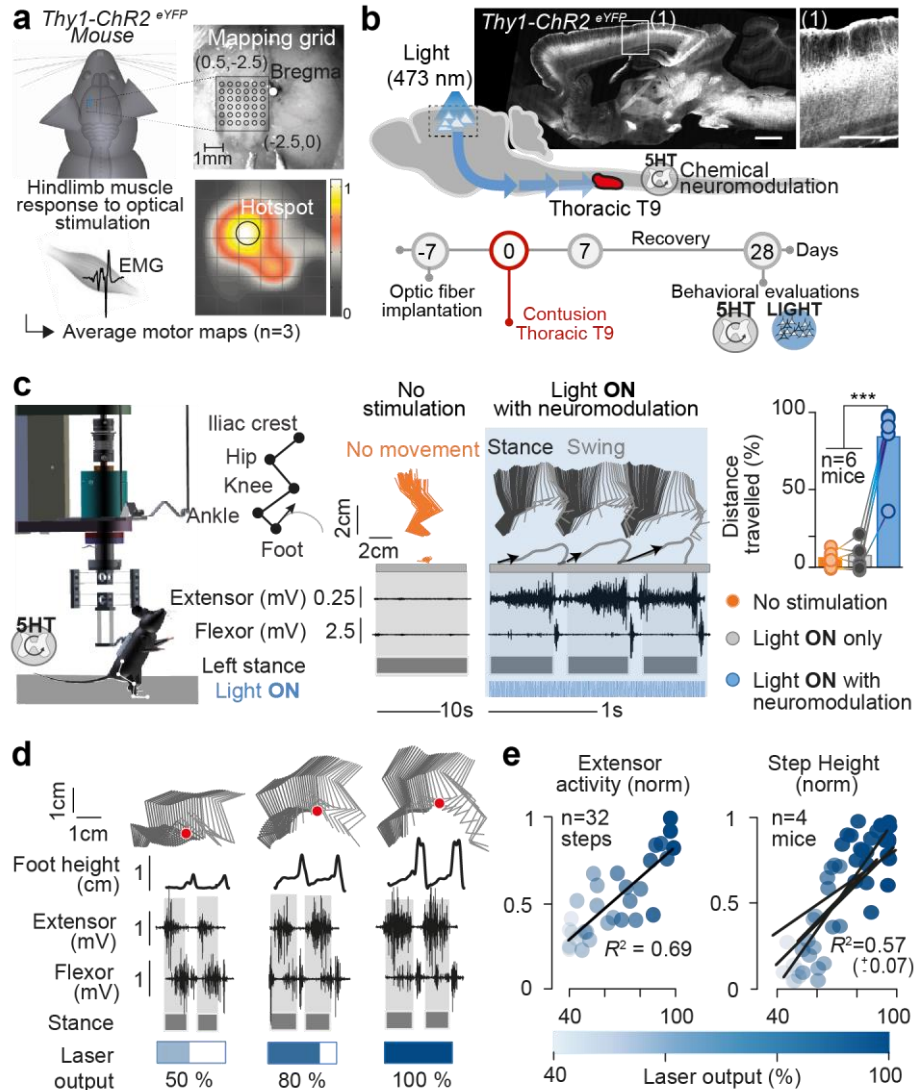
Fig. 5 | Cortical control of leg movements in mice
a, Short bursts of optical stimulation were delivered using a mapping grid positioned over the leg motor cortex region, as shown in the photograph. The amplitude of motor evoked potentials recorded in the flexor muscle of the contralateral ankle was measured for each site of stimulation to elaborate a motor map. The average heat map of 3 mice was computed, showing leg muscle activity amplitude for each optical stimulation location. **b**, Expression of ChR2 in the brain of Thy1-ChR2-eYFP mice, including an enlargement (1) showing expression in layer V of the hindlimb motor cortex (scale bars 1 mm left, 500 μm right). Scheme and timeline summarizing the experiment. Before contusion, mice receive bilateral implantation of optic fibers into the identified hotspot of the motor cortex. Mice were tested 28 days after contusion. **c**, Mice were tested bipedally using a robot providing vertical and mediolateral body weight support. Leg kinematics and ankle muscle activity are shown using the same conventions as in Fig. 1. Bar plot shows the relative distance traveled along a 40-cm-long runway under the different experimental conditions (n = 6 mice). ***p < 0.001. One-way ANOVA followed by Bonferroni's post hoc test. **d**, Modulation of leg kinematics and muscle activity during optical stimulation intensity increments, indicated at the bottom. The red dot on the kinematics diagram represents the maximal step height. **e**, Relationships between optical stimulation intensity and extensor muscle activity (left, 1 mouse) and step height (right, 4 mice; each regression line corresponds to a mouse).

Contusions abolished corticospinal tract projections below injury

Behavioral evaluations showed that the motor cortex could access lumbar circuits during neuromodulation. These results prompted us to assess the possible survival of corticospinal tract projections that could activate lumbar circuits.

To label the fibers and synapses from motor cortex projection neurons, we co-injected a Cre-dependent adeno-associated viral (AAV) vector carrying synaptophysin-GFP with an AAV-Cre in the leg motor cortex of *Flex-TdTomato* reporter mice (Fig. 6.1a). The contusion abolished all projections from labeled corticospinal tract neurons (Fig. 6.1a,b and Supplementary Fig. 6a-c). Labeling of corticospinal tract axons with protein kinase C-γ immunostaining confirmed the complete interruption of this pathway (Supplementary Fig. 6.1c). These results indicate that alternative descending pathways are responsible for activating lumbar circuits during optogenetic motor cortex stimulation.

Contusions spare subsets of glutamatergic vestibulospinal and ventral gigantocellular projections

To identify projection neurons that maintained connectivity across contusion and could be responsible for relaying the cortical command downstream, we conducted retrograde neuroanatomical tracing from lumbar segments. The contusion interrupted nearly all projections from neurons located in the thoracic and cervical segments above the injury, in the red nucleus and, as expected, in the motor cortex (Supplementary Fig. 6d). Only a subset of projection neurons located in the vestibular nuclei, raphe, parapyramidal region and ventral gigantocellular reticular nuclei (vGi) retained connectivity with lumbar segments (Fig. 6.1c,d). These neurons amounted to 16.6 ± 3.3% of all the retrogradely labeled cells counted in these regions in intact mice (Fig. 6.1d).

We used immunohistochemistry to determine the cellular identity of these projection neurons. We found that neurons located in the vestibular nuclei and vGi colocalized with glutamate, while neurons situated in the raphe and parapyramidal regions expressed serotonin (Fig. 6.1d and Supplementary Fig. 6g).

To validate these results, we labeled projection neurons with residual synapses in lumbar segments using injections of AAV2-retro-cre in the L1-L2 segments of *Flex-TdTomato* reporter mice. We visualized the brain, brainstem and spinal cord using CLARITY-optimized light-sheet microscopy (Fig. 6.2e-g). This experiment confirms the depletion of corticospinal tract synapses within lumbar segments (Fig. 6.2g). The largest number of neurons with residual projections to lumbar segments were found in the vGi (Fig. 6.2f).

Silencing vGluT2ON vGi neurons blocks cortical control of locomotion

Serotonergic neuromodulation of lumbar circuits was essential to restoration of movements, indicating that residual slow acting serotonergic projections are unlikely to have contributed to
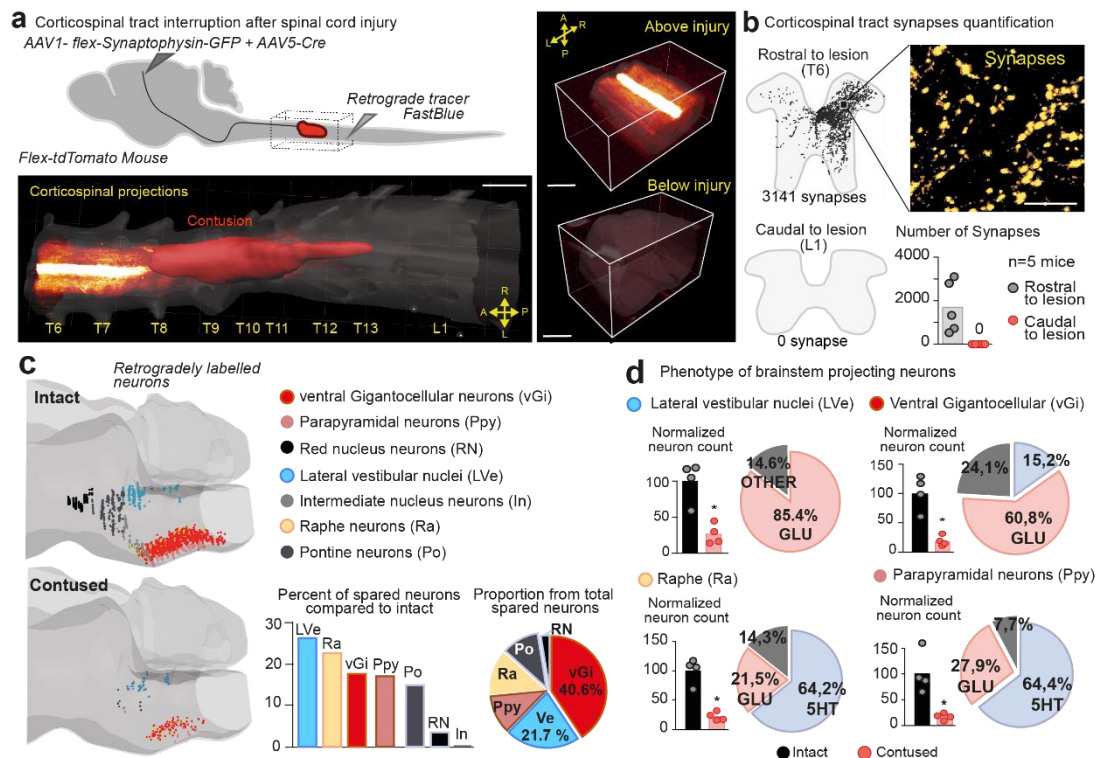
Fig. 6.1 | The contusion interrupts all corticospinal tract projections but spares subsets of brainstem pathways

a, AAV5-Cre was jointly injected with AAV1-flex-Synaptophysin-GFP into the motor cortex of *Flex-tdTomato* reporter mice to label corticospinal tract fibers and synapses. A large block of spinal cord containing the contusion was cleared using CLARITY. A representative 3D rendering (bottom left) of a CLARITY-processed spinal cord imaged by light-sheet microscopy shows the complete interruption of corticospinal tract fibers by the contusion. 3D images (right) from above and below contusion show the complete absence of corticospinal tract projections below injury. Scale bars 1 mm left, 500 µm right. **b**, Automatic spot detection showing synapses from cortical projection neurons detected in the gray matter at thoracic (T6) and lumbar (L1) segments. Representative photograph of synapses from cortical projection neurons in the T6 segment. Scale bar, 20 µm. Bar plot shows the number of synapses in gray matter sections above and below contusion (n = 5 mice). No synapses were detected in sections below the contusion. **c**, Coronal snapshots of 3D brainstem reconstructions in intact and contused mice. Each neuron is represented by a single dot. Bar plot represents the ratio of neuron counts in intact mice (n = 4 mice) over contused mice (n = 4 mice) for each identified region. Circular plot represents the proportion of spared neurons per region with respect to the total number of spared neurons in contused mice. **d**, The phenotype of brainstem projecting neurons was studied with immunohistochemistry in the four regions with highest percentage of spared neurons. Bar plots represent the mean neuron count in intact (n = 4) and contused (n = 4) mice for each region, normalized to the average count in intact mice. Individual plots represent independent animals. The polar plots display the average percentage of neurons (± s.e.m.) colocalizing with glutamate or serotonin with respect to the total number of neurons retrogradely labeled from lumbar segments in the identified region in 4 mice. *p < 0.05, two-tailed Mann–Whitney test.

behavioral observations. We thus hypothesized that glutamatergic neurons identified in the vGi and/or vestibular nuclei, both of which modulate locomotion (Hagglund, Borgius et al. 2010, Bachmann, Matis et al. 2013, Basaldella, Takeoka et al. 2015), were responsible for relaying the cortical command to lumbar execution centers. To address this question, we silenced these cells using a designer receptor exclusively activated by designer drug (DREADD) (Fig. 7a). To selectively target glutamatergic neurons in the vGi, we performed stereotaxic injections of a Cre-dependent AAV2/1 vector carrying the Gi/o-coupled DREADD (hM4Di) coupled to an mCherry tag in Thy1-ChR2-YFP::Vglut2-Cre mice (Vglut2 is also known as Slc17a6). Post-mortem evaluations confirmed transgene expression restricted to vGi neurons (Supplementary Fig. 7).

e Brain projection neurons with synapses in the lumbar spinal cord

f vGi projection neurons with synapses in the lumbar spinal cord

g Motor cortex projection neurons with synapses in the lumbar spinal cord
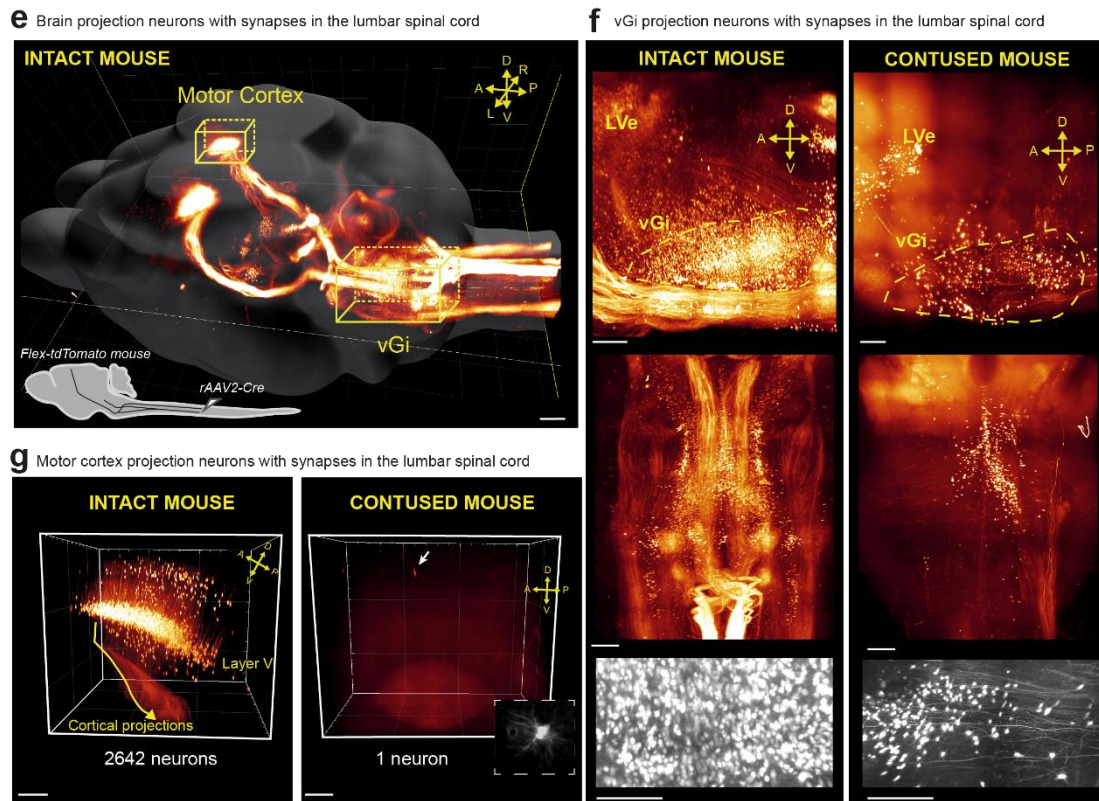
Fig. 6.2 | The contusion interrupts all corticospinal tract projections but spares subsets of brainstem pathways

e, 3D rendering of a CLARITY-processed brain showing all projection neurons with synapses in the lumbar spinal cord. Bottom, scheme showing the injection of AAV2-retro-Cre into lumbar (L1 and L2) segments of a *Flex-tdTomato* mouse. Scale bar, 2 mm. **f**,**g**, 3D images comparing number of vGi (**f**) and motor cortex (**g**) neurons projecting to the lumbar spinal cord in an intact and a contused mouse. This experiment was reproduced twice with CLARITY with similar results and was quantified in a group of 6 mice using classical histology (Supplementary Fig. 6d). Scale bars, motor cortex and vGi views, 500 µm; motor cortex inset, 30 µm; vGi enlargements in white, 200 µm.

In intact mice, silencing DREADD-positive vGluT2 neurons in the vGi (vGluT2ON neurons) exerted no detectable effect on basic and skilled locomotion (Supplementary Fig. 7). The same mice then received a contusion that caused leg paralysis. As observed in previous experiments, optogenetic stimulation of the motor cortex during neuromodulation instantly induced locomotion (Fig. 7b). Silencing vGluT2ON vGi neurons abolished these movements ($p < 0.001$, Fig. 7b). The optogenetic stimulation induced a forward tilt of the trunk (plus 4.2 ± 1.3 deg compared to standing) and rhythmic forelimb movements (4.72 ± 0.73 Hz), but the cortical command failed to engage lumbar circuits (Supplementary Fig. 7).

Before contusion, optogenetic stimulation (5 ms, 40 Hz) elicited reproducible motor evoked potentials in leg muscles (Fig. 7c). These responses vanished after contusion, but reappeared a few weeks later with longer latencies (increase in the length of latency: 25.9 ± 10.4 ms, Fig. 7c). Silencing vGluT2ON vGi neurons reduced or even suppressed these responses, indicating that these neurons relayed the cortical command to leg motor neurons.

We used the same procedure to silence vGluT2ON neurons located in the extended vestibular region, as confirmed post-mortem (Fig. 7d and Supplementary Fig. 7). Silencing glutamatergic vestibular neurons exerted no detectable impact on locomotion induced by optogenetic motor

47

cortex stimulation (Fig. 7d). The absence of deficits also indicate that, at our dosage (CNO 5 mg/kg), the suppression of locomotion during glutamatergic vGi neuron inactivation was not due to a nonspecific modulation of serotonergic receptors following CNO administration (Gomez, Bonaventura et al. 2017). These results reveal that glutamatergic vGi projection neurons relayed the motor cortex command downstream to produce locomotion during neuromodulation.
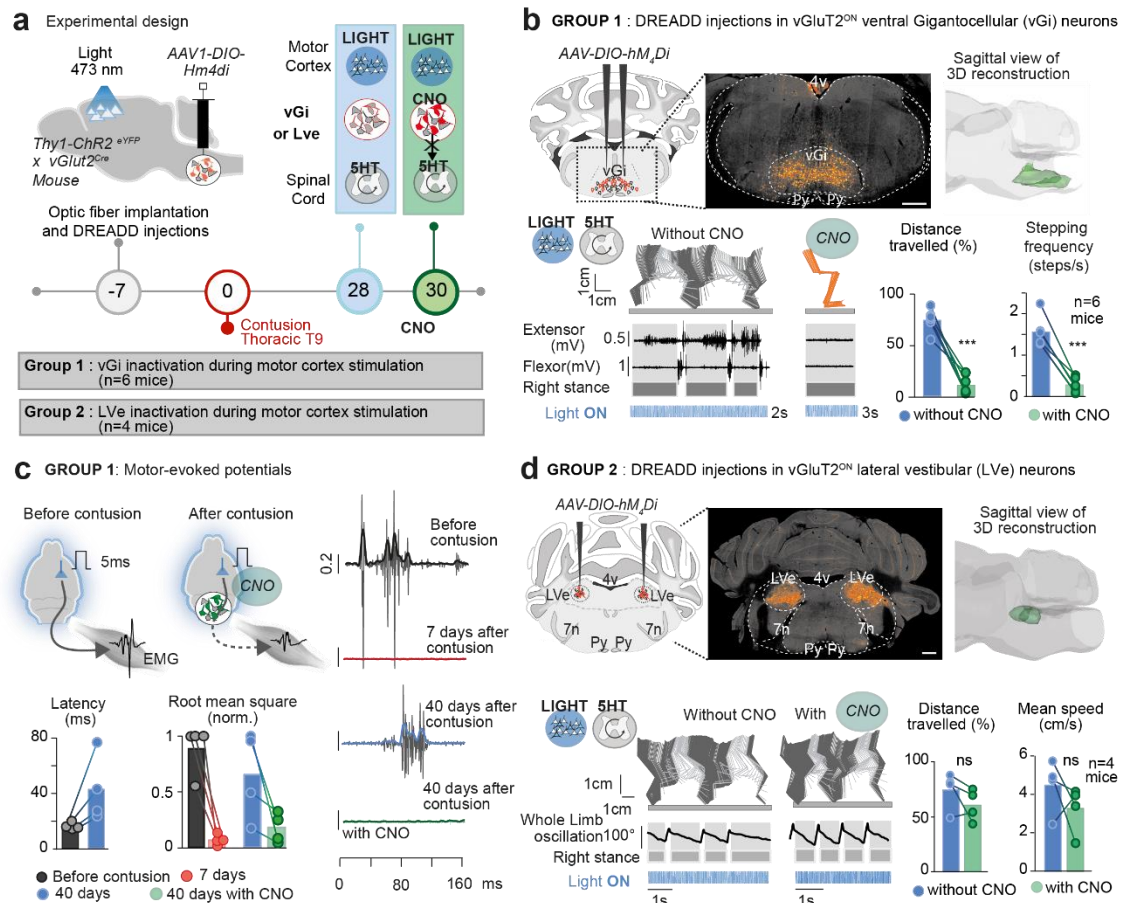
Fig. 7 | vGluT2ON vGi neurons relay the cortical command below injury
a, Scheme and timeline summarizing the experiments and behavioral conditions; LVe, lateral vestibular. **b**, Scheme and photograph showing expression of hM4Di in vGluT2ON vGi neurons (scale bar, 500 µm). Snapshot shows the 3D volume containing vGluT2ON hM4Di-expressing neurons in the vGi. Leg kinematics and muscle activity are shown during motor cortex stimulation before and during CNO administration using the same conventions as Fig. 1. Bar plot shows the relative distance traveled and the stepping frequency on the runway without and with CNO (n = 6 mice). ***$p < 0.001$. Two-tailed paired Student's t-test. Py, pyramidal tract; 4 V, fourth ventricle. **c**, Scheme of motor-evoked potential (MEP) recordings in the flexor muscles of the ankle in response to a single pulse of optical stimulation applied to the motor cortex. Representative MEP signals are plotted before contusion (black), 7 days after contusion (red), 40 days after contusion (blue) and 40 days after contusion during DREADD-mediated silencing of vGluT2ON vGi neurons (green). Thin gray traces represent raw EMG responses. Thick lines represent smoothed signals of EMG responses for each condition. The plots report the average latency and root mean square of MEPs for each mouse (n = 4 mice). Two-tailed Mann–Whitney test for latency (*$p = 0.0286$) and Kruskal–Wallis test for the root mean square (*$p = 0.0102$). **d**, Scheme and photograph showing bilateral expression of hM4Di in vGluT2ON neurons in the lateral vestibular nuclei (scale bar, 500 µm); 7n, seventh cranial nerve. Snapshot shows the 3D volume containing vGluT2ON hM4Di-expressing neurons in the lateral vestibular nuclei. Leg kinematics are shown during motor cortex stimulation before and during CNO administration. Bar plot shows the relative distance traveled ($p = 0.25$) and the mean speed ($p = 0.375$) on the runway without and with CNO (n = 4 mice); ns, not significant. Two-tailed Wilcoxon signed-rank test.

vGi projections survive contusions due to their distributed location in the white matter

These experiments implied that contusions systematically spared subsets of glutamatergic vGi projections. To study the mechanisms underlying this survival, we labeled the axonal projections from vGluT2ON vGi neurons using stereotaxic injections of AAV2/1-flex-tdTomato in Vglut2-Cre mice (Fig. 8a). CLARITY-optimized microscopy (Fig. 8b-e) showed that descending projections from vGluT2ON vGi neurons separated into two distinct pathways, expanding bilaterally in the lateral and ventral regions of the spinal cord white matter (Fig. 8c). Due to this distributed spatial topography, contusions systematically spared a subset of vGluT2ON vGi projections, regardless of the inherently variable damage location (Fig. 8d).

Quantification of white matter axon density revealed that only $6.5 \pm 2.3\%$ of axons from vGluT2ON vGi neurons survived contusions (Fig. 8f). Spared axons were more numerous in the lateral columns than in the ventral funiculi (Fig. 8f). These experiments show that the uniquely distributed topology of vGi projections in the white matter was the key mechanism allowing their survival after contusions.

Neurorehabilitation mediates motor cortex-dependent recovery of leg movements

We next investigated whether rehabilitation triggered a reorganization of the identified cortico-vGi-spinal circuits that mediated recovery in rats. We labeled the fibers and synapses of motor cortex projection neurons using injection of AAV-DJ-hSyn-flex-mGFP-2A-Synaptophysin-mRuby in leg motor cortex. There was a twofold increase in fiber density in the vGi of trained rats compared to both intact and untrained rats ($p < 0.05$).

These fibers established many synaptic contacts with vGi projection neurons that retained connections to lumbar segments (Fig. 9a and Supplementary Fig. 8a). Similar remodeling occurred in the red nucleus ($p < 0.05$; Supplementary Fig. 8e), but not in the vestibular regions (Supplementary Fig. 8d).

To probe the functional contribution of this reorganization, we silenced the leg motor cortex bilaterally using DREADD (Fig. 9b and Supplementary Fig. 9). In intact rats, motor cortex inactivation exerted no detectable effects during swimming. We only observed minimal foot misplacements during skilled locomotion along a ladder ($p = 0.00036$, Supplementary Fig. 9). Silencing the motor cortex of the same rats after contusion and training abolished volitional leg movements during swimming ($p = 0.0007$, Fig. 9b). These results demonstrate that neurorehabilitation triggered a pronounced remodeling of motor cortex projections in the vGi and that the production of volitional leg movements after training was contingent on these projections.
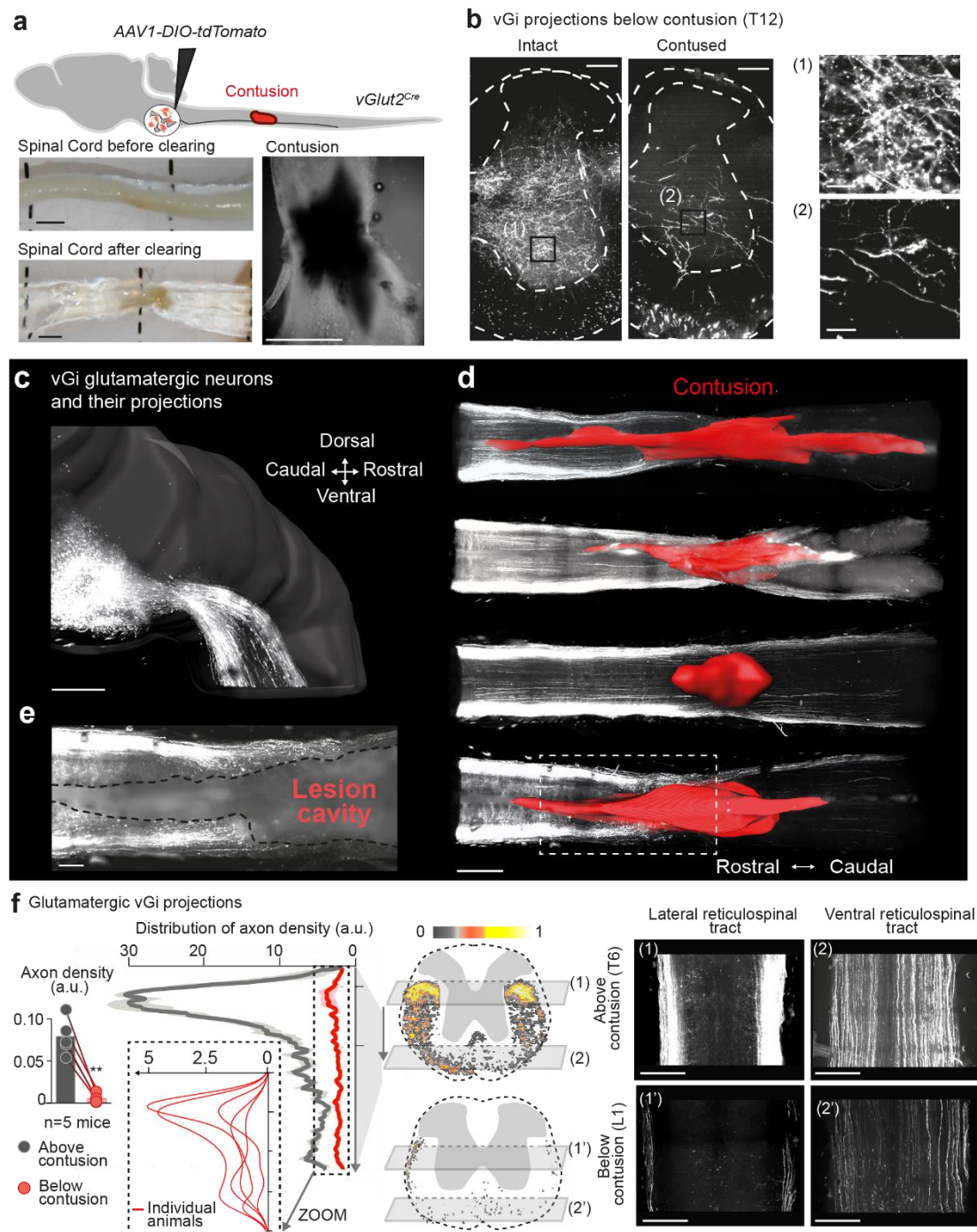
Fig. 8 | Variable topography of vGluT2ON vGi projection neurons enables their survival after contusion
a, Strategy for labeling axons of vGluT2ON neurons located in the vGi. The photographs show a segment of spinal cord containing the contusion before and after clearing. Note that the contusion cavity did not clear completely, and could thus be visualized with wide-field microscopy, as shown. Scale bar, 2 mm. **b**, CLARITY-processed spinal cords segments showing axons from vGluT2ON vGi neurons at spinal level T12 below the level of the contusion, both in intact and contused mice. Scale bars 250 µm. **c**, 3D rendering of a CLARITY-processed brainstem showing vGluT2ON neurons in the vGi and their axonal projections to the lateral and ventral spinal cord white matter. Only one side of the brainstem is shown. Scale bar, 500 µm. **d**, Four examples of 3D rendering of CLARITY-processed spinal cords showing the partial interruption of axons from vGluT2ON vGi neurons at the level of the contusion cavity, reconstructed in red. Scale bar, 1 mm. **e**, The interruption of vGluT2ON vGi projections at contusion level. Scale bar, 250 µm. **f**, Bar plot represents the mean axon density (n = 5 mice) above and below contusion. Curve plot represents the dorsoventral density distribution of glutamatergic vGi axons above (gray) and below (red). Thick line represents average distribution of n = 5 animals; shaded area, s.e.m. Individual dorsoventral distributions below injury are displayed as a zoom from the overview plot. Representative heat maps of vGluT2ON vGi projections in the gray matter are provided for slices above and below injury. Right, longitudinal sections showing axons from vGluT2ON vGi in the ventral and lateral spinal cord white matter. Scale bars, 500 µm. **p < 0.001, two-tailed paired Student's t-test.

Training-specific reorganization of vGi projections restore supraspinal control of movements

We then studied whether the recovery of volitional leg movements relied on the anatomical and functional reorganization of vGi projection neurons. To label these projections, we performed stereotaxic injections of AAV2/1-CMVGFP in the vGi. Compared to rats examined 1 week after contusion (subacute), trained rats exhibited a threefold increase in the density of vGi projections below the injury ($p < 0.001$, Fig. 10a). This reorganization occurred in distinct gray matter territories relevant for motor control. In thoracic segments below the injury, fiber density increased in intermediate laminas ($p = 0.0032$, Fig. 10a), where they established close appositions with spinal projection neurons connected to lumbar segments (Fig. 10b). These neurons amplify the descending locomotor command (Cowley, Zaporozhets et al. 2008). In lumbar segments, vGi projections sprouted in ventral laminas ($p = 0.0024$, Fig. 10a), wherein premotor circuits and leg motor neurons reside (Fig. 10b).

To assess the contribution of vGi projections, we used a doxycycline-inducible tetanus toxin technique (Kinoshita, Matsui et al. 2012) that allowed reversible inactivation of vGi neurons with synaptic projections to lumbar segments (Fig. 10c and Supplementary Fig. 10). All rats had recovered volitional locomotion. The inactivation of vGi neurons with residual projections below injury abolished this recovery ($p < 0.001$; Fig. 10c). Locomotion recovered when we ceased doxycycline administration ($p = 0.694$; Fig. 10c). Inactivation of vGi neurons in intact rats did not induce detectable deficits during either basic or skilled locomotion (Supplementary Fig. 10). These experiments establish causal relationships between the reorganization of vGi projections and recovery of volitional locomotion. Other supraspinal pathways failed to compensate for the blocked synaptic transmission from vGi neurons, indicating that these specific cells were necessary to mediate locomotion after injury in trained rats.

Reorganization of serotonergic projections

Trained rats regained volitional locomotion without serotonergic neuromodulation therapies. These observations suggest that serotonergic neurons located in the raphe and parapyramidal regions, which maintained projections to lumbar segments (Supplementary Fig. 8), also reorganized during rehabilitation. To evaluate this hypothesis, we stained serotonergic fibers with immunohistochemistry (Supplementary Fig. 11). Spared serotonergic fibers below the contusion showed no sign of sprouting in untrained rats, and instead exhibited a pathological increase in caliber ($p = 0.0191$; Supplementary Fig. 11). Rehabilitation prevented this swelling (Supplementary Fig. 11). Moreover, trained rats exhibited lamina-specific increase in serotonergic fiber density in the ventral gray matter of segments containing motor circuits.
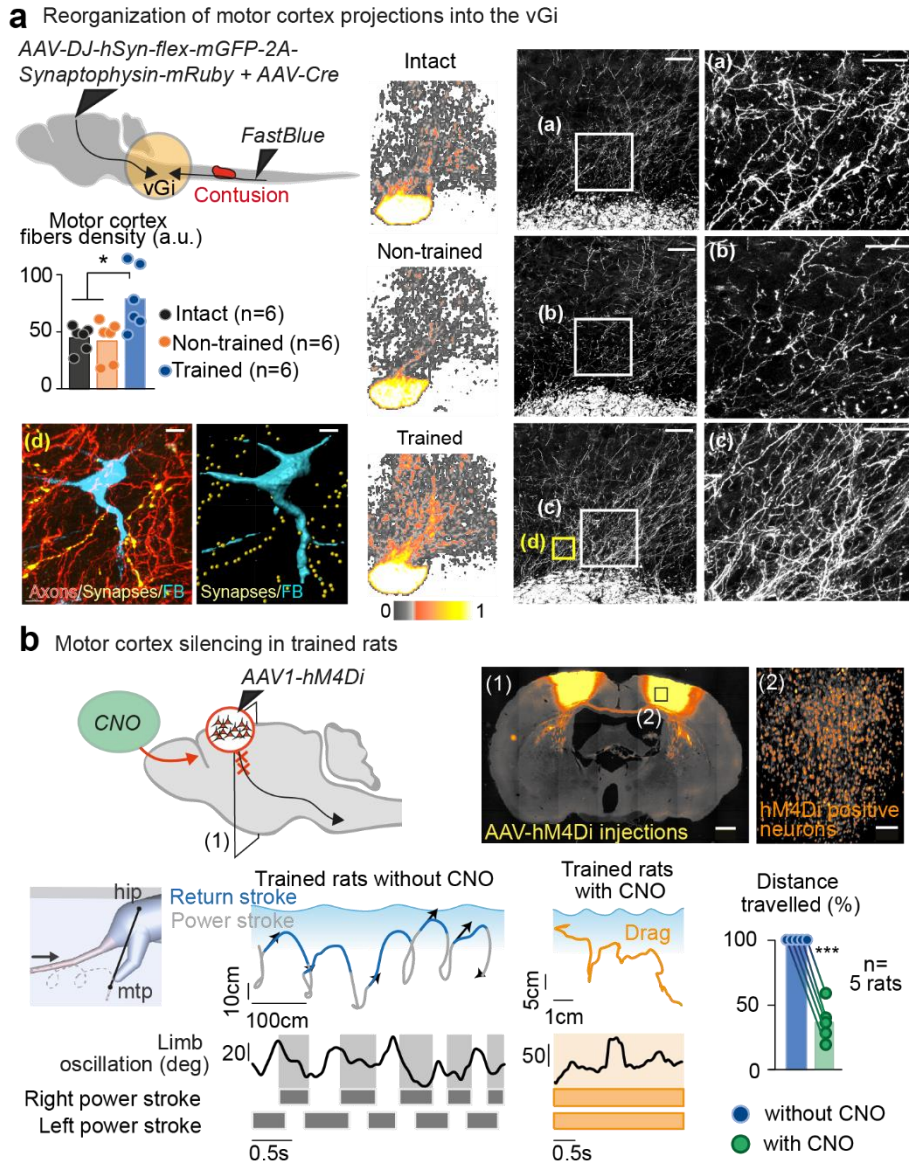
Fig. 9 | Neurorehabilitation promotes a reorganization of motor cortex projections
a, Top left, scheme illustrating the strategy for labeling the axons and synapses of motor cortex projection neurons, and spared vGi neurons projecting to the lumbar region. Heat maps (second column) and plots (center left) report the density of motor cortex projections in the vGi of intact (n = 6), untrained (n = 6) and trained (n = 6) rats. *p = 0.0107, one-way ANOVA followed by Bonferroni's post hoc test. Right, representative photographs of motor cortex projections in the vGi, including enlargements of the boxed regions. Scale bars, left 100 μm, right 25 μm. Bottom left, representative photograph and 3D reconstruction of close appositions from motor cortex synapses onto a vGi neuron with spared projections to the lumbar spinal cord. Scale bars, 10 μm. **b**, Top, scheme and photograph showing expression of hM4DiON neurons in the leg motor cortex of rats. Scale bar, left 1 mm, right 100 μm. Bottom left, leg kinematics and ankle muscle activity shown before and during motor cortex inactivation. Bottom right, plots showing the relative distance traveled along the pool of water (n = 5 rats). Mtp, metatarsophalangeal joint. ***p = 0.0007. Two-tailed paired Student's t-test.
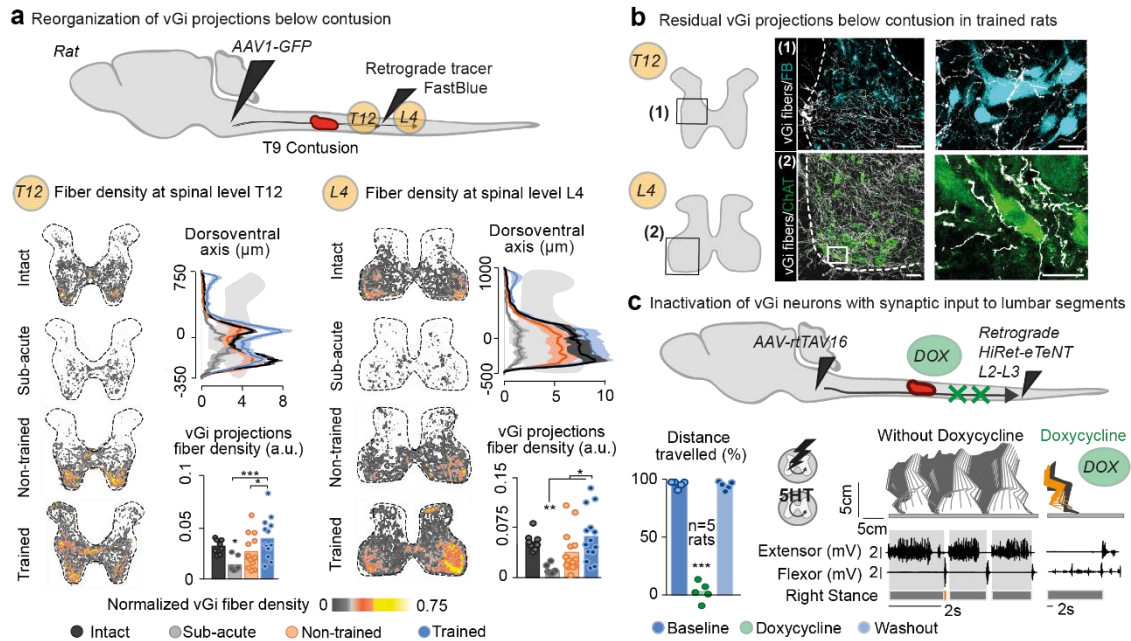
Fig. 10 | Neurorehabilitation promotes reorganization of vGi projection circuits
a, Diagram illustrating the strategy for labeling axonal projections from neurons located in the vGi. Heat maps are shown for a representative animal from each experimental group along the gray matter in thoracic (T12) and lumbar (L4) segments. Curve plots represent the dorsoventral distribution of axon density along the gray matter. Thick lines represent the average distributions of n = 4 intact rats (black), n = 4 subacute rats (1 week post-injury, gray), n = 7 untrained (9 weeks post-injury, orange) and n = 7 trained (9 weeks post-injury, blue) rats; shaded areas, s.e.m. Bar plots report the mean density of vGi axons in T12 (p = 0.0032) and L4 (p = 0.0024) segments and individual values for each animal (2 slices per animal). *p < 0.05; **p < 0.01; ***p < 0.001. One-way ANOVA followed by Bonferroni's post hoc test. **b**, Representative photographs of vGi axons projecting in laminas containing spinal neurons projecting to L2 and leg motor neurons located at L4. Scale bars, 100 µm left and 20 µm right. Close appositions of vGi axons with premotor neurons or motor neurons were frequent. FB, Fast Blue. **c**, Scheme illustrating the reversible inactivation of vGi neurons with residual projection to lumbar segments. Leg kinematics and ankle muscle activity is shown before and after inactivation using the same conventions as Fig. 1. Bar plots show the relative distance traveled along the runway (n = 5 rats). ***p < 0.001. One-way ANOVA followed by Bonferroni's post hoc test.

3.3. Discussion

We modeled a clinically relevant severe contusion SCI in rodents and found that this injury abolished all motor cortex projections to lumbar segments. Despite this interruption, electrochemical neuromodulation of lumbar circuits immediately enabled motor cortex to regain adaptive control over the paralyzed legs. Glutamatergic reticulospinal neurons located in the vGi nuclei relayed the cortical command downstream. With neurorehabilitation, neuromodulation therapies promoted an extensive reorganization of cortico-reticulo-spinal circuits that mediated a motor cortex-dependent recovery of walking, stair climbing and swimming without requiring neuromodulation. We discuss the critical role of cortico-reticulo-spinal circuits in enabling motor control after contusion, the reorganization of these circuits supporting motor cortex-dependent recovery, and the implication of these findings for repair interventions.

Cortico-reticulo-spinal circuits enable movement after contusion

Volitional locomotion involves an exquisitely organized motor-circuit communication matrix (Pivetta, Esposito et al. 2014). Concretely, cortical projection neurons transfer their command to lumbar segments both directly and indirectly through multiple midbrain and brainstem pathways operating in parallel. After moderate cut injuries, reorganization of intraspinal (Bareyre, Kerschensteiner et al. 2004, Takeoka, Vollenweider et al. 2014) and corticospinal tract (Friedli, Rosenzweig et al. 2015, Hilton, Anenberg et al. 2016, Hollis, Ishiko et al. 2016) projection circuits enables spontaneous recovery. By contrast, our severe contusions profoundly disrupted the communication matrix, leading to permanent deficits. Contusions only spared a few fibers originating from heterogeneous regions of the midbrain and brainstem. Yet common to all analyzed mice and rats was the systematic sparing of fibers from glutamatergic projection neurons located in the vGi.

Despite their survival, residual vGi projections failed to produce functional movements. The exogenous increase in lumbar circuit excitability with electrochemical neuromodulation was necessary to uncover the functionality of the residual cortico-reticulo-spinal circuitry. These results corroborate observations in paraplegic people who regain volitional movements during electrical spinal cord stimulation (Angeli, Edgerton et al. 2014, Gerasimenko, Gorodnichev et al. 2015).

We analyzed whether alternative routes may participate in this phenomenon. For example, vestibulospinal projection neurons, which modulate locomotion (Basaldella, Takeoka et al. 2015), also survived contusions. However, the inactivation of glutamatergic neurons located in the extended vestibular regions did not alter locomotor performance. The red nucleus can also act as a relay to produce forelimb movements after injuries (Siegel, Fink et al. 2015). However, contusions rarely spared rubrospinal projections. Yet many trained rats displayed a sprouting of motor cortex projections in the red nucleus. While we cannot exclude the possibility that this reorganization implies a contribution of rubrospinal pathways to locomotion, the variability

between rats and complete interruption of this pathway in mice suggest that the recovery was not contingent on residual rubrospinal projections. Instead, inactivation experiments revealed that glutamatergic vGi neurons were essential to the generation of locomotion. These results indicate that recovery from contusions involves mechanisms that are partly different from those previously described after restricted cut injuries. Reticulospinal projection circuits have been linked to skilled forelimb functions in intact mice (Esposito, Capelli et al. 2014), confirming that the reticular formation constitutes an important bridge between the motor cortex and spinal circuits for movement production (Nathan 1994, Matsuyama, Mori et al. 2004). Various studies suggest that cortical commands can be rerouted to the spinal cord through brainstem pathways following SCI (Belhaj-Saif and Cheney 2000, Ballermann and Fouad 2006, Zaaimi, Edgley et al. 2012, Zörner, Bachmann et al. 2014) and stroke (Koch, Schulz et al. 2016). Here we establish causal links between residual cortico-reticulo-spinal circuits and recovery after SCI.

The anatomy and function of reticulospinal pathways are well conserved across mammals (Nudo and Masterton 1988). Experiments in non-human primates and humans show that reticulospinal systems contribute to recovery after corticospinal tract lesions or SCI (Zaaimi, Edgley et al. 2012, Baker and Perez 2017). Moreover, due to their distributed location in the white matter (Nathan, Smith et al. 1996, Ballermann and Fouad 2006), reticulospinal pathways are prone to sparing after SCI in humans (Kakulas 1999). Consequently, we propose that cortico-reticulo-spinal circuits also mediate volitional movements during stimulation in people with motor paralysis (Angeli, Edgerton et al. 2014, Gerasimenko, Gorodnichev et al. 2015).

Motor cortex-dependent recovery of natural behaviors

In intact rodents, the motor cortex contributes to learning new motor skills (Kawai, Markman et al. 2015), but plays a minimal role during locomotion (Miri, Warriner et al. 2017). We confirmed this in intact rats. However, our results are consistent with models (van den Brand, Heutschi et al. 2012, Hilton, Anenberg et al. 2016, Hollis, Ishiko et al. 2016) in which the rodent motor cortex orchestrates the production of movements during recovery from neurological disorders.

After neurorehabilitation, contused rats could transform contextual information into task-specific commands to walk, climb a staircase and swim. These executions were contingent on motor cortex activity. However, the command was not transmitted through the corticospinal tract. Instead, task-specific cortical information was conveyed to the spinal cord via vGi neurons that maintained connections to lumbar segments. Neurorehabilitation triggered a collateralization of cortical projections to the vGi and a pronounced growth of vGi reticulospinal fibers in gray matter territories below the injury.

Spontaneous recovery has been associated with a similar reorganization of reticulospinal fibers after cut injuries (Ballermann and Fouad 2006, Takeoka, Vollenweider et al. 2014, Zörner, Bachmann et al. 2014). Here, we confirm the ability of the reticulospinal system to reorganize after contusions leading to paralysis and document direction of this growth to specific segments and laminas that are relevant for motor control. Training also augmented the density of serotonergic fibers in the ventral region of lumbar segments, which likely played a key role in the

recovery of volitional movements without neuromodulation. These results suggest that the new vGi (and serotonergic) projections targeted specific spinal neurons. While the identification of these integration nodes is outside the scope of our study, it will be important to investigate the postsynaptic partners of reticulospinal collaterals in the future. The molecular cues that guide training-specific reorganization also deserve clarification, since they may open new avenues for enhancing spinal cord repair.

Implications for spinal cord repair

Previous studies in animal models and humans with complete paraplegia reported the recovery of volitional movements following neurorehabilitation enabled by neuromodulation therapies (van den Brand, Heutschi et al. 2012, Angeli, Edgerton et al. 2014, Gerasimenko, Gorodnichev et al. 2015). However, motor control only occurred in the presence of neuromodulation therapies. By contrast, rats with contusions leading to permanent paralysis regained the ability to walk freely and swim without any neuromodulation. These carry-over effects were unexpected. They suggest that neuromodulation therapies enabled activity-dependent reorganization of cortico-reticulo-spinal circuits during neurorehabilitation and that the extent of this neuroplasticity was sufficient to restore natural locomotor behaviors without neuromodulation.

3.4. Supplementary material
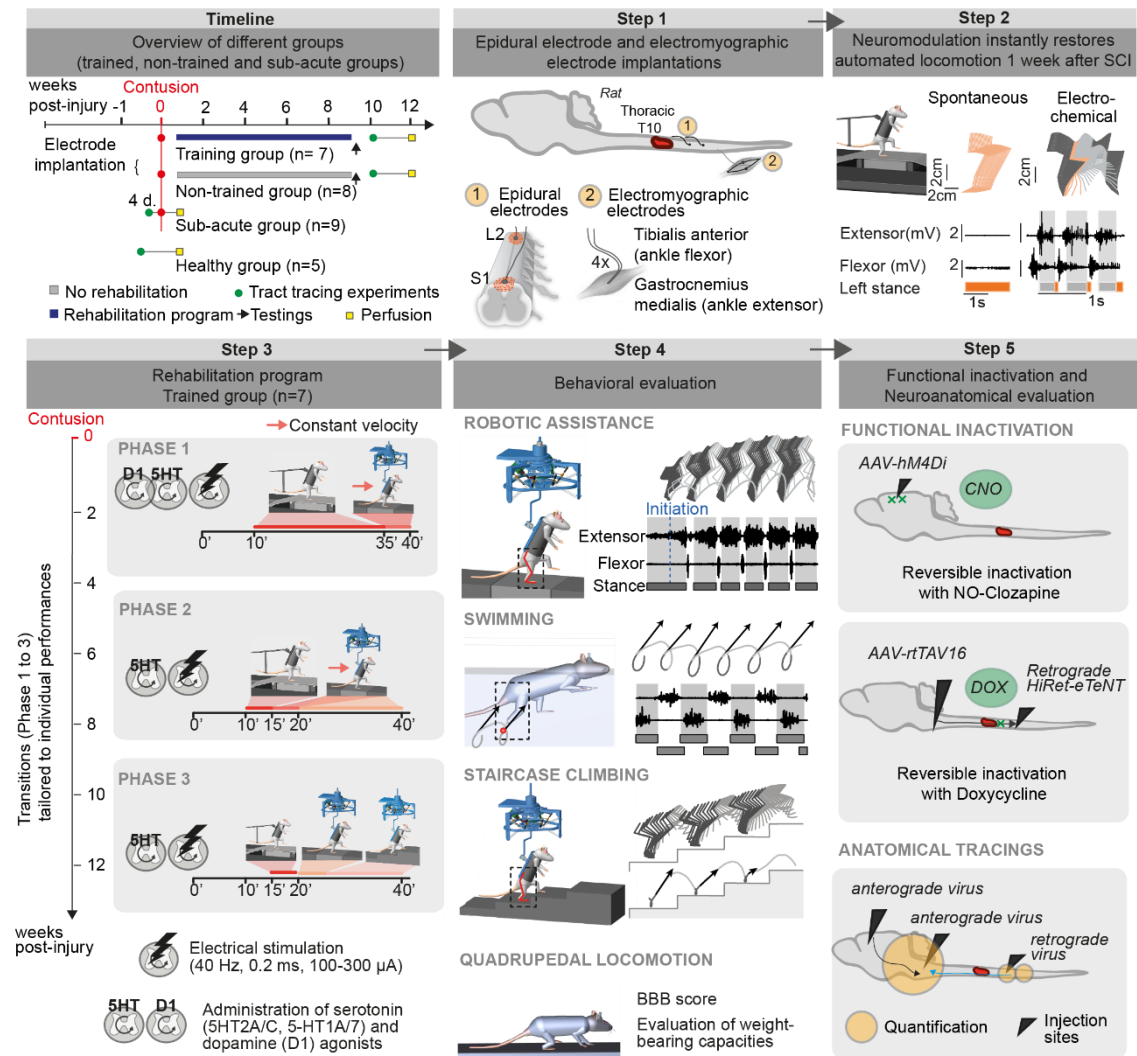
Supplementary Figure 1 | General methods and experimental groups
(**Timeline**) Summary of the experimental procedures and timeline for the main groups of animals. (**Step 1**)
Surgical implantation of chronic epidural electrodes over the midline of L2 and S1 spinal cord segments to
deliver electrical neuromodulation therapies. Bipolar electrodes are inserted into a pair of flexor (tibialis
anterior) and extensor (medial gastrocnemius) muscles of the ankle to record electromyographic activity.
(**Step 2**) A severe contusion was performed at the mid-thoracic level. Leg kinematics and muscle activity
are shown for a rat tested on a treadmill 1 week after contusion, both without and with electrochemical
neuromodulation. (**Step 3**) Design of the task-specific training regimen throughout the period of recovery,
including the transition from automatic stepping on a treadmill to overground walking with robotic assistance,
to stair climbing. The features and time-dependent adaptations of the electrochemical neuromodulation
therapy are shown. Briefly, the type and concentration of administered chemicals is constantly adjusted to
the current motor performance of the rats. (**Step 4**) Behavioral tasks to evaluate leg motor control. (**Step 5**)
Schematic overview of the functional inactivation and anatomical experiments that were used to evaluate
the reorganization of neuronal pathways.
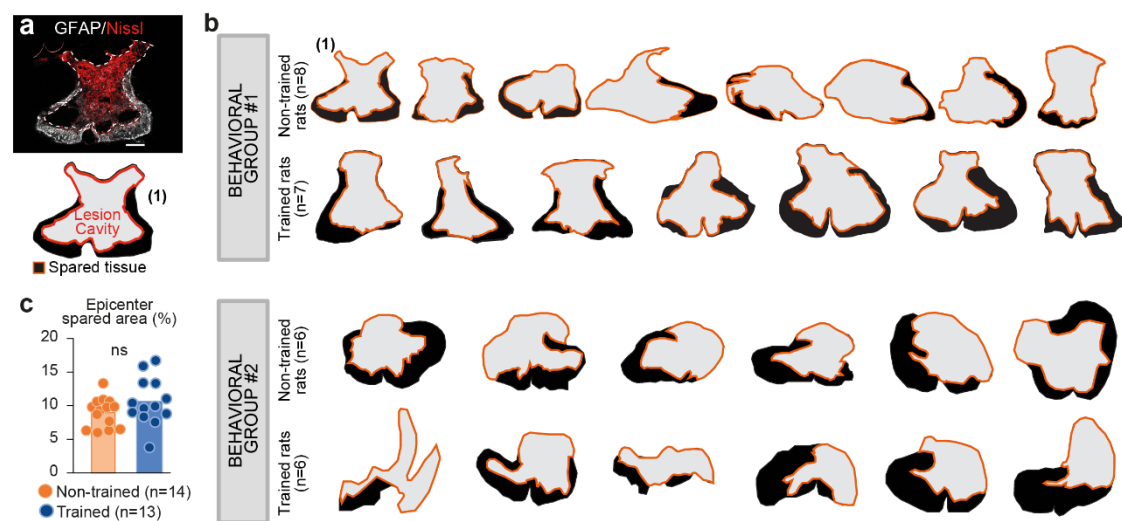
Supplementary Figure 2 | Characterization of spinal cord contusion in rats
a. Photograph of a coronal section through the contusion epicenter (GFAP, Glial fibrillary acidic protein), which was used to trace the contour of the contusion cavity, as illustrated below. Scale bar, 250µm. **b.** The contours of the lesion cavity at the epicenter are shown for all the main experimental rats used for behavioral and anatomical evaluations. **c.** The bar graph reports the area of spared tissue at the lesion epicenter for pooled non-trained (n = 14) and trained (n = 13) rats. ns, not significant, Student's t-test.
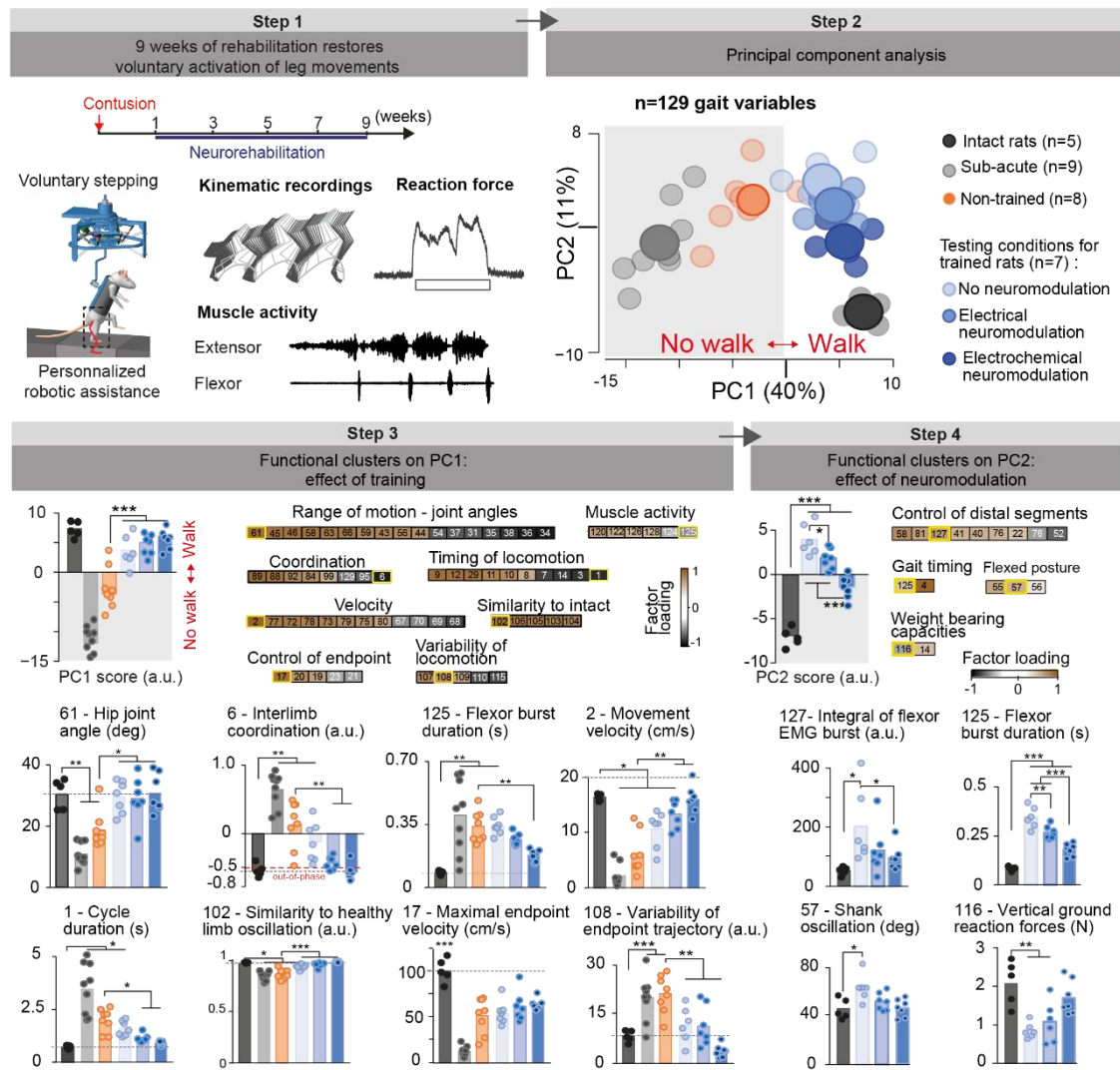
Supplementary Figure 3 | Behavioral evaluations of gross and detailed motor performance
(**Step 1**) Rats were evaluated during overground locomotion in a bipedal posture with robotic assistance. They were tested without neuromodulation, with electrical neuromodulation, and with electrochemical neuromodulation. Rats were trained to step overground with the gravity-assist during 9 weeks. Stepping performance (kinematics, muscle activity and ground reaction forces) was evaluated for different testing conditions at the end of the training period and compared to the motor output of non-trained rats. (**Step 2**) A PC analysis was applied on a total of 129 parameters characterizing global and fine details of leg motor control (table S1). The gait cycles of each rat under each neuromodulation condition (single dot, averaged of 10 to 20 gait cycles per rat) and averaged per group and conditions (large dots) are represented in new space defined by PC1 and PC2 (%, percent of explained variance). PC1 differentiated the effects of training, distinguishing the ability to move forward (walking) versus movements in place or falling backward (not able to walk). PC2 distinguished the effects of the neuromodulation conditions on leg motor control. (**Step 3**) The score of each rat on PC1 was extracted to quantify motor performance, i.e. the relative difference to intact (no injury) rats. The parameters that correlated highly with PC1 were extracted and regrouped in functional clusters that we named for clarity. The bar plots report the mean values for one parameter per each cluster, highlighted in yellow in the cluster. (**Step 4**) The same procedure was applied for parameters correlating with PC2, to identify the specific effects of neuromodulation conditions. *p < 0.05; **p < 0.01; ***p < 0.001, one-way ANOVA followed by Bonferroni's post-hoc test.

59
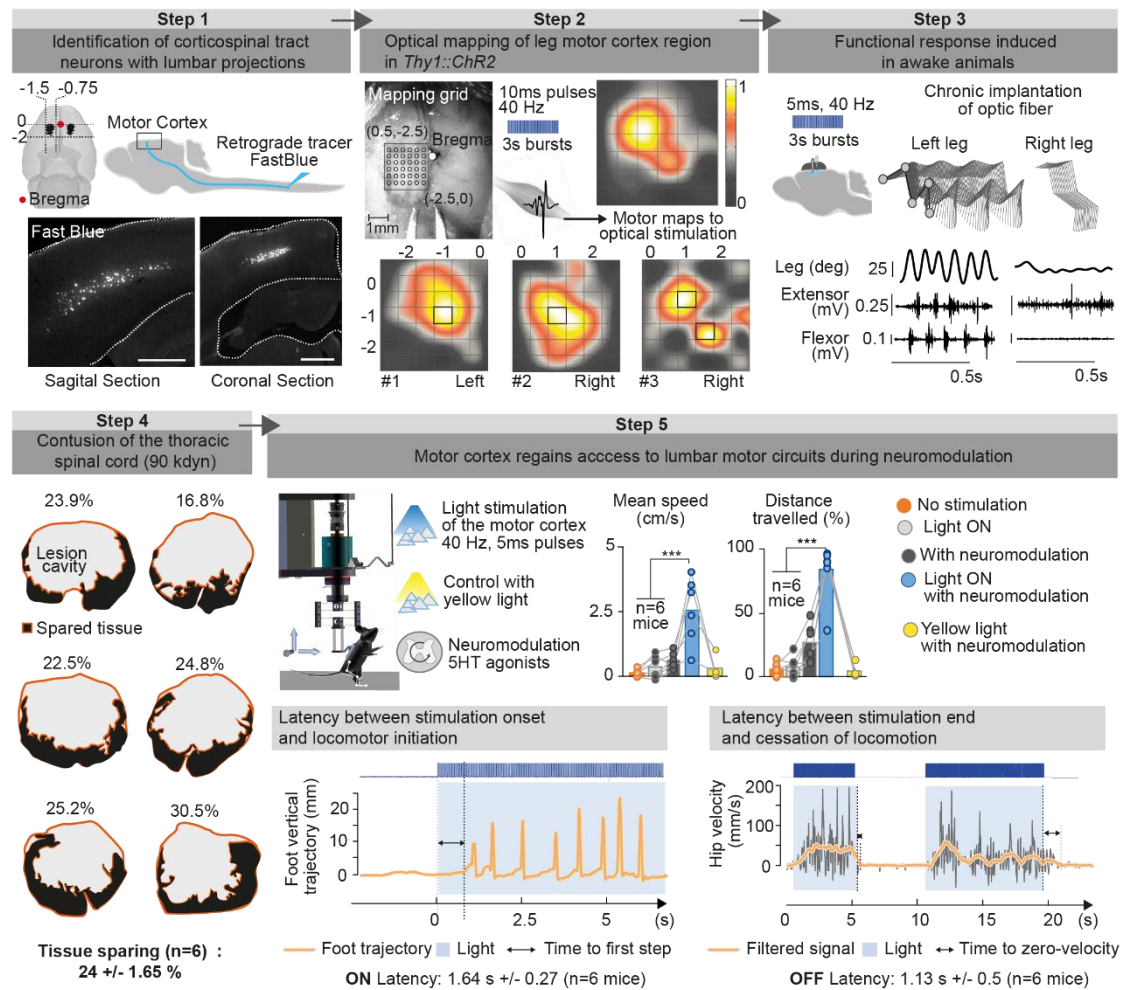
Supplementary Figure 4 | Optical manipulation of leg motor cortex activity in mice
(**Step 1**) To identify corticospinal tract neurons projecting to lumbar spinal segment, the retrograde tracer FastBlue was injected in the lumbar segments of *Thy1:ChR2-YFP* mice. Photographs show a sagittal and coronal view of FastBlue-labelled cells in the motor cortex. Scale bar 500µm. The scheme shows a 3D reconstruction of all the labelled cells. (**Step 2**) Short bursts of optical stimulation were delivered using a mapping grid positioned over the motor cortex region identified in Step1, as shown in the photograph. The amplitude of the motor evoked potentials recorded in the contralateral flexor muscles of the ankle was measured for each site of stimulation in order to elaborate a motor map for each tested mouse (bottom, squares indicate hotspots), and all mice combined (top). (**Step 3**) Optic fibers were implanted chronically in the region identified in Step 2. Stick diagram decomposition of leg movements, amplitude of leg oscillations, and electromyographic activity of the tibialis anterior (flexor) and gastrocnemius medialis (extensor) of the left and right legs in response to optical stimulation of the right motor cortex in suspended, awake mice. (**Step 4**) Mice received a contusion of the spinal cord at the T9 spinal segment level. For each experimental mouse, the lesion was reconstructed in order to visualize spared tissue (black) and lesion cavity (grey). (**Step 5)** Scheme showing the experimental conditions to test the mice with contusion. Bar plots reporting the mean speed and relative travelled distance under the different experimental conditions (n = 6 mice). Note the absence of behavioral effects when a non-specific yellow light was delivered over the motor cortex. ***p < 0.001, one-way ANOVA followed by Bonferroni's post-hoc test. **Bottom left,** the latency between the delivery of optical stimulation and the onset of locomotion was measured as the duration between the onset of the optical stimulation and the first vertical elevation of the foot. Bottom right, the latency between the termination of optical stimulation and the cessation of locomotion was measured as the duration between the end of the optical stimulation and the zero crossing of the filtered hip velocity profile.

60
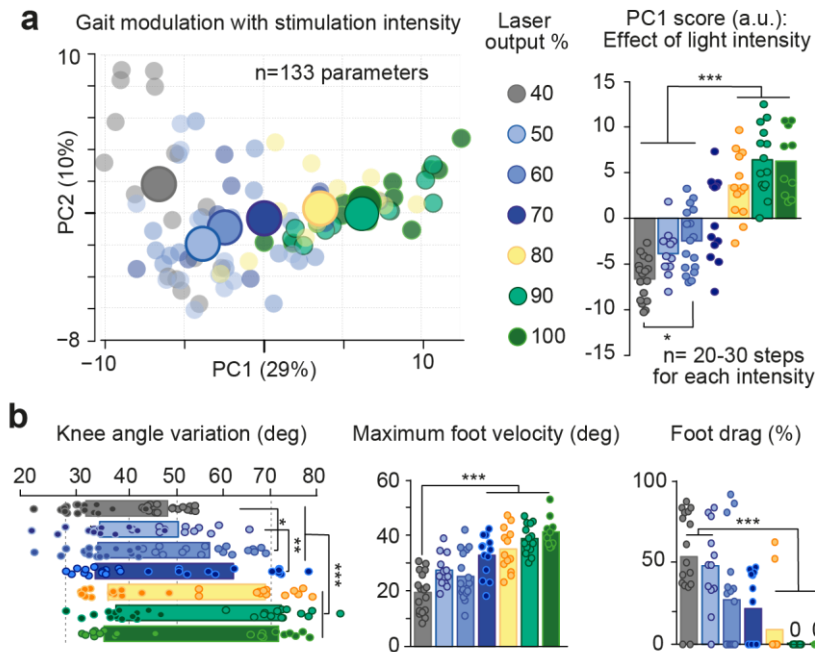
Supplementary Figure 5 | The motor cortex regains adaptive control of leg movements during neuromodulation

a. Leg kinematics were recorded during continuous stepping on a treadmill with different levels of optical intensities (laser output, %). A total of 133 parameters characterizing gait patterns were measured and submitted to a principal component (PC) analysis. The plot shows each gait cycle (small dot) in the new, reduced space created by PC1 and PC2. Large spots represent average per stimulation intensity. The bar plot on the right reports mean PC1 values, averaged over individual values for each gait cycle (individual dots). The number of gait cycles varies for each light intensity: n = 17 steps (40%), n = 11 (50%), n = 17 (60%), n = 13 (70%), n = 13 (80%), n = 14 (90%), n = 10 (100%). Laser output is expressed in percentage of the maximal light intensity (60mW). **b.** The bar plots show average values of single gait parameters for each stimulation intensity. $p < 0.05$; $p < 0.01$; $p < 0.001$, one-way ANOVA followed by Bonferroni's post-hoc test.
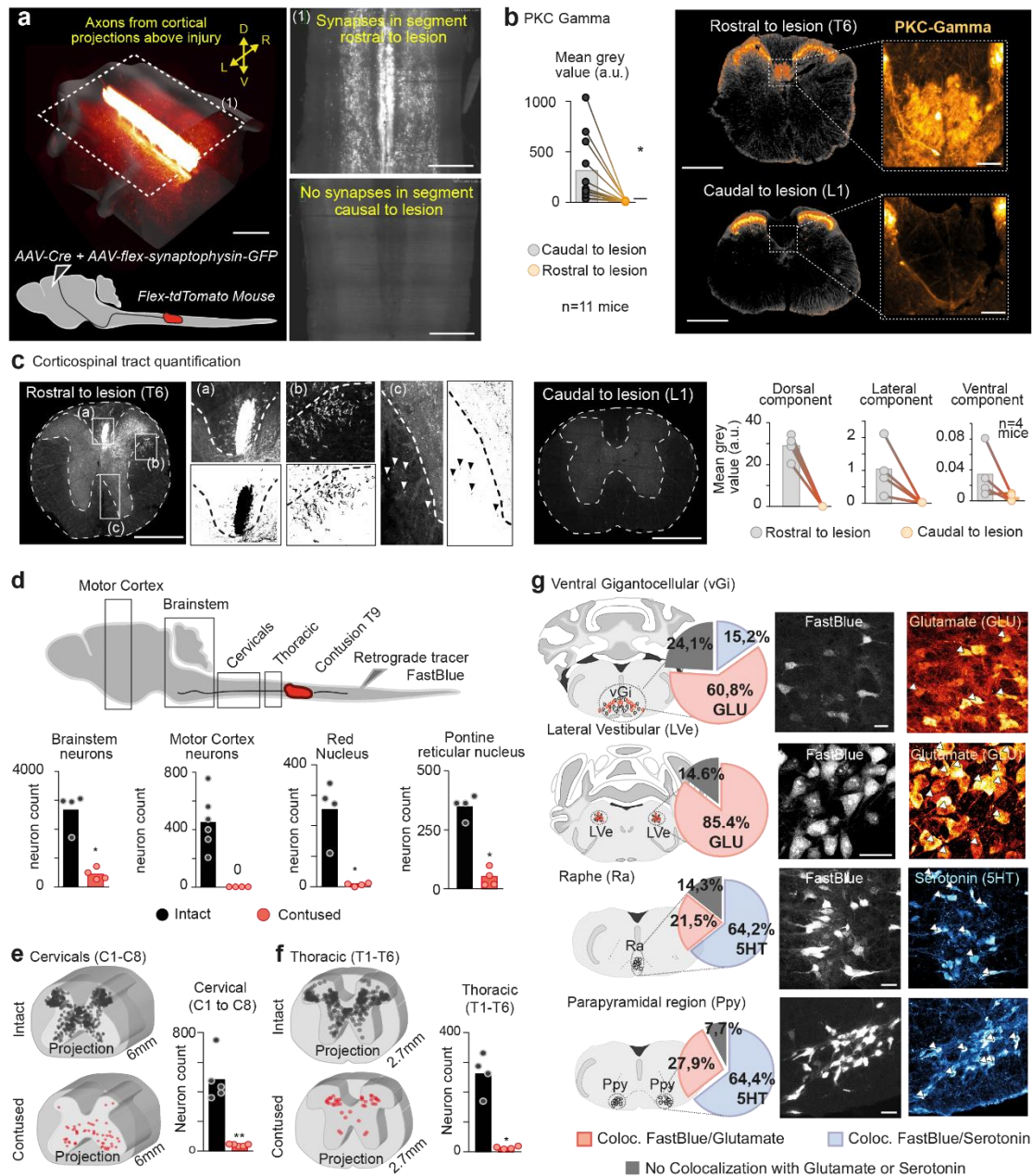
Supplementary Figure 6 | Characterization of projection neurons with residual connection below the contusion in mice

a. To visualize the interruption of the corticospinal tract in 3D, an AAV-Cre was co-injected with an AAV-flex-Synaptophysin-GFP into the motor cortex of *Flex-tdTomato* mice to label corticospinal tract fibers in the spinal cord. A large block of spinal cord containing the contusion was cleared using CLARITY. A representative 3D rendering of a CLARITY-processed spinal segment rostral to the contusion shows corticospinal tract fibers. Longitudinal photographs of spinal segments rostral and caudal to contusion show the synapses from corticospinal tract neurons. Scale bar 500µm. **b.** To verify the interruption of corticospinal tract projections independent of viral injections, spinal cord sections rostral (T6) and caudal (L1) to the contusion were stained with Protein Kinase C gamma (PKC-Gamma) antibodies, which label corticospinal tract axons. The bar plot reports the mean relative (arbitrary unit, a.u.) intensity of the PKC-Gamma signal in segments caudal and rostral to the contusion. Scale bars 500µm, 50 µm insets. $*p < 0.05$, paired Student's t-test. **c.** To quantify the interruption of corticospinal tract projections from the leg region of the motor cortex, fluorescence of the main corticospinal tract component in the dorsal column, the lateral component and the ventral component was measured in spinal cord sections rostral (T6) and caudal (L1) to the contusion. Scale bars 500µm, 50 µm insets. Bar plots show the mean relative (arbitrary unit, a.u.) intensity of corticospinal tract axons projecting in the different regions of the white matter. **d.** Diagram illustrating the injections of the retrograde tracer FastBlue in the lumbar spinal cord to identify projection neurons with residual connections below the contusion. The diagram illustrates the various regions where neurons were found and analyzed. Bar plots report the number of neurons in these regions (n = 4 each for intact and contused mice). 3D cervical **e.** and **f.** thoracic spinal cord reconstructions in intact and contused mice, including quantifications. $*p < 0.05$, $**p < 0.01$, Mann-Whitney test. **g.** The phenotype of brainstem neurons with residual projections below the contusion was studied with immunohistochemistry. Photographs show neurons retrogradely labelled from lumbar segments and the colocalisation with glutamate or serotonin (white arrows). Scale bars 25µm. The polar plots display the mean percentage (+- s.e.m) of neurons co-localising with glutamate or serotonin with respect to the entire population of neurons retrogradely labelled from lumbar segments in intact mice (n = 4 mice).

62
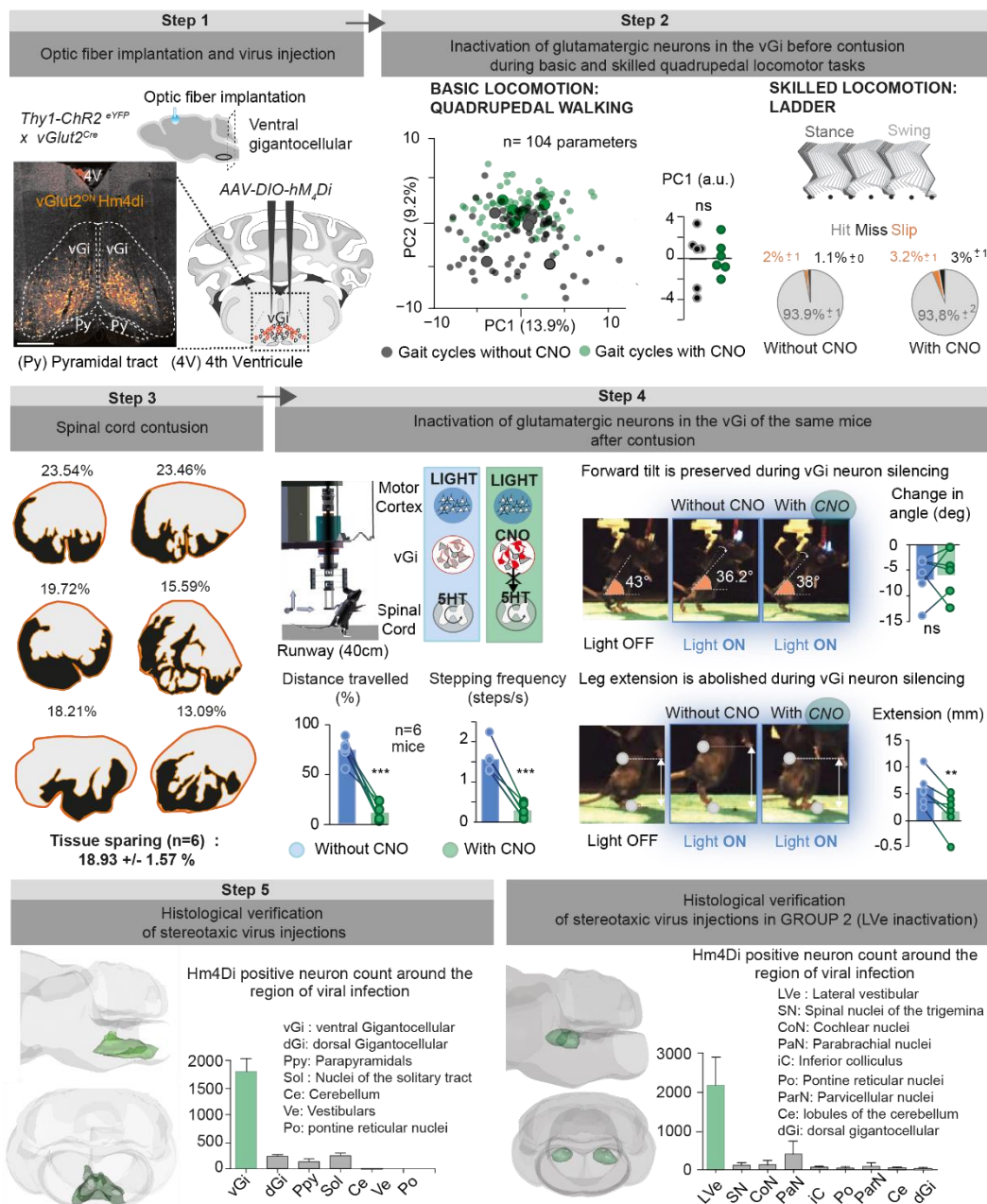
Supplementary Figure 7 | Inactivation of vGi neurons suppresses cortical control of locomotion
(**Step1**) Strategy to express DREADDs specifically in glutamatergic neurons of the vGi, while manipulating the activity of motor cortex projection neurons with light (n = 6 mice). Photograph showing expression of *hM4Di* in *vGluT2ON* vGi neurons. Scale bar, 500μm. (**Step 2**) Intact (no injury) mice were tested before and after CNO during quadrupedal locomotion along a flat surface and a horizontal ladder. A PC analysis was applied on 104 gait parameters characterizing the walking pattern. Gait cycles (small dot, individual gait cycles; large dots, average per mouse and condition) measured along the flat surface are represented in the new space created by PC1 and PC2 (%, explained variance). No significant difference was detected between both conditions. The stick diagram decomposition of leg movements shows the progression along the horizontal ladder. The polar plot reports the mean relative percent of hits, misses and slips onto the rungs of the ladder for both conditions (±s.e.m). Silencing *vGluT2ON* vGi neurons did not alter skilled leg movements. (**Step 3**) The same mice received a severe contusion. For each experimental mouse, the lesion was reconstructed in order to visualize spared tissue (black) and lesion cavity (grey). (**Step 4**) Experimental conditions to evaluate the cortical control of leg movements before and after silencing *vGluT2ON* vGi neurons. Mice were tested bipedally under chemical neuromodulation (5HT agonists). The bar plots represents the mean distance travelled and the mean stepping frequency when delivering optical motor cortex stimulation without and with CNO (n = 6 mice). The snapshots illustrate the forward tilt of the trunk and whole leg extension when delivering optical stimulation. The bar plots report the mean values of these parameters (n = 6 mice). **$p < 0.01$, ***$p < 0.001$, two-tailed paired Student's t-test. (**Step 5**) Post-mortem evaluation of hM4Di positive neurons in the vGi and potential infection in neighbouring regions for all experimental animals (n = 6 mice), shown as mean ±s.e.m. The coronal and dorsoventral snapshots of the brainstem show the 3D volume containing *vGluT2ON hM4Di* expressing neurons. Post-mortem evaluation of hM4Di positive neurons in the lateral vestibular nuclei (n=4 mice) shown as mean ±s.e.m., and 3D volume containing *vGluT2ON hM4Di* expressing neurons is shown in the right panel.
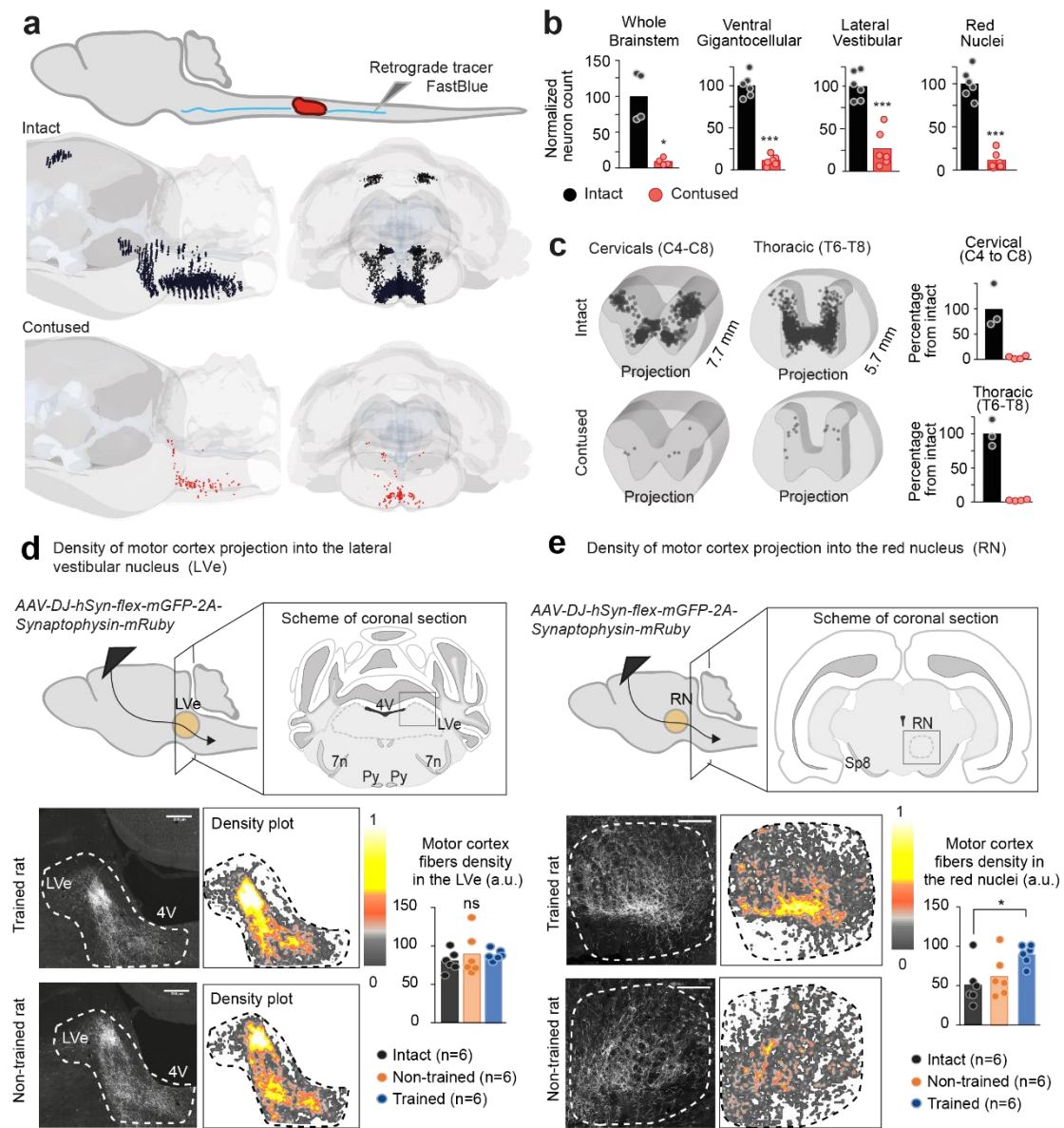
Supplementary Figure 8 | Characterization of projection neurons with residual connection below the contusion in rats, and reorganization of motor cortex projections in the brainstem

a. Diagram illustrating the injections of the retrograde tracer FastBlue in the lumbar spinal cord to identify projection neurons with residual connections below the contusion in rats. Coronal and dorsoventral snapshots of 3D brain and brainstem reconstructions in intact and contused (non-trained) rats. Each neuron is represented by a single dot. **b.** The bar plots report the relative number of identified neurons in the whole brainstem (n = 4 each for intact and contused rats) and selected regions from the brainstem (n = 6 each for intact and contused). **c.** 3D cervical and thoracic spinal cord reconstructions in intact and contused rats, including quantifications. *p < 0.05, **p < 0.01, ***p < 0.001, non-paired Student's t-test (b) or Mann-Whitney test (c). **d. and e.** Scheme illustrating motor cortex injections and regions for the quantification of motor cortex projections. Representative photographs and corresponding heat maps of motor cortex projections in the lateral vestibular nuclei **d.** and red nuclei **e.** of intact (n = 6), non-trained (n = 6) and trained (n = 6) rats. Scale bars, 200 μm. *p < 0.05, one-way ANOVA followed by Bonferroni's post-hoc test.

64
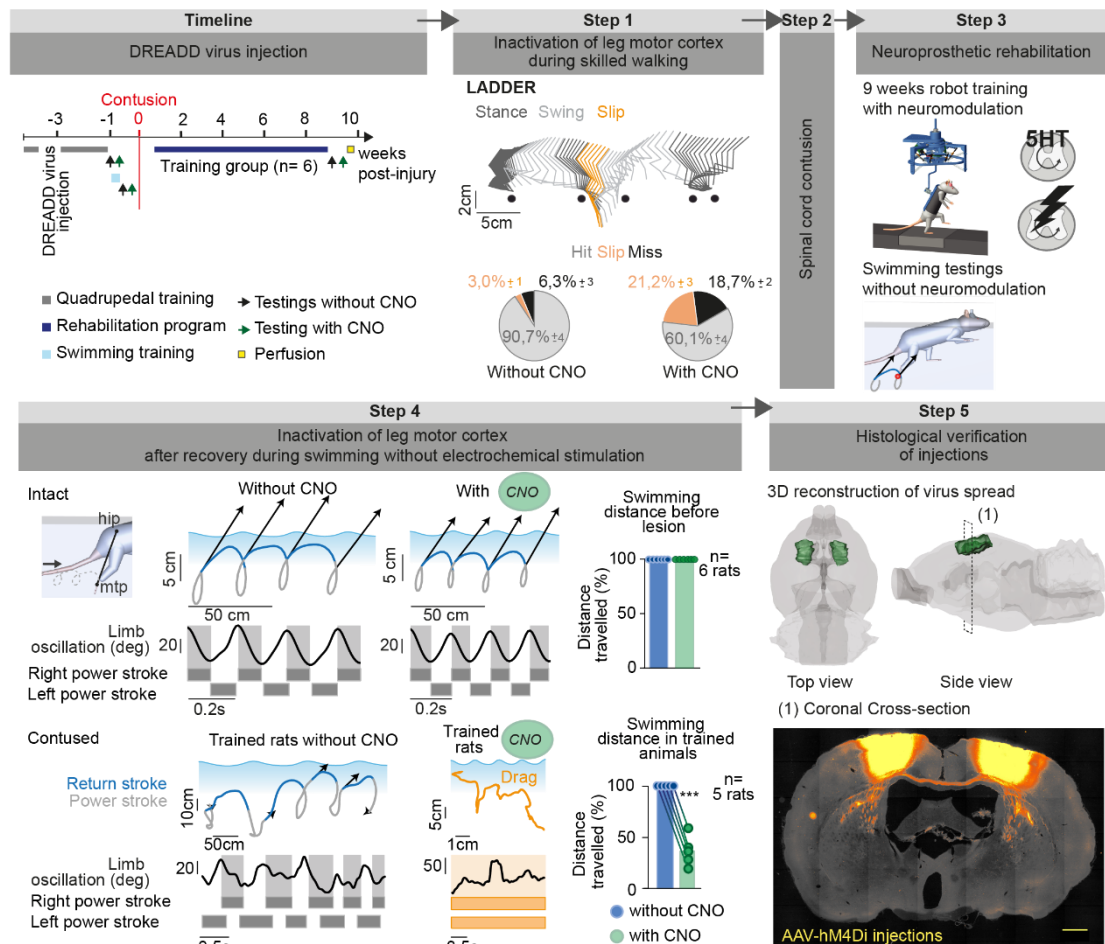
Supplementary Figure 9 | Silencing of leg motor cortex neurons abolishes leg motor control in trained rats

(**Timeline**) Timeline of experimental procedures in intact (n = 6) and contused rats (n = 5). (**Step 1**) Intact rats were evaluated during locomotion along the irregularly spaced rungs of a ladder, before and after CNO administration. The circular plots report the percent of hits, misses and slips onto the rungs of the ladder for both conditions. (**Step 2**) The rats received a 250 kdyn contusion. (**Step 3**) They followed the standard neurorehabilitation protocols as described in Supplementary Fig. 1. (**Step 4**) Stick diagram decomposition of leg movements during swimming. Successive leg endpoint trajectories, including velocity vector at return stroke onset, together with the oscillation of the limb and occurrence of left and right power strokes during swimming. A representative sequence is shown for intact and contused rats, both without and with CNO. Contused rats were tested without neuromodulation. ***p < 0.001, paired Student's t-test. (**Step 5**) 3D reconstruction of the cortical region with neurons expressing hM4Di, including a photograph through the coronal plane marked (1). Scale bar, 500 µm.
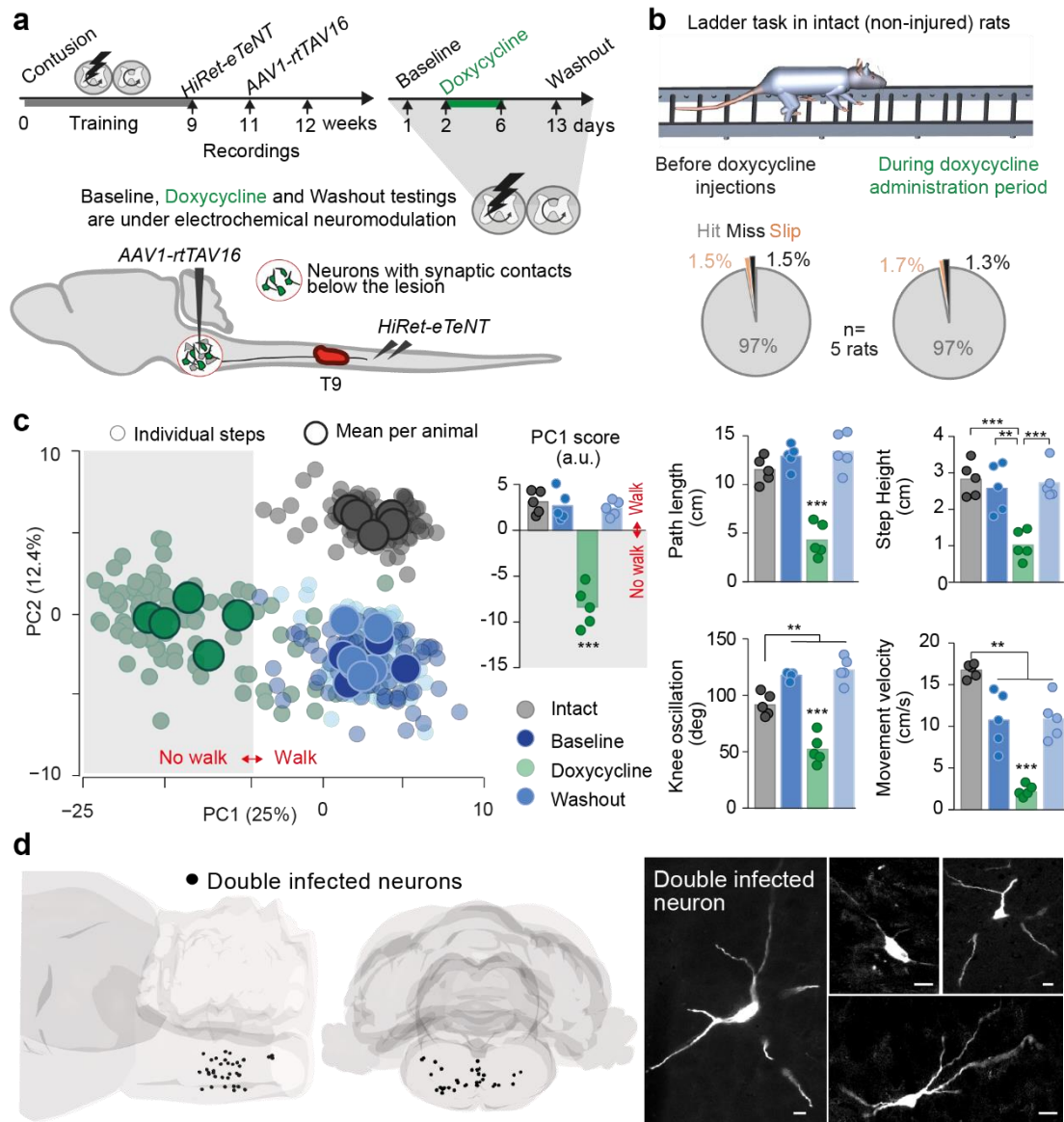
Supplementary Figure 10 | Inactivation of vGi neurons projecting below the contusion abolishes leg motor control in trained rats

a. Timeline of experimental procedures and strategy for the reversible inactivation of vGi neurons with projections to lumbar segments, both in intact (n = 5 rats) and contused rats (n = 5 rats). **b**. Intact rats (no injury) were evaluated during locomotion along the irregularly spaced rungs of a ladder, before and after repeated doxycycline administration. The circular plots report the percent of hits, misses and slips onto the rungs of the ladder for both conditions **c**. PC analysis using the same conventions as in Fig. 1. All the individual gait cycles are shown, as well as the average for each rat. The bar plot near the PC analysis reports the mean values of the score on PC1 which differentiated trials with forward progression (walking) from trials without initiation (not walking). The other bar plots report the mean values of basic gait parameters illustrating the robust deterioration of leg motor control during inactivation of vGi neurons with residual projections to lumbar segments in trained rats. **p < 0.01, ***p < 0.001, one-way ANOVA followed by Bonferroni's post-hoc test. **d**. 3D reconstruction of all neurons expressing both transgenes, including photographs showing the morphology of these neurons. Scale bars, 25 µm.
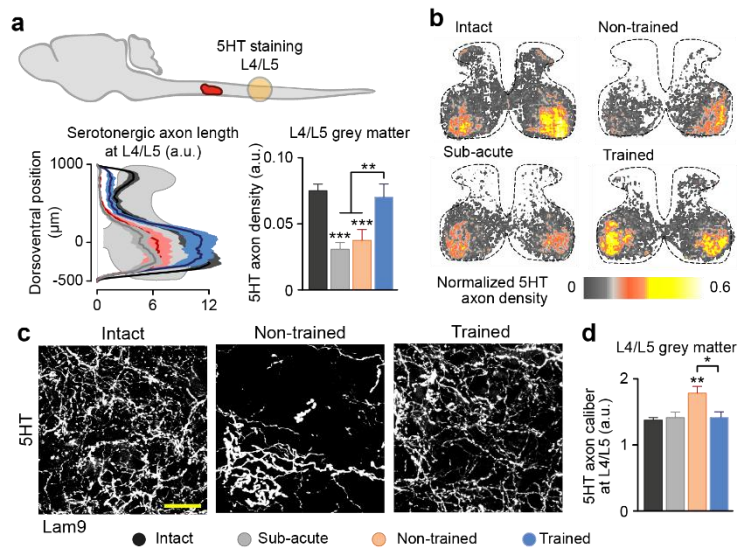
Supplementary Figure 11 | Reorganization of serotonergic (5HT) axons in the lumbar spinal cord
a. Scheme showing the location at which the density of 5HT axons was evaluated. Density plot of 5HT axons along the dorsoventral extent of the spinal cord (bold line represents the mean distribution for all animals, shaded region represents s.e.m.), and bar graphs reporting the mean axon density of 5HT axons and individual animals within L4/L5 spinal segments. **b.** Representative heat maps of 5HT axons, visualized at L4/L5. **c.** Representative images of 5HT axons in the lamina 9 of L4 segment. Scale bar, 25 μm (d) Bar graph reporting the mean caliber of 5-HT axons at L4/L5. Scale bars, 25μm.*p < 0.05, **p < 0.01, one-way ANOVA followed by Bonferroni's post-hoc test.

OVERVIEW OF GROUPS					
SPECIES	ANALYSIS	GROUP	N	FIGURE NUMBER	EPICENTER SPARED AREA (mean +- s.e.m.)
RATS	Behavioral assessments and quantification of vGi projections in the spinal cord	INTACT	5	Fig.1, Fig. 2b-2f, Fig. 8a Sup. Fig.1, Sup. Fig. 3	-
		SUB-ACUTE	9		12.7 +- 1.1
		NON-TRAINED	8		8.04 +- 0.7
		TRAINED	7		12.29 +- 1.2
	Supplementary behavioral assessments and quantification of cortical projections in the brainstem	INTACT	6	Fig.2d, Fig. 7a Sup. Fig. 8	-
		NON-TRAINED	6		10.26 +- 0.61
		TRAINED	6		8.66 +- 1.16
	Hindlimb motor cortex inactivation with DREADDs	TRAINED	5	Fig.7b Sup. Fig. 9	9.93 +- 0.89
	Inactivation of vGi neurons with synaptic inputs to the lumbar spinal cord	TRAINED	5	Fig.8c Sup. Fig. 10	N/A
MICE	Motor cortex activation after contusion	CONTUSED	6	Fig. 3c-3d Sup. Fig. 4, Sup. Fig. 5	23.97 +- 1.65
	Inactivation of glutamatergic neurons in the vGi with DREADDs	CONTUSED	6	Fig. 5b-5c Sup. Fig. 7	18.93 +- 1.57
	Inactivation of glutamatergic neurons in the LVe with DREADDs	CONTUSED	4	Fig. 5d Sup. Fig. 7	20.83 +- 2.50

Supplementary Table 1 | Overview of experimental groups

#		Computed parameter
Rat	Mouse	
		Gait Timing
1	1	Cycle duration
2	2	Movement velocity
3	3	Stance duration
4	4	Swing duration
5	5	Stance duration in percentage of whole cycle
6	6	Interlimb coordination
7	7	Double stance (in percentage of gait cycle duration)
8	8	Stride length
9	9	Step length
10	10	Step height
11	11	Step height normalized to stance height
12	12	Path length
		Endpoint trajectory shape
13	13	Stance width
14		Body weight support by the postural prosthesis
15	14	Maximal backward position of the foot
16	15	Maximal forward position of the foot
17	16	Maximal endpoint velocity
18	17	Timing of the maximal enpoint velocity
19	18	Endpoint acceleration
20	19	Endpoint velocity
21	20	orientation of the velocity vector at swing onset
22		Drag duration
23		relative drag duration (percent of swing duration)
		Stability
24	21	Amplitude of lateral trunk position
25	22	Sagital trunk movement
26	23	Sagital trunk velocity
27	24	Variability of vertical hip-midpoint oscillation
28	25	Variability of medio-lateral hip rotation
29	26	Forward movement of the center of mass
30	27	Lateral oscillation of the center of mass
		Joint angles and limb segment oscillations
31	28	Crest oscillation (minimal elevation)
32	29	thigh oscillation (minimal elevation)
33	30	Shank oscillation (minimal elevation)
34	31	Foot oscillation (minimal elevation)
35		Toe oscillation (minimal elevation)
36	32	Whole limb oscillation (minimal elevation)
37	33	Crest oscillation (maximal elevation)
38	34	thigh oscillation (maximal elevation)
39	35	Shank oscillation (maximal elevation)
40	36	Foot oscillation (maximal elevation)
41		Toe oscillation (maximal elevation)
42	37	Whole limb oscillation (maximal elevation)
43	38	Hip joint angle (maximal)
44	39	Knee joint angle (maximal)
45	40	Ankle joint angle (maximal)
46		MTP joint angle (maximal)
47	41	Whole limb adduction
48	42	Foot adduction
49	43	Hip joint angle (minimal)
50	44	Knee joint angle (minimal)
51	45	Ankle joint angle (minimal)
52		MTP joint angle (minimal)
53	46	Whole limb abduction
54	47	Foot abduction
55	48	Crest oscillation
56	49	Thigh oscillation
57	50	Shank oscillation
58	51	Foot oscillation
59		Toe oscillation
60	52	Whole limb oscillation
61	53	Hip joint angle
62	54	Knee joint angle
63	55	Ankle joint angle
64	56	MTP joint angle
65	57	Whole limb medio-lateral oscillation
66	58	Foot rotation
		Velocity
67	59	Whole limb angle velocity (minimal)
68	60	Hip joint anlge velocity (minimal)
69	61	Knee joint angle velocity (minimal)
70	62	Ankle joint angle velocity (minimal)
71		MTP joint angle velocity (minimal)
72	63	Whole limb angle velocity (maximal)
73	64	Hip joint anlge velocity (maximal)
74	65	Knee joint angle velocity (maximal)
75	66	Ankle joint angle velocity (maximal)
76		MTP joint angle velocity (maximal)
77	67	Whole limb angle velocity
78	68	Hip joint anlge velocity
79	69	Knee joint angle velocity
80	70	Ankle joint angle velocity
81		MTP joint angle velocity
		(Intra-limb) coordination
82	71	Temporal coupling between crest and thigh oscillation
83	72	Temporal coupling between thight and shank oscillation
84	73	Temporal coupling between shank and foor oscialltion
85		Temporal coupling between foot and toe oscillation
86	74	correlation of crest and thigh oscillation
87	75	Correlation of thigh and leg oscillation
88	76	Correlation of leg and foot oscillation
89		Correlation of foot and toe oscillation
90	77	Correlation of hip and knee oscillation
91	78	Correlation of knee and ankle oscillation
92	79	Correlation of ankle and MTP oscillation
93	80	Timing of crest-thigh (minimal)
94	81	Timing of crest-thigh (maximal)
95	82	Timing of thigh-shank (minimal)
96	83	Timing of thigh-shank (maximal)
97	84	Timing of shank-foot (minimal)
98	85	Timing of shank-foot (maximal)
99		Degree of linear coupling between joint oscillations (PC1)
100		Degree of linear coupling between joint oscillations (PC2)
101		Degree of linear coupling between joint oscillations (PC3)
		Similarity to healthy gait
102		Correlation between limb oscillation of healthy and injured leg
103		Correlation between hip oscillation of healthy and injured leg
104		Correlation between knee oscillation of healthy and injured leg
105		Correlation between ankle oscillation of healthy and injured leg
106		Correlation between MTP oscillation of healthy and injured leg
		Variability of gait
107	86	Variability of foot trajectory in the forward direction
108	87	Variability of foot trajectory in the sagital place
109	88	Variability of foot trajectory in the 3-dimensioal room
110	89	Variability of gait cycle duration
111	90	Variability of stride length
112	91	Variability of double stance duration
113	92	Variability of step height
114	93	Variability of path length
115	94	Variability of max endpoint velocity
		Kinetics
116		vertical ground reaction force
		Muscle activity parameters
117		Burst onset of extensor
118		Burst end of extenson
119		Burst duration of extensor
120		Mean amplitude of extensor
121		Integral of extensor activity
122		Root mean square of extensor activity
123		Burst onset flexor
124		Burst end of flexor
125		Burst duration of flexor
126		Mean amplitude of flexor
127		Integral of flexor activity
128		Root mean square of eflexor activity
129		Co-contraction of the flexor and extensor muscle

Supplementary Table 2 | Kinematic, Kinetic and EMG parameters

IV. Chapter 2

ESTABLISHMENT OF AN EXPERIMENTAL SET-UP FOR CHRONIC CALCIUM IMAGING IN FREELY-MOVING RATS

Abstract

The need to chronically follow the activity of specific and large neuronal populations during behavioral testing has become central in experimental paradigms studying plasticity and learning. Hence, calcium imaging is a powerful tool to decipher neuronal correlates of behavior, and recent developments aiming at minimizing perturbations have yielded a commercially available solution for endoscopic recordings in freely-moving animals. While this technology was originally developed for mice and enables the tracking of the same neurons over several weeks, important adaptations had to be implemented in order to translate this method to rats. We describe the selection, refinement and optimization of surgical as well as recording procedures, resulting in a detailed protocol that was validated for chronic calcium recordings of the corticolumbar population in freely-moving rats.

4.1. Introduction

Previous results, including the work presented in the first chapter of this thesis, indicate that the motor cortex is involved in leg motor control of locomotion after recovery from a spinal cord injury (van den Brand, Heutschi et al. 2012, Asboth, Friedli et al. 2018). More specifically, the corticolumbar neurons have direct synaptic connections onto lumbar spinal circuits controlling leg movement in intact animals. The need to record the activity of this specific population of neurons during locomotion and across recovery has thus emerged as central in the study of functional plasticity mechanisms.

While electrophysiological recordings are widely used to monitor neuronal activity, they are limited to a restricted number of neurons and over a limited period of time, as recordings extinguish after a few weeks. This inherent limitation in stability makes this technique a poor tool for chronic study designs interrogating neuroplasticity and learning. Furthermore, electrophysiological recordings do not allow the clear identification of the recorded neurons. They present a major lack of specificity regarding biophysiological properties, such as number, type, position, and projection pattern (Jercog, Rogerson et al. 2016). All these limitations can be addressed by the use of an alternative approach, which leverages intrinsic physiological properties of the circuits of interest: calcium activity recordings have arisen as a powerful tool to investigate neuronal processing over chronic time scales and to correlate population-scale neuronal activity to behavior (Ziv and Ghosh 2015).

Neural activity causes rapid changes in intracellular calcium concentration (Baker, Hodgkin et al. 1971, Tank, Sugimori et al. 1988, Helmchen, Imoto et al. 1996). In turn, calcium indicators display fluorescence levels that vary accordingly to intracellular calcium concentration. The transfer function from neural activity to fluorescence signal, though non-linear, is monotonic, which establishes this method as a robust read-out of neural activity. Protein engineering leads to constantly improving generations of sensors, and the last generations of genetically-encoded calcium indicators (GECI) reaches a satisfying sensitivity while allowing a simple non-invasive delivery throughout large populations of neurons (Chen, Wardill et al. 2013, Dana, Sun et al. 2018). The GECIs of the GCaMP family, based on Förster resonance energy transfer, are the most widely used (Tian, Hires et al. 2009, Chen, Wardill et al. 2013). By leveraging the advantages of genetic engineering and viral delivery strategies, GECIs enable to target specific neuronal populations. Thus, in contrast to electrophysiological recordings, calcium imaging techniques give access to spatial, anatomical and genetic identity over large neuronal populations, without introducing a bias towards active cells (Jercog, Rogerson et al. 2016). Thanks to an increased stability, recordings can as well extend over longer periods of time, rendering possible the tracking of single neurons over several months in experimental paradigms interrogating neuroplasticity and learning (Komiyama, Sato et al. 2010, Huber, Gutnisky et al.

2012, Margolis, Lutcke et al. 2012, Peters, Chen et al. 2014, Peron, Freeman et al. 2015, Jercog, Rogerson et al. 2016).

GECIs are commonly delivered to the target population through adeno-associated viruses (AAV). This transduction method leads to high intracellular GECI concentration required for calcium imaging (Huber, Gutnisky et al. 2012, Zariwala, Borghuis et al. 2012). However, GECI expression levels are known to increase over the course of weeks and months, ultimately resulting in nuclear filling. In these neurons, physiology and fluorescence responses become aberrant (Tian, Hires et al. 2009, Chen, Wardill et al. 2013). The time window available for recording thus depends on the virus titer, volume of injection and promoter, and typically ranges from a several days to several months (Tian, Hires et al. 2009, Chen, Wardill et al. 2013). The use of transgenic mice enables to overcome this limitation by providing relatively stable protein expression levels over several months (Zariwala, Borghuis et al. 2012).

Until recently, calcium imaging studies were performed with 2-photon microscopy. This technique offers optical sectioning, increased spatial resolution and reduced background noise in imaging. Yet, it requires head-fixing, thus dramatically limiting – if not altering – animal behavior. Despite an important gain in knowledge on cortical computation of sensory, motor, visual and decision making processes (Chen, Andermann et al. 2013), such restrictive recording conditions remain highly non-ecological and collide with the inherent design of studies such as spatial navigation, social interaction behaviors, anxiety or locomotion (Ravassard, Kees et al. 2013, Aghajan, Acharya et al. 2015, Jercog, Rogerson et al. 2016). Recently tackling this issue, the development of miniaturized integrated microscopy has greatly expanded the range of animal behaviors that can be interrogated concurrently to neuronal activity recordings. The integration in a single case of all necessary optical components rendered 1-photon imaging of large-scale populations possible in freely-moving animals (Ghosh, Burns et al. 2011, Ziv and Ghosh 2015, Aharoni, Khakh et al. 2019).

The integrated microscope commercialized by the company Inscopix weights less than 2 grams and is composed of a light-emitting diode, an objective lens, a fluorescence filter cube, and a high-resolution, high-sensitivity CMOS image sensor. It enables single-channel epifluorescence imaging, offering a tissue penetration of only 150μm away from the objective (Flusberg, Nimmerjahn et al. 2008, Ziv and Ghosh 2015). In turn, the combination of this integrated microscope with the use of endoscopic probes opens access to virtually any brain area (Ziv, Burns et al. 2013, Ziv and Ghosh 2015, Resendez, Jennings et al. 2016). An implanted gradient refractive index (GRIN) lens serves as an optical relay between the microscope and the target brain tissue (Barretto, Messerschmidt et al. 2009). Chronic imaging is rendered possible thanks to a partially removable set-up on the animal, whereby the microscope is mounted on a head-plate system permanently secured on the skull of the animal (Helmchen, Fee et al. 2001,

Flusberg, Nimmerjahn et al. 2008, Ziv and Ghosh 2015, Jercog, Rogerson et al. 2016, Resendez, Jennings et al. 2016).

In order to record the activity of the same population of corticolumbar neurons during locomotion in the intact rat and throughout recovery from a spinal contusion, we aimed to use the Inscopix nVista system, combined with an AAV-mediated delivery of the GECI GCaMP6m. The Inscopix solution commercialized in 2015 was restricted to an ensemble of simple GRIN lens probes, baseplates, as well as the miniscope and acquisition system. This technology was originally developed for mice and for recording periods extending up to 6 weeks, such as the very first – and to date the only – study in rats was published only very recently (Cameron, Murugan et al. 2019), and the longest reported time range of recordings in freely-moving rodents is 45 days (Ziv, Burns et al. 2013). As a consequence, a number of procedures – including surgery and recording protocols – needed adaptation and optimization, in the main goal of ensuring successful translation to rats and increasing stability. We first established an intersectional viral targeting strategy in order to achieve stable and reliable GCaMP expression in the corticolumbar neuron population over several months. We then established a technical pipeline for lens probe implantation and behavioral recordings, which we validated for chronic calcium imaging in the rat L5 motor cortex for periods extending up to 4 months.

4.2. Results

Validation of a strategy for chronic GECI expression in the rat corticolumbar population

We sought to express stably and specifically the GCaMP6m calcium indicator in corticolumbar neurons for the time range of approximately 3 months, corresponding to healthy locomotor training, contusion and neuroprosthetic rehabilitation. The use of transgenic lines is usually preferred over viral vector delivery methods, due to more stable protein expression levels, thus avoiding detrimental secondary effects such as cytoplasmic accumulation, nuclear filling and consequential neuronal death. However, our experimental design involved rats, as the neuroprosthetic rehabilitation protocol yields mitigated outcomes in mice. While transgenic F*lex-GCaMP* mouse lines are available, the corresponding genetic tools are not yet developed in rats.

As a consequence, we opted for an AAV-mediated delivery of GECI, leveraging the flexibility and specificity of an intersectional viral targeting approach to achieve specificity (Fig. 11A). Thus, we used a conditional expression strategy, by injecting a retrograde rAAV-Cre vector in the right lumbar spinal cord and the AAV5-hSyn-flex-GCaMP6m vector in the left leg motor cortex. We confirmed the

A Injection of viral construct

	Full name	Origin	Titer (GC/mL)
AAV-flex-GCaMP6m	AAV5-hSyn-flex-GCaMP6m	Upenn	1.45E+13
rAAV-Cre	rAAV2-pmSyn1-EBFP-Cre	Addgene	6.87 E+12

B Coordinates for injections and lens placement

		AP	ML	DV
Craniotomy	MC	-1 -> -2	+2 -> +3.7	-
Viral injections	MC	-1.1, -1.9	+2, +2.6	-1.45
	SC	Δ = 1	-0.65	-0.8
Lens implantation	MC	-1 -> -2	2.65	-2

Fig. 11 | GECI expression strategy for chronic corticolumbar neurons calcium imaging in rats
A. Schematic representation of the intersectional injection strategy for GCaMP6m expression in corticolumbar neurons. Table of specifications of the viral vectors used. **B.** Coordinates of craniotomy, viral injections and lens probe implantation. Picture during the surgical procedure, showing the positioning of injection points and relative position of lens implantation within the craniotomy. Confocal photograph of a coronal section corresponding to (A), showing the GECI expression in corticolumbar neurons. Dotted line represents the trace left by the lens implant in brain tissue. Scale bars 10 µm.

consistent and stable expression of GCaMP in motor cortex L5 neurons (Fig. 11B). After 20 weeks, histological analysis revealed no sign of nuclear filling or neuronal death, validating the virus titers used in our delivery strategy (Fig. 11B).

Translation to rats of the lens probe implantation surgical procedure

The nVista recording system commercialized by Inscopix was originally developed for calcium imaging in freely-moving mice. Therefore, the consumables as well as surgical procedures were not suited for rat applications, and *a fortiori* for stable recordings over several months. With a trial-and-error approach, we adapted and optimized the surgical protocol for lens probe implantation. We used a Prism lens probe (P/N 1050-002184, later 1050-002203, Inscopix, Palo Alto, USA) which offers a 90° angle of the optical path, thus accessing the brain tissue beside the lens and enabling the imaging of a cortical column. Individual steps were adapted according to the resulting field of view (FoV) (1) visually inspected in the anaesthetized rat, (2) visually inspected in the freely-moving animal, following baseplate installation several weeks after implantation, and (3) analyzed during calcium movie processing subsequent to recordings. The main obstacles encountered in this early optimization phase, as well as the corresponding developed solutions are described in the table below (Table 1).

Problem	Cause	Troubleshooting
Difficulties to appropriately hold the lens probe during implantation. Requirements: - consistent, straight, stable and non-damaging grip to enable implantation - ability to transparently release once fixed to the skull	- Lens probe too short for rat application - No suitable holder provided or recommended	- Home-build gripper coated with heat-shrink sleeve - Inscopix released cuffed lens probes and the ProView implant kit early 2018
- Full or partially dark FoV - Dark spots on the FoV, preventing motion correction during image processing	Blood or resorbed bleeding	- Proceed to viral vector injection and lens implantation during the same surgery - Strictly stop bleeding before proceeding to further steps - Increase lens probe stabilization to prevent post-surgical bleeding - Remove from the home cage environment all elements that could lead to collisions with the headcap
Bright spots in the FoV	Presence of autofluorescent debris in the FoV, originating from dura pieces or brain damage	- Remove dura over the whole craniotomy before brain incision and lens implantation - Add a step during surgical procedure to create an incision in the brain, preparing the path for lens implantation. This enables correct penetration of the lens while minimizing brain compression, thus avoiding tissue damage
No cells and no dF in the FoV	- Failed GECI expression - Bad lens DV targeting	- Histological check for viral expression and adjust GECI delivery strategy - Histological check for lens DV placement relative to GECI-expressing population, and adjust implantation coordinates - Add a step during surgical procedure to create an incision in the brain preparing the path for lens implantation. This enables correct penetration of the lens while minimizing brain compression, resulting in increased consistency of DV targeting
dF in the FoV but not in focus	Improper ML targeting of the lens, too far from GECI-expressing population	- Histological check for lens ML placement and adjust ML implantation coordinates - Proceed to viral vector injection and lens implantation during the same surgery, in order to reduce variability in coordinates measurement

Table 1 | Troubleshooting of the lens probe implantation surgical procedure
FoV: field of view, dF: variation of fluorescence, DV: dorsoventral, ML: mediolateral.

One of the most important points of improvement was the strict requirement, at any step of the surgery, to completely suppress bleeding before proceeding forward. The optimized surgical protocol for lens probe implantation in the rat L5 hindlimb motor cortex is precisely described step-by-step as follows (Fig. 12). Viral vector injection is to be performed as usual between steps 2 and 3.

1.1 Skull incision: remove a small piece of skin in the shape of a pointed oval around the initial midline incision.

1.2 Push away and retract all layers of skin and muscle to each side. Dry and clean the surface of the skull with Q-tips. After reaching the lateral suture, push the tissue further down and separate all muscle layers from the skull with the blade. Scratch the skull surface with the scalpel tip to increase adherence of the cement on further steps. Dry the skull again and use a cauterizer to stop any possible bleeding. Drill holes in the skull for the screws with a hand drill: 3 smaller holes for the smaller screws serving to stabilize the lens and 2 bigger holes for the bigger screws serving to stabilize the baseplate and electrode connector at further steps in the experimental design. The smaller holes are positioned as follows relative to bregma (AP: anteroposterior, ML: mediolateral), to ensure space for the ProView kit holder on later steps of this surgery: [AP +2.8, ML +2.5]; [AP -1.5, ML -1.7]; [AP -6.2, ML +4]. The bigger holes are located further, towards the lateral part of the other hemisphere, one rostral and one caudal.

1.3 Fix the 2 big screws (stainless steel screw AMS90/8B B000FN68PI, Antrin miniature specialities) and the 3 small screws (stainless steel screw AMS90/1F-100 B000FN68KS, Antrin miniature specialities). If not available, ensure choosing screws of similar length, in order to prevent interference with the adequate position of the miniscope at the time of baseplating later in the experimental design. Do not screw the bigger screws further than 2.75 turns in order to avoid pressure on the brain tissue below the skull.

2.1 Perform craniotomy (coordinates specified in Fig. 11B) with a fine motorized drill. Make sure to clean any bone debris from the craniotomy, by scratching the edges with tweezers and cleaning the opening with gelfoam (Pfizer, Canada) and saline.

2.2 Remove dura in the craniotomy. Start from the edge of the craniotomy furthest away from the side corresponding to the imaging face of the lens. Puncture dura with a fine needle, then carefully pull and cut the dura along the edges of the craniotomy with the help of fine tweezers and fine angled spring scissors. Keep the tissue hydrated with saline while peeling off the dura and clean with gelfoam as soon as bleeding occurs. In that case, keep flushing saline and aspirating with Q-tips through the gelfoam until all bleeding stops. Ensure that there is no dura left in the craniotomy, especially on the side of imaging, and strictly no bleeding, before proceeding to the next steps. From completion of this step on, proceed further as rapidly as possible, and make sure to always keep the brain tissue hydrated with the help of gelfoam with saline. In case of bleeding during future steps, stop immediately the procedure and do not engage further before bleeding has been fully stopped.

6.4 Make a brain incision to create the path for lens implantation. Place the microscalpel (dissecting knife fine tip FST 10055-12) at the surface of the brain parallel to the desired face of imaging, at the rostral end of the craniotomy and mediolateral coordinate of lens implantation (Fig. 11B). Visually check for dura or other debris on the path of the blade.

6.4 Lower the knife very slowly (approximately 0.01mm/s) until the desired DV coordinate of lens implantation (Fig. 11B). The knife should penetrate easily in the brain tissue and not generate compression.

6.4 Once the target DV coordinate has been reached, slowly slide the dissecting knife caudally towards the opposite edge of the craniotomy. In the case of important blood vessels on the path of the incision, proceed nevertheless and ensure to stop the bleeding afterwards. The blood vessel is very likely to hinder smooth cutting, by dragging along brain tissue with the knife. In that case, it is suggested to use slight z motions around the target DV coordinate concurrently with anteroposterior travelling of the blade, to help obtaining a clear cut. After reaching the caudal edge of the craniotomy, remove the knife and immediately cover the brain tissue with gelfoam soaked with saline in order to prevent blood to settle in the newly made incision. Whenever bleeding appears, repeat flushing with saline and aspirating until all bleeding stops.

4.1 Prepare the lens probe. Clean the lens with ethanol and then saline before positioning it in the Proview implant kit holder. Secure by tightening the side screw.Position the lens above the incision. Check under the surgery microscope that the lens is clean, well attached to the cuff and straight. Clean again with saline if necessary.

6.4 The nVista microscope can be placed on top of the lens in the holder for imaging during implantation, in case the targeted cell population is already expressing the GECI (not applicable in this project).

5.1 Insert the lens by lowering the z arm of the stereotaxic frame. Proceed with very slow speed (approximately 5µm/s) and as steadily as possible. The brain tissue should not bend or get compressed during insertion. If compression occurs and the lens does not penetrate into brain tissue, do not proceed further and remove the lens. Check for possible remaining dura and for the exact positioning of the lens above the incision. Repeat insertion.Once the lens is at its final position, fill in the exposed brain tissue in the craniotomy with Kwik-Cast (WPI, Sarasota USA). Then use Superbond (Super-bond C&B, Sun Medical, Shiga, Japan) mixed with carbon powder (#484164, Sigma-Aldrich, Germany) to fix the lens to the skull and at least two of the three small anchor screws. Take care not to drop Superbond above the cuff or apply on the holder. During this step and the following ones, make sure to keep the skull surface clean and dry to improve adherence, and to retract as much as possible the skin on the sides in order to prevent blood and fluids to come in contact with the casting resin.
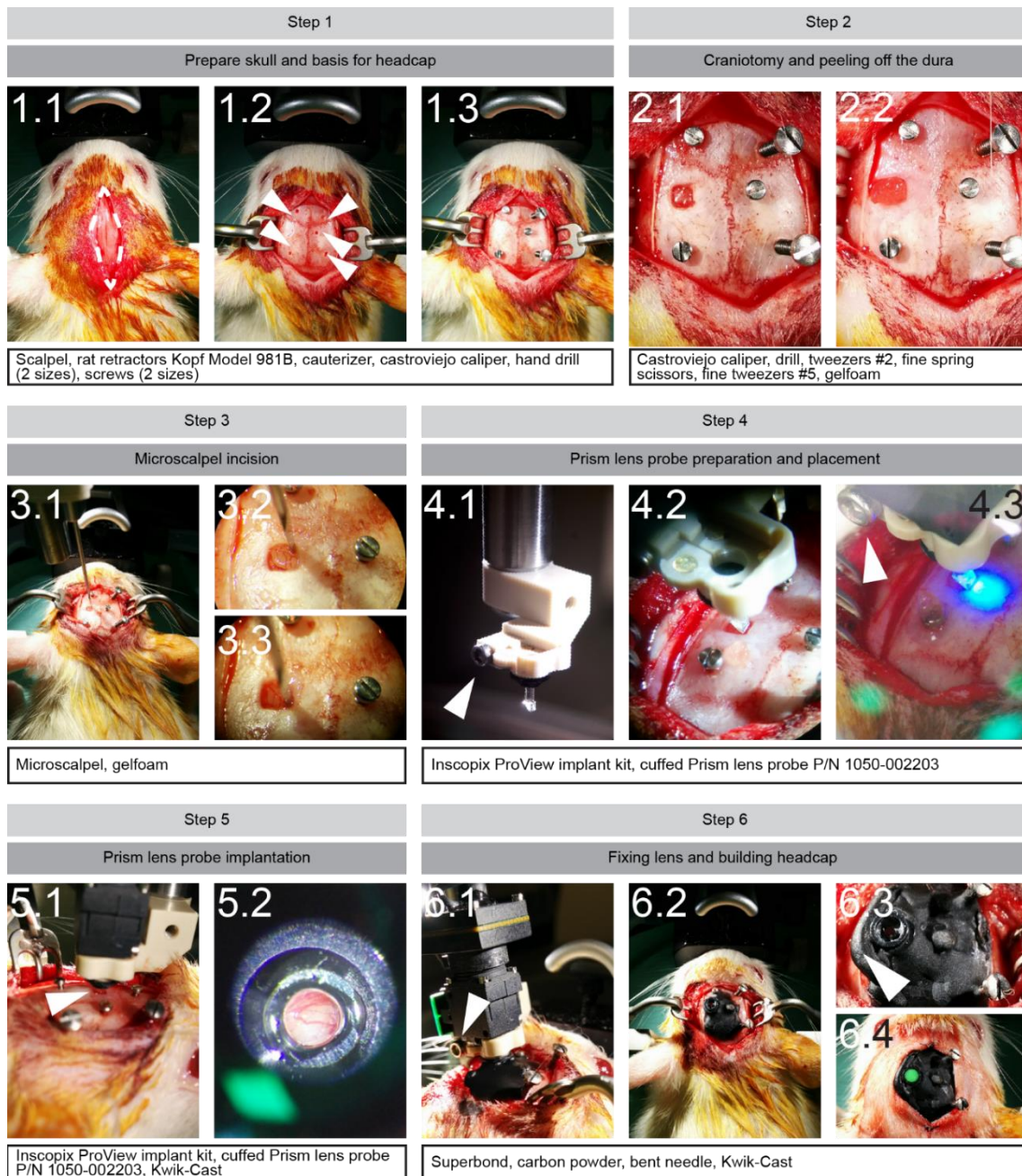
Fig. 12 | Optimized surgical protocol for prism lens implantation
Description of the methodological steps is detailed in the main text. Specific tools and material needed for each step are listed in the box below the pictures. Arrowheads: **4.1**, **4.3** and **6.1.** Side screw of the implant kit, to hold and secure the cuffed lens probe and the microscope if applicable. **5.1.** Implanted lens, the remaining space between the skull and the cuff will be filled with dental cement for fixation. **6.3.** Side extension of the superior part of the headcap, creating a notch to stabilize the positioning of the skin.

6.1 Side view of the set-up. The lens is secured with Superbond to the skull and the screws; no Superbond flows above the cuff onto the holder. The skin is safely retracted to the side to avoid touching the headcap. Let the Superbond cast, then release the lens cuff by fully unscrewing the side screw and carefully removing the holder by lifting up the z arm of the stereotaxic frame.Add Superbond to build up the headcap. Consolidate and secure further on the 3 small screws and at the base of the 2 bigger screws. Take care not to drop resin on the lens; Kwik-Cast can be applied in the cuff on top of the lens in order to proceed safely.

6.4 Use dental cement or Superbond of high viscosity to create an approximate $1cm^2$ flat square surface around the lens, and make the headcap protrude further than the skull on the medial side. This prepares the foundation for later baseplate installation, and the side notch will secure the position of the skin, preventing it to set up either under the headcap or on top of the headcap and the lens.

6.4 Place the skin in the notch, add some stitches if needed so that no more skull is exposed. Fill in the cuff with Kwik-Cast in order to protect the lens from scratches and dirt (for better caution, proceed to this step as soon as the lens has been released from the ProView implant kit, cf step 6.2.).

Translation to rats of the experimental recording set-up

Similarly to the surgical procedure, the translation of the recording set-up from mice to rats is not limited to a simple scale-up in size. The first attempts of use in the rat emphasized mechanical instabilities and vulnerabilities of the system, whose design was not adapted to the constraints into play with an animal of a higher body weight. The problems encountered with recordings, as well as the corresponding solutions developed in response are recapitulated in the following table (Table 2).

Problem	Cause	Troubleshooting
Baseplate set screw stuck	- Defect of the screw hole by design or production	Carefully check quality of screw hole and ease of screwing/unscrewing before baseplating
- Baseplate set screw worn out - Adjustment tool worn out	- Head movement of the rat during screwing/unscrewing - Forcing and/or imperfect alignment of the adjustment tool to the set screw during screwing/ unscrewing	- Develop behavioral techniques to keep the rat calm for the time of screwing/unscrewing - Stop screwing as soon as resistance is felt - Regularly renew adjustment tools - Replace set screw regularly, as soon as the first signs of wearing out appear
- Important brain motion or loss of focus	- Microscope motion in the baseplate due to pull on the cable - Imperfect securing with baseplate set screw	- Installation of a pulley to follow animal position and minimize mechanical constraints on the cable - Permanent manual adjustment of cable position above the head of the animal - Replace set screw regularly, as soon as the first signs of wearing out appear - Permanent visual inspection of the FoV during recordings

Table 2 | Troubleshooting of the recording procedure
FoV: field of View.

Transparency of the lens probe implant on locomotor performance

In order to control for the effect of the lens probe implant, we analyzed the locomotion on a linear runway and a horizontal ladder in healthy animals implanted in the left motor cortex (Fig. 13). We compared the gait pattern of each hindlimb within animals, and used non-implanted naïve rats as a second control.

Principal component analysis of the gait pattern during quadrupedal runway walking revealed no difference between right and left hindlimbs. The euclidian distance separating both hindlimbs for each animal in the new 3-dimensional space composed of the 3 first PCs was not significantly different in the group of implanted animals compared to the control group (ns, $p = 0.6623$, Student's t-test) (Fig. 13A). Additionally, the error rate on the horizontal ladder task, engaging fine paw placement, did not significantly differ between the implanted and the control group (ns, $p = 0.0625$, Student's t-test) (Fig. 13B). These results indicate that the lens probe implant does not alter natural or fine locomotion in the intact animal.
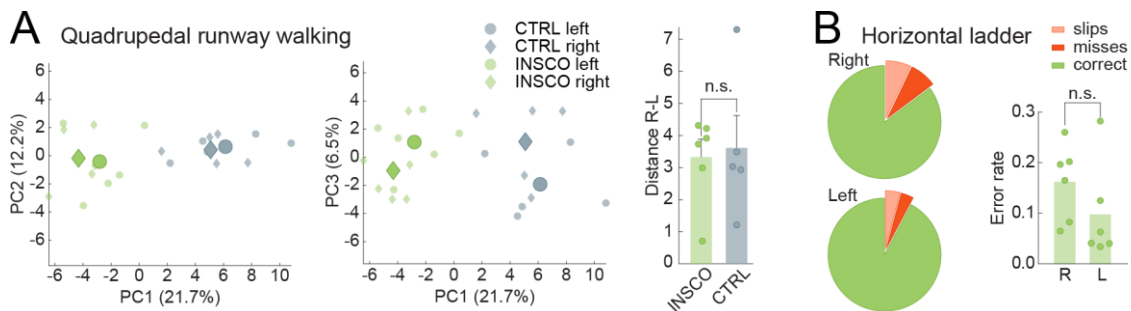
Fig. 13 | Transparency of the lens probe implant on locomotion
A. A PC analysis was applied on a total of 129 parameters characterizing global and fine details of leg motor control (table S1). The gait cycles of each rat (single dot, averaged of 10 gait cycles per rat) and averaged per group and side (large dots) are represented in the new space defined by PC1 and PC2 (%, percent of explained variance) (right graph) or PC1 and PC 3 (left graph). INSCO: group implanted with the lens probe in the left motor cortex, CTRL: control naïve rats. Bar plot of the euclidian distance between both hindlimbs in the space composed of PC1-PC3. **B.** Circular plots report error rate for right (R) and left (L) hindlimb (slips and misses) during the horizontal ladder task in the implanted rats. Bar plot shows the average error per side for each rat (circles). ns, $p > 0.05$, not significant, paired Student's t-test.

4.3. Discussion

Perspectives on the technological translation process

We established a longitudinal framework to perform chronic calcium recordings of the corticolumbar neurons in the freely-moving rat, based on the commercially available solution offered by Inscopix and originally developed for mice. We thus demonstrated the feasibility of translation, and extension of the experimental time up to 3 months.

The advantages of the intersectional viral targeting approach are two-sided: biophysiological specificity of the imaged population and regulation of GECI expression. The conditional expression strategy enabled to overcome the common problem of GECI accumulation that usually limits the maximal length of the experimental recording period to several weeks (Chen, Wardill et al. 2013).

All the adaptations presented in this chapter have been implemented through a trial-and-error process. Preliminary groups of animals are not presented here and were needed to identify the most adapted GECI delivery approach, and later to adapt each step of the surgical and recording protocols. The obstacles encountered along the development of this framework led to consequences ranging from simple delays to forced abortion of specific time points, tasks or testing conditions, and dropping data corresponding to whole sessions. Over 2 years of optimization, the yield in lens implantation surgery increased from less than 10% to approximately 90% of animals usable for further enrolment in the experimental paradigm.

Along the encounter of these technical hurdles and the development of customized solutions, a continuous dialogue was maintained with the customer support of the company Inscopix. As an "early adopter" of the nVista system, the extent of technical advice and support available at the time of development was restricted. While the community of Inscopix users and the company itself are growing larger, knowledge continues to get updated and adapted to more specific situations, thanks to experience feedback during workshops, conferences and user meetings. In this context, our pioneering work in rat translation has brought invaluable expertise to the community. Our precise and unique surgery protocol for lens probe implantation established here is currently commonly used as a reference by the company Inscopix for advising new customers worldwide in the rat application.

Technical validation of endoscopic calcium recordings in freely-moving animals

We found no significant effect of the lens probe implant on locomotion in the healthy rat, during both natural and fine motor control tasks. This validates our experimental plan to perform endoscopic calcium imaging recordings in the leg motor cortex in the aim of studying the functional plasticity of corticolumbar neurons throughout recovery after SCI.

V. Chapter 3

FUNCTIONAL DYNAMICS OF CORTICOLUMBAR NEURONS THROUGHOUT CONTUSION AND RECOVERY

Abstract

After a contusion spinal cord injury, the formation of a cortico-reticulo-spinal detour circuit mediates the recovery of voluntary control over the paralyzed legs. This circuit-level reorganization, enabled by neuroprosthetic rehabilitation, translates a cortex-dependent recovery of natural locomotor behaviors. In the aim of understanding the computational logics underlying this remodeling, we tracked the activity of the corticolumbar population thanks to calcium recordings in freely-moving rats throughout training-enabled recovery. The corticolumbar population-level representation of locomotion was stable in the intact animal. Similarly, individual neuronal classifications were mostly stable, and their limited dynamics suggested a segregation of movement-related representations. While the lesion-induced cell body shrinkage prevented further investigation of individual neuronal fates across the injury, we observed that population activity accounted for locomotion with high fidelity after recovery, enabling the maintaining of a strong behavioral decoding performance. Surprisingly, the recovery of leg motor control did not correlate with any dynamic change in corticolumbar population activity, and fractions of movement-related cells remained remarkably stable as well. These early results initiate the investigation of functional plasticity mechanisms during recovery after SCI as a specific form of motor learning.

5.1. Introduction

Despite decades of research, motor cortex involvement in motor control and learning is far from being fully elucidated. Motor control in healthy, and *a fortiori* in the injured mammal, is a remarkably complex and redundant process (Lemon 2008, Pivetta, Esposito et al. 2014). Although not needed for natural locomotion in intact animals, the motor cortex does contribute to learning new motor skills (Muir and Whishaw 1999, Kawai, Markman et al. 2015). In turn, several studies have shown the pivotal role taken over by the motor cortex in recovery after a spinal cord injury. While many functional and anatomical studies focus on the spared elements of the CST after a mild to moderate injury (Bareyre, Kerschensteiner et al. 2004, Hilton, Anenberg et al. 2016, Hollis, Ishiko et al. 2016), our severe lesion model completely interrupts direct cortical inputs onto lumbar circuits in the spinal cord (Asboth, Friedli et al. 2018). The reorganization of motor circuits thus leverages alternative spared elements, previously known to be involved in rearrangements occurring after more moderate (Zörner, Bachmann et al. 2014) and less clinically relevant (van den Brand, Heutschi et al. 2012) injury models. In the first chapter of this thesis, we demonstrated the establishment of a cortico-reticulo-spinal relay that mediates the recovery of voluntary leg motor control, highlighting the motor cortex-dependency of recovered natural motor behaviors after a severe contusion (Asboth, Friedli et al. 2018).

Yet, the cellular and circuit-level organization of the motor cortex reveals a high anatomical and functional diversity, emphasizing the limitations of experimental assays regarding it as a coherent and rigid building block of the motor-circuit communication matrix. Neuronal phenotypes, as well as horizontal and vertical circuit organization and projection patterns are mere examples of the complexity of this system (Weiler, Wood et al. 2008, Mao, Kusefoglu et al. 2011, Harrison, Ayling et al. 2012). This level of fine organization cannot be further overlooked in the aim of unraveling high-precision mechanisms of motor control. Refined research paradigms have thus emerged thanks to powerful technological advances, such as genetic engineering, optogenetic tools or 2-photon microscopy. Circuit-level dissection, as well as targeting, recording and interrogation of specific neuronal populations, cortical layers and subneuronal compartments have greatly contributed to gain valuable knowledge in the fine-scale mechanisms of cortical motor control and learning (Komiyama, Sato et al. 2010, Huber, Gutnisky et al. 2012, Peters, Chen et al. 2014, Chen, Kim et al. 2015, Guo, Graves et al. 2015, Peters, Lee et al. 2017, Heindorf, Arber et al. 2018).

Although motor map boundaries remain unchanged during motor learning of unskilled movements (Kleim, Hogg et al. 2004), layer 2/3 excitatory neurons do undergo important plasticity. Up to date, recordings of cortical calcium activity mainly focused on the investigation of L2/3, due to the limitation of light penetration in brain tissue with 2-photon imaging. These studies established that learning correlates with a strengthening of neuronal representations of the learnt task (Huber,

Gutnisky et al. 2012), and that population activity converges towards the establishment of reproducible spatiotemporal patterns (Peters, Chen et al. 2014). This dynamics of functional organization is accompanied by a transient spine turnover, suggesting that dendritic remodeling of layer 2/3 neurons in the motor cortex underlies motor learning. A recent study based on 2-photon imaging of corticospinal dendrites pushed the exploration further to L5 neurons, demonstrating that such activity dynamics, correlating with motor learning, is not restricted to L2/3 (Peters, Lee et al. 2017). Motor learning is as well accompanied by an anatomical plasticity of dendritic spines of L5 motor cortex neurons. Moreover, this structural remodeling is specific to the neurons projecting directly to the spinal levels where the circuits controlling the muscles engaged in the learnt task are located (Wang, Conner et al. 2011). These results establish that motor cortical populations undergo a profound and precisely-organized reshaping with motor learning. Specifically, not only the motor cortex on a finer scale, but also its output channel – namely the corticospinal population – is plastic.

Thus, in the aim of refining our understanding of motor cortex involvement in the recovery of locomotion after SCI, we further concentrated our research efforts on the corticolumbar (CL) population. The cortex-dependent recovery of natural locomotor tasks following contusion led us to explore the mechanisms of recovery as a form of motor learning. Based on the results of the first chapter of this thesis, we hypothesized that CL neurons drive the changes observed with recovery enabled by rehabilitative training, and as such, undergo important functional plasticity reflecting this reorganization. To test these assumptions, we sought to follow the activity of the same CL neurons during locomotion throughout a SCI and neuroprosthetic rehabilitation. Thanks to chronic calcium recordings in freely-moving rats, we investigated the activity of this specific population during various motor tasks before injury, and at different time points after contusion.

5.2. Results

Experimental design

To investigate the involvement of corticolumbar neurons in the control of leg movement in intact rats and throughout recovery after a spinal cord injury, we performed calcium imaging recordings during locomotor tasks in intact rats and at different time points after contusion in a trained group of animals (n = 6) and an untrained group undergoing spontaneous recovery (n = 5). One animal of the trained group was excluded from analysis because of the reduced number of neurons imaged. The experimental design and timeline are described in Fig. 14.

The spinal cord contusion spared 9.5% (±0.7%) of neural tissue at the lesion epicenter in the trained group, and 6.6% (±0.9%) in the untrained group. Post-mortem histological verification confirmed that the lesion completely interrupted the corticolumbar tract (Fig. 14(Step5)). The trained group went through neuroprosthetic rehabilitation as previously described (van den Brand, Heutschi et al. 2012, Asboth, Friedli et al. 2018), during a period ranging from 6 to 10 weeks. The evolution and duration of training depended on individual performance (Supplementary Fig. 1). During the recovery period, rats were recorded during various locomotor tasks and under various neuromodulation conditions, at time points corresponding to early, middle and late recovery (Table 3 and Table 4).

The time points along recovery were defined by the experimenter as follows for the trained group, during bipedal treadmill and overground walking with electrochemical neuromodulation. Matching time points were used for the control untrained group.

- Early: approximately 14 days after contusion. On the treadmill and with 80 to 90% of body-weight support against gravity, the animal is fully dragging the legs and needs manual assistance from the experimenter to produce movements. The stepping is weak and inconsistent, mostly non-plantar and non-weight-bearing. The animal is not able to initiate or sustain locomotion overground with vertical support.

- Middle: approximately 21-30 days after contusion. On the treadmill and with body-weight support around 60%, the animal exhibits a consistent gait pattern with clear alternating movements of flexion and extension on both legs, as well as plantar stepping. Experimenter's assistance is mostly limited to trunk stabilization and partial and occasional support for specific movements depending on each animal's performance, such as help against knee endorotation, or one-sided flexion and/or extension. The animal is able to have some volitional leg muscle contractions on the treadmill or overground. These contractions contribute to an increased extension sustaining locomotion during overground bipedal walking, though insufficient to initiate locomotion or propel the animal forward.
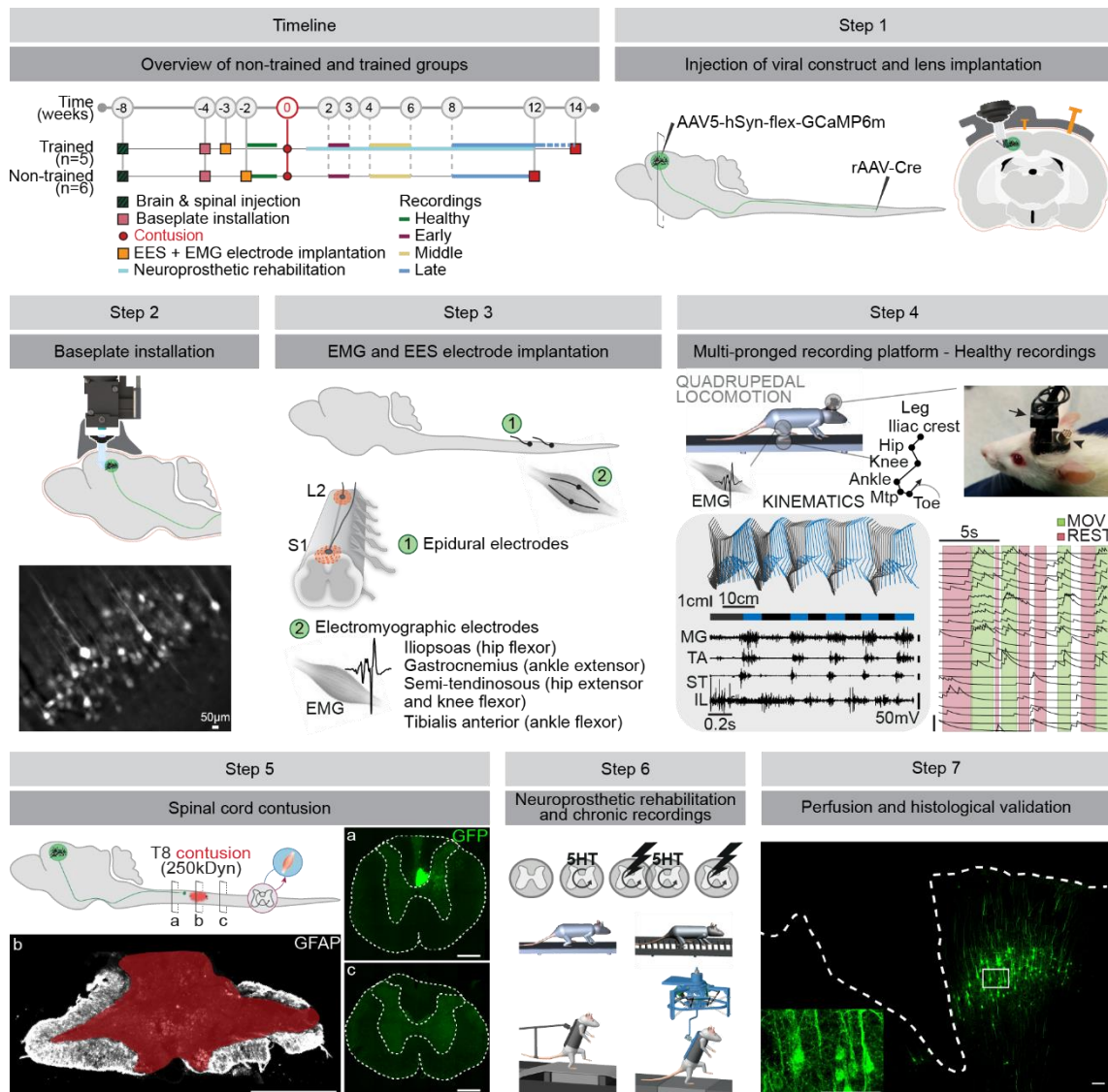
Fig. 14 | Experimental design for chronic calcium imaging of the rat corticolumbar population throughout neurorehabilitation-enabled recovery following contusion

(Timeline) Summary of the experimental procedures and timeline for the group of trained (n = 6) and contused untrained (n = 5) rats. EES: electrical epidural stimulation, EMG: electromyographe. **(Step1)** All rats were injected with the intersectional viral construct enabling specific expression of the GECI in corticolumbar neurons (Fig. 11). Optical access to the GECI-expressing population was rendered possible thanks to implantation of an endoscopic lens probe. Schematic view of a coronal section of the implant, showing the implanted cuffed lens probe and its relative position to the GECI-expression neurons, screws (orange) and the cement head-cap with the side notch for skin positioning. **(Step2)** Installation of the baseplate for a stable chronic access to the FoV. The miniscope can be attached and detached for each imaging sesion. **(Step3)** Epidural electrodes for electrical stimulation and EMG electrodes for muscle activity recordings in the leg contralateral to the lens implant. **(Step4)** Scheme of the rat within the multipronged platform for synchronized recordings. Stick diagram showing the movement kinematics of the leg and corresponding EMG. Mtp: metatarsophalangeal joint, MG: medial gastrocnemius, TA: tibialis anterior, ST: semi-tendinosous, IL: iliopsoas. Picture of the implants on the head of the animal, arrow: nVista microscope attached to the baseplate, arrowhead: connector for EES and EMG electrodes. **(Step5)** Spinal contusion at the T8 spinal level. Photograph of a representative coronal section through the contusion epicenter (GFAP, glial fibrillary acidic protein). Photographs above (a) and below (c) the injury with GFP signal expressed in the corticolumbar axons. Scale bars 500μm. **(Step6)** Scheme of the various recorded tasks (quadrupedal runway, quadrupedal horizontal ladder, treadmill and robot) and neuromodulation conditions (spontaneous, pharma, combo, EES). **(Step7)** Confocal photograph of a coronal section at the level schematized in (Step1). Dotted line marks the edge of brain tissue and trace of the lens. Scale bars 10μm.

- Late: from approximately 42 days on after contusion. The animal sustains a consistent gait pattern on the treadmill without manual assistance, with a typical vertical support against gravity of 50%. Overground, the animal is able to consistently fully initiate and sustain locomotion with a vertical support ranging from 0 to 10%, thanks to clear volitional leg muscle contractions leading to strong alternating extensions and flexions. The animal's locomotor performance has reached the recovery plateau.

The locomotor tasks recorded are described as follows:

- QUAD: quadrupedal walking on a linear runway, no external assistance.

- Ladder: quadrupedal walking on a horizontal irregular ladder, no external assistance.

- Treadmill (TM): bipedal walking on a treadmill belt, moving at 11cm/s. The rat is wearing a jacket and attached to the robotic system enabling the bipedal position and providing an adjustable vertical support against gravity.

- Single pulse: no walking. The animal is positioned in the jacket and maintained in a standing bipedal position while electrical stimulation is delivered at 1Hz through the epidural electrodes.

- Robot: bipedal walking on a linear runway. The rat is wearing a jacket and attached to the robotic system enabling the bipedal position and providing an adjustable vertical assistance against gravity. The robotic system is transparent, such as movement can be initiated by external drives only (rat or experimenter) (Dominici, Keller et al. 2012).

The neuromodulation conditions are defined as follows.

- SPONT: spontaneous, natural conditions.

- PHARMA: pharmacological stimulation by injection of the serotonergic agonists quipazine and 8-OH-DPAT. The drugs are injected systemically 5 min before the beginning of motor training, and their action lasts for approximately 30min.

- EES: electrical epidural stimulation at 40Hz at the L2 and S1 spinal levels.

- COMBO: combination of pharmacological and electrical stimulations.

The planning of recorded tasks, time points and neuromodulation conditions (Table 3 and Table 4) was designed to address specific questions, account for constraints inherent to the experimental paradigm, and control for individual effects of the electrochemical neuromodulation.

- Quadrupedal runway: natural locomotor task. The only motor task that can be performed both by intact and injured animals.

- Ladder: enables to test for fine motor control. Only applicable in intact animals.

- Robot: the motor task used for neurorehabilitative training, involving the production of volitional descending drives during electrochemical enabling of lumbar circuits. Only applicable in injured animals.

- Treadmill: passive motor task as opposed to the active robot task. Only applicable in injured animals. Intended to disentangle between causal descending drives and possible ascending signals arising from sensory feedback.

- Single pulse: tested at the middle or late recovery time point in order to control for the backpropagation and/or feedback effect of electrical neuromodulation.

- Spont: natural locomotion, applicable at intact and late recovery stages. At other time points, animals are not able to perform the motor task without neuromodulation.

- Pharma: tested in intact animals to control for the effect of chemical neuromodulation as part of the neuroprosthesis used after SCI.

- EES: tested in the late recovery stage to disentangle between the pharmacological and electrical neuromodulation effects of the neuroprosthesis used after SCI.

- Combo: full neuromodulation therapy by electrochemical stimulation, daily used during rehabilitative training to reactivate dormant spinal circuits below the lesion.

Animal #	Session	Condition	Task
127	20181106	SPONT	QUAD
	20181107	PHARMA	QUAD
	20181108	SPONT	QUAD
	20181127	COMBO	QUAD
	20181128	SPONT	QUAD
	20181129	COMBO	QUAD
	20181217	COMBO	QUAD
	20181218	SPONT	QUAD
	20181219	COMBO	QUAD
	20190107	SPONT	QUAD
	20190108	SPONT	QUAD
	20190109	COMBO	QUAD
128	20181120	SPONT	QUAD
	20181122	PHARMA	QUAD
	20181127	SPONT	QUAD
	20181128	SPONT	QUAD
	20181129	SPONT	QUAD
	20181217	COMBO	QUAD
	20181218	SPONT	QUAD
	20181219	COMBO	QUAD
	20190104	COMBO	QUAD
	20190107	SPONT	QUAD
	20190108	COMBO	QUAD
	20190128	COMBO	QUAD
	20190129	SPONT	QUAD
	20190130	COMBO	QUAD
130	20181106	SPONT	QUAD
	20181107	PHARMA	QUAD
	20181108	SPONT	QUAD
	20181127	COMBO	QUAD
	20181128	SPONT	QUAD
	20181129	COMBO	QUAD
	20181217	COMBO	QUAD
	20181218	SPONT	QUAD
	20181219	COMBO	QUAD
	20190107	SPONT	QUAD
	20190108	SPONT	QUAD
	20190109	COMBO	QUAD
131	20181106	SPONT	QUAD
	20181107	PHARMA	QUAD
	20181108	SPONT	QUAD
	20181127	COMBO	QUAD
	20181128	SPONT	QUAD
	20181129	COMBO	QUAD
	20181217	COMBO	QUAD
	20181218	SPONT	QUAD
	20181219	COMBO	QUAD
	20190107	SPONT	QUAD
	20190108	SPONT	QUAD
	20190109	COMBO	QUAD
132	20181106	SPONT	QUAD
	20181107	PHARMA	QUAD
	20181108	SPONT	QUAD
	20181127	COMBO	QUAD
	20181128	SPONT	QUAD
	20181129	COMBO	QUAD
	20181217	COMBO	QUAD
	20181218	SPONT	QUAD
	20181219	COMBO	QUAD
	20190107	SPONT	QUAD
	20190108	SPONT	QUAD
	20190109	COMBO	QUAD

Legend: Healthy, Early, Middle, Late

Table 3 | Data collected with the contused untrained group, across tasks, conditions and time points
Kinematics data, EMG and calcium activity were recorded during quadrupedal linear runway walking before injury (healthy) in the spontaneous condition (SPONT) and with pharmacological stimulation (PHARMA), as well as at time points that matched early, middle and late recovery stages of the trained group in spontaneous (SPONT) condition and with electrochemical neuromodulation (COMBO). This study has been designed as a control to compare with the trained group. The collected data has not been analyzed yet.

Animal #	Session	Condition	Task	Selected for further analysis	Used for further analysis
104	20180717	SPONT	QUAD	✓	✓
104	20180718	SPONT	LADDER		
104	20180719	PHARMA	QUAD	✓	✓
104	20180723	SPONT	QUAD	✓	✓
104	20180724	PHARMA	QUAD	✓	✓
104	20180725	SPONT	QUAD	✓	✓
104	20180809	SPONT/COMBO	TM		
104	20180815	SPONT/COMBO	QUAD	✓	✓
104	20180829	COMBO	ROBOT		
104	20180830	SPONT	SINGLE PULSE		
104	20180830	SPONT/COMBO	TM		
104	20180903	SPONT/COMBO	QUAD	✓	✓
104	20180918	SPONT/COMBO	QUAD	✓	✓
104	20180925	COMBO	ROBOT	✓	✓
104	20180926	SPONT/COMBO	TM		
104	20180928	COMBO	ROBOT	✓	✓
105	20180717	SPONT	QUAD	✓	✓
105	20180718	SPONT	LADDER		
105	20180719	PHARMA	QUAD	✓	✓
105	20180723	SPONT	QUAD	✓	✓
105	20180725	SPONT	QUAD	✓	✓
105	20180813	SPONT/COMBO	QUAD	✓	✓
105	20180813	SPONT/COMBO	TM		
105	20180816	COMBO	ROBOT		
105	20180828	SPONT/COMBO	QUAD	✓	
105	20180829	COMBO	ROBOT		
105	20180903	SPONT	SINGLE PULSE		
105	20180903	SPONT/COMBO	TM		
105	20180912	COMBO	ROBOT	✓	
105	20180914	SPONT/COMBO	QUAD	✓	
105	20180918	COMBO	ROBOT	✓	
105	20180926	SPONT/COMBO	TM		
105	20181002	EES	QUAD	✓	✓
106	20180717	SPONT	QUAD	✓	✓
106	20180718	SPONT	LADDER		
106	20180719	PHARMA	QUAD	✓	✓
106	20180723	SPONT	QUAD	✓	✓
106	20180725	SPONT	QUAD	✓	✓
106	20180813	SPONT/COMBO	QUAD	✓	✓
106	20180813	SPONT/COMBO	TM		
106	20180814	COMBO	TM		
106	20180816	COMBO	ROBOT		
106	20180823	COMBO	ROBOT		
106	20180828	SPONT/COMBO	QUAD	✓	✓
106	20180830	SPONT	SINGLE PULSE		
106	20180830	SPONT/COMBO	TM		
106	20180903	SPONT/COMBO	QUAD	✓	✓
106	20180907	COMBO	ROBOT	✓	✓
106	20180927	COMBO	ROBOT	✓	✓
106	20181009	EES	ROBOT		
106	20181010	EES	ROBOT		
106	20181016	EES	ROBOT		
106	20181018	EES	QUAD	✓	✓
106	20181019	SPONT	QUAD	✓	✓
108	20180717	SPONT	QUAD	✓	✓
108	20180718	SPONT	LADDER		
108	20180723	SPONT	QUAD	✓	✓
108	20180724	SPONT	LADDER		
108	20180725	SPONT	QUAD	✓	✓
108	20180813	SPONT/COMBO	QUAD	✓	✓
108	20180813	SPONT/COMBO	TM		
108	20180816	COMBO	ROBOT		
108	20180822	COMBO	ROBOT		
108	20180828	SPONT/COMBO	QUAD	✓	✓
108	20180829	COMBO	ROBOT		
108	20180830	SPONT	SINGLE PULSE		
108	20180830	SPONT/COMBO	TM		
108	20180913	COMBO	ROBOT	✓	
108	20180926	SPONT/COMBO	TM		
108	20180927	COMBO	ROBOT	✓	
108	20180928	SPONT/COMBO	QUAD	✓	✓
108	20181002	SPONT/EES	QUAD	✓	✓
108	20181003	EES	QUAD	✓	✓
108	20181009	EES	ROBOT		
108	20181010	EES	ROBOT		
108	20181016	EES	ROBOT		
109	20180717	SPONT	QUAD	✓	✓
109	20180718	SPONT	LADDER		
109	20180719	PHARMA	QUAD	✓	✓
109	20180723	SPONT	QUAD	✓	✓
109	20180724	PHARMA	QUAD	✓	✓
109	20180724	SPONT	LADDER		
109	20180725	SPONT	QUAD	✓	✓
109	20180813	SPONT/COMBO	QUAD	✓	✓
109	20180813	SPONT/COMBO	TM		
109	20180829	COMBO	ROBOT	✓	✓
109	20180830	SPONT	SINGLE PULSE		
109	20180830	SPONT/COMBO	TM		
109	20180903	SPONT/COMBO	QUAD	✓	✓
109	20180928	COMBO	ROBOT	✓	✓
109	20181002	EES	QUAD	✓	✓
109	20181003	SPONT	QUAD	✓	✓
109	20181009	EES	ROBOT		
109	20181010	EES	ROBOT		
109	20181016	EES	ROBOT		

Legend: ■ Healthy ■ Early ■ Middle ■ Late

Table 4 | Data collected with the contused trained group, across tasks, conditions and time points
Kinematics data, EMG and calcium activity were recorded during various locomotor tasks and neuromodulation conditions, in the healthy animal and at the early, middle and late recovery stages. Data collected during all quadrupedal sessions under SPONT, PHARMA, EES and COMBO conditions, as well as during the robot task under the COMBO condition at late recovery have been analyzed and further used in this study.

92

Field of view stability and chronic neuron identification

Altogether, calcium activity recordings were performed in 10 rats from 13 days before up to 81 days after contusion, corresponding to a period ranging between 48 and 142 days after viral vector injection and lens probe implantation for the trained group, and between 51 and 139 days for the untrained group. The full recording period for each animal covered 80.8 days (±3.7), with a maximum of 95 days for the trained group, and 66.4 days (±1.4) for the untrained group (Fig. 15A). To our knowledge, this is the first reported occurrence of such extended chronic endoscopic calcium recordings in freely-moving rodents.

Neuron identification and further calcium activity analysis was performed on the data collected from the trained group, and was restricted to quadrupedal tasks at all time points available, and partly the robot task at late time point of recovery (Table 4). The analysis of the remaining sessions, including other neuromodulation conditions and locomotor tasks, is currently ongoing. Neuron identification was performed using CNMF-e (Zhou, Resendez et al. 2018). The number of dynamic neurons identified across all animals and sessions ranged from 27 to 146 (Fig. 15C). We recorded in average 82 (±13) neurons per animal, and in each animal, the number of neurons varied of 22% (±4%) across sessions. However, this variability was not accompanied by a general trend with time, which validates the stability and robustness of the experimental set-up, as well as the non-toxicity of the GECI delivery approach (see chapter 2). Additionally, the number of neurons identified on robot sessions tended to be reduced compared to quadrupedal sessions, although this effect was not significant ($p = 0.0625$, Wilcoxon matched-pairs sign rank test). As this effect was independent of the age of the implant, we suggest that this decrease is due to technical issues. Contrary to the quadrupedal task, where the animal is completely free in its environment, the design of the robot task involves the presence of diverse pieces of equipment in the vicinity of the animal's head. Notably, the jacket, as well as the backrest and rods of the robot can enter in contact with the baseplate or the microscope, leading to an increased motion in the recorded field of view (FoV). We confirmed the important instability of the FoV and the subsequent suboptimal motion correction on the recordings corresponding to this task. Thus, we suggest that the observed reduction in the number of neurons identified on these sessions is due to a weakness in the optical stability of the FoV.

Neuron registration is not possible chronically and across injury

In order to follow the very same neurons throughout SCI and recovery, we sought to proceed to cell registration with the CellReg algorithm (Sheintuch, Rubin et al. 2017). Only 5.1% (±1.2%) of all cells per animal could be registered across all analyzed sessions. This fraction increased if the number of sessions to register was reduced: 7.9% (±1.7%) over quadrupedal sessions, 33.1% (±5.6%) over robot sessions, 36.2% (±2.9%) over healthy sessions, 23.9% (±5.1%) over post-injury sessions and 44.9% (±3.1%) over the last healthy session and the first session post-injury only. Using the registration method integrated in the Inscopix Data Processing Software, and based on the same algorithm by Sheintuch et al., did not yield more satisfying results.
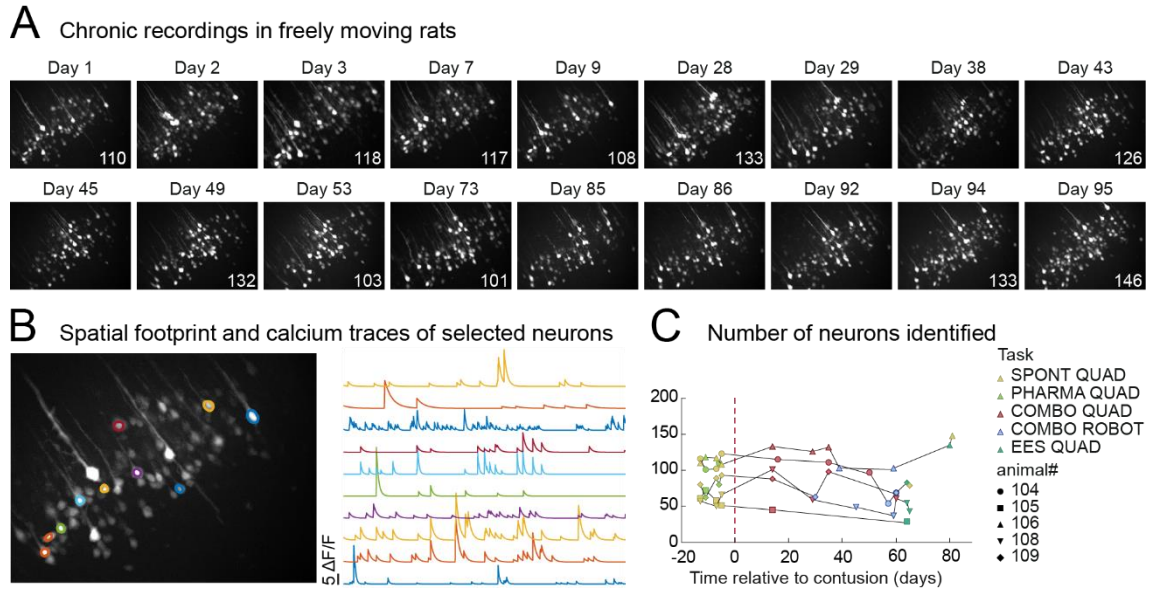
Fig. 15 | Cell identification in chronic calcium in freely-moving rats
A. Projection of the standard deviation of the pre-processed calcium movies obtained during longitudinal recordings recordings in one rat (#106). The number in the lower right corner indicates the number of neurons identified by CNMF-e on each session. **B.** An example FoV showing the spatial footprint of the neurons, with the position and corresponding calcium traces of a selected subset of neurons. **C.** Number of neurons identified by CNMF-e in each animal across all analyzed sessions of different behavioral tasks before and after contusion. The vertical bar indicates the time point of contusion.

Cell registration was then performed on couples of sessions only (Fig. 16A). The number of neurons registered on two consecutive sessions tended to drop right after contusion (Fig. 16B). In order to further explore this effect, we computed a similarity score for the FoV between pairs of sessions, thus quantifying the dynamics of neuronal spatial footprints. The similarity score exhibited the same tendency to drop when comparing pairs of sessions across injury (Fig. 16A). A simple linear regression revealed a negative correlation between the time separating the two sessions and the number of neurons registered ($R^2 = 0.588$, ±0.021) (Fig. 16C). However, a distinction could be made between pairs of sessions registered across the lesion and pairs of pre-lesion or post-lesion sessions. We confirmed this effect, showing that the lesion is accompanied by a significant drop in the performance of longitudinal registration (*$p = 0.0290 < 0.05$, Kruskal-Wallis, followed by Dunn's multiple comparisons post-hoc test) (Fig. 16D).
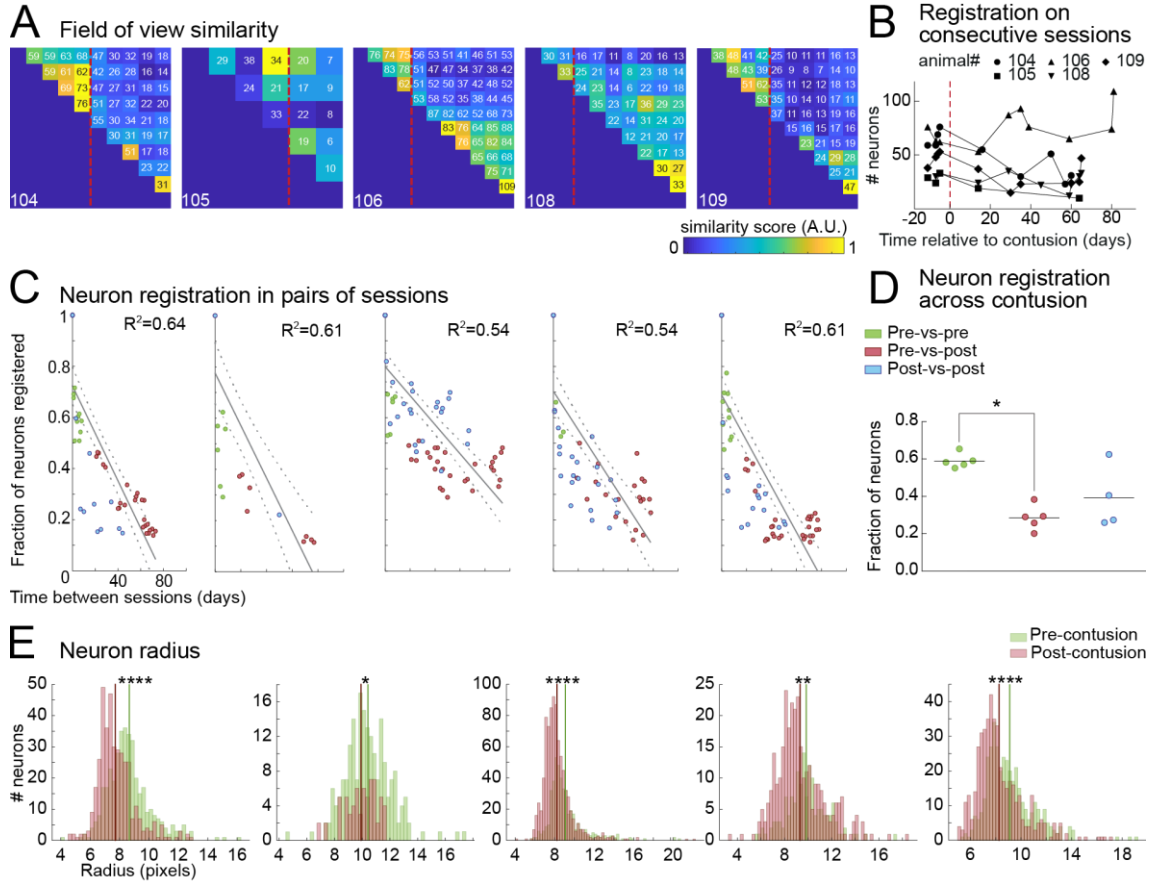
Fig. 16 | Cell registration in chronic calcium recordings across contusion
A. Similarity matrix per animal indicating the field of view similarity score (A.U.) calculated between pairs of sessions. Red vertical bar corresponds to the contusion. The number in each box indicates the number of neurons registered in the corresponding pair of sessions. **B.** Number of neurons registered on pairs of consecutive sessions for each animal. Red vertical bar corresponds to the contusion. **C.** Linear fit per animal of the ratio of registered neurons with the time separating the 2 registered sessions. **D.** Fraction of neurons registered on pairs of sessions before, across and after the lesion, averaged per animal. *p < 0.05, Kruskal-Wallis, followed by Dunn's multiple comparisons post-hoc test. **E.** Distribution of the neuron radii before and after contusion, Vertical bars indicate the mean of each population. *p < 0.05, **p < 0.01, ****p < 0.0001, Student's t-test.

In order to check for a possible anatomical change in the FoV with the contusion, we compared the population distribution of neuronal radius before and after the lesion. Each animal displayed a significant reduction in neuron size after contusion (*p < 0.05, Student's t-test) (Fig. 16E), leading us to suggest that important anatomical changes in the neuronal cell bodies lead to the decreased performance of longitudinal registration. Interestingly, the number of identified neurons was not reduced with the contusion (Fig. 15C).

As a conclusion, cell registration across longer periods of time and across contusion and recovery was not straightforward, most probably because of a combination of two limitations: technical issues linked to the robustness of cell identification and registration algorithms, and a physiological reality linked to anatomical changes following injury.

Corticolumbar population activity during natural walking in the intact animal

The activity of corticolumbar neurons was analyzed during the spontaneous quadrupedal walking task in the intact state in n = 5 animals. The task was repeated 3 times (H1, H2 and H3), with 8 days separating the first and the third session. Corticolumbar activity was stable across sessions (ns, $p > 0.05$, Friedman test), and significantly higher during movement than rest (**$p = 0.0040 < 0.01$, one-tailed Wilcoxon sign-rank test) (Fig. 17A). Neurons were then classified into movement-active (MA), rest-active (RA), indiscriminately active (IA) and silent (S) for each of the 3 repetitions (Fig. 17B). Fractions of neurons belonging to each class were stable across animals (ns, Kruskal-Wallis test) and across sessions (ns, Friedman test) (Fig. 17C), with an average of 10.1% MA, 9.2% RA, 72.9% IA and 7.8% S. Furthermore, the activity of movement- and rest-active classified neurons during respectively movement and rest was stable across the 3 sessions (ns, $p > 0.05$, Friedman test) (Fig. 17D).

This stability validates the robustness of the method and emphasizes the consistency of motor cortex representation of natural locomotion. While an approximate 20% of the neuronal population had a movement-related representation, evenly distributed between movement-active and rest-active, the greater part of the corticolumbar population was indiscriminately active.
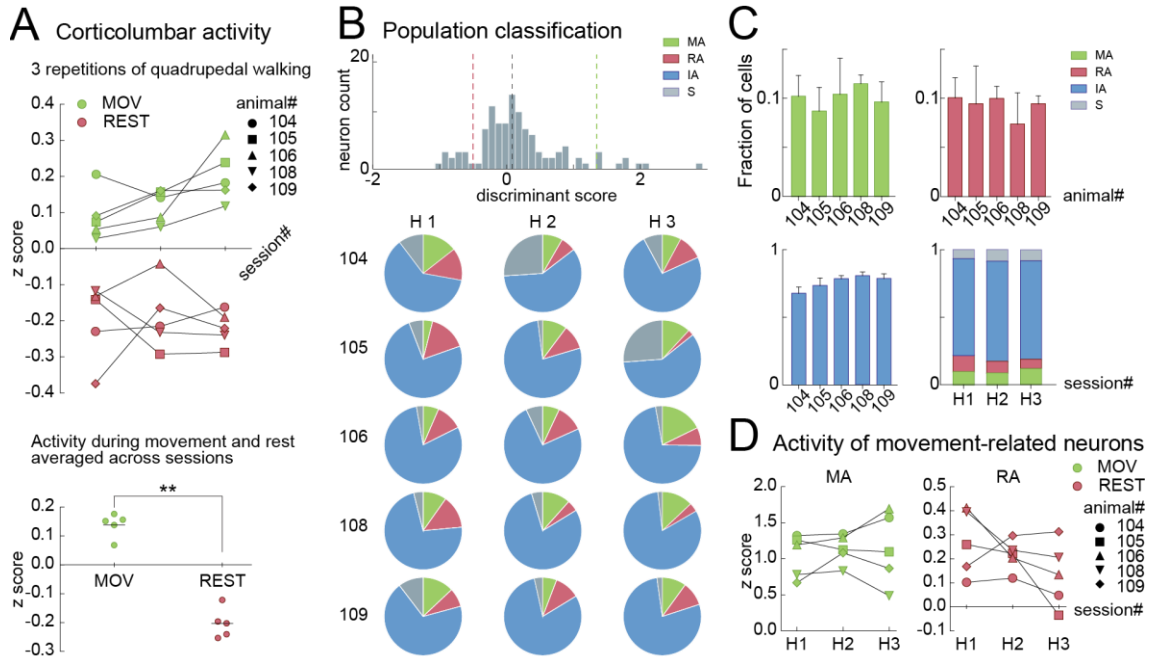
Fig. 17 | Population activity and classification during quadrupedal walking in the intact animal
A. Population calcium activity of corticolumbar neurons during manually marked movement (MOV) and rest periods for each animal on 3 repetitions of healthy spontaneous quadrupedal walking sessions. Corticolumbar activities are stable across time (ns, $p > 0.05$, Friedman test). Bar graph shows the activity during MOV and REST averaged across the 3 sessions, each dot is one animal. **$p < 0.01$, one-tailed Wilcoxon sign-rank test. **B.** Example of the population distribution of the discriminant score. Gray vertical bar corresponds to the median. Activity below the 10 percentile of the shuffled distribution marked by the red vertical line defines the rest-active classification; activity above the 90 percentile marked by the green vertical line defines the movement-active classification. Circular plots show the population classification for each animal on the 3 repetitions of healthy quadrupedal walking sessions. **C.** Fraction of cells in each movement-active (MA), rest-active (RA) representations and indiscriminately active (IA) class averaged over the 3 sessions for each animal, showing inter-subject stability (ns, $p > 0.05$, one-way ANOVA). Stacked bar graph shows the distribution of population classifications averaged across animals over the 3 sessions. S: silent. **D.** Activity of MA neurons during movement and RA neurons during rest periods for each animal on the 3 sessions. ns, $p > 0.05$, Friedman test.

96

Stability of individual neuron classifications during natural walking in the intact animal

We further investigated individual neuronal representations of locomotion, by performing longitudinal registration of the identified cells on the 3 repetitions of the spontaneous quadrupedal task in the intact state. An average of 36% (±3%) of identified neurons was registered (Fig. 18A). The overall classification of registered neurons was representative of the whole population (ns, Wilcoxon matched-pairs sign rank test, data not shown). In addition, neurons bearing different representations were spatially intermingled (Fig. 18B) and the distribution of classes was stable across animals (ns, Kruskal-Wallis test, data not shown) and across days (ns, Friedman test, data not shown).

For further analysis, we cumulated the registered neurons over all animals (192 unique neurons, 5 animals, 3 sessions per animal). We analyzed single class transitions between two consecutive recording sessions (Fig. 18C), as well as individual neuronal fates following the representation of the same neurons over the 3 recording sessions (Fig. 18D). Individual neuronal representations were overall stable, with 74.4% of single transitions within the same class, and 62.3% of neurons retaining their representation over the 3 sessions. Especially, indiscriminately active neurons were highly stable: 85.6% neurons stayed stable across single transitions and 76.43% over the 3 sessions. As IA represented the great majority of the population, 56.0% of the whole population constituted a stable pool of IA neurons. In turn, 59.5% of movement-active neurons stayed stable across single transitions and 41.7% over the 3 sessions. On the contrary, the classes of rest-active and silent neurons were highly labile: only 15.6% of RA and 25.0% of S neurons were stable on 2 consecutive sessions.

We observed no direct transitions between the two movement-related representations, from MA to RA and inversely (Fig. 18C). As a consequence, all new MA and RA classified neurons originated from the IA class. Furthermore, neurons did not switch movement-related representations indirectly via IA either (Fig. 18D). As a consequence, MA and RA representations formed two separate representations in the execution of natural walking, with dynamics consisting in varying degrees of correlation to movement.

While virtually no previously MA neuron became silent, a small proportion (2.1% of neurons, 19.1% of the original RA population) of RA neurons switched to silent. Conversely, no transitioning from silent to movement-tuned representations was observed, directly or indirectly via IA, while transitions from silent to IA and inversely commonly occurred.

These results, despite a low number of observations rendering the interpretation delicate, lead us to suggest a model of corticolumbar representations during the execution of natural locomotion (Fig. 18D) whereby:

- indiscriminately active neurons constitute the great majority of the population, with an important core of stable neurons representing more than half of the population.

- movement-active and rest-active representations form two segregated pools of neurons.

- approximately half of the movement-active population is stable, and the dynamics of the other half consists in changing correlations to movement, with no switching of movement-related representation.

- rest-active neurons mainly have varying correlations with movement, and might become silent via a transitory decorrelation to movement.

- silent neurons have varying correlations with movement. Their further possible fate is unknown.
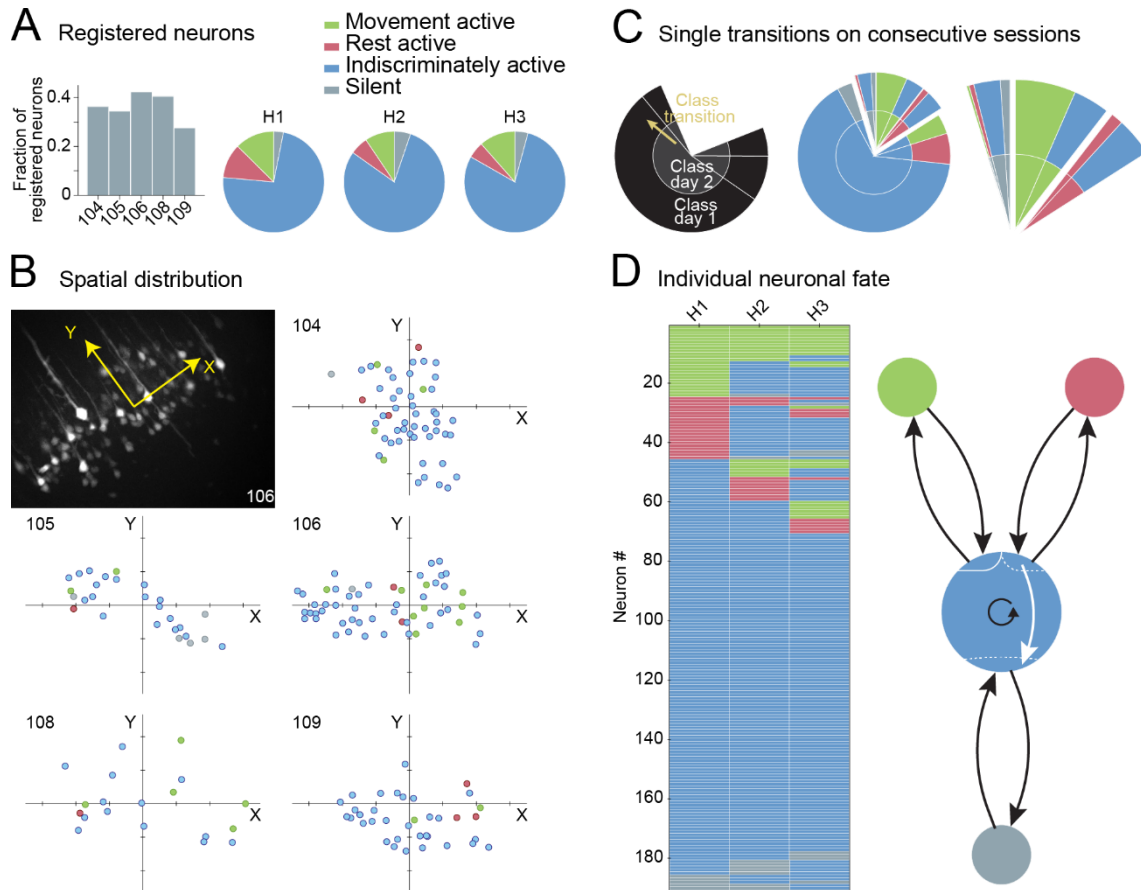
Fig. 18 | Stability of individual corticolumbar neurons classifications during natural walking in the intact animal
A. Bar graph shows the ratio of neurons registered across the 3 healthy spontaneous quadrupedal walking sessions (H1, H2, H3) in each animal. Registered neurons were further cumulated over all animals. Population classification of the registered neurons into movement-active, rest-active, indiscriminately active and silent. **B.** Spatial distribution of the registered neurons on session H3 for each animal. Neurons of different classes are spatially intermingled **C.** Single transitions of registered neurons on consecutive recording sessions. Inner circular plot indicates neuron's class on the departing session and outer plot the class on the arrival session. **D.** Individual neuron representations on the 3 consecutive recording sessions and scheme summarizing the model of neuronal representations dynamics over time during the execution of natural locomotion.

Corticolumbar population-level encoding of motor behavior

We sought to determine how well leg muscle activity is represented by the CL neurons. For this, we performed a linear regression of general CL calcium activity with the recorded EMG data on the trials of healthy quadrupedal walking. The linear model presented a periodic pattern that matched the EMG power during the manually marked movement phases (Fig. 19A). Decoding performance scaled up with the size of the neuronal population (Fig.19B), showing that muscle
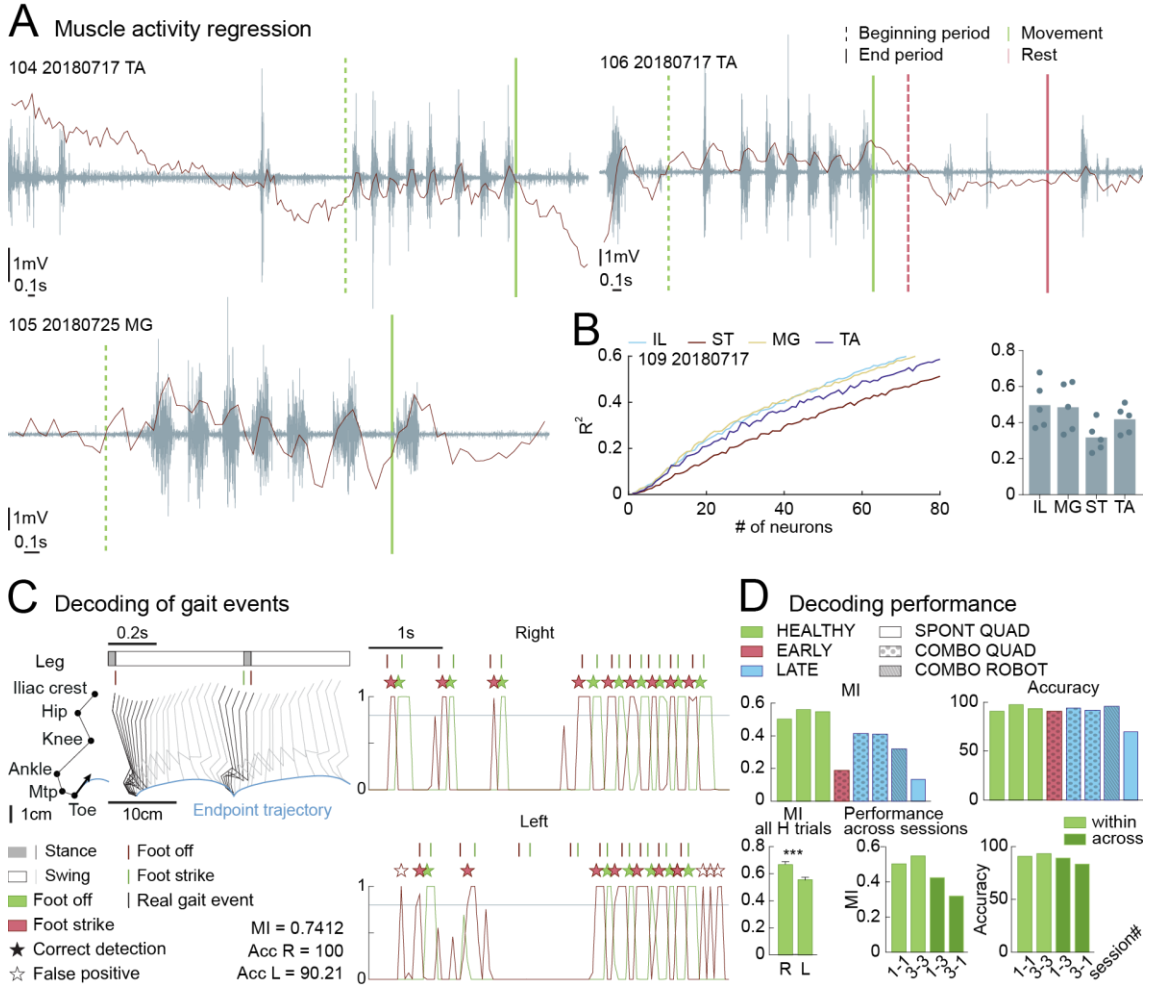
Fig. 19 | Population-level representation of locomotion in the intact animal and across lesion
A. Examples of linear fitting of calcium data to EMG signals for single trials of healthy walking. Vertical bars indicated the beginning (dotted) and the end (full line) of movement (green) and rest (red) periods manually selected for analysis. Title indicates the animal identity, date of the session and muscle selected for the analysis. **B.** Example of a neuron dropout test showing the performance of the linear fitting with the size of the neuronal population used for the regression. IL: iliopsoas, ST: semi-tendinosous, TA: tibialis anterior, MG: medial gastrocnemius. Bar graph shows the maximal regression performance (obtained with the whole based on the whole neuronal population) for each muscle averaged across all trials of healthy quadrupedal walking for each animal. Each dot represents one animal. **C.** Stick diagram showing the kinematics of the leg during walking and the corresponding gait events used for decoding. Mtp: metatarsophalangeal joint. Mutual information (MI) graphs for foot of and foot strike gait events on right and left leg for a representative trial. Vertical bars correspond to real events marked manually. Detection threshold is set at 0.8. Full star: correct detection, empty star: false positive, acc: accuracy. **D.** Upper graphs: mutual information (left) and accuracy (right) for both hindlimbs on the 3 healthy spont quad sessions, one early combo quad, two late combo quad, one late combo robot and one late spont quad session. Lower graphs: MI averaged on all cumulated trials of healthy spont walking on right and left hindlimb. ***p < 0.001, two-tailed Student's t-test. Graphs on the left show MI and accuracy of the decoder when training and testing intra-sessions (light green) or across different sessions (dark green) of healthy quadrupedal walking. Sessions 1 and 3 were used.

activity is encoded at the population rather than single neuron level. Overall, the corticolumbar neuronal activity accounted with high fidelity for individual muscle activities (average regression scores for all animals ranged from 0.32 for the semi-tendinosous to 0.50 for the iliopsoas).

Further exploring the representation of behavioral features in the CL population, we aimed to predict foot strike and foot off gait events (Fig. 19C) based on the calcium activity of all neurons. Using the data from one animal, we built a decoder based on linear discriminant analysis for each of the three healthy quadrupedal spont, one early quadrupedal combo, two late quadrupedal combo, one late robot combo and one late quadrupedal spont session (Fig. 19C,D). Gait events were decoded with high performance on both hindlimbs, not only during natural walking in the intact state (accuracy acc = 93.7% ±2.0%), but also during quadrupedal walking early after lesion (acc = 90.5%), at the late time point of recovery (acc = 92.7% ±1.1%), and during the robot task (acc = 95.5%) (Fig. 19C,D). Although still high, the decoding accuracy was significantly lower for the left leg, ipsilateral to the implant (84.1% for all healthy trials, ±0.9), compared to the right leg (86.9% for all healthy trials, ± 0.9%) (**p = 0.0099 < 0.01, Student's t-test). This expected result can be explained by the significantly lower mutual information (MI) (***p = 0.0002 < 0.001, Student's t-test) (Fig. 19D). Similarly, the mutual information dropped early after injury (MI = 0.187) compared to the intact state (MI = 0.536 ±0.031), and increased again at the late time point (MI = 0.412 ±0.002), suggesting a possible strengthening of the population-level representation of locomotion with recovery. However, the corresponding decoding accuracies remained high, which could be explained by the scarcity of actual gait events occurring at the early stage after lesion. This inherent aspect of the experimental design limits our ability to investigate the neuronal correlates of locomotion early after injury. Interestingly, at the late time point, quadrupedal walking under the spontaneous condition exhibited a lower MI (MI = 0.132, acc = 69.5%) than under the combo neuromodulation, which this time also translated into a drop in decoding accuracy (Fig. 19D). Whether this decrease in decoding performance is due to a notable behavioral difference or to a direct neuromodulatory effect of the electrochemical neuroprosthesis is yet to be determined.

We then assessed the stability of the population-level representation of locomotion during intact walking, by using the decoder built on one session to predict gait events on another session. We used H1 and H3 sessions of healthy spontaneous quadrupedal walking for this analysis. Although the overall performance was lower for across-sessions decoding compared to within-session, both MI and accuracy remained high (MI = 0.371 ±0.052, acc = 86.1% ±2.9%) (Fig. 19D). These results suggest a stability of the representation of locomotion in the corticolumbar population in the intact state, which will be confirmed by extending this analysis to the other recorded animals. Furthermore, the investigation of the decoding performance across injury and with recovery will enable to assess the stability of the population-level representation of locomotion with the relearning of walking.

All together, these results demonstrate the ability to predict motor behavior from the optical read-out of calcium activity in the brain of freely-moving rats over several months, not only in the intact animal but also after injury and recovery. Both in the intact state and after recovery has been

reached, the population-level representation of natural locomotion was high. The careful control of behavioral data, and integration of other animals in this analysis is needed in order to conclude about the dynamics accompanying recovery.

Corticolumbar activity and population-level classifications during quadrupedal walking after contusion

CL neurons activity was analyzed during quadrupedal runway walking early after injury and late after recovery, with electrochemical neuromodulation, in n = 4 animals. Neuronal activity was stable during both walking and resting periods (ns, $p > 0.05$, Friedman test), and was consistently reduced during rest compared to movement at both time points (*$p < 0.05$, one-tailed Wilcoxon sign-rank test) (Fig. 20A).

Neurons were then classified, and fractions of movement-related neurons and of indiscriminately active neurons were not significantly different across time points (ns, Friedman test) (Fig. 20B). Importantly, we noted a high inter-animal variability in the dynamics of the fractions of movement-related neurons across injury, which might account for the absence observable effect.

The activity of movement-related neurons did not significantly change after the contusion (ns, Friedman test) (Fig. 20C). However, there was a tendency for an increase in the activity of rest-active neurons during rest at the early time point after injury, compared to intact. This observation might be due to the complexity of distinguishing between motor intention and execution early after injury.

Effect of the pharmacological stimulation on corticolumbar activity

In order to check for the effect of pharmacological stimulation on CL neurons during a natural locomotor task, we compared neuronal activity in intact animals between the spontaneous and pharma neuromodulation conditions, and after recovery between the spontaneous and combo conditions. No significant difference was found (ns, paired two-tailed Wilcoxon sign-rank test) (Fig. 20D), indicating that the pharmacological stimulation *per se*, as part of the electrochemical neuromodulation therapy, does not importantly affect CL activity. This conclusion appeared surprising, as it would have been reasonable to hypothesize that the systemic injection of serotonergic agonists, originally aimed at enabling lumbar spinal circuits, does modulate brain circuits as well. The absence of effect shown here, however, serves as a partial control for the combo neuromodulation condition.
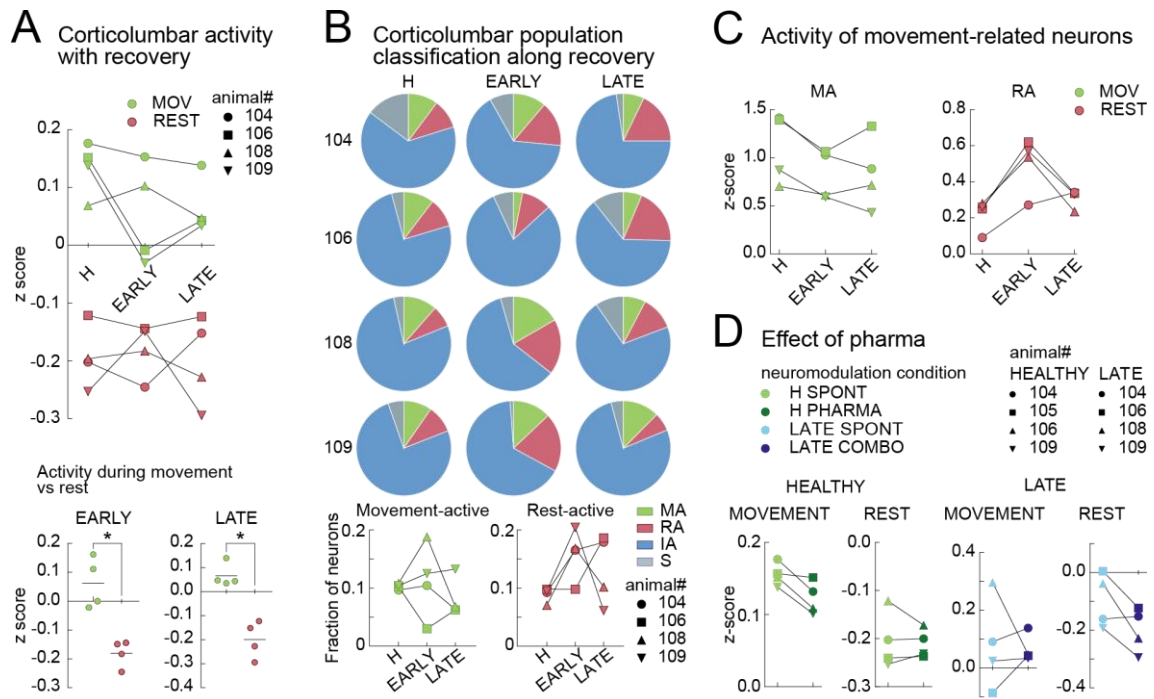
Fig. 20 | Corticolumbar population activity and classification across recovery
A. Population activity of corticolumbar neurons during movement (MOV) and rest periods on quadrupedal walking task in the healthy, early and late time points. MOV: movement, H: healthy. ns, p > 0.05, Friedman test. Bar graph shows the activity during MOV and REST at early and late time points; each dot is one animal. *p < 0.05, one-tailed Wilcoxon sign-rank test. **B.** Classification of corticolumbar neurons during quadrupedal walking at the 3 time points of recovery for each animal. MA: movement-active, RA: rest-active, IA: indiscriminately active, S: silent. Graphs show the fraction of neurons with movement-related representations across the 3 time points for each animal. ns, repeated measures one-way ANOVA. **C.** Activity of the movement active (MA) and rest-active (RA) neurons during respectively movement and rest periods. ns, p> 0.05, Friedman test. **D.** Activity of all corticolumbar neurons during movement and during rest without and with the neuromodulation therapy: at the healthy time point under spontaneous and pharma conditions and at the late recovery time point under spontaneous and combo conditions. ns, p > 0.05, paired two-tailed Wilcoxon sign-rank test.

5.3. Discussion

Proof of concept for chronic endoscopic calcium recordings in freely-moving rats

We have performed a proof-of-concept for chronic calcium imaging in freely-moving rats. Only recently, the very first study in this species was published, reporting experiments lasting for approximately 20 days (Cameron, Murugan et al. 2019). Over up to 95 days of recordings, we gathered an exceptional amount of data. To date, the longest study design of unconstrained endoscopic calcium recordings reports 45 experimental days in mice (Ziv, Burns et al. 2013). Thus, we performed the first study, to our knowledge, achieving chronic recordings extending over several months in rodents.

Limitations of cell registration across sessions

The number of neurons identified over the long time range of our experiment was overall stable in all animals, validating our method for chronic studies of neuronal population activity. Despite the stable quality of the FoV over more than 4 months, longitudinal registration did not yield the originally expected results. Two reasons can be invoked to explain this hurdle, one of technical and one of anatomical source. The technical limitation encountered during the registration process is a common problem among the community of 1-photon calcium imaging users, especially in chronic studies extending over several weeks or months (no published data available, knowledge exchange). The development of better computational algorithms to optimize cell identification and registration will hopefully generate robust solutions, rendering possible to follow the exact same neurons in large populations throughout several months of experimentation. Such a technical improvement would greatly increase the power of calcium imaging in freely-moving animals as a technique to investigate the neural correlates of recovery and learning.

The anatomical limitation, on the other hand, is constitutive to our specific experimental design. Corticospinal axon severing is known to lead to consequent neuronal death (46%) (Giehl and Tetzlaff 1996, Lu, Blesch et al. 2001), as well as important anatomical changes such as cell body atrophy and shrinkage (49%) in surviving neurons (Giehl and Tetzlaff 1996, Tseng and Prince 1996, Wannier, Schmidlin et al. 2005, Brock, Rosenzweig et al. 2010, Nielson, Strong et al. 2011). While we did not observe any effect suggesting neuronal death, the consistent reduction in neuron radius in our study is coherent with these histological results. This limitation, as a direct biophysiological consequence the lesion, cannot be overcome without drastic modification of our experimental paradigm.

Emergence of new challenges with recordings in freely-moving animals

While head-fixed recordings lacked ecological value due to important physical constraints on the animal, they thereby ensured a certain experimental control and consistency. The introduction of

freely-moving recordings, on the counterpart of opening avenues for the study of locomotion or social interactions, greatly increases the variability in animal behavior. The extreme complexity of behavioral read-out is thus a new challenge, adding up to the constitutive intricacy of disentangling motor behavior from motor intention in our specific experimental design. To best account for this, all behavioral videos were manually marked for data rejection with highly selective criteria. Any unclear animal behavior was excluded from the dataset in the sake of experimental consistency, though strongly detrimental to the resulting amount of data available for analysis.

Variety and complexity of the behavioral experimental design

The three different time points along recovery have been selected in the aim of following CL dynamics along the reorganization of the motor-circuit communication matrix after contusion. The wide variety of tasks and neuromodulation conditions recorded, although adding tremendous complexity to the study, was designed to answer the need for controls while performing motor tasks adapted to the impaired motor capabilities of animals after lesion. Due to the important experimental effort required by neuroprosthetic rehabilitation, the number of animals in our experiment is reduced in comparison with other studies investigating motor learning, limiting the interpretation of our results due to inter-subject variability. Additionally, the restricted number of individual neurons recorded represents a further limitation, and is an inherent downside of both the specificity of the neuronal population studied and the use 1-photon as opposed to 2-photon imaging.

However, further analysis of the collected data will enable to strengthen our understanding of corticolumbar involvement in locomotion. For example, the analysis of CL activity and individual neuron representations during the healthy ladder task will yield precious information about the execution of skilled movement as opposed to natural walking behaviors.

Corticolumbar activity during natural locomotion

We have shown the stability of corticolumbar activity and of the fraction of movement-related neurons during the execution of natural locomotion in the intact animal. Corticospinal neuron activity is known to correlate with movement in rodents (Komiyama, Sato et al. 2010, Li, Chen et al. 2015, Peters, Lee et al. 2017) and primates (Evarts 1965, Churchland, Cunningham et al. 2012). We found an approximate of 10% of movement-active and 10% of rest-active neurons, consistent with a previous study reporting various correlations of corticospinal activity with movement in a lever-press task (Peters, Lee et al. 2017). However, in that study, the authors found a surprisingly higher fraction of rest-active cells – nearly twice as much as movement-active – which resulted in a general reduction of CS activity during movement. They suggest that such a representation and activity pattern might be specific to deeper cortical layers (Isomura, Harukuni et al. 2009), as they had previously observed an opposite effect in L2/3 neurons (Peters, Chen et al. 2014). These findings were not repeated here: on the contrary, we report, similarly to L2/3, an increase of general activity during movement in corticolumbar neurons. The second hypothesis

formulated by the authors, involving a task-specific dependency of the observed drop in CS activity, seems more compliant with our results.

In our study, a major part (73%) of CL neurons were indiscriminately active, while this population represented only 22% of CS neurons in the previously mentioned study (Peters, Lee et al. 2017), although the same computation method was used for classification. Besides the difference in the fractions of rest-active neurons that only partly accounts for this effect, this divergence is driven by the distribution between silent and indiscriminately active cells. This discrepancy might be explained by specificities in the respective experimental designs, be it in the animal behavior or the data collection and analysis: natural walking vs skilled motor execution, recording of leg vs forelimb motor cortex, recording with 1-photon vs 2-photon microscopy, analysis and classification of neurons based on calcium signals from cell bodies vs apical dendrites.

In regard of our distribution, and although representations do not necessarily link directly to causality, the role of the greater part of CL neurons in the execution of healthy locomotion still needs to be questioned. Huber et al. also report a sparse coding of the studied behavioral features (touch, lick and whisk) during the execution of a sensorimotor task, where only 42% of active recorded L2/3 neurons in the vibrissal motor cortex were classified as behavior-tuned (Huber, Gutnisky et al. 2012). Indiscriminately active neurons might be involved in cognitive processing, or be correlated to non-tracked behavioral features, notably sensory-related representations engaged in sensorimotor integration and learning.

Individual CL neurons representations of leg movement in the intact animal

Huber et al. further investigated individual neurons representations. The authors showed that cells become more or less correlated with behavior with motor execution and across learning days but do not switch between different features of behavior (Huber, Gutnisky et al. 2012). This variability in single neuron representations remained after the stabilization of both population-level representations and motor performance. Similarly, Peters et al. demonstrated the dynamic representation of single CS neurons during motor learning. Interestingly, in their study, movement-active cells did transition to rest-active and to indiscriminately active, while rest-active cells transitioned mainly to silent (Peters, Lee et al. 2017).

While our analysis was restricted to class-transitions during stable repetitions of a natural behavior, we report that 42% of movement-active, while only 5% of rest-active neurons stayed stable across the 3 repetitions of the task. The dynamics of representations mostly consisted in varying levels of correlation with movement, and CL neurons did not switch between movement-active and rest-active representations. However, the number of observations remained limited in our study, and the additional data collected with the untrained group will help strengthen our conclusions.

The necessity of being able to register neurons across injury and in recording sessions separated of several months is central in the further analysis of individual neuronal representations dynamics with recovery. This would enable to ascertain the variability of individual neuronal encoding of behavioral features during learning, as opposed to execution of a locomotor task. For the time

being, whether a different pattern of possible class transitions emerges during learning, as observed in the aforementioned studies, thus remains an open question.

Population-level representation of movement and learning

Beyond the analysis of single neurons, we highlighted the population-level encoding of behavioral features such as individual muscle activity and gait events, corroborating previous results showing that neuronal population, rather than single neurons, bear the strongest relationship with movement (Cohen and Nicolelis 2004, Afshar, Santhanam et al. 2011).

Early motor learning is associated with changes in L5 motor cortex activity patterns that directly translate into corresponding changes in muscle activity (Kargo and Nitz 2004), suggesting a non-plastic relationship between neuronal activity and output movement at early stages. Electrophysiological recordings in the L5 motor cortex first showed an increase in the fraction of cells correlated with movement (Costa, Cohen et al. 2004, Kargo and Nitz 2004). Later, a 2-photon calcium imaging study demonstrated the same effect in L2/3 dynamics during sensorimotor learning (Huber, Gutnisky et al. 2012). Interestingly, the initial increase in the fraction of movement-related neurons during motor learning is followed by a decrease to original levels at later time points (Peters, Chen et al. 2014). This finding highlights possible fine-scale temporal dynamics – possibly translating exploration followed by consolidation – that might not be captured in our experimental design. Surprisingly, we found no dynamics in the fraction of movement-related cells along recovery.

Sensorimotor learning is also known to be accompanied by an increase in activity (Heindorf, Arber et al. 2018) and variability (Peters, Lee et al. 2017) in CS neurons. Unexpectedly, we found no effect of the contusion and of recovery on the activity of corticolumbar neurons during locomotion. The important inter-animal variability might account for this observed absence of dynamics. Moreover, our paradigm is inherently different from usual motor learning studies. Our longer time scales, as well as the necessity of longitudinal animal training, make it delicate to put in perspective with compact studies whereby animals learn a motor task within a couple of days to reach a performance plateau. The injury leads to the perturbation not only of the very behavior tested, but also intrinsically of motor circuits prior to the phase of interrogation through recording. In this regard, the functional plasticity of early motor recovery is probable to differ from usual studies of motor learning in the intact animal.

Furthermore, the population-level representation of a learnt behavior is known to strengthen with learning (Huber, Gutnisky et al. 2012), first exhibiting variability before reaching stability, which is consistent with a model of motor learning whereby an initial phase of exploration is followed by consolidation. We decoded behavioral features from CL calcium activity across injury and recovery, over the time range of several months, exhibiting a high performance in the intact state and after recovery. We also highlighted the stability of the population-level representation of locomotion in the intact state. However, the interpretation of learning-related dynamics across recovery is rendered delicate by the study design, due to the animal's limited motor abilities early after injury.

Despite great challenges introduced by the complex experimental design, the analysis of additional data collected from both the trained and the untrained group will help further explore the corticolumbar representation of locomotion in the intact state and during recovery after SCI.

VI. Chapter 4

ANATOMICAL PLASTICITY OF THE CORTICOLUMBAR CONNECTOME AFTER CONTUSION

Abstract

Despite the complete interruption of the corticospinal tract by a severe contusion, the motor cortex retains indirect connections to the spinal circuits below the lesion. Yet insufficient to elicit voluntary movement, these spared circuits enable an immediate cortical control over the paralyzed legs during spinal electrochemical stimulation. Neuroprosthetic rehabilitation encourages the plasticity of remaining motor circuits, and the resulting training-dependent anatomical remodeling of cortical and reticulospinal projections underlies the recovery of leg motor control. We sought to thoroughly investigate the anatomical plasticity with contusion and training of the corticolumbar neurons, which are the main source of corticofugal axons in the leg motor cortex. An exhaustive brain mapping of the corticolumbar connectome enabled to identify the regions of collateral projections. The precise quantification of brain and spinal collateral synapses revealed a training-dependent strengthening of corticolumbar projections in the thoracic spinal segments above the lesion. However, no effect of neuroprosthetic rehabilitation was found on the density of collateral synapses throughout brain and brainstem target regions. The cortical neurons involved in the functional and anatomical plasticity specifically observed after neuroprosthetic rehabilitation might belong to a distinct cortical population.

6.1. Introduction

In the first chapter of this thesis, we have shown that rats with a paralyzing spinal contusion recover voluntary control over the legs thanks to neuroprosthetic rehabilitation, and this restoration of function is motor-cortex dependent (Asboth, Friedli et al. 2018). Additionally, it is known that functional plasticity of corticospinal neurons accompanies motor learning (Peters, Lee et al. 2017). In case of learning in the intact animal, the reshaping of the relationship between the activity of motor cortex output neurons and the motor outcome does not necessarily translate in a neuroanatomical plasticity in corticospinal circuits. This degeneracy might provide robustness against internal noise and external unpredicted changes of the environment. However, a spinal cord injury drastically disrupts the anatomical organization of corticospinal neurons prior to the occurrence of functional plasticity and learning. Previous studies have shown the extensive anatomical remodeling of corticospinal neurons after SCI, including important sprouting throughout the whole central nervous system, midline crossing of spared CST components and formation of new synapses into the spinal cord above and below injury (Weidner, Ner et al. 2001, Bareyre, Kerschensteiner et al. 2005, van den Brand, Heutschi et al. 2012, Zörner, Bachmann et al. 2014, Hilton, Anenberg et al. 2016, Hollis, Ishiko et al. 2016).

As well, in the context of a severe spinal cord injury leading to the complete interruption of the corticospinal tract, important anatomical plasticity occurs at various levels of the brain, brainstem and spinal cord above the lesion. Several brainstem centers, such as the bilateral vestibular nuclei, the reticular formation and the parapyramidal regions receive a near four-fold increase in cortical fibers after a double hemisection (van den Brand, Heutschi et al. 2012). Similarly, the density of cortical fibers exhibits a significant increase in the spinal cord above injury (T4-T5 level), leading to the formation of propriospinal relays. Moreover, we showed in the first chapter of this thesis that the establishment of a cortico-reticulo-spinal relay bypassing a severe spinal contusion involves the drastic sprouting of cortical fibers in the ventral gigantocellular nuclei of the brainstem (Asboth, Friedli et al. 2018). The functional carry-over effect evidenced in this study suggests that the important neuroplasticity observed with training is sufficient for the recovery of natural locomotion in the absence of neuromodulation. All these anatomical rearrangements were observed with neuroprosthetic rehabilitation only, and were absent in the non-trained or treadmill-trained animals.

In the light of these results, we hypothesize that within the leg motor cortex, the corticolumbar population, directly projecting onto the spinal circuits controlling leg movement in the intact animal, is the major contributor to the increase in cortical fibers density observed in the brainstem following neuroprosthetic rehabilitation. We aimed to verify this hypothesis, and further investigate the neuroplasticity of corticolumbar collaterals after a contusion and with training. For this, we achieved an exhaustive mapping of the brain and spinal corticolumbar connectome in intact,

contused and trained rats, and quantified the density of corticolumbar synapses in a selected subset of target regions.

6.2. Results

Experimental design

For the anatomical analysis of the corticolumbar connectome, rats were separated into 3 groups: healthy (n = 5), contused (n = 6) and trained (n = 5) (Fig. 21). Animals were injected unilaterally with the AAV-DJ-hSyn-flex-mGFP-2A-Synaptophysin-mRuby viral vector in the leg motor cortex and with the retrograde rAAV-Cre in the contralateral lumbar spinal cord to achieve the specific labeling of
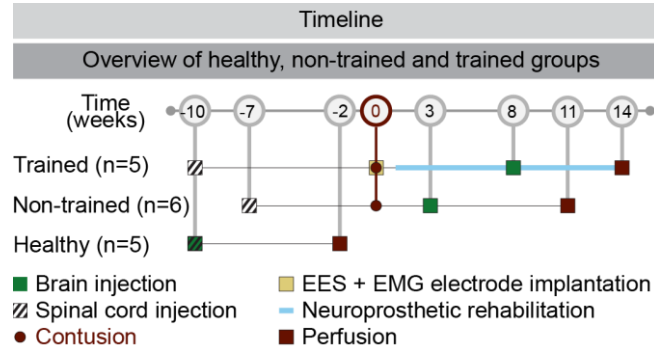
Fig. 21 | Timeline and experimental groups for the anatomical analysis of the corticolumbar connectome plasticity

corticolumbar collateral axons with GFP and synapses with mRuby (Fig. 24C,D, Fig. 33). The trained group of animals underwent neuroprosthetic rehabilitation as previously described (Supplementary Fig. 1) (van den Brand, Heutschi et al. 2012). The timeline of interventions is detailed in Fig. 21. The contusion spared 9.7% of spinal tissue (± 0.7%) in the contused untrained group and 9.9% (± 1.0%) in the trained group. Histological evaluation of the contusion revealed an anatomically complete lesion in one animal of the trained group, which was consequently discarded from further analysis.

The spinal corticolumbar connectome is strengthened by training

Corticolumbar synapses were quantified in the spinal cord (Fig. 22) by group of spinal segments. Briefly, microscopy photographs of 4 coronal sections per group of spinal segment were selected and the synapse area was quantified by manual thresholding thanks to an in-house coded algorithm based on R. We averaged synapse densities per animal and per group of spinal segments. To account for possible variations due to the viral injections, we normalized the synapse area by the labelled area of the corticolumbar tract at the level of the pyramids in the brainstem for each animal. For this quantification, the untrained group counted n = 4 animals; one animal was discarded because of tissue damage at the level of the pyramids.

We further average the data per group for the representation of the spatial distribution of synapses and statistical analysis. In healthy animals, the rostro-caudal profile of corticolumbar synapse density presented a local maximum at spinal segments C5-C8, and increased continuously along thoracic segments, until reaching a maximum at the sites of injection of the retrograde viral vector, at spinal segments L4 to L6 (Fig. 22L). In both groups of lesioned animals, synapse densities decreased when approaching the contusion, at spinal segments T6-T7, and synapses were totally

absent from spinal segments T8 and caudally, confirming the complete interruption of the corticolumbar tract by the lesion (Fig. 22L).

For the trained group, we observed a 212% increase (compared to the intact group) in the density of synapses at spinal levels T4-T5 above the injury. This increase was significant only after neuroprosthetic rehabilitation (*p = 0.027 < 0.05, Kruskal-Wallis test followed by Dunn's multiple comparison post-hoc test) (Fig. 22D,L,M). Additionally, corticolumbar collateral synapses were mainly located in the intermediate zone laminae IV and VII of the spinal gray matter, which was consistent with the spatial distribution in the intact animal (Fig. 22D). All other synapse densities were unchanged across groups and spinal segments (Fig. 22A-C,E-L). These results confirm a training-dependent increase in corticospinal connections in the spinal cord above the lesion.

Fig. 22 | Quantification of the spinal corticolumbar connectome A-K. Spatial distribution of the corticolumbar collateral synapses per group of spinal segment, represented by heat maps (A.U.) of the normalized synapse density averaged per group: healthy (left), untrained (middle) and trained (right). **L.** Rostro-caudal profile of the normalized synapse density averaged across animals for each group. *p < 0.05, Kruskal-Wallis test followed by Dunn's multiple comparison test. M. Detail of the quantified synapse area at spinal segments T4-T5 normalized to the healthy group. Each dot represents one animal. *p < 0.05, Kruskal-Wallis test followed by Dunn's multiple comparison test.

Mapping of the brain corticolumbar connectome

For the mapping and quantification of the brain corticolumbar connectome, 4 animals in the healthy group and 1 animal in the contused untrained group had to be discarded because of tissue damage along histological processing. As a result, only n = 1 healthy animal was analyzed. To address this issue, we repeated the group of healthy animals, and n = 3 additional animals are currently being processed.

An exhaustive brain screening revealed 24 brain and brainstem regions receiving collateral projections from corticolumbar neurons. These regions were consistently identified in all analyzed animals (Fig. 23-30):

- ipsilaterally to the injection side: caudate putamen (Fig. 23C), reticular thalamus (Fig. 24E), anterior component of the secondary sensory cortex (S2ant) (Fig. 25C), zona incerta (Fig. 25E), posterior component of the secondary sensory cortex (S2post) (Fig. 26C), ventral posteromedial nucleus of the thalamus (VPM) (Fig. 26D), parafascicular nucleus (Fig. 26E), anterior pretectal nucleus (Fig. 26F), red nucleus (Fig. 27C), mediate geniculate nucleus (Fig. 27D), substantia nigra reticulata (Fig. 27E), midbrain reticular formation (Fig. 27F), periaqueductal gray matter (PAG) (Fig. 28.1C), colliculi (Fig. 28.1D), pons part oral (Fig. 28.1E), pons (Fig. 28.2F), lateral parabrachial nuclei (Fig. 29C), and ventral gigantocellular nucleus (vGi) (Fig. 30C).

- contralaterally to the injection side: caudate putamen (Fig. 23D), primary motor cortex (M1contra) (Fig. 23E), anterior part of the secondary sensory cortex (Fig. 26D), pons (Fig. 28.2G), ventral gigantocellular nucleus (Fig. 30D), and vestibular nucleus (Fig. 30E).

Fig. 23 | Brain mapping of the corticolumbar connectome | 0mm-3mm caudal to bregma
A. Schematic sagittal view of the brain, showing the approximate position of the coronal planes imaged. **B.** Schematic representation of the coronal plane imaged. Striped area represents the motor cortex on the side of injection. Dashed contours represent the identified and imaged target areas of corticolumbar collaterals. **C, D and E.** Confocal pictures of a representative **(1)** healthy, **(2)** contused non-trained and **(3)** trained animal of the brain regions indicated in (B). In green is GFP marking axons, in red mRuby marking synapses. Scale bars 10µm. **C.** Caudate putamen. **D.** Contralateral caudate putamen. **E.** Contralateral motor cortex.

Fig. 24 | Brain mapping of the corticolumbar connectome | 0.5mm-3.2mm caudal to bregma
A. Schematic sagittal view of the brain, showing the approximate position of the coronal planes imaged. **B.** Schematic representation of the coronal plane imaged. Striped area represents the motor cortex on the side of injection. Dashed contours represent the identified and imaged target areas of corticolumbar collaterals. **C.** Image of the coronal section represented in (B) showing injection site and the beginning of the corticolumbar tract. **D, Di and E.** Confocal pictures of a representative **(1)** healthy, **(2)** contused non-trained and **(3)** trained animal of the brain regions indicated in (B). In green is GFP marking axons, in red mRuby marking synapses. **Di and E.** Scale bars 10µm. **D.** Injection site in the motor cortex. Scale bars 100 µm. **Di.** Higher magnification of the inset in (D). **E.** Reticular thalamus.
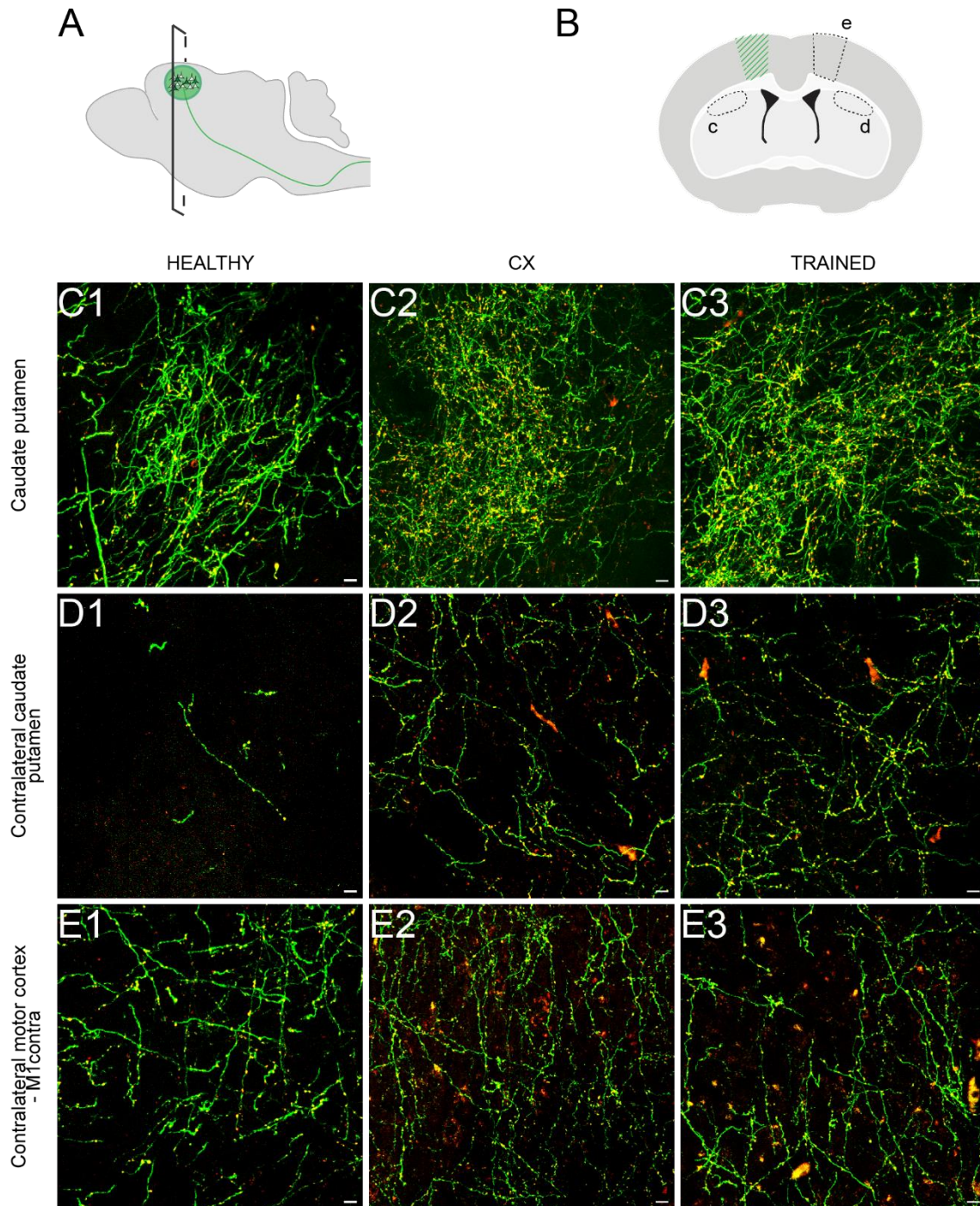
Fig. 25 | Brain mapping of the corticolumbar connectome | 1.5mm-4.8mm caudal to bregma
A. Schematic sagittal view of the brain, showing the approximate position of the coronal planes imaged. **B.** Scheme of the coronal plane imaged. Dashed contours represent the identified and imaged target areas of corticolumbar collaterals. **C, D and E.** Confocal pictures of a representative **(1)** healthy, **(2)** contused non-trained and **(3)** trained animal of the brain regions indicated in (B). In green is GFP marking axons, in red mRuby marking synapses. Scale bars 10µm. **C.** Anterior part of the secondary sensory cortex. **D.** Contralateral secondary sensory cortex. **E.** Zona incerta.

Fig. 26 | Brain mapping of the corticolumbar connectome | 2.8 mm-5.2mm caudal to bregma
A. Schematic sagittal view of the brain, showing the approximate position of the coronal planes imaged. **B.** Scheme of the coronal plane imaged. Dashed contours represent the identified and imaged target areas of corticolumbar collaterals. **C, D, E and F.** Confocal pictures of a representative **(1)** healthy, **(2)** contused non-trained and **(3)** trained animal of the brain regions indicated in B. Green: GFP marking axons, red: mRuby marking synapses. Scale bars 10µm. **C.** Posterior part of the secondary sensory cortex. **D.** Ventral posteromedial thalamus. **E.** Parafascicular nucleus. **F.** Anterior pretectal nucleus.
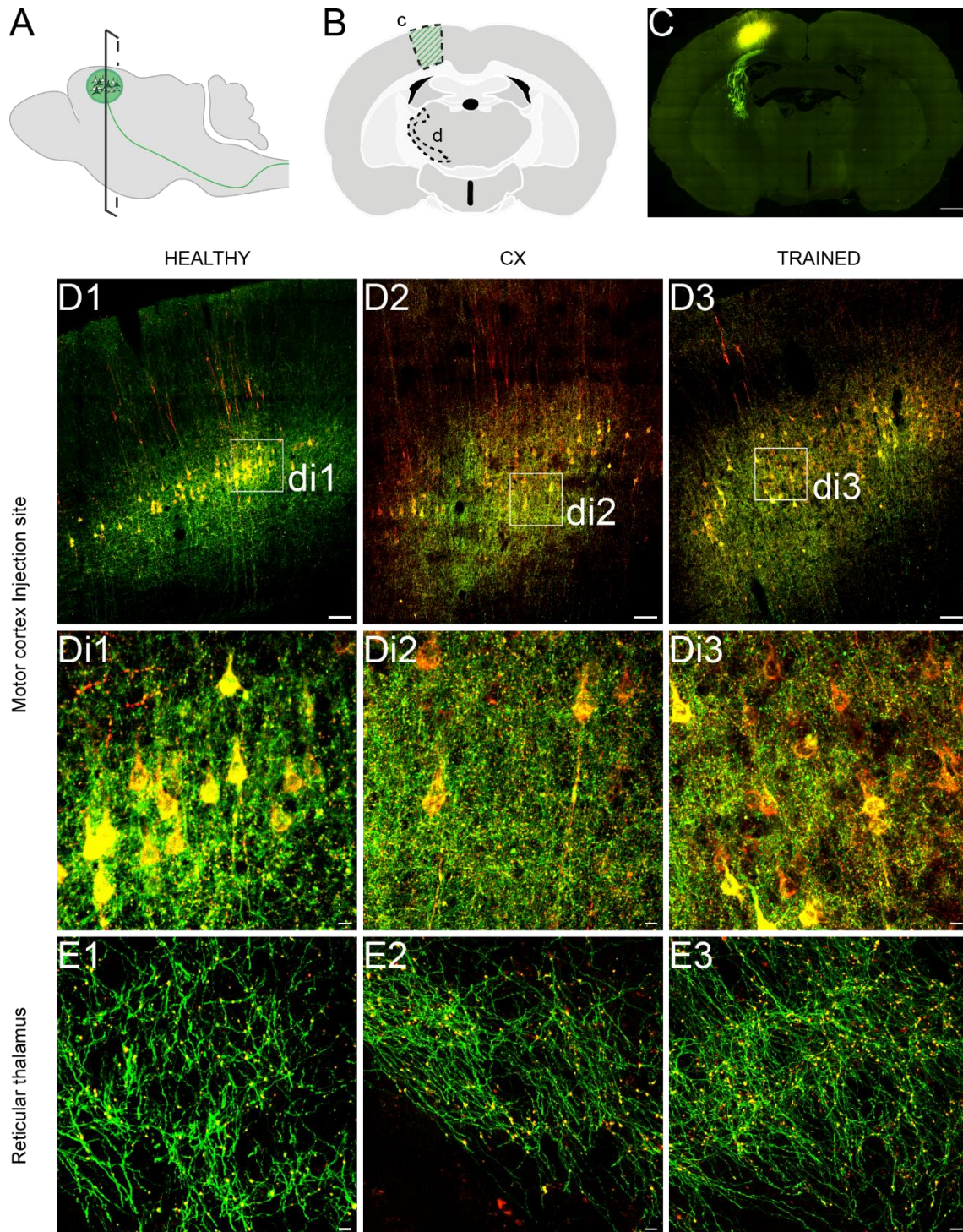
Fig. 27 | Brain mapping of the corticolumbar connectome | 4.2mm-7.0mm caudal to bregma
A. Schematic sagittal view of the brain, showing the approximate position of the coronal planes imaged. **B.** Scheme of the coronal plane imaged. Dashed contours represent the identified and imaged target areas of corticolumbar collaterals. **C, D, E and F.** Confocal pictures of a representative **(1)** healthy, **(2)** contused non-trained and **(3)** trained animal of the brain regions indicated in (B). In green is GFP marking axons, in red mRuby marking synapses. Scale bars 10µm. **C.** Red nucleus. **D.** Mediate geniculate nucleus. **E.** Substantia nigra reticulata. **F.** Midbrain reticular formation.
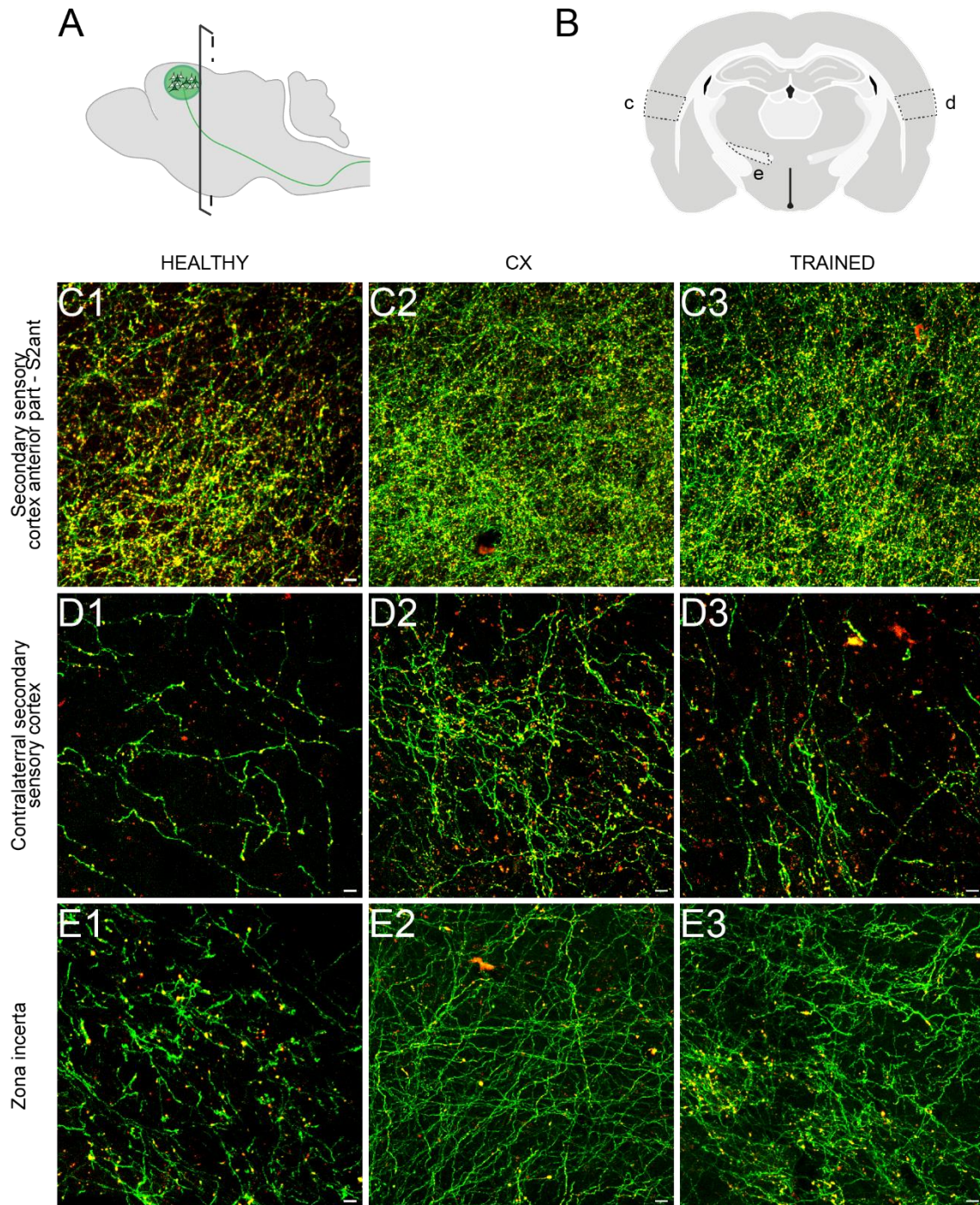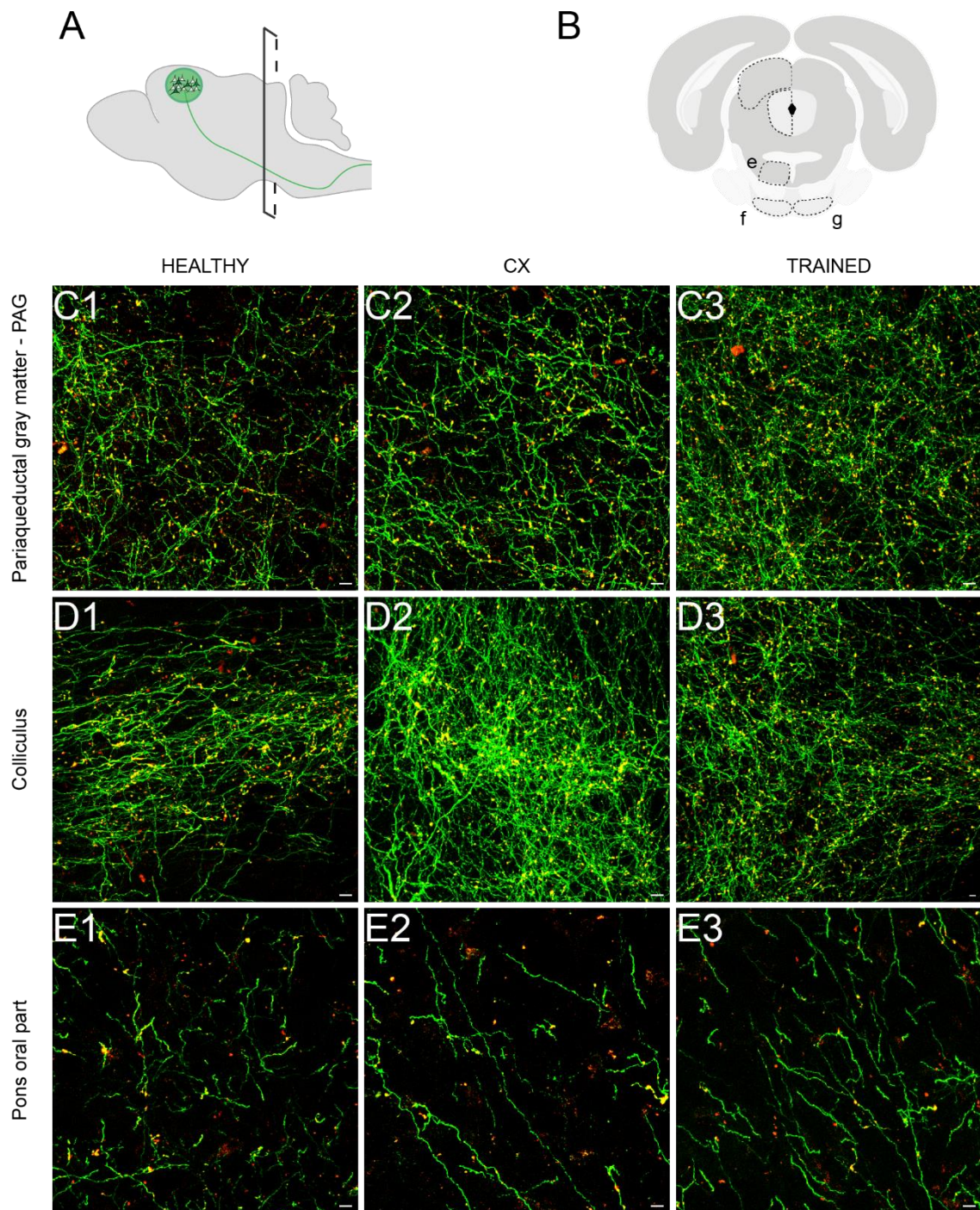
Fig. 28.1 | Brain mapping of the corticolumbar connectome | 6mm-9.0mm caudal to bregma

A. Schematic sagittal view of the brain, showing the approximate position of the coronal planes imaged. **B.** Scheme of the coronal plane imaged. Dashed contours represent the identified and imaged target areas of corticolumbar collaterals. **C, D, E, F and G.** Confocal pictures of a representative **(1)** healthy, **(2)** contused non-trained and **(3)** trained animal of the brain regions indicated in (B). In green is GFP marking axons, in red mRuby marking synapses. Scale bars 10µm. **C.** Periaqueductal gray matter. **D.** Colliculi. **E.** Pons part
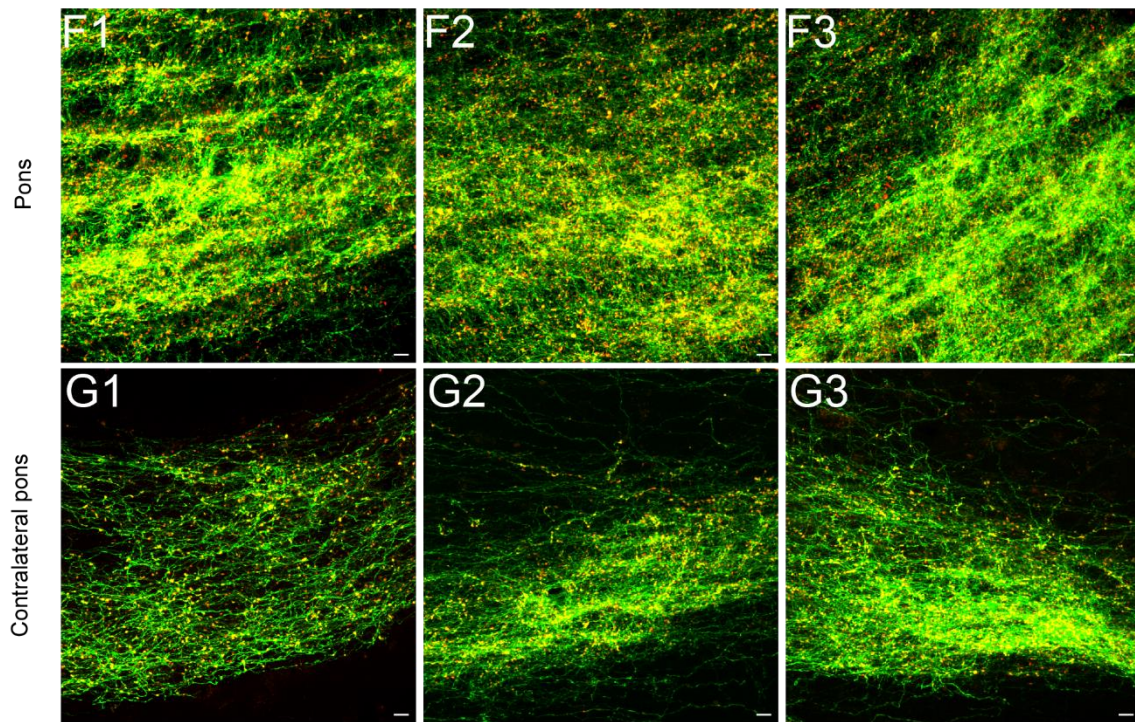
Fig. 28.2 | Brain mapping of the corticolumbar connectome | 6mm-9.0mm caudal to bregma
F and G. R Confocal pictures of a representative **(1)** healthy, **(2)** contused non-trained and **(3)** trained animal of the brain regions indicated in (B). In green is GFP marking axons, in red mRuby marking synapses. Scale bars 10µm. **F.** Pons. **G.** Contralateral pons.
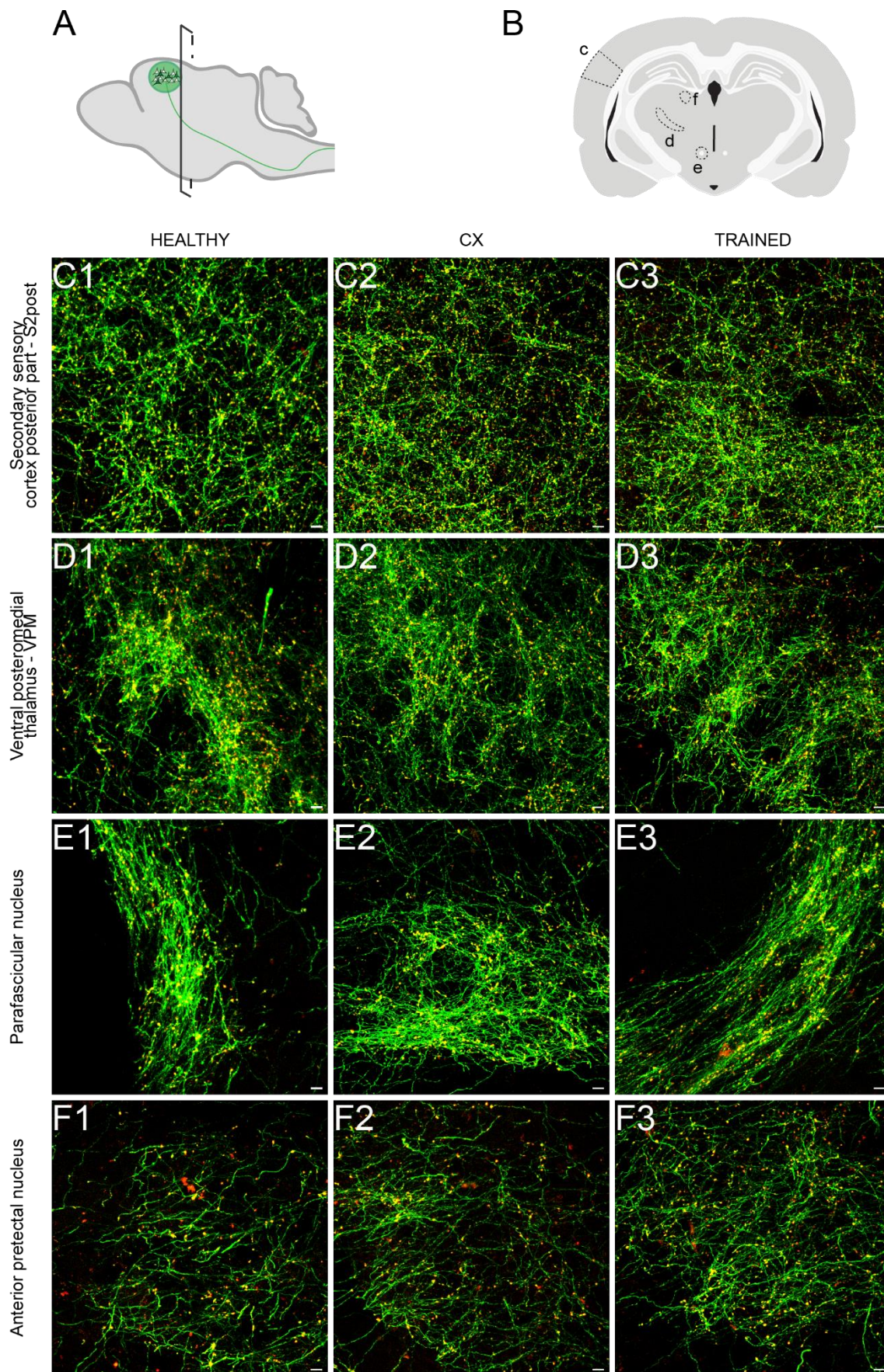

HEALTHY   CX   TRAINED
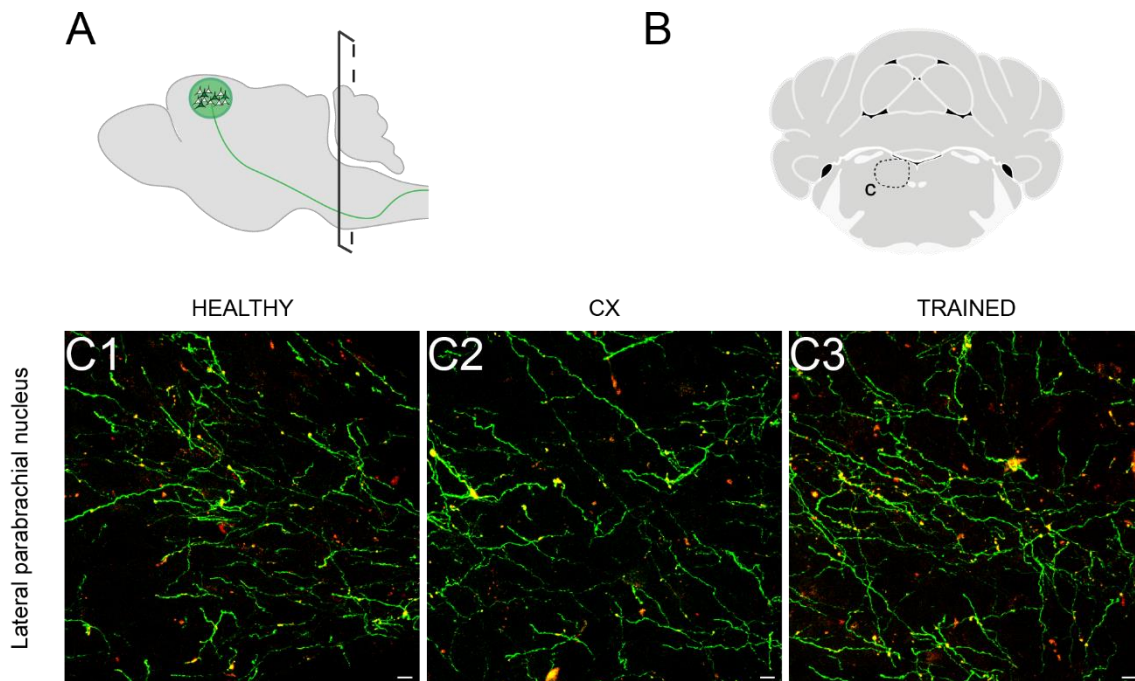
Fig. 29 | Brain mapping of the corticolumbar connectome | 9.2mm-9.8mm caudal to bregma
A. Schematic sagittal view of the brain, showing the approximate position of the coronal planes imaged. **B.** Scheme of the coronal plane imaged. Dashed contours represent the identified and imaged target areas of corticolumbar collaterals. **C.** Confocal pictures of a representative **(1)** healthy, **(2)** contused non-trained and **(3)** trained animal of the brain regions indicated in (B). In green is GFP marking axons, in red mRuby marking synapses. Scale bars 10µm.
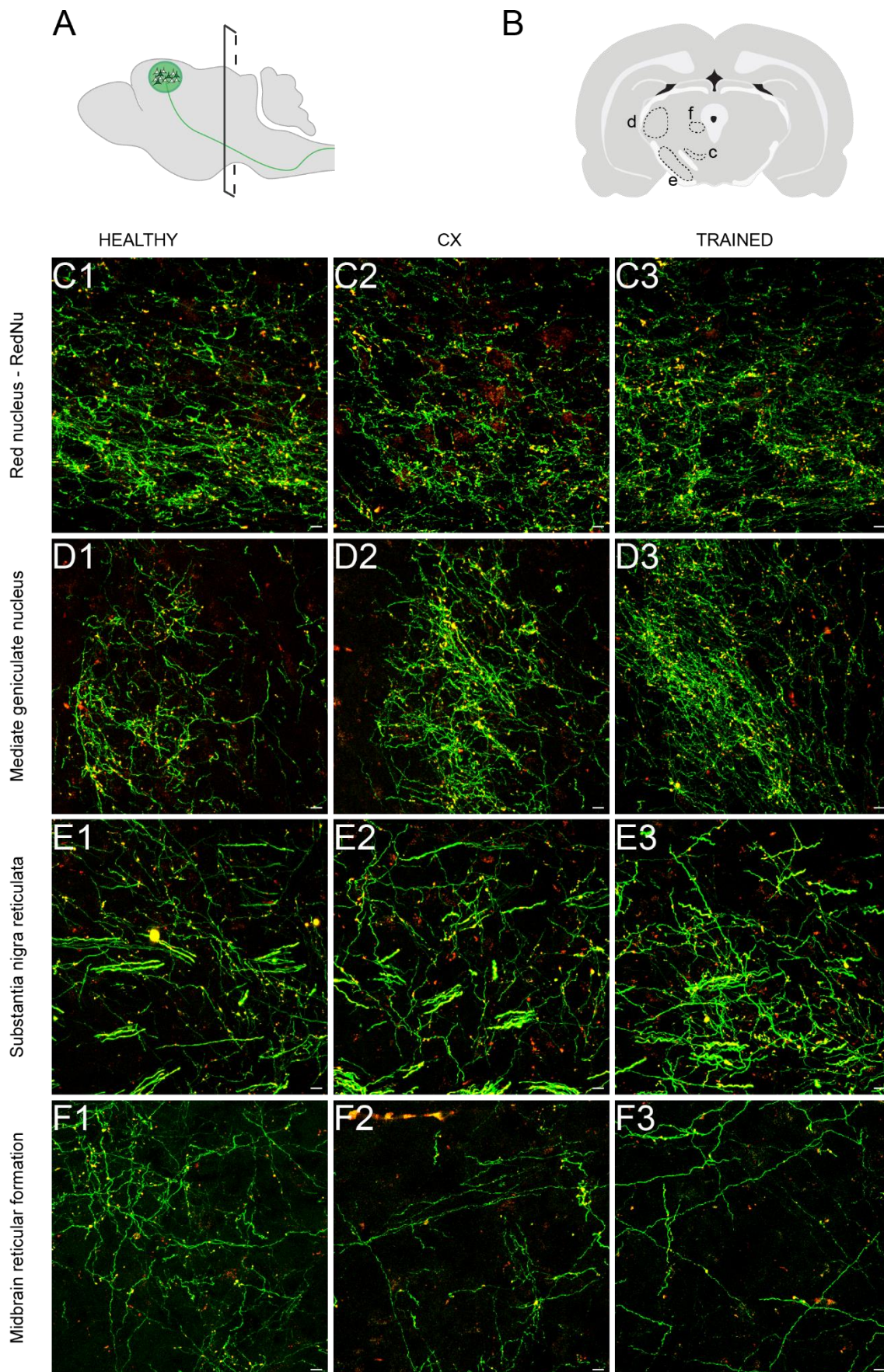
121
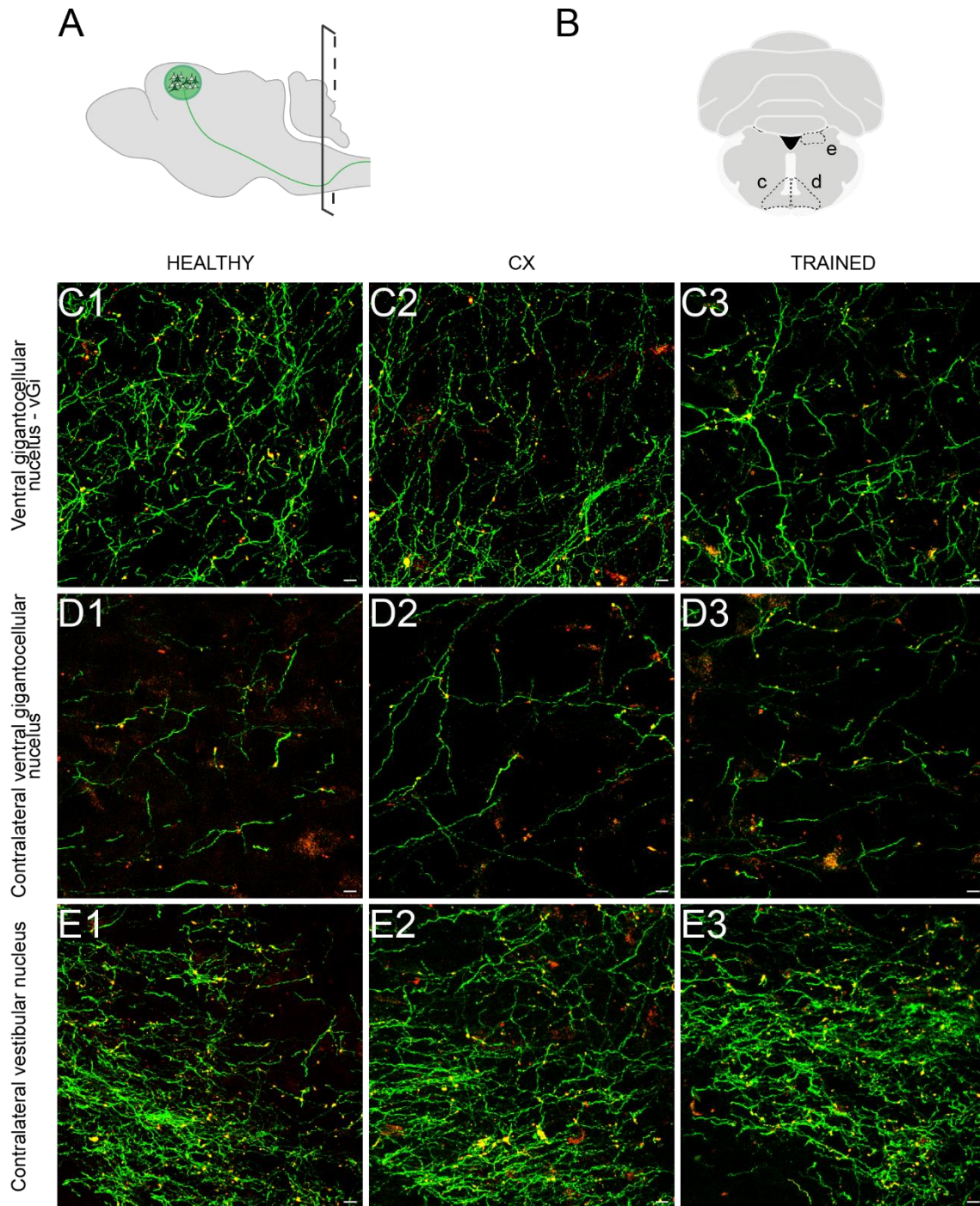
Fig. 30 | Brain mapping of the corticolumbar connectome | 10.0mm-14.0mm caudal to bregma
A. Schematic sagittal view of the brain, showing the approximate position of the coronal planes imaged. **B.** Scheme of the coronal plane imaged. Dashed contours represent the identified and imaged target areas of corticolumbar collaterals. **C, D and E.** Confocal pictures of a representative **(1)** healthy, **(2)** contused non-trained and **(3)** trained animal of the brain regions indicated in (B). In green is GFP marking axons, in red mRuby marking synapses. Scale bars 10μm. **C.** Ventral gigantocellular nucleus. **D.** Contralateral ventral gigantocellular nucleus. **E.** Contralateral vestibular nucleus.

Design of a pipeline for synapse quantification in brain target regions

Based on the previous brain screening, we selected 7 regions for corticolumbar collateral synapse quantification. We developed an in-house semi-automated pipeline based on ImageJ (National Institute of Health, USA) (Fig. 31):

- Step1: 5 stacked sections per target brain region were selected per animal. Depending on the rostro-caudal extent of the region, consecutive sections were separated of 120 or 240μm. Consistency across animals was ensured by checking anatomical landmarks.

- Step 2: Images of the synapses were acquired with the Zeiss LSM 880 laser confocal scanning microscope (20x objective), and tile scanning was used in order to ensure the full coverage of the region of interest (ROI).

- Step 3: Brain segmentation was performed by manual drawing on ImageJ, and area consistency across animals was ensured by reporting the ROI across animals on sections of corresponding rostro-caudal coordinate. Manual adjustment was then done to fit each anatomical section individually.

- Step 4: Image noise was removed using different methods depending on the brain region and the quality of the signal. In case of a background ramp in pixel intensity (see PAG), background subtraction was performed followed by a median filter. In case of strong cell autofluorescence (see vGi), a gray scale attribute filter was applied followed by a median filter. The fine adjustment and selection of image processing parameters was done manually on representative images and then reported to the whole batch of images for a single brain region.

- Step 5: Manual thresholding was applied, aided by visual comparison with the original acquisition image. In case of a previous gray scale attribute filter, this step enabled to remove aberrant signals of large pixel area, mainly originating from autofluorescent cells. The resulting image was binarized into a mask.

- Step 6: Optional shape filtering on the binarized image, enabling to remove aberrant signals of large pixel area. If the image was previously processed with gray scale attribute filtering, this step is redundant. The resulting image was binarized and the final pixel area was measured and cumulated over the 5 stacked images per animal.

In order to account for a possible variability introduced by viral injection, we quantified the pixel area of the corticolumbar tract at the level of the pyramids, following the same method. The total synapse area for each brain region per animal was normalized to the pixel area of the pyramids.
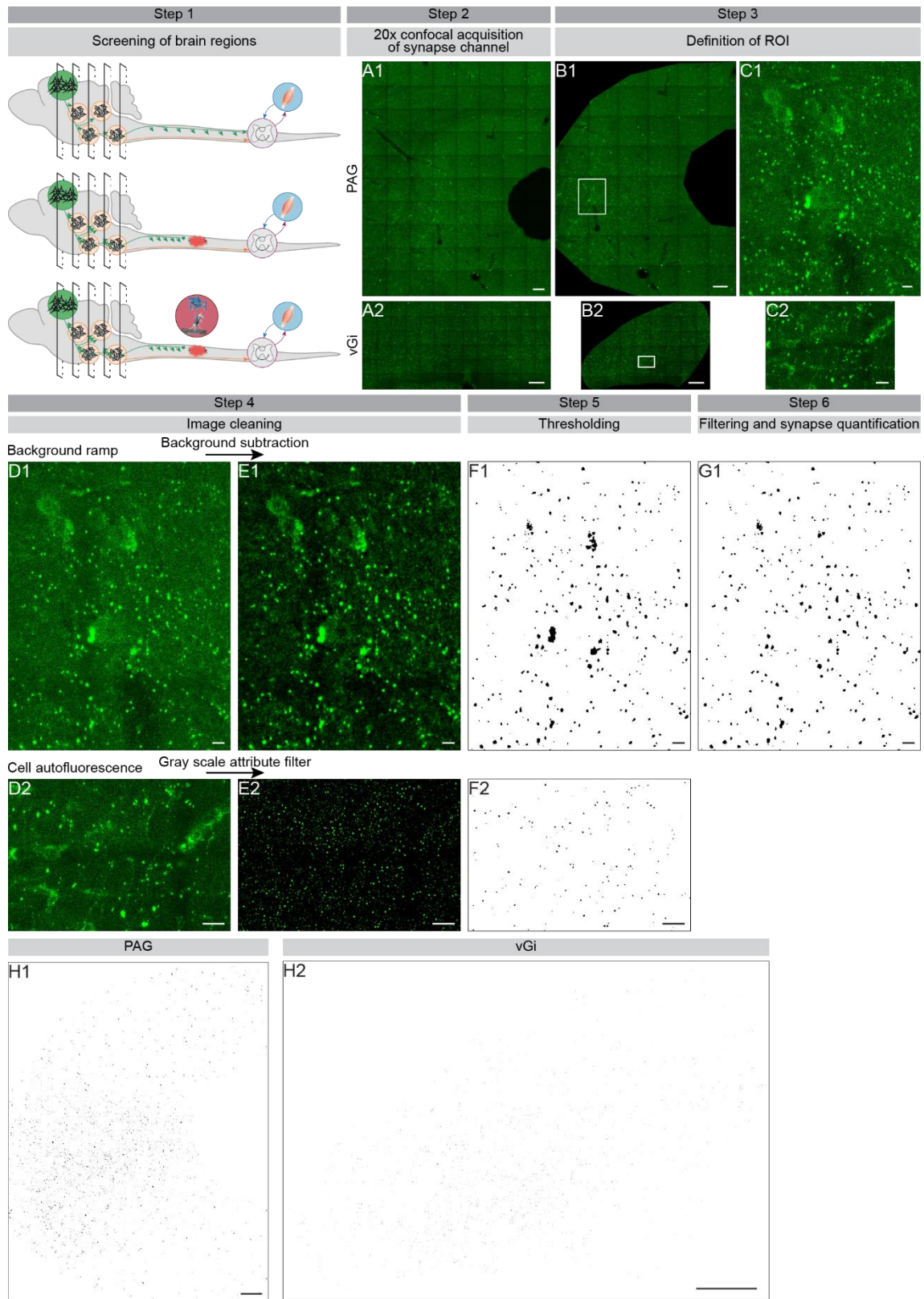
Fig. 31 | Pipeline for the semi-automated quantification of synapses in target brain areas
(Step 1) Schematic representations of the healthy, untrained and trained animal groups. **A-I.** For each step, (1) and (2) designate the successive images obtained after the processing of the original images (A), respectively (A1) PAG and (A2) vGi in a representative trained animal. **A, B, H, I.** Scale bars 100 µm. **A.** Confocal tile image of the brain region of interest. **B.** Image after manual drawing of the ROI and clearing outside. **C-G.** Scale bars 10µm. **C.** Higher magnification of the inset in (B). Scale bars 10µm. **D.** Higher magnification of (C). **E.** Resulting image after cleaning image noise by various filtering methods. **F.** Masks obtained after binarization of (E). **G1.** Mask obtained after shape filtering by size of pixel area (F1). **H.** Final mask obtained after completion of the full pipeline used for pixel area measurement.

The brain corticolumbar connectome is not affected by training

Corticolumbar synapses were quantified in the following brain regions: M1contra, S2ant, S2post, VPM, RedNu, PAG and vGi (Fig. 32). As only one animal was analyzed as a healthy control, conclusions cannot be drawn and merely further hypothesis can be formulated as of the effect of contusion. Furthermore, none of the following presented results are statistically significant, highlighting an important variability within each the two groups of contused animals.

The overall synapse area, normalized to the pyramids and cumulated on the 7 brain regions of interest was not different between the untrained and the trained group (ns, Mann-Whitney test) (Fig. 32A). Surprisingly, the contusion seemed to lead to a reduction in the density of corticolumbar collateral synapses in M1contra as well as S2post (Fig. 32B,D). We noted a tendency for an increase in synapse density in S2ant, VPM, PAG and vGi with the contusion, as well as in the VPM, RedNu, PAG and vGi with training in comparison to the untrained group.

These indicative yet inconclusive results regarding the neuroplasticity of the corticolumbar synapses in a selected subset of brain target regions need to be strengthened. The addition of healthy controls will enable to analyze the effect of contusion. Furthermore, both the untrained and trained groups would benefit from an increase in sample size, in order to mitigate the important intra-group variability.
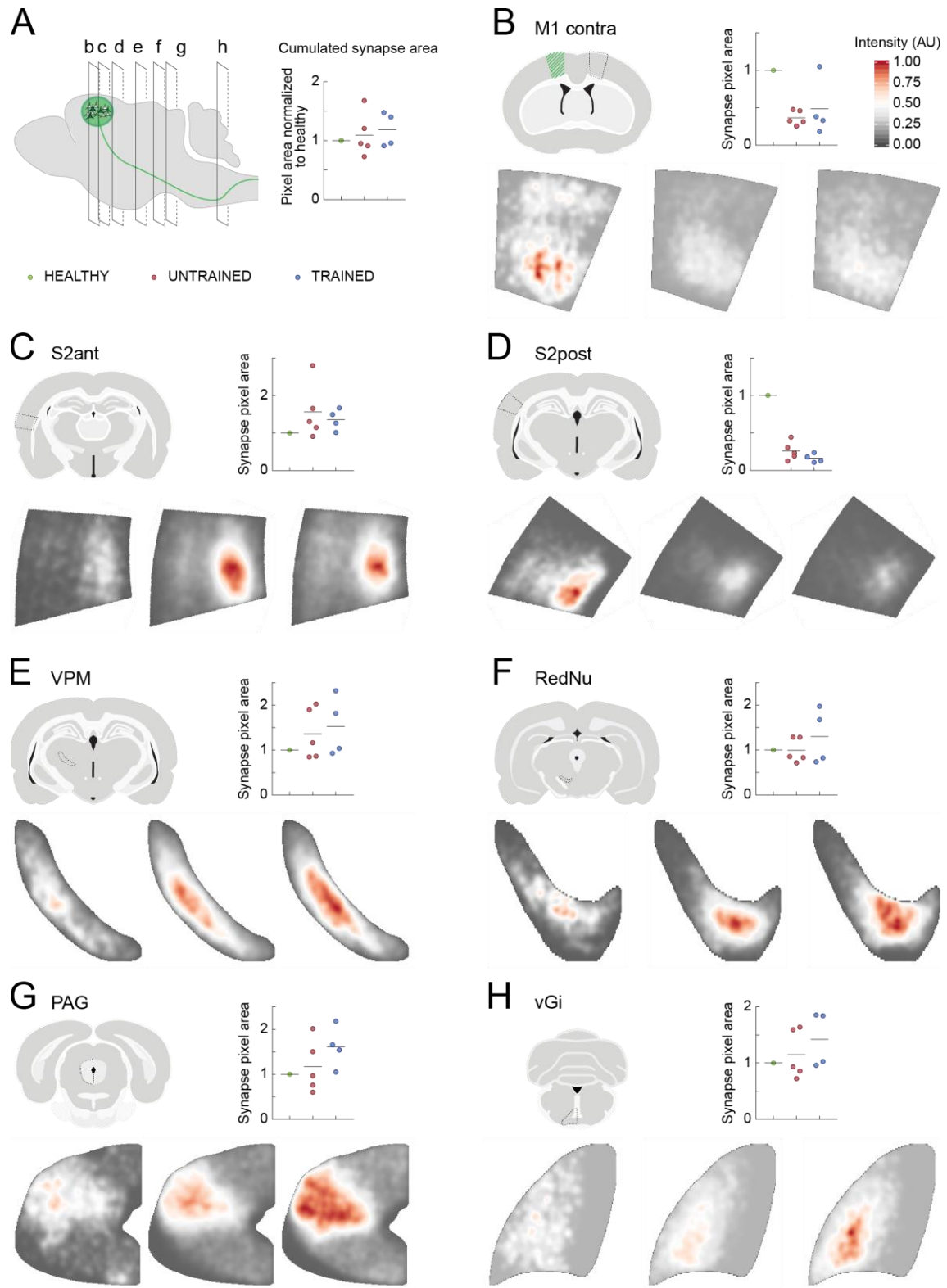
Fig. 32 | Quantification of the brain corticolumbar connectome
A. Schematic representation of a sagittal view of the brain, with the positions of coronal sections corresponding to (B-H). **A-H.** Graphs show the corticolumbar collateral synapse area normalized to the pyramids and cumulated over the 7 quantified brain regions (A) or for each quantified brain area (B-H), normalized to the healthy animal. Each dot represents one animal. **B-H.** Schematic representation of the coronal section corresponding to the quantified brain area (dotted contour). The three heat maps represent the spatial distribution of synapses on registered brain regions for the healthy animal (left), and averaged across animals for the untrained (middle) and trained (right) groups. ns, Mann-Whitney test.

126

6.3. Discussion

Plasticity of the spinal corticolumbar connectome with training

We have quantified and compared the density of corticolumbar collateral synapses in the spinal cord gray matter of intact, contused untrained and contused trained rats. The training led to a significant increase in the density of synapses in the thoracic spinal segments T4-T5 above the lesion. This effect was observed only in the animals which had received neuroprosthetic rehabilitation, corroborating previous findings of cortical fibers sprouting after a double hemisection in rats (van den Brand, Heutschi et al. 2012). The spatial distribution of these enriched corticolumbar collateral synapses in the thoracic spinal gray matter was conform to the pattern of projection in the intact animal, with the main target areas located in intermediate laminae, where most premotor neurons connecting to the lumbar spinal cord are located (Cowley, Zaporozhets et al. 2008, Sengul and Watson 2012, Ni, Nawabi et al. 2014). The possible sparing of propriospinal neurons across the lesion and their involvement in the amplification of the descending motor command after SCI needs to be further investigated. In turn, this would enable to assess the role of the evidenced corticolumbar collateral thoracic sprouting in regaining access to the lumbar spinal cord after injury (Bareyre, Kerschensteiner et al. 2004, Courtine, Song et al. 2008, van den Brand, Heutschi et al. 2012).

Generation of new data for the quantification of the intact brain CL connectome

Furthermore, we have performed an exhaustive brain mapping of the corticolumbar connectome in healthy, contused and trained rats, consistently identifying 24 regions of projection. The lack of a healthy control group is currently being addressed with the histological processing of three additional animals. Quantification and analysis of these new data will enable to ascertain the effect of contusion on the neuroplasticity of corticolumbar collaterals. In addition, some of the brain regions analyzed do display a very important intra-group scattering, such as the VPM, RedNu, PAG and vGi. To address this weakness, larger groups would be needed.

Absence of training effect on the brain corticolumbar connectome

We observed an absence of training effect on the density of corticolumbar collateral synapses in the brain and brainstem. This result was surprising in the light of the findings presented in the first chapter of this thesis (Asboth, Friedli et al. 2018). Indeed, we had noted a significant increase in cortical fibers in the vGi in the group of trained animals, which had led us to suggest that corticolumbar synapses would undergo the same drastic effect, thus being the major contributor to the cortico-reticulo-spinal relay enabling the recovery of leg motor control with training. We can invoke two possible explanations to this difference in outcomes: a methodological reason and a neuroanatomical reality.

First, we used different pipelines for the two quantifications, which can raise the question of consistency. Despite our best efforts to automatize the image processing, manual intervention of the experimenter cannot be bypassed. To control for this aspect, two different experimenters proceeded to the thresholding for two different brain regions. Although some slight differences were observed, they were not significant. For a same brain region, all quantifications across animals and groups were performed by the same experimenter for both studies, such as any possible individual bias would not impact the resulting data. This leads us to state confidence in the robustness and the consistency of the methods used.

Alternatively, the observed discrepancy in experimental outcomes may reflect a neuroanatomical reality. Indeed, in the study presented in chapter 1, animals had undergone a highly intensive training, enabling them to walk without the help of chemical stimulation. For the goal of the connectome quantification described in the present chapter, once animals reached the recovery of locomotion with electrochemical neuromodulation, training was not carried further. Thus, the intensity of training and the final level of motor performance of animals can be interrogated regarding their importance in neuroplasticity effects.

However, and most importantly, the lack of specificity of the anatomical tracing performed in the previous study, in contrast to our precise intersectional targeting strategy used here, leads us to hypothesize that the anatomical plasticity mediating the establishment of the cortico-reticulo-spinal relay is not driven by the corticolumbar neurons. While the axons traced in the previous experiment did originate in the leg area of the motor cortex, they might belong to a separate population of neurons, which lacks synaptic connections onto the lumbar spinal cord. Further circuit-level dissection, with anatomical labeling using intersectional strategies, will be needed to determine the precise nature of the possible alternative source of these corticofugal axons.

VII. Materials & methods

Table of contents

7.1. Animal procedures

7.1.1. Animals

Animal models

Experiments were conducted on adult female Lewis rats (180–220 g body weight, 14–30 weeks of age) and adult male or female C57BL/6 mice (15–35 g body weight, 12–30 weeks of age). Thy1::ChR2 (Jackson Laboratory 12350), Vglut2Cre (Jackson Laboratory 016963) and RosaTomato (Jackson Laboratory 07909) transgenic mouse strains were used and maintained on a mixed genetic background (129/C57BL/6). Housing, surgery, behavioral experiments and euthanasia were performed in compliance with the Swiss Veterinary Law guidelines. Animal care, including manual bladder voiding, was performed twice daily for the first 3 weeks after injury and once daily for the remaining post-injury period. All procedures and surgeries were approved by the Veterinary Office of the canton of Vaud and the Veterinary Office of the Canton of Geneva (Switzerland).

Experimental groups

For the cortico-reticulo-spinal relay study, the main group involved 16 rats that were randomly divided into an untrained (n=9) and a trained (n=7) group. One of the trained rats was excluded due to a lesion extent that substantially exceeded the mean variability of the rest of the group. For the calcium imaging study, the main group involved 11 rats that were randomly divided into an untrained (n=5) and a trained group (n=6). One of the trained animals was excluded from analysis because of an insufficient number of neurons identified in the field of view. Several recording sessions of another of the trained animal were excluded because of too important brain motion that could not be corrected.

For the corticolumbar connectome study, the main group involved 16 groups that were randomly divided into healthy (n=5), untrained (n=6) and trained (n=5). One of the trained rats was excluded after neuromorphological evaluation, due to the anatomical completeness of the lesion. 4 of the healthy rats and one of the untrained rats were excluded due to improper histological processing of the biological tissues.

7.1.2. Surgical procedures

Anesthesia

For all surgical procedures, animals were anesthetized with isoflurane inhalation (induction at 4.0-5.0%, sustaining at 1.0-2.0%). Prior to induction, the following premedication was injection subcutaneously: 0.03mL of Dorbene as a relaxant, and 0.03 ml qsp 0.5 ml NaCl 0.9% Rimadyl (Carprophen) as an analgesic and anti-inflammatory drug.

Spinal cord contusion

Under aseptic conditions and general anesthesia, a partial laminectomy was made at the midthoracic level (T9 vertebra). Contusion injury was applied using a force-controlled spinal cord impactor (IH-0400 Impactor, Precision Systems and Instrumentation LLC, USA). The applied force was set to 250 kdyn (1 dyn = 10 µN) in rats and 90 kdyn in mice. The spinal cord displacement induced by the impact was measured for each animal.

Implantation of epidural electrical stimulation (EES) electrodes

For positioning epidural stimulation electrodes in rats, a partial laminectomy was performed over spinal segments L2 and S1. Stimulating electrodes were created by removing a small part of the insulation (~400 µm notch) from Teflon-coated stainless steel wires (AS632, Cooner Wire, USA), which were subsequently secured at the midline overlying spinal segments L2 and S1 by suturing the wires to the dura. A common ground wire (~1 cm of Teflon removed at the distal end) was inserted subcutaneously over the right shoulder. All wires were connected to a percutaneous amphenol connector (Omnetics Connector Corporation, USA) cemented to the skull of the animal.

Implantation of chronic electromyographic (EMG) electrodes

Bipolar intramuscular electrodes (Cooner Wire; AS632 and AS632-1 for rats and mice, respectively) were inserted in muscles to record electromyographic (EMG) activity. For the study presented in the first chapter of this thesis, EMG electrodes were implanted bilaterally in the medial gastrocnemius (ankle extensor, in rats) or vastus lateralis (knee extensor, in mice) and tibialis anterior (ankle flexor). For the calcium imaging study presented in the third chapter of this thesis, EMG electrodes were implanted unilaterally on the right leg, contralateral to the brain implant, in the iliopsoas (hip flexor), semi-tendinosous (hip extensor and knee flexor), medial gastrocnemius (ankle extensor) and tibialis anterior (ankle flexor). All wires were connected to a percutaneous amphenol connector (Omnetics Connector Corporation, USA) cemented to the skull of the animal.

Virus production

Viruses used in this study were either produced locally or acquired commercially. The following plasmids were used: pCAG-FLEX-tdTomato, CMV-cre and pCAG-FLEX-synGFP (kindly provided by S. Arber), CMV-GFP (upon request), hSyn-DIO-hM4Di(Gi)-mCherry (Addgene, Plasmid #44362), hSyn-hM4Di(Gi)-mCherry (kindly provided by E. Bezard), CMV-rtTAV16 (kindly provided by T. Isa). AAV2/1 and AAV2/5 production was carried out in 293AAV HEK cells following standard procedures, yielding vector suspensions with the following titers: AAV2/5-CMV-cre (1.12E+14 VG/ml), AAV2/1-CMV-GFP (1.85E+13 VG/ml), AAV2/1-CAG-FLEX-tdTomato (6.5E+12 VG/ml), AAV2/1-CAG-SynGFP (6.5 E+12 VG/ml), AAV2/1-hSyn-hM4Di-mCherry (2.41E+13 VG/ml), AAV2/1-hSyn-DIO-hM4Di-mCherry (4.9E+12 VG/ml), AAV2/1-CMV-rtTAV16 (4E+12 VG/ml). Lentivirus production was carried out in HEK 293 T/17 cells to obtain the retrograde lentiviral vector HiRet-TRE-EGFP.eTeNT (titer 5E+9 VG/ml), carrying enhanced tetanus neurotoxin light chain (eTeNT) and enhanced GFP (EGFP) downstream of the tetracycline-responsive element (TRE). The following viruses were obtained commercially: AAV5-Syn.FLEX-GCaMP6m-WPRE.SV40 (UPenn Vector Core Facility, reference CS0603, titer 2.90E+13), AAV-DJ-hSyn-FLEX-mGFP-2 A-synaptophysin-mRuby (Stanford Vector Core Facility, reference AAV DJ GVVC-AAV-100, titer 1.15E+14 GC/ml) and AAV-pmSyn1-EBFP-Cre (Addgene, Plasmid #51507) together with the AAV2-retro helper52 (Addgene, Plasmid 81070, titer 4.2E+12 GC/ml). All flexed AAV vectors used in the present study showed transgene expression only upon Cre-mediated recombination. Injection volumes, coordinates and experimental purpose using these viruses are described specifically for each study.

Intraspinal injections

Tracer or virus delivery was performed through stereotaxic injections using high-precision instruments. Injections were performed using either glass pipettes driven with the Nanoliter pump (Nanoliter 2010 injector, World Precision Instruments) or the Hamilton injection system (for Fast Blue injections) at a rate of rate of 3nL/s. The needle was then held into place 2 min after the end of each injection, in order to prevent reflux with needle withdrawal.

Under isoflurane anesthesia, a partial laminectomy was performed over lumbar spinal segments. For Fast Blue tracings, rats received three injections of 200 nL separated by 1 mm at the following coordinates: 800 µm lateral of the midline and 1.2-1.5 mm below the dorsal surface of the spinal cord. For viral injections (Fig. 33A,B), rats received 6 injections of 250 nL separated by 1mm at the following coordinates, either unilaterally contralateral to the brain injections for tracing and calcium imaging experiments, or bilaterally for DREADD-mediated inactivation experiment: 0.65mm lateral from the midline and 0.8mm below the dorsal surface of the spinal cord. For mice, three injections of 200 nL Fast Blue or 100 nL AAV-retro-cre separated by 1 mm were performed. The injection coordinates were 200 µm lateral of the midline and -0.5 mm below the dorsal surface of the spinal cord.

Brain injections

Virus delivery was performed through stereotaxic injections using high-precision instruments. Injections were performed using either glass pipettes driven with the Nanoliter pump (Nanoliter 2010 injector, World Precision Instruments) at a rate of rate of 3nL/s. The needle was then held into place 2 to 3 min after the end of each injection, in order to prevent reflux during withdrawal. Viral delivery to the ventral gigantocellular (vGi) for tract-tracing and inactivation experiments was performed in rats and/or mice. Under isoflurane anesthesia, a craniotomy was performed over the brainstem medulla oblongata. Injection coordinates for mice were -5.6,-5.8 mm caudal, ±0.3 mm mediolateral to bregma and -5.6 mm ventral from the surface of the cerebellum (four injections total, 100 nL per injection, injected with a Nanoliter pump). Injection coordinates for rats were -11, -11.5, -12 mm caudal, ±1.5 mm mediolateral to bregma and 8.5 mm ventral from the surface of the cerebellum (six injections total, 250 nL per injection, injected with a Hamilton injection system).

In mice, coordinates for targeting the lateral vestibular nucleus were -4.6 caudal, ±1.25 mediolateral to bregma and -3.2 ventral from the surface of the cerebellum.

Viral delivery to the motor cortex was performed in rats and/or mice. Injection coordinates for mice were 0, -0.5, -1, -1.5 mm caudal, ±1, 1.5 mm mediolateral to bregma and -0.5 mm ventral from the surface of the brain (six injections per side, 100 nL per injection). Injection coordinates for rats in the cortico-reticulo-spinal relay and the corticolumbar connectome studies were -0.5, -1.5, -2.5 mm caudal, ±2,3 mm mediolateral to bregma and 1.45mm ventral from the surface of the brain (six injections per side, 250 nL per injection) (Fig. 33A). Injection coordinates for the calcium imaging studies were -1.1, -1.9 mm caudal, +2, +2.6mm mediolateral to bregma, and an additional injection site at -1.5mm caudal, +2.3mm mediolateral to bregma, and -1.45 ventral from the surface of the brain (5 injection sites, 250 nL/injection) (Fig. 11B).

Lens probe implantation

For the lens probe implantation in the motor cortex, the procedure is illustrated in detail in Fig. 12 and described step by step in the paragraph "Results" of the corresponding chapter (chapter 2, item 4.2.). Prism lens probe (P/N 1050-002184, later 1050-002203, NA = 0.36, working distance = 100-300µm, Inscopix, Palo Alto, USA) implantation was consistently performed on the left side, and coordinates were -1 to -2mm caudal (the face of the lens measures 1mm and is positioned in the sagittal plane), +2.65mm mediolateral to bregma, and -2mm ventral from the surface of the brain (Fig. 11B).

A Injection of viral construct

AAV-DJ

rAAV-Cre

Laminectomies
Caudal half of T13
Rostral half of L1

1mm

B Viral vectors and injection coordinates

	Full name	Origin	Titer (GC/mL)
AAV-DJ	AAV-DJ-hSyn-flex-GFP-Syn-mRuby	Stanford vector core	1.32E13
rAAV-Cre	rAAV2-pmSyn1-EBFP-Cre	Addgene	6.87 E12

	AP	ML	DV
MC	-0.5, -1.5, -2.5	+2, +3	-1.45
SC	Δ = 1	-0.65	-0.8

C Axon and synapse labelling with AAV-DJ viral vector

GFP   mRuby   Merge

Fig. 33 | Viral vector strategy to label axons and synapses for the study of the corticolumbar connectome
A. Schematic representation of the intersectional injection of viral constructs to label the collateral axons and synapses of corticolumbar neurons. Photograph during the surgical process, representing the position of injection sites relative to skull sutures. **B.** Specifications of viral vectors used and injection coordinates (in mm, relative to bregma) used for the AAV-DJ-mediated tracing **C.** Representative confocal images of the axons labelled with GFP (green), synapses with mRuby (red) and merge image in a coronal section of the periacqueductal gray matter in a contused animal. Scale bars 10μm.

Post-operative care

Analgesia (buprenorphine, Essex Chemie AG, Switzerland, 0.01–0.05 mg per kg, s.c.) was provided for 1 to 3 days after viral injections, spinal cord contusion, electrode implantations, or lens implantation, the duration of analgesia treatment being adapted according to the general state and recovery curve of the animal. Antibiotics (Baytril 2.5%, Bayer Health Care AG, Germany, 5-10 mg per kg, s.c. or Clamoxyl, Zoetis, France, 0.5mL per kg, s.c.) were provided twice a day for 5 days after respectively spinal cord contusion and electrode implantation surgeries.

Baseplate installation

3 to 4 weeks were left after the lens probe implantation in order to allow tissue stabilization and expression of the calcium indicator. The rat was anesthetized with isoflurane inhalation only and placed in the cranial stereotaxic frame. A baseplate was attached and secured with the baseplate screw onto the miniature microscope (nVistaHD, Inscopix, Palo Alto, USA), and the system was lowered above the lens until the correct focal distance, which enabled clear visualization of brain tissue. If fluorescence signals were visualized, the baseplate was fixed to the skull with Superbond (Super-bond C&B, Sun Medical, Shiga, Japan), using the two bigger screws (see lens implantation protocol) as additional anchors. Once the resin casted and the

baseplate was secured on the skull, the microscope was released by unscrewing of the baseplate screw, and a baseplate cover was attached in order to protect the lens form scratches and dirt.

7.1.3. Behavior

Neurorehabilitation procedure

Experiments with mice did not involve rehabilitation procedures.

The trained rats (n = 7 for the cortico-reticulo-spinal relay study, n=6 for the calcium imaging study, and n=5 for the corticolumbar connectome study) followed a comprehensive rehabilitation program for 2 months, starting 7 days after contusion, as described in detail previously (van den Brand, Heutschi et al. 2012). Briefly, rats were trained 5 to 6 days per week for 40 min per day. To reactivate lumbar motor circuits during training, we applied an electrochemical neuromodulation therapy consisting of a serotoninergic replacement therapy and epidural electrical stimulation (van den Brand, Heutschi et al. 2012). Five minutes before training, the rats received a systemic (i.p.) administration of quipazine (5-HT2A/C, 0.2–0.3 mg/kg) and 8-OH-DPAT (5-HT1A/7, 0.05–0.2 mg/kg) that was adjusted daily based on locomotor performance. Specifically, quipazine was adjusted to modulate extension components while 8-OH-DPAT was adjusted to modulate flexion components of the gait pattern. During training, continuous epidural electrical stimulation (0.2 ms, 100-300 µA, 40 Hz) was delivered through L2 and S1 electrodes. Training was conducted bipedally on a treadmill (11 cm/s) with adjustable robotic body weight support against gravity (Robomedica, USA). Starting 2 weeks after injury, rats were additionally trained over ground with the robotic bodyweight support system (Dominici, Keller et al. 2012). The content of each training session evolved with the actual capacities of the rats and training objectives. Positive reinforcement was used to encourage the rats to perform the tasks. The experiments and procedures are summarized in Supplementary Fig. 1.

Behavioral testing of leg motor control

For the cortico-reticulo-spinal relay study, leg motor control was evaluated in mice in different testing conditions 4 weeks after spinal cord contusion. In rats, leg motor control was evaluated on a treadmill, along a straight runway with or without robotic assistance, up a ladder, up a staircase (4 steps) and during swimming across a straight pool of water. Rats participated in two sets of behavioral evaluations, at 1 (subacute) and 9 (chronic) weeks post-injury. They were tested in different experimental neuromodulation conditions. To ensure that the specificity of the task was not responsible for their incapacity to initiate and sustain locomotion, untrained rats practiced locomotion with the robotic postural interface for about 10 min per day during 5 sessions before behavioral recordings.

Motor-evoked potentials

We measured evoked potentials in ankle flexor muscles in response to short light pulses in the motor cortex (10 ms pulses, 15-20 mW light power, 475 nm) of *Thy1::ChR2* mice crossed with *Vglut2^Cre* mice that received AAV2/1-hSyn-DIO-hM4D-mCherry injections in the vGi (Fig. 7c). Motor evoked potentials were measured at different time points and different experimental conditions: before contusion and every week after contusion (until maximum 40 days), with CNO i.p. injection or without CNO injections to evaluate contribution of vGlut2^{ON} vGi neurons to the measured motor evoked responses. Animals were awake and held still during motor cortex activation. EMG recordings were synchronized with the stimulation onset using custom-developed Tucker-Davis Technology code. Analysis was performed in Matlab. The EMG signal was rectified, filtered (Savitzky-Golay smoothing filter) and summed. Signals with movement artifacts were excluded. Only animals with chronic stable EMG were included in this experiment. The root mean square of the EMG envelope was quantified for each motor evoked potential and averaged for each animal (n = 4 mice) over 10 repetitions.

Optogenetic experiments

Mapping of the motor cortex region was performed acutely using the following coordinates: 0 to -2.5 anteroposterior and 0 to ±2.5 mediolateral from bregma with incremental steps of 0.5 mm. The mapping was performed in *Thy1::ChR2* transgenic mice (Wang, Peca et al. 2007) under ketamine-xylazine anesthesia. The animal's head was fixed in a stereotaxic frame. Bipolar electrodes were implanted in the tibialis anterior and medial gastrocnemius muscles to record muscle activity. A craniotomy was then performed over the targeted area. A laser (Laserglow, 473 nm Blue DPSS Laser System) transmitted blue light through an optic fiber (200 µm core diameter, 0.22 NA, Thorlabs) that was held in a 1.25mm ferrule at the surface of the dura matter. Light stimulation was delivered over 3 s and consisted of 10ms-long pulses delivered at 40 Hz. The evoked leg muscle activity was filtered (bandpass 10-500 Hz), rectified and summed for each stimulation spot of the mapping grid. Measures were normalized to the maximum value recorded for each animal.

For chronic experiments, optic fibers were implanted in the right and left motor cortex using the coordinates of the hotspot identified during the mapping experiments (-1 mm anteroposterior, -1.5 mm lateral, -0.5 mm ventral). The ferrule was fixed with dental cement. Light was transmitted to the brain through a ferrule-to-ferrule connection cable. Intensity of blue light stimulation was estimated to range from 8 to 45 mW/mm^2 at -0.5 mm under the tip of the fiber (estimation based on the brain tissue light transmission calculator, open access from the Deisseroth laboratory, https://web.stanford.edu/group/dlab/cgi-bin/graph/chart.php). Laser pulses were driven by an external stimulator (A-M Systems) to ensure precise control of stimulation features. Responses to light were tested 4 days after fiber implantation to ensure the quality of the implant. Yellow light stimulation (Laserglow, 589 nm Yellow DPSS Laser System) was delivered during control experiments to verify that the behavioral effects were specifically related to the modulation of motor cortex neurons expressing ChR2 with blue light, thus excluding potential heat effects.

The latency between motor cortex activation and the onset of locomotion was measured as the time between the onset of light stimulation and the first step, defined from a threshold set as 5% of the maximum value of the vertical foot elevation. The cessation of locomotion was measured as the time between the end of light stimulation and the 10% crossing of the filtered hip velocity profile. A total of 3 to 5 trials were averaged per mouse and statistics were performed on the mean of all animals (n = 6 mice, Supplementary Fig. 6a,b).

Body tilting was measured geometrically on static images of the recorded videos, taken immediately before and after stimulation, using a customized Matlab script. Analysis was performed blinded. A total of 3 to 5 trials were averaged per mouse and statistics were performed on the mean of all animals (n = 6 mice, Supplementary Fig. 8, Step 4).

DREADD-mediated inactivation experiments

To reversibly silence glutamatergic neurons in regions of interest, we used virally mediated expression of an engineered G-protein-coupled receptor exclusively activated by the otherwise inert drug-like small molecule clozapine N-oxide (CNO) (Roth 2016). In Thy1 ChR2::Vglut2Cre mice, AAV2/1-hSyn-DIO-hM4Di-mCherry was injected bilaterally in the vGi or in the lateral vestibular nuclei (coordinates provided above). First behavioral evaluations were performed 2 to 3 weeks after virus injection. Testing was performed 20 to 50 min after i.p. injection of CNO (5 mg/kg of body weight, diluted in saline). Experiments were performed blinded (saline or CNO injections were randomly distributed over both experimental days). The number of neurons expressing hM4Di (mCherry) was evaluated post-mortem in the region of interest and the spread of infection to neighboring regions is reported for all experimental animals. The reconstruction of the 3D volume containing hM4Di-expressing neurons was performed with Neurolucida software. Four mice were excluded from the experiment due to off-target injections.

In rats, a non-flexed DREADD virus (AAV2/1-hSyn-hM4D-mCherry) was injected bilaterally to the motor cortex (coordinates given above). A total of 4.5 μl was injected per side. Swimming performance was evaluated 40 to 60 min after CNO i.p. injection (5 mg/kg of body weight).

Double virus-mediated inactivation experiments

We reversibly prevented synaptic release from vGi neurons with projections to lumbar segments using a double virus construct (Supplementary Fig. 10) (Kinoshita, Matsui et al. 2012). We first placed four injections of 250 nL of HiRet-TRE-EGFP.eTeNT per hemicord in spinal segments L2/L3 (coordinates described above). Fourteen days later, rats received six injections of AAV2/1-CMV-rtTAV16 bilaterally in the vGi (300 nl per injection, coordinates given above). AAV2/1-CMV-rtTAV16 encodes the Tet-on sequence, a variant of the reverse tetracycline transactivator (rtTAV16) under the control of the cytomegalovirus (CMV) promoter. Seven days after the second injection, the administration of doxycycline was initiated to induce the expression of eTeNT. Doxycycline was administered i.p. (10 mg/kg of body weight) using saline solution as a vehicle. Trained rats (n = 5) were tested overground under robotic assistance and electrochemical

neuromodulation before doxycycline administration (baseline), during doxycycline administration (5 days after initiation), and 7 days after the cessation of doxycycline administration. Doxycycline was administered a second time during the 5 days before death to ensure expression of EGFP in inactivated neurons. In all experimental rats, we counted the number of neurons expressing EGFP throughout the brainstem and reconstructed the double-infected neurons in the rat brain template using Neurolucida. Three rats were excluded from the experiment because post-mortem analysis showed off-target virus injections.

Kinematic, kinetic and muscle activity recordings

All procedures used have been detailed previously (Dominici, Keller et al. 2012, van den Brand, Heutschi et al. 2012, Takeoka, Vollenweider et al. 2014). During both treadmill and over-ground conditions, bilateral leg kinematics were captured using the Vicon high-speed motion capture system (Vicon Motion Systems, UK), consisting of 12 infrared cameras (200 Hz). Reflective markers were attached bilaterally at the iliac crest, the greater trochanter (hip joint), the late,ral condyle (knee joint), the lateral malleolus (ankle), the distal end of the fifth metatarsophalangeal joint and, for the rats, the tip of the fourth toe. The body was modeled as an interconnected chain of rigid segments, and joint angles were generated accordingly. Ground reaction forces were recorded using a biomechanical force plate (2 kHz; HE6X6, AMTI, YSA) located below the treadmill belt or in the middle of the runway. Electromyographic signals (2 kHz) were amplified, filtered (10–1,000 Hz bandpass), stored, and analyzed offline to compute the amplitude, duration and timing of individual bursts. For both the left and right legs, 15 step cycles were extracted randomly over several trials on the runway for each rat under each experimental condition and time points. A 20-s interval was used when no or minimal leg movements were observed.

During swimming, leg kinematics were captured by two Basler cameras (100 Hz; Basler Vision Technologies, Germany). Black dots were drawn on the shaved skin over the same anatomical landmarks on both legs. Leg movements were reconstructed as a virtual segment connecting the iliac crest and the metatarsophalangeal joint marker. KinemaTracer (Kissei Comtec Co., Japan) motion tracking software was used to obtain 2D coordinates of hindlimb movements. Electromyographic signals were recorded concomitantly to video acquisition.

Calcium recordings in freely-moving rats

For imaging sessions, the baseplate screw was untightened to release the baseplate cover, and the nVista miniscope (Inscopix, Palo Alto, CA, USA. Objective lens NA = 0.5, FoV 650 μm x 900 μm, CMOS sensor 1280 x 800 pixels) was positioned in the baseplate, then secured by tightening the screw. The animal was awake during this process and minimally constrained to ensure immobility without inducing unnecessary stress. On the first day of imaging, the turret of the miniscope was adjusted for precise adjustment of the focal plane. To ensure imaging the exact same focal plane in each animal over multiple days, a static overlay of the FoV on the first recording session was used to daily align the FoV. Calcium movies were recorded using the nVista acquisition software (Inscopix, Palo Alto, CA, USA) and externally triggered

by a TTL pulse sent by the Vicon system (Vicon Motion Systems, UK) for synchronization with the acquisition of behavioral, kinematic and EMG. Calcium movies were acquired at a rate of 20 frames per second, with a LED power of 1.6 mW/mm^2 (excitation wavelength 475 ± 15 nm).

7.2. Histological analyses

7.2.1. Preparation and processing of biological tissue

Perfusion and histological tissue preparation

At the end of the defined experimental period (and ensuring a minimum of 50 days for spinal tracings in rats) rats and mice were deeply anesthetized by an i.p. injection of respectively 0.5 or 0.8mL Pentobarbital-Na (50mg/mL), and then transcardially perfused with respectively 80 or 250mL PBS solution containing 100'000IU/L heparin (Liquemin, Roche, Switzerland), followed by 250mL of cold 4% phosphate buffered paraformaldehyde, pH 7.4. The brain and spinal cord were dissected out and postfixed overnight in the paraformaldehyde solution.

For further histological treatment, tissues were transferred to 30% sucrose in phosphate buffer for cryoprotection for 3 nights, then embedded in Tissue Tek O.C.T. (Sakura Finetek Europe B.V., The Netherlands), frozen at -54° using a Snapfrost (SF_II, Excilone, France) and cut to a thickness of 40 µm on a cryostat. In case of further tissue clearing, the samples were transferred to 0.1 PBS after post-fixation

Immunohistochemistry

All antibodies used in this study were obtained commercially and have been validated with positive and negative controls for each experiment. Mounted or free-floating sections (40 µm) were washed three times in 0.1 M PBS and blocked in 5% (5HT, NeuN) or 10% (GFAP, GFP) normal goat serum containing 0.3% Triton. Sections were then incubated in primary antibody diluted in the blocking solution overnight at 4 °C (GFAP, NeuN) or at room temperature (GFP, 5HT), or 3 nights at room temperature (glutamate). Primary antibodies used were rabbit anti-GFAP (1:1,000, Dako #Z0334, USA), anti-5HT (1:5,000, Sigma Aldrich #S5545, Germany), anti-glutamate (1:1,000, Sigma #G6642, USA), mouse anti-NeuN (1:300, Chemicon #MAB5262, Millipore Corporation, USA), chicken anti-GFP (1:500, Life Technologies #A10262, USA), goat anti-ChAT (1:500, Chemicon #AB144P, Temecula, CA, USA) and rabbit anti-PKC gamma (1:500, Santa Cruz Biotechnology #sc-166385, Santa Cruz, USA). Sections were again washed three times in 0.1 M PBS and incubated with the appropriate secondary antibody (Alexa Fluor 488 goat anti-rabbit #A11034, goat anti-mouse #A11001, goat anti-chicken #A11039, donkey anti-goat #A11055; Alexa Fluor 555 goat anti-rabbit #A21428, goat anti-mouse #A21422, goat anti-chicken #A21437; or Alexa Fluor 647 goat anti-rabbit #A21245, goat anti-mouse #A21235; Molecular Probes, Life Technologies, USA) in blocking solution.

The Tyramide System Amplification (TSA)-Cyanine 3 kit (PerkinElmer NEL744001KT, USA) was used to visualize BDA-labeled fibers. Sections were first washed and endogenous peroxidase activity was quenched by 30 min incubation in 0.1% H2O2. After overnight incubation at 4 °C with streptavidin–horseradish peroxidase (1:200) in 0.1 M PBS-Triton (1%), sections were again washed and incubated in TSA cyanine 3 (1:100) for 45 s (spinal cord sections) or 3 min (brainstem sections), respectively. NeuroTrace (Life Technologies #N21482, USA) was used as a Nissl counterstain at a dilution of 1:50 in 0.1 M PBS. Slides were finally washed, air-dried and cover slipped with Mowiol.

CLARITY and 3D image acquisition

Tissues were cleared using CLARITY (Chung, Wallace et al. 2013). Mice were perfused with 4% PFA as previously described and tissue was postfixed overnight in 4% PFA. Tissue was then transferred to a bis-free acrylamide solution (with 4% PFA) for 2 d at 4 °C, allowing diffusion of the hydrogel solution into the tissue. For the polymerization process, the brain or spinal cord were entirely immersed in bis-free acrylamide solution. Tubes were flushed with nitrogen gas for a couple of seconds and immediately closed to remove oxygen and were submerged in a 37 °C water bath for 3 h or until the solution had polymerized. The gel was then carefully removed and tissue was immersed in an SDS solution (clearing solution) which was changed every day for 4 d after the polymerization process. For active clearing, we used the X-Clarity Tissue clearing system developed by Logos Biosystems. A clearing solution was continually circulated through an adequate chamber with precise conditions: 37 °C temperature, 1.5 A current, 30 r.p.m. pump speed. The clarification process lasted 10–12 h for the spinal cord and 8 h for the brainstem.

Prior to imaging, the sample was washed with 0.1 M PBS + 0.1% Triton overnight and then placed in Histodenz 24 h before imaging (0.02 M PB, 0.1% Tween-20, 0.01% azide, pH 7.5). Fluorescence imaging of CLARITY samples presented in Fig. 6 was performed using a light-sheet fluorescence microscope (Carl Zeiss LSFM Z.1, Zena, Germany) with a Fluar 5× objective lens. We used a customized sample holder to immerse the mouse spinal cord or half brains in a chamber (adapted to a 5× objective) filled with Histodenz. Each plane was illuminated from the right and the left side.

To image whole brains including a part of the spinal cord at high spatial resolution (lateral resolution ~0.3 µm, axial resolution ~5 µm, with a 4× objective), we used a custom-made light-sheet microscope optimized to image labeled clarified tissue (Fig. 4e-g). The design of this microscope has been published (Tomer, Ye et al. 2014). Briefly, the sample is illuminated by two digitally scanned light sheets coming from opposite directions. Emitted fluorescence is collected by high-numerical-aperture objectives (Olympus XLSLPLN25XGMP N.A. 1.0, XLPLN10XSVMP N.A 0.6 or XLFLUOR4X N.A. 0.28), filtered (Brightline HC 525/50 and 609/54, Semrock) and imaged on an Orca-Flash4.0 LT digital CMOS camera at a frequency ranging between 5 and 10 fps. A self-adaptive positioning of the light sheets across z-stacks acquisition ensures optimal image quality over up to 1 cm of tissue. Images were reconstructed

in 3D using the Grid Collection Stitching plugin tool in Fiji or TeraStitcher (BMC Bioinformatics, Italy). Volume reconstructions (brain, spinal cord and lesions) were performed using the Surface tool from Imaris.

7.2.2. Histological evaluations

Evaluation and quantification of the spinal cord contusion

The extent and location of spinal cord damage was evaluated in each contused experimental animal. The lesion cavity was cut in serial coronal sections (40 µm) that were stained using GFAP and Nissl antibodies. For 3D vizualisation, the entire extent of the lesion cavity was reconstructed in 3D using Neurolucida (MBF Bioscience, USA). The maximal projection surface was generated for each rat and mouse to visualize the spared white and gray matter regions. For each lesion in the cortico-reticulo-spinal study, we calculated the spared spinal cord surface with respect to the distance from the epicenter of the lesion, the spared area at the epicenter, and the total volume of damaged spinal cord tissue.

The percentage of spared tissue at the epicenter was calculated using Fiji and normalized using the mean surface of sections rostral and caudal to the contusion, taking into account the compression of the spinal cord.

Neuromorphological quantification

For the cortico-reticulo-spinal relay study, fiber density (GFP, tdTomato) was measured using 3 to 5 confocal image stacks per region (vGi, T12 spinal cord, L4 spinal cord) per animal (Fig. 6). Images were acquired with standard imaging settings and analyzed using custom-written Matlab (MathWorks, USA) scripts according to previously described methods (van den Brand, Heutschi et al. 2012). Confocal output images were binarized by means of an intensity threshold and divided into square regions of interest (ROI). The investigator was blinded during intensity thresholding. Densities were computed within each ROI as the ratio of traced fibers (number of pixels) per ROI area. Image acquisition was performed using a Leica TCS SPE or Zeiss LSM 880 laser confocal scanning microscopes and stacks were processed offline using Imaris software (Bitplane, USA) and ImageJ (National Institute of Health, USA).

Fast Blue cell bodies projecting to the site of injections were identified in the brain, brainstem and spinal cord (cortex, brainstem, cervical C1-C8 and thoracic T1-T6 segments) and reconstructed in rat or mouse templates using Neurolucida software (MBF Biosciences, USA). Templates were reconstructed using the Allen Brain Atlas and Nissl stained coronal brain or spinal cord sections evenly spaced. The data were imported into AMIRA software to generate 3D representations.

To determine spatial enrichment of synapse density in the lateral horn of the spinal cord, we implemented a custom image analysis pipeline that allows to preprocess, trace, register and combine a large amount of images from histology. Briefly, we implemented preprocessing and manual tracing of horns in ImageJ (National Institute of Health, USA), then post-processing, registration and image summarization in R, using image analysis package imageR and medical

image registration package RNiftyReg. We quantified 3 sections per spinal segment and per animal. To determine spatial enrichment of synapse density in brain regions, we implemented a custom image analysis pipeline based developed on ImageJ (National Institute of Health, USA), which is described in detail in the corresponding section of chapter 4 of this thesis (chapter 3, item 6.2, Fig. 31). We quantified 5 stacked sections per brain area and per animal. The resulting spinal and brain synapse areas were further normalized to the pixel area of the corticolumbar tract at the pyramids for each animal. Area values were then averaged per spinal segment or brain region and per animal. For the representation of the spatial distribution of synapses, thresholded images were averaged across animals in each group.

7.3. Data analysis

7.3.1. Behavioral data analysis

Analysis of kinematic, kinetic and muscle activity

A total of 104 (for mice) and 129 (for rats) parameters quantifying kinematics, kinetics and muscle activity features were computed for each leg and each gait or stroke cycle according to methods described in detail previously (Dominici, Keller et al. 2012, van den Brand, Heutschi et al. 2012). All parameters are reported in Supplementary Table 2. To evaluate differences between experimental conditions and groups, as well as the most relevant parameters to explain these differences, we implemented a multistep statistical procedure based on PC analysis (Dominici, Keller et al. 2012, Takeoka, Vollenweider et al. 2014). PC analyses were applied to data from all individual gait cycles or swim strokes for all rats together. Data were analyzed using the correlation method, which adjusts the mean of the data to 0 and the s.d. to 1. This method of normalization allows the comparison of variables with disparate values (large vs. small values) as well as different variances. The various steps, methods, results and interpretation of the analysis are detailed in Supplementary Figs. 1 and 3.

Behavioral data segmentation

In order to select appropriate data and rule out any bias induced by the experimenter or uncharacterized behavior of the animal, all behavioral videos where viewed and frames were manually cut out in case of interaction of the experimenter on the lower half of the animal body, of animal moving in a non-straight fashion, grooming, or any other unpredicted or unclear behavior (cables pulling, falls, hesitant locomotion…). The remaining frames were further marked by the experimenter as resting and walking periods.

7.3.2. Analysis of calcium recordings

Preprocessing of calcium recording movies

Calcium videos were pre-processed with the Inscopix Data Processing Software (Inscopix, Palo Alto, CA, USA). All calcium movies of one session were imported and concatenated into a single time series. Movies were corrected for defective pixels ansd spatially binned by a factor 2. Aberrant frames with loss of focus and/or excessive brain motion were trimmed out. A spatial bandpass was applied (0.005 pixel^{-1}-0.5 pixel^{-1}). Lateral brain movement was then corrected with the integrated motion correction algorithm (Thevenaz, Ruttimann et al. 1998), where the first frame of the movie was selected as a reference for shifting each individual frame in X and Y to match contrast features. The pixel values were then normalized by generation of $\Delta F/F_0$, where F_0 is the mean frame calculated over the whole movie.

Several recording sessions of two animals of the trained group were excluded because of important brain motion that could not be corrected.

Field of view similarity score

Calcium movies were projected according to pixel maximal values. To compute the similarity index between two movies, we used a 2-dimensional matched filter method. Each pixel of the first projection image was multiplied by the corresponding pixel of the second projection image. The similarity score was obtained by summation of the result over the whole image. To account for possible shifts and rotations between the two projection images, this process was performed for all possible shifts in X and Y and all possible rotations. The final similarity score was the maximal value obtained across all possible translations and rotations.

Cell identification

For the detection of cells from calcium movies and extraction of the corresponding spatial footprints and activity traces, we applied CNMF-e (Zhou, Resendez et al. 2018) for one-photon microendoscopic data. Thresholds on the minimum local correlation and the minimum peak-to-noise ratio (PNR) for detecting seed pixels were determined in each session separately. Following the first initialization step, the background component was updated and missing neurons were selected from the residual using a second greedy component initialization step. Next, CNMF-e was applied for four iterations of updating model variables (spatial footprints, temporal activity and background activity). The first three iterations were performed automatically. Manual interventions (e.g. merging/deleting components) were integrated before the last iteration.

After detection, cells were further selected based on their radius and circularity. The spatial footprint of each detected cell was normalized to its maximal value, then filtered with a threshold set at 0.6. The length of the resulting long and short axes were measured and the cell radius was set as half of the average of this bidirectional measure. Neurons with a radius

smaller than 3 pixels or larger than 30 pixels, as well as neurons with abnormal shape (circularity < 0.5) were deleted. For the analysis of neuronal activity, cell traces were normalized using a z-score, and population activities were calculated by averaging across cells for each animal.

One of the n = 6 trained animals was excluded from analysis because of an insufficient number of neurons identified.

Cell classification

Based on the behaviorally marked movement and rest periods, we extracted 1s movement and rest epochs from the calcium data using a 50ms sliding window. The average activity of each neuron i during movement epochs $C_{mov,i}$ and rest epochs $C_{rest,i}$ was calculated. The discriminant score of each neuron was calculated as follows:

$$DS_i = \frac{mean(C_{mov,i}) - mean(C_{rest,i})}{std(C_{mov,i}) + std(C_{rest,i})} \ .$$

Based on the population distribution for each recording session, neurons with a discriminant score above the 90 percentile of the distribution were classified as movement-active, while those with a discriminant score below the 10 percentile were classified as rest-active. Among the cells that were not classified as movement-tuned, those with both an average ΔF/F and a spike rate above the 5 percentile of the classified cells were classified as indiscriminately active. The rest of the cells were classified as silent.

Cell registration

Cell images of all sessions were adjusted to the same size by adding the necessary number of pixels in X and Y. We then used the TurboReg (Thevenaz, Ruttimann et al. 1998) image registration algorithm to align the cell projection map of each session to a reference through linear and non-linear transformation. Each neuron's spatial footprint was then modified accordingly. This processing corrected for translations, rotations and focus-dependent magnification changes between sessions, and yielded a single location of each cell in the reference coordinate system. Cell registration was then performed in all sessions using the CellReg (Sheintuch, Rubin et al. 2017) toolbox based on a probabilistic model of center distance.

Muscle regression

EMG power was calculated from the raw signals and then filtered (bandpass 1-8Hz). A linear model of the calcium data was fitted to the resulting signal for the regression analysis on the sessions of healthy quadrupedal walking. Regression scores were averaged per animal across sessions.

Gait decoding

Left and right foot off and foot strike events were manually marked on the behavioral videos as fo and fs time points. For each side, three sets of features were extracted: C_{fo}, C_{fs} and C_{other} as follows:

$$C_{rfo} = \begin{bmatrix} x_1(rfo(i)) \\ x_1(rfo(i) - \Delta t) \\ \vdots \\ x_1(rfo(i) - (N_{TP} - 1) \cdot \Delta t) \\ x_2(rfo(i)) \\ \vdots \\ x_{N_{CH}}(rfo(i) - (N_{TP} - 1) \cdot \Delta t) \end{bmatrix}$$

$$C_{rfs} = \begin{bmatrix} x_1(rfs(i)) \\ x_1(rfs(i) - \Delta t) \\ \vdots \\ x_1(rfs(i) - (N_{TP} - 1) \cdot \Delta t) \\ x_2(rfs(i)) \\ \vdots \\ x_{N_{CH}}(rfs(i) - (N_{TP} - 1) \cdot \Delta t) \end{bmatrix}$$

$$C_{rother} = \begin{bmatrix} x_1(t_i) \\ x_1(t_i - \Delta t) \\ \vdots \\ x_1(t_i - (N_{TP} - 1) \cdot \Delta t) \\ x_2(t_i) \\ \vdots \\ x_{N_{CH}}(t_i - (N_{TP} - 1) \cdot \Delta t) \end{bmatrix},$$

where x_i is the calcium trace of neuron i, N_{TP} is the number of time points used in the feature vector, Δt is the time difference between two time points, and t_i is the time point 10ms away from fo and fs. A two-class rLDA decoder was built for each side. The feature lengths, dimensions and regularization coefficients were chosen based on cross-validation.

7.3.3. Statistical procedures

All data are reported as mean values ±sem (standard deviation of the mean). No statistical methods were used to predetermine sample sizes, but our sample sizes are similar to those reported in previous publications. Behavioral assays were replicated when possible, and averaged per animal. Statistics were then performed over the mean of animals. All statistical analysis was performed in GraphPad Prism (USA) using two-tailed paired or unpaired Student's t-tests, one-way ANOVA for neuromorphological evaluations with more than two groups, and two-way repeated-measures ANOVA for functional assessments and neuronal activity evaluations. The post-hoc Tukey or Bonferroni test was applied. The significance level was set as $p < 0.05$. In the first chapter, the non-parametric Mann-Whitney and Wilcoxon signed-rank tests were used in comparisons of fewer than 5 animals, assuming that data distribution was not normal.

VIII. Integration & perspectives

8.1. Perspectives for the development of optical brain-computer interfaces

We sought to understand the functional plasticity of the motor-circuit communication matrix underlying recovery of voluntary leg movement after a contusion SCI. To this aim, we developed a technical implant and a methodology to perform chronic calcium imaging in freely-moving rats. Our pioneering study provides an early proof-of-concept for technological and biological stability (chapter 2), as well as for feasibility of behavioral decoding from an optical read-out of brain activity over a period of several months and across injury (chapter 3).

The translation from electrophysiological to optical calcium recordings that are more enduring represents a major effort in the development of future generations of brain-computer interfaces (BCI). Recently, an optical BCI in the non-human primate demonstrated the ability to decode movement direction based on calcium recordings of apical dendrites from deep cortical neurons (Trautmann, O'Shea et al. 2019). The authors opted for an optical chamber, arguing that the implantation of endoscopic material might importantly disrupt local and nearby circuits. They thus had optical access to superficial brain tissue, including cell bodies of superficial layer neurons, as well as apical dendrites from deep layers neurons. The chronic implant integrated strategies for brain tissue stabilization, and enabled to perform chronic 2-photon recordings coupled with online decoding for periods extending up to 42 days in the head-fixed rhesus macaque.

Here we show, in a different yet complementary approach, that a single-photon endoscopic imaging solution yields satisfying outcomes in chronic offline decoding, opening the way for

miniaturized portable devices. The further development and combination of recent technological achievements will lead to the new generation of freely-moving optical brain-computer interface applications.

8.2. Further elucidating the functional and anatomical plasticity of motor cortex L5 neurons with recovery

We demonstrated the cortex-dependent recovery of natural locomotion after a contusion spinal cord injury (Asboth, Friedli et al. 2018). Precise circuit-interrogation experiments allying optogenetic stimulation and chemogenic inhibition enabled to identify a cortico-reticulo-spinal detour circuit that mediates the recovered leg motor control, and whose establishment is training-dependent.

The following functional and anatomical studies presented in this thesis sought to reveal plasticity mechanisms of corticolumbar neurons correlating with the recovery enabled by neuroprosthetic rehabilitation. Analysis of the results of the calcium imaging study are currently ongoing. Unfortunately, the impossibility to perform longitudinal registration across the 4 months of recordings – and 2 months of injury followed by recovery – represents a major impediment to the interpretation of the present results. In turn, the anatomical study of the corticolumbar connectome revealed surprisingly no neuroplasticity effect of neuroprosthetic rehabilitation. While we know that the motor cortex redirects its descending command onto vGi excitatory neurons to regain access to the lumbar spinal cord, it remains to be confirmed whether or not corticolumbar neurons, despite the absence of sprouting, play a role in this descending drive. To fully complete this study, further investigation is currently being performed. We designed an experiment of functional inactivation with chemogenic tools, aiming to elucidate the role of corticolumbar neurons in the recovered control of leg movement, by testing a skilled hindlimb motor task (hip flexion) in the intact animal and after neuroprosthetic rehabilitation.

However, our results suggest that corticolumbar neurons are not the specific population involved in the functional and anatomical remodeling of the motor-circuit communication matrix that mediates recovery. Thereby, the nature of the neuronal population driving the formation of the cortico-reticulo-spinal relay remains to be elucidated. Further understanding of the fine organization of the leg motor cortex is thus critical. Circuit-dissection with neuroanatomical tracings and functional interrogation experiments will start questioning the identity and role of its constituting neuronal populations in the context of recovery after SCI.

8.3. Motor recovery after SCI in the frame of sensorimotor integration and learning

Anatomical substrate of motor learning

Motor learning translates into a temporal refinement of layer 5b neurons activity in the motor cortex (Li, Ko et al. 2017, Peters, Lee et al. 2017). In addition, it is accompanied by an extensive dendritic plasticity, the remodeling being specific to the neuronal populations that directly contact the spinal circuits controlling the muscles involved in learning (Wang, Conner et al. 2011). The stabilization of such learning-related structural changes correlates with the retention of new motor memories (Xu, Yu et al. 2009). Concurrently, motor learning is accompanied by structural plasticity in L2/3 neurons (Rioult-Pedotti, Fau et al. , Komiyama, Sato et al. 2010). Thus, intracortical synaptic reorganization is strongly believed to mediate the increased precision in motor cortex output signal and of, in turn, motor outcome.

Similarly, a spinal cord injury induces important spine changes in cortical L5 neurons, illustrating local rearrangements of cortical circuits (Ghosh, Sydekum et al. 2009) The main mechanism of motor map plasticity following injury is the reorganization of neuronal connectivity through morphological remodeling of pyramidal neuron dendrites in layers 2/3 and 5 (Greenough, Larson et al. 1985, Withers and Greenough 1989). Hence, despite fundamental differences, recovery after spinal cord injury, and *a fortiori* training-enhanced recovery, are strongly believed to share functional and anatomical mechanisms of motor learning.

Taking a step back: ensemble analysis and sensorimotor integration

In this thesis we focused on the motor cortex descending output to the lumbar circuits. However, in the ultimate goal of reaching a global understanding of the motor-circuit communication matrix remodeling, corticolumbar plasticity during injury and with recovery cannot be studied independently from the inherent reorganization of other motor-involved circuits.

It is known that motor output is encoded at the neuronal population level within the motor cortex. Behavioral predictions during a motor task are more accurate from neuronal ensembles than from individual neurons in the L5 motor cortex neurons (Laubach, Wessberg et al. 2000) and the premotor cortex (Afshar, Santhanam et al. 2011). As such, neuronal ensembles, encompassing various neuronal types, bear precious information about movement that is ignored when studying a precisely targeted neuronal population (Huber, Gutnisky et al. 2012, Peters, Chen et al. 2014). Hence, the constant chase for specificity is necessarily intertwined with loss of information, and while no trade-off provides satisfactory outcome in the unraveling of incredibly complex mechanisms, there is a paramount need for a perpetual back-and-forth between high-end precision and integration at the circuit- or whole-system level.

The motor cortex is further known to integrate a wide range of inputs, essentially arising from intracortical, thalamic and brainstem circuits (Wise and Donoghue 1986). The major excitatory

input to L5b in the motor cortex originates from L2/3 neurons (Weiler, Wood et al. 2008, Anderson, Sheets et al. 2010), which in turn integrate massive input from the somatosensory cortex (Mao, Kusefoglu et al. 2011). Thus, L2/3, upstream from the processing in L5b, plays a major role in linking sensory input to motor output (Wolpert, Diedrichsen et al. 2011, Huber, Gutnisky et al. 2012, Heindorf, Arber et al. 2018). In this aspect, motor control is indistinguishable from sensorimotor integration.

Sensorimotor learning

In turn, sensorimotor learning is associated with the formation and stabilization of spatiotemporal patterns of coordinated neurons, emphasizing the central importance of circuit-level plasticity. Komiyama et al. first highlighted the emergence, with learning of a licking task, of fine-scale correlations between neurons bearing the same representation (Komiyama, Sato et al. 2010). How the activity of individual neurons correlate to each other in the paradigm of a spinal cord injury, especially across neurons of the same movement-related representation, and how these patterns of activity evolve with recovery still remains to be investigated.

In the frame of sensorimotor integration, learning is associated with functional plasticity of both L2/3 neurons and corticospinal neurons (Peters, Chen et al. 2014, Peters, Lee et al. 2017). While L2/3 activity patterns converge towards an increased consistency in the representation of similar movements, CS activity patterns evolve towards an increased separation between representations of dissimilar movements. The combination of these two opposite yet complementary strategies ultimately leads to the refinement of motor output commands in response to sensory stimuli.

Whether the recovery process after SCI answers to mechanisms similar to sensorimotor learning in the intact animals is a central question. Analysis of corticospinal neurons activity during a passive motor task, such as treadmill walking, would enable to start disentangle descending commands from the integration of possible sensory signals in the cortex along recovery. Experiments exploring the functional plasticity of L2/3 neurons after contusion and with training would bring critical knowledge about the strategies of integration of the new motor-circuit communication matrix. Finally, beyond cortical circuits, the further investigation of the functional and anatomical reorganization of spared ascending systems would clarify the role of sensory feedback in recovery, thus closing the loop and ultimately bringing answers to the post-lesional integration of the "sensorimotor-circuit communication matrix".

8.4. Implications for clinical translation

Despite the recovery of voluntary leg movement after contusion thanks to neurorehabilitation, important motor deficits remain, emphasizing the necessity to combine neuroprosthetics and robotics with spinal cord repair interventions in the future. In this respect, the reorganization of cortico-reticulo-spinal circuits opens new perspectives to guide targeted repair interventions. Due to the dependence on corticospinal tract inputs for manual skills in humans, biological strategies have primarily focused on regenerating this system. However, corticospinal tract axons are more recalcitrant to regrowth after injury (Kadoya, Lu et al. 2016). Instead, reticulospinal projections have been one of the more amenable systems to regeneration (Lu, Wang et al. 2012), suggesting that targeting these projections specifically in combination with rehabilitation could lead to robust recovery.

These results warrant clinical studies. The implementation of neuroprosthetic rehabilitation in clinical settings requires a series of innovative neurotechnologies, including implantable stimulation system operating in real time (Capogrosso, Milekovic et al. 2016), safe pharmacological cocktails (Radhakrishna, Steuer et al. 2017) and a gravity assist to enable active locomotion in natural conditions (Mignardot, Le Goff et al. 2017) . These neurotechnologies have all been developed and approved for research use in humans. While challenges lie ahead, neuroprosthetic rehabilitation may become medical practice for improving recovery from SCI.

Publications & contributions

Mignardot, J.-B., C. G. Le Goff, R. van den Brand, M. Capogrosso, N. Fumeaux, H. Vallery, S. Anil, J. Lanini, I. Fodor, G. Eberle, A. Ijspeert, B. Schurch, A. Curt, S. Carda, J. Bloch, J. von Zitzewitz and G. Courtine (2017). "A multidirectional gravity-assist algorithm that enhances locomotor control in patients with stroke or spinal cord injury." Science Translational Medicine **9**(399): eaah3621.

> I participated in the early design of force personalization, by analyzing the biomechanical effects of the upward and forward forces applied on the gravity assist during standing. I also participated in the collection of data.

Asboth, L., L. Friedli, J. Beauparlant, C. Martinez-Gonzalez, S. Anil, E. Rey, L. Baud, G. Pidpruzhnykova, M. A. Anderson, P. Shkorbatova, L. Batti, S. Pages, J. Kreider, B. L. Schneider, Q. Barraud and G. Courtine (2018). "Cortico-reticulo-spinal circuit reorganization enables functional recovery after severe spinal cord contusion." Nat Neurosci **21**(4): 576-588.

> I led the experiment of chemogenic inactivation of hindlimb motor cortex in rats. This work involved experimental design, surgeries, animal training, behavioral testing, recordings and subsequent analysis, as well as anatomical processing of histological tissues and subsequent analysis.

List of abbreviations

#

5HT   Serotonin

A

AIS   ASIA Impairment Scale

ASIA   American Spinal Injury Association

AAV   Adeno-associated virus

AP   Antero-posterior

B

BDA   Biotinylated Dextran Amine

C

ChR2   Channelrhodospin-2

CL   Corticolumbar

CNO   Clozapine-N-Oxide

COMBO   Combined electrical and pharmacological stimulations

CS   Corticospinal

CST   Corticospinal tract

D

dF   Variation of fluorescence

DOX   Doxycycline

DREADD   Designer receptor exclusively activated by designer drugs

DV   Dorso-ventral

E

EES   Epidural electrical stimulation

EMG   Electromyography

F

FoV   Field of view

G

GFAP   Glial Fibrillary Acidic Protein

GFP   Green Fluorescent Protein

GRIN   Gradient refractive index

H

H   Healthy

I

IA   Indiscriminately active

IL   Iliopsoas

i.p.   Intraperitoneal

L
L2/3	Layer 2/3
L5	Layer 5

M
M1contra	Contralateral motor cortex
MA	Movement-active
MC	Motor cortex
MEP	Motor evoked potential
MG	Medial gastrocnemius
MI	Mutual Information
ML	Medio-lateral
MOV	Movement
MTP	Metatarsophalangeal joint

N
ns	Not significant

P
PAG	Periaqueductal gray matter
PC	Principal component
PHARMA	Pharmacological stimulation

Q
QUAD	Quadrupedal

R
RA	Rest-active
RedNu	Red nucleus
ROI	Region of interest

S
S	Silent
S2ant	Secondary sensory cortex, anterior part
S2post	Secondary sensory cortex, posterior part
s.c.	Sub-cutaneous
SCI	Spinal cord injury
ST	Semi-tendinosous
SPONT	Spontaneous

T
TA	Tibialis anterior
TM	Treadmill

V
vGi	Ventral Gigantocellular
vGlut2	Vesicular Glutamate transporter 2
VPM	Ventral posteromedial nucleus of the thalamus

References

Afshar, A., G. Santhanam, B. M. Yu, S. I. Ryu, M. Sahani and K. V. Shenoy (2011). "Single-trial neural correlates of arm movement preparation." <u>Neuron</u> **71**(3): 555-564.

Aghajan, Z. M., L. Acharya, J. J. Moore, J. D. Cushman, C. Vuong and M. R. Mehta (2015). "Impaired spatial selectivity and intact phase precession in two-dimensional virtual reality." <u>Nat Neurosci</u> **18**(1): 121-128.

Agnati, L. F., D. Guidolin, M. Guescini, S. Genedani and K. Fuxe (2010). "Understanding wiring and volume transmission." <u>Brain Res Rev</u> **64**(1): 137-159.

Aharoni, D., B. S. Khakh, A. J. Silva and P. Golshani (2019). "All the light that we can see: a new era in miniaturized microscopy." <u>Nature Methods</u> **16**(1): 11-13.

Ahuja, C. S., J. R. Wilson, S. Nori, M. R. N. Kotter, C. Druschel, A. Curt and M. G. Fehlings (2017). "Traumatic spinal cord injury."

Alstermark, B., J. Ogawa and T. Isa (2004). "Lack of monosynaptic corticomotoneuronal EPSPs in rats: disynaptic EPSPs mediated via reticulospinal neurons and polysynaptic EPSPs via segmental interneurons." <u>J Neurophysiol</u> **91**(4): 1832-1839.

Anderson, C. T., P. L. Sheets, T. Kiritani and G. M. G. Shepherd (2010). "Sublayer-specific microcircuits of corticospinal and corticostriatal neurons in motor cortex." <u>Nature Neuroscience</u> **13**(6): 739-744.

Anderson, M. A., J. E. Burda, Y. Ren, Y. Ao, T. M. O'Shea, R. Kawaguchi, G. Coppola, B. S. Khakh, T. J. Deming and M. V. Sofroniew (2016). "Astrocyte scar formation aids central nervous system axon regeneration." <u>Nature</u> **532**(7598): 195-200.

Anderson, M. A., T. M. O'Shea, J. E. Burda, Y. Ao, S. L. Barlatey, A. M. Bernstein, J. H. Kim, N. D. James, A. Rogers, B. Kato, A. L. Wollenberg, R. Kawaguchi, G. Coppola, C. Wang, T. J. Deming, Z. He, G. Courtine and M. V. Sofroniew (2018). "Required growth facilitators propel axon regeneration across complete spinal cord injury." <u>Nature</u> **561**(7723): 396-400.

Angeli, C. A., V. R. Edgerton, Y. P. Gerasimenko and S. J. Harkema (2014). "Altering spinal cord excitability enables voluntary movements after chronic complete paralysis in humans." <u>Brain</u>.

Antri, M., C. Mouffle, D. Orsal and J. Y. Barthe (2003). "5-HT1A receptors are involved in short- and long-term processes responsible for 5-HT-induced locomotor function recovery in chronic spinal rat." <u>Eur J Neurosci</u> **18**(7): 1963-1972.

Armand, J. (1982). "The origin, course and terminations of corticospinal fibers in various mammals." Prog Brain Res **57**: 329-360.

Asante, C. O., C. A, M. Fisher, F. M, B. L, B. A, S. P and J. Martin (2010). "Cortical control of adaptive locomotion in wild-type mice and mutant mice lacking the ephrin-Eph effector protein alpha2-chimaerin." (1522-1598 (Electronic)).

Asanuma, H. and H. Sakata (1967). "Functional Organization of a Cortical Efferent System Examined with Focal Depth Stimulation in Cats." Journal of Neurophysiology **30**(1): 35-54.

Asboth, L., L. Friedli, J. Beauparlant, C. Martinez-Gonzalez, S. Anil, E. Rey, L. Baud, G. Pidpruzhnykova, M. A. Anderson, P. Shkorbatova, L. Batti, S. Pages, J. Kreider, B. L. Schneider, Q. Barraud and G. Courtine (2018). "Cortico-reticulo-spinal circuit reorganization enables functional recovery after severe spinal cord contusion." Nat Neurosci **21**(4): 576-588.

Bachmann, L. C., A. Matis, N. T. Lindau, P. Felder, M. Gullo and M. E. Schwab (2013). "Deep Brain Stimulation of the Midbrain Locomotor Region Improves Paretic Hindlimb Function After Spinal Cord Injury in Rats." Science Translational Medicine **5**(208): 208ra146-208ra146.

Baker, P. F., A. L. Hodgkin and E. B. Ridgway (1971). "Depolarization and calcium entry in squid giant axons." The Journal of physiology **218**(3): 709-755.

Baker, S. N. and M. A. Perez (2017). "Reticulospinal Contributions to Gross Hand Function after Human Spinal Cord Injury." J Neurosci **37**(40): 9778-9784.

Ballermann, M. and K. Fouad (2006). "Spontaneous locomotor recovery in spinal cord injured rats is accompanied by anatomical plasticity of reticulospinal fibers." Eur J Neurosci **23**(8): 1988-1996.

Bareyre, F. M., M. Kerschensteiner, T. Misgeld and J. R. Sanes (2005). "Transgenic labeling of the corticospinal tract for monitoring axonal responses to spinal cord injury." Nat Med **11**(12): 1355-1360.

Bareyre, F. M., M. Kerschensteiner, O. Raineteau, T. C. Mettenleiter, O. Weinmann and M. E. Schwab (2004). "The injured spinal cord spontaneously forms a new intraspinal circuit in adult rats." Nat Neurosci **7**(3): 269-277.

Barretto, R. P. J., B. Messerschmidt and M. J. Schnitzer (2009). "In vivo fluorescence imaging with high-resolution microlenses." Nature methods **6**(7): 511-512.

Barthelemy, D., M. Willerslev-Olsen, H. Lundell, F. Biering-Sorensen and J. B. Nielsen (2015). "Assessment of transmission in specific descending pathways in relation to gait and balance following spinal cord injury." Prog Brain Res **218**: 79-101.

Basaldella, E., A. Takeoka, M. Sigrist and S. Arber (2015). "Multisensory Signaling Shapes Vestibulo-Motor Circuit Specificity." Cell **163**(2): 301-312.

Basso, D. M., M. S. Beattie and J. C. Bresnahan (1996). "Graded histological and locomotor outcomes after spinal cord contusion using the NYU weight-drop device versus transection." Exp Neurol **139**(2): 244-256.

Beauparlant, J., R. van den Brand, Q. Barraud, L. Friedli, P. Musienko, V. Dietz and G. Courtine (2013). "Undirected compensatory plasticity contributes to neuronal dysfunction after severe spinal cord injury." Brain.

Belhaj-Saif, A. and P. D. Cheney (2000). "Plasticity in the distribution of the red nucleus output to forearm muscles after unilateral lesions of the pyramidal tract." J Neurophysiol **83**(5): 3147-3153.

Brock, J. H., E. S. Rosenzweig, A. Blesch, R. Moseanko, L. A. Havton, V. R. Edgerton and M. H. Tuszynski (2010). "Local and Remote Growth Factor Effects after Primate Spinal Cord Injury." The Journal of Neuroscience **30**(29): 9728.

Brosamle, C. and M. E. Schwab (1997). "Cells of origin, course, and termination patterns of the ventral, uncrossed component of the mature rat corticospinal tract." J Comp Neurol **386**(2): 293-303.

Brown, A. R. and M. Martinez (2018). "Ipsilesional Motor Cortex Plasticity Participates in Spontaneous Hindlimb Recovery after Lateral Hemisection of the Thoracic Spinal Cord in the Rat." J Neurosci **38**(46): 9977-9988.

Brown Thomas, G. and S. Sherrington Charles (1912). "On the instability of a cortical point." Proceedings of the Royal Society of London. Series B, Containing Papers of a Biological Character **85**(579): 250-277.

Brus-Ramer, M., J. B. Carmel, S. Chakrabarty and J. H. Martin (2007). "Electrical stimulation of spared corticospinal axons augments connections with ipsilateral spinal motor circuits after injury." J Neurosci **27**(50): 13793-13801.

Cameron, C. M., M. Murugan, J. Y. Choi, E. A. Engel and I. B. Witten (2019). "Increased Cocaine Motivation Is Associated with Degraded Spatial and Temporal Representations in IL-NAc Neurons." Neuron **103**(1): 80-91.e87.

Canedo, A. (1997). "Primary motor cortex influences on the descending and ascending systems." Prog Neurobiol **51**(3): 287-335.

Capogrosso, M., T. Milekovic, D. Borton, F. Wagner, E. M. Moraud, J.-B. Mignardot, N. Buse, J. Gandar, Q. Barraud, D. Xing, E. Rey, S. Duis, Y. Jianzhong, W. K. D. Ko, Q. Li, P. Detemple, T.

Denison, S. Micera, E. Bezard, J. Bloch and G. Courtine (2016). "A brain–spine interface alleviating gait deficits after spinal cord injury in primates." <u>Nature</u> **539**: 284.

Carhart, M. R., J. He, R. Herman, S. D'Luzansky and W. T. Willis (2004). "Epidural spinal-cord stimulation facilitates recovery of functional walking following incomplete spinal-cord injury." <u>IEEE Trans Neural Syst Rehabil Eng</u> **12**(1): 32-42.

Carmel, J. B., H. Kimura and J. H. Martin (2014). "Electrical stimulation of motor cortex in the uninjured hemisphere after chronic unilateral injury promotes recovery of skilled locomotion through ipsilateral control." <u>J Neurosci</u> **34**(2): 462-466.

Castro, A. J. (1972). "Motor performance in rats. The effects of pyramidal tract section." <u>Brain Res</u> **44**(2): 313-323.

Chen, J. L., M. L. Andermann, T. Keck, N. L. Xu and Y. Ziv (2013). "Imaging neuronal populations in behaving rodents: paradigms for studying neural circuits underlying behavior in the mammalian cortex." <u>J Neurosci</u> **33**(45): 17631-17640.

Chen, S. X., A. N. Kim, A. J. Peters and T. Komiyama (2015). "Subtype-specific plasticity of inhibitory circuits in motor cortex during motor learning." <u>Nat Neurosci</u> **18**(8): 1109-1115.

Chen, T.-W., T. J. Wardill, Y. Sun, S. R. Pulver, S. L. Renninger, A. Baohan, E. R. Schreiter, R. A. Kerr, M. B. Orger, V. Jayaraman, L. L. Looger, K. Svoboda and D. S. Kim (2013). "Ultrasensitive fluorescent proteins for imaging neuronal activity." **499**(7458): 295-300.

Chung, K., J. Wallace, S. Y. Kim, S. Kalyanasundaram, A. S. Andalman, T. J. Davidson, J. J. Mirzabekov, K. A. Zalocusky, J. Mattis, A. K. Denisin, S. Pak, H. Bernstein, C. Ramakrishnan, L. Grosenick, V. Gradinaru and K. Deisseroth (2013). "Structural and molecular interrogation of intact biological systems." <u>Nature</u> **497**(7449): 332-337.

Churchland, M. M., J. P. Cunningham, M. T. Kaufman, J. D. Foster, P. Nuyujukian, S. I. Ryu and K. V. Shenoy (2012). "Neural population dynamics during reaching." <u>Nature</u> **487**(7405): 51-56.

Cohen, D. and M. A. Nicolelis (2004). "Reduction of single-neuron firing uncertainty by cortical ensembles during motor skill learning." <u>J Neurosci</u> **24**(14): 3574-3582.

Costa, R. M., D. Cohen and M. A. Nicolelis (2004). "Differential corticostriatal plasticity during fast and slow motor skill learning in mice." <u>Curr Biol</u> **14**(13): 1124-1134.

Courtine, G., M. B. Bunge, J. W. Fawcett, R. G. Grossman, J. H. Kaas, R. Lemon, I. Maier, J. Martin, R. J. Nudo, A. Ramon-Cueto, E. M. Rouiller, L. Schnell, T. Wannier, M. E. Schwab and V. R. Edgerton (2007). "Can experiments in nonhuman primates expedite the translation of treatments for spinal cord injury in humans?" <u>Nat Med</u> **13**(5): 561-566.

Courtine, G., Y. Gerasimenko, R. van den Brand, A. Yew, P. Musienko, H. Zhong, B. Song, Y. Ao, R. M. Ichiyama, I. Lavrov, R. R. Roy, M. V. Sofroniew and V. R. Edgerton (2009). "Transformation of nonfunctional spinal circuits into functional states after the loss of brain input." **12**(10): 1333-1342.

Courtine, G., R. R. Roy, J. Raven, J. Hodgson, H. McKay, H. Yang, H. Zhong, M. H. Tuszynski and V. R. Edgerton (2005). "Performance of locomotion and foot grasping following a unilateral thoracic corticospinal tract lesion in monkeys (Macaca mulatta)." Brain **128**(Pt 10): 2338-2358.

Courtine, G., B. Song, R. R. Roy, H. Zhong, J. E. Herrmann, Y. Ao, J. Qi, V. R. Edgerton and M. V. Sofroniew (2008). "Recovery of supraspinal control of stepping via indirect propriospinal relay connections after spinal cord injury." Nat Med **14**(1): 69-74.

Cowley, K. C., E. Zaporozhets and B. J. Schmidt (2008). "Propriospinal neurons are sufficient for bulbospinal transmission of the locomotor command signal in the neonatal rat spinal cord." J Physiol **586**(6): 1623-1635.

Dana, H., Y. Sun, B. Mohar, B. Hulse, J. P. Hasseman, G. Tsegaye, A. Tsang, A. Wong, R. Patel, J. J. Macklin, Y. Chen, A. Konnerth, V. Jayaraman, L. L. Looger, E. R. Schreiter, K. Svoboda and D. S. Kim (2018). "High-performance GFP-based calcium indicators for imaging activity in neuronal populations and microcompartments." bioRxiv: 434589.

Danilov, C. A. and O. Steward (2015). "Conditional genetic deletion of PTEN after a spinal cord injury enhances regenerative growth of CST axons and motor function recovery in mice." Experimental Neurology **266**: 147-160.

Davey, N. J., H. C. Smith, E. Wells, D. W. Maskill, G. Savic, P. H. Ellaway and H. L. Frankel (1998). "Responses of thenar muscles to transcranial magnetic stimulation of the motor cortex in patients with incomplete spinal cord injury." J Neurol Neurosurg Psychiatry **65**(1): 80-87.

De Leon, R. D., J. A. Hodgson, R. R. Roy and V. R. Edgerton (1998). "Full weight-bearing hindlimb standing following stand training in the adult spinal cat." J Neurophysiol **80**(1): 83-91.

de Leon, R. D., J. A. Hodgson, R. R. Roy and V. R. Edgerton (1998). "Locomotor capacity attributable to step training versus spontaneous recovery after spinalization in adult cats." J Neurophysiol **79**(3): 1329-1340.

Dimitrijevic, M. R., Y. Gerasimenko and M. M. Pinter (1998). "Evidence for a spinal central pattern generator in humans." Ann N Y Acad Sci **860**: 360-376.

Ditunno, J. F., Jr., W. Young, W. H. Donovan and G. Creasey (1994). "The international standards booklet for neurological and functional classification of spinal cord injury. American Spinal Injury Association." Paraplegia **32**(2): 70-80.

Dobkin, B. H. and L. A. Havton (2004). "Basic advances and new avenues in therapy of spinal cord injury." Annual review of medicine **55**: 255-282.

Dominici, N., U. Keller, H. Vallery, L. Friedli, R. van den Brand, M. L. Starkey, P. Musienko, R. Riener and G. Courtine (2012). "Versatile robotic interface to evaluate, enable and train locomotion and balance after neuromotor disorders." Nat Med **18**(7): 1142-1147.

Donoghue, J. P. and S. T. Kitai (1981). "A collateral pathway to the neostriatum from corticofugal neurons of the rat sensory-motor cortex: an intracellular HRP study." J Comp Neurol **201**(1): 1-13.

Duffy, P., X. Wang, C. S. Siegel, N. Tu, M. Henkemeyer, W. B. J. Cafferty and S. M. Strittmatter (2012). "Myelin-derived ephrinB3 restricts axonal regeneration and recovery after adult CNS injury." Proceedings of the National Academy of Sciences **109**(13): 5063.

Edgerton, V. R., G. Courtine, Y. P. Gerasimenko, I. Lavrov, R. M. Ichiyama, A. J. Fong, L. L. Cai, C. K. Otoshi, N. J. Tillakaratne, J. W. Burdick and R. R. Roy (2008). "Training locomotor networks." Brain Res Rev **57**(1): 241-254.

Esposito, M. S., P. Capelli and S. Arber (2014). "Brainstem nucleus MdV mediates skilled forelimb motor tasks." Nature **508**(7496): 351-356.

Evarts, E. V. (1965). "RELATION OF DISCHARGE FREQUENCY TO CONDUCTION VELOCITY IN PYRAMIDAL TRACT NEURONS." J Neurophysiol **28**: 216-228.

Fawcett, J. W. (2019). "The Struggle to Make CNS Axons Regenerate: Why Has It Been so Difficult?" Neurochemical Research.

Fawcett, J. W., A. Curt, J. D. Steeves, W. P. Coleman, M. H. Tuszynski, D. Lammertse, P. F. Bartlett, A. R. Blight, V. Dietz, J. Ditunno, B. H. Dobkin, L. A. Havton, P. H. Ellaway, M. G. Fehlings, A. Privat, R. Grossman, J. D. Guest, N. Kleitman, M. Nakamura, M. Gaviria and D. Short (2006). "Guidelines for the conduct of clinical trials for spinal cord injury as developed by the ICCP panel: spontaneous recovery after spinal cord injury and statistical power needed for therapeutic clinical trials." Spinal Cord **45**: 190.

Fedirchuk, B., J. Nielsen, N. Petersen and H. Hultborn (1998). "Pharmacologically evoked fictive motor patterns in the acutely spinalized marmoset monkey (Callithrix jacchus)." Experimental Brain Research **122**(3): 351-361.

Filli, L., A. K. Engmann, B. Zorner, O. Weinmann, T. Moraitis, M. Gullo, H. Kasper, R. Schneider and M. E. Schwab (2014). "Bridging the gap: a reticulo-propriospinal detour bypassing an incomplete spinal cord injury." J Neurosci **34**(40): 13399-13410.

Flusberg, B. A., A. Nimmerjahn, E. D. Cocker, E. A. Mukamel, R. P. Barretto, T. H. Ko, L. D. Burns, J. C. Jung and M. J. Schnitzer (2008). "High-speed, miniaturized fluorescence microscopy in freely moving mice." Nat Methods **5**(11): 935-938.

Fouad, K., V. Pedersen, M. E. Schwab and C. Brosamle (2001). "Cervical sprouting of corticospinal fibers after thoracic spinal cord injury accompanies shifts in evoked motor responses." Curr Biol **11**(22): 1766-1770.

Freund, P., J. Rothwell, M. Craggs, A. J. Thompson and S. Bestmann (2011). "Corticomotor representation to a human forearm muscle changes following cervical spinal cord injury." Eur J Neurosci **34**(11): 1839-1846.

Friedli, L., E. S. Rosenzweig, Q. Barraud, M. Schubert, N. Dominici, L. Awai, J. L. Nielson, P. Musienko, Y. Nout-Lomas, H. Zhong, S. Zdunowski, R. R. Roy, S. C. Strand, R. van den Brand, L. A. Havton, M. S. Beattie, J. C. Bresnahan, E. Bézard, J. Bloch, V. R. Edgerton, A. R. Ferguson, A. Curt, M. H. Tuszynski and G. Courtine (2015). "Pronounced species divergence in corticospinal tract reorganization and functional recovery after lateralized spinal cord injury favors primates." Science Translational Medicine **7**(302): 302ra134-302ra134.

Gao, W.-J. and Z.-H. Zheng (2004). "Target-specific differences in somatodendritic morphology of layer V pyramidal neurons in rat motor cortex." The Journal of comparative neurology **476**: 174-185.

Garcia-Alias, G., K. Truong, P. K. Shah, R. R. Roy and V. R. Edgerton (2015). "Plasticity of subcortical pathways promote recovery of skilled hand function in rats after corticospinal and rubrospinal tract injuries." Exp Neurol **266**: 112-119.

Gerasimenko, Y., R. Gorodnichev, A. Puhov, T. Moshonkina, A. Savochin, V. Selionov, R. R. Roy, D. C. Lu and V. R. Edgerton (2015). "Initiation and modulation of locomotor circuitry output with multisite transcutaneous electrical stimulation of the spinal cord in noninjured humans." J Neurophysiol **113**(3): 834-842.

Ghosh, A., F. Haiss, E. Sydekum, R. Schneider, M. Gullo, M. T. Wyss, T. Mueggler, C. Baltes, M. Rudin, B. Weber and M. E. Schwab (2010). "Rewiring of hindlimb corticospinal neurons after spinal cord injury." Nat Neurosci **13**(1): 97-104.

Ghosh, A., S. Peduzzi, M. Snyder, R. Schneider, M. Starkey and M. E. Schwab (2012). "Heterogeneous spine loss in layer 5 cortical neurons after spinal cord injury." Cereb Cortex **22**(6): 1309-1317.

Ghosh, A., E. Sydekum, F. Haiss, S. Peduzzi, B. Zorner, R. Schneider, C. Baltes, M. Rudin, B. Weber and M. E. Schwab (2009). "Functional and anatomical reorganization of the sensory-motor cortex after incomplete spinal cord injury in adult rats." J Neurosci **29**(39): 12210-12219.

Ghosh, K. K., L. D. Burns, E. D. Cocker, A. Nimmerjahn, Y. Ziv, A. E. Gamal and M. J. Schnitzer (2011). "Miniaturized integration of a fluorescence microscope." **8**(10): 871-878.

Giehl, K. M. and W. Tetzlaff (1996). "BDNF and NT-3, but not NGF, prevent axotomy-induced death of rat corticospinal neurons in vivo." <u>Eur J Neurosci</u> **8**(6): 1167-1175.

Girgis, J., D. Merrett, S. Kirkland, G. A. Metz, V. Verge and K. Fouad (2007). "Reaching training in rats with spinal cord injury promotes plasticity and task specific recovery." <u>Brain</u> **130**(Pt 11): 2993-3003.

Gomez, J. L., J. Bonaventura, W. Lesniak, W. B. Mathews, P. Sysa-Shah, L. A. Rodriguez, R. J. Ellis, C. T. Richie, B. K. Harvey, R. F. Dannals, M. G. Pomper, A. Bonci and M. Michaelides (2017). "Chemogenetics revealed: DREADD occupancy and activation via converted clozapine." <u>Science</u> **357**(6350): 503.

Greenough, W. T., J. R. Larson and G. S. Withers (1985). "Effects of unilateral and bilateral training in a reaching task on dendritic branching of neurons in the rat motor-sensory forelimb cortex." <u>Behavioral and Neural Biology</u> **44**(2): 301-314.

Grill, R., K. Murai, A. Blesch, F. H. Gage and M. H. Tuszynski (1997). "Cellular delivery of neurotrophin-3 promotes corticospinal axonal growth and partial functional recovery after spinal cord injury." <u>J Neurosci</u> **17**(14): 5560-5572.

Guo, J.-Z., A. R. Graves, W. W. Guo, J. Zheng, A. Lee, J. Rodríguez-González, N. Li, J. J. Macklin, J. W. Phillips, B. D. Mensh, K. Branson and A. W. Hantman (2015). "Cortex commands the performance of skilled movement." <u>eLife</u> **4**: e10774.

Hagglund, M., L. Borgius, K. J. Dougherty and O. Kiehn (2010). "Activation of groups of excitatory neurons in the mammalian spinal cord or hindbrain evokes locomotion." <u>Nat Neurosci</u> **13**(2): 246-252.

Hallett, M. (2007). "Transcranial magnetic stimulation: a primer." <u>Neuron</u> **55**(2): 187-199.

Han, Q., C. Cao, Y. Ding, K.-F. So, W. Wu, Y. Qu and L. Zhou (2015). "Plasticity of motor network and function in the absence of corticospinal projection." <u>Experimental Neurology</u> **267**: 194-208.

Harkema, S., Y. Gerasimenko, J. Hodes, J. Burdick, C. Angeli, Y. Chen, C. Ferreira, A. Willhite, E. Rejc, R. G. Grossman and V. R. Edgerton (2011). "Effect of epidural stimulation of the lumbosacral spinal cord on voluntary movement, standing, and assisted stepping after motor complete paraplegia: a case study." <u>Lancet</u> **377**(9781): 1938-1947.

Harkema, S. J. (2008). "Plasticity of interneuronal networks of the functionally isolated human spinal cord." <u>Brain research reviews</u> **57**(1): 255-264.

Harrison, T. C., O. G. Ayling and T. H. Murphy (2012). "Distinct cortical circuit mechanisms for complex forelimb movement and motor map topography." Neuron **74**(2): 397-409.

Heindorf, M., S. Arber and G. B. Keller (2018). "Mouse Motor Cortex Coordinates the Behavioral Response to Unpredicted Sensory Feedback." Neuron **99**(5): 1040-1054 e1045.

Helmchen, F., M. S. Fee, D. W. Tank and W. Denk (2001). "A miniature head-mounted two-photon microscope. high-resolution brain imaging in freely moving animals." Neuron **31**(6): 903-912.

Helmchen, F., K. Imoto and B. Sakmann (1996). "Ca2+ buffering and action potential-evoked Ca2+ signaling in dendrites of pyramidal neurons." Biophys J **70**(2): 1069-1081.

Hilton, B. J., E. Anenberg, T. C. Harrison, J. D. Boyd, T. H. Murphy and W. Tetzlaff (2016). "Re-Establishment of Cortical Motor Output Maps and Spontaneous Functional Recovery via Spared Dorsolaterally Projecting Corticospinal Neurons after Dorsal Column Spinal Cord Injury in Adult Mice." J Neurosci **36**(14): 4080-4092.

Hollis, E. R., 2nd, N. Ishiko, T. Yu, C. C. Lu, A. Haimovich, K. Tolentino, A. Richman, A. Tury, S. H. Wang, M. Pessian, E. Jo, A. Kolodkin and Y. Zou (2016). "Ryk controls remapping of motor cortex during functional recovery after spinal cord injury." Nat Neurosci **19**(5): 697-705.

Huber, D., D. A. Gutnisky, S. Peron, D. H. O/'Connor, J. S. Wiegert, L. Tian, T. G. Oertner, L. L. Looger and K. Svoboda (2012). "Multiple dynamic representations in the motor cortex during sensorimotor learning."

Isomura, Y., R. Harukuni, T. Takekawa, H. Aizawa and T. Fukai (2009). "Microcircuitry coordination of cortical motor information in self-initiation of voluntary movements." Nat Neurosci **12**(12): 1586-1593.

J. Casale, E., A. R. Light and A. Rustioni (1988). "Direct projection of the corticospinal tract to the superficial laminae of the spinal cord in the rat." The Journal of comparative neurology **278**: 275-286.

James, N. D., K. Bartus, J. Grist, D. L. H. Bennett, S. B. McMahon and E. J. Bradbury (2011). "Conduction Failure following Spinal Cord Injury: Functional and Anatomical Changes from Acute to Chronic Stages." The Journal of Neuroscience **31**(50): 18543.

Jankowska, E. and S. A. Edgley (2006). "How can corticospinal tract neurons contribute to ipsilateral movements? A question with implications for recovery of motor functions." Neuroscientist **12**(1): 67-79.

Jercog, P., T. Rogerson and M. J. Schnitzer (2016). "Large-Scale Fluorescence Calcium-Imaging Methods for Studies of Long-Term Memory in Behaving Mammals." <u>Cold Spring Harb Perspect Biol</u> **8**(5).

Jordan, L. M., J. Liu, P. B. Hedlund, T. Akay and K. G. Pearson (2008). "Descending command systems for the initiation of locomotion in mammals." <u>Brain Res Rev</u> **57**(1): 183-191.

Kadoya, K., P. Lu, K. Nguyen, C. Lee-Kubli, H. Kumamaru, L. Yao, J. Knackert, G. Poplawski, J. N. Dulin, H. Strobl, Y. Takashima, J. Biane, J. Conner, S.-C. Zhang and M. H. Tuszynski (2016). "Spinal cord reconstitution with homologous neural grafts enables robust corticospinal regeneration." <u>Nat Med</u> **advance online publication**.

Kakulas, B. A. (1999). "A review of the neuropathology of human spinal cord injury with emphasis on special features." <u>J Spinal Cord Med</u> **22**(2): 119-124.

Kargo, W. J. and D. A. Nitz (2004). "Improvements in the signal-to-noise ratio of motor cortex cells distinguish early versus late phases of motor skill learning." <u>J Neurosci</u> **24**(24): 5560-5569.

Kawai, R., T. Markman, R. Poddar, R. Ko, A. L. Fantana, A. K. Dhawale, A. R. Kampff and B. P. Olveczky (2015). "Motor cortex is required for learning but not for executing a motor skill." <u>Neuron</u> **86**(3): 800-812.

Keller, A. (1993). "Intrinsic Synaptic Organization of the Motor Cortex." <u>Cerebral Cortex</u> **3**(5): 430-441.

Kiehn, O. (2006). "Locomotor circuits in the mammalian spinal cord." <u>Annu Rev Neurosci</u> **29**: 279-306.

Kinoshita, M., R. Matsui, S. Kato, T. Hasegawa, H. Kasahara, K. Isa, A. Watakabe, T. Yamamori, Y. Nishimura, B. Alstermark, D. Watanabe, K. Kobayashi and T. Isa (2012). "Genetic dissection of the circuit for hand dexterity in primates." <u>Nature</u> **487**(7406): 235-238.

Kleim, J. A., S. Barbay and R. J. Nudo (1998). "Functional reorganization of the rat motor cortex following motor skill learning." <u>J Neurophysiol</u> **80**(6): 3321-3325.

Kleim, J. A., T. M. Hogg, P. M. VandenBerg, N. R. Cooper, R. Bruneau and M. Remple (2004). "Cortical synaptogenesis and motor map reorganization occur during late, but not early, phase of motor skill learning." <u>J Neurosci</u> **24**(3): 628-633.

Koch, P., R. Schulz and F. C. Hummel (2016). "Structural connectivity analyses in motor recovery research after stroke." <u>Ann Clin Transl Neurol</u> **3**(3): 233-244.

Komiyama, T., T. R. Sato, D. H. O/'Connor, Y.-X. Zhang, D. Huber, B. M. Hooks, M. Gabitto and K. Svoboda (2010). "Learning-related fine-scale specificity imaged in motor cortex circuits of behaving mice." Nature **464**(7292): 1182-1186.

Kuypers, H. G. (1960). "Central cortical projections to motor and somato-sensory cell groups. An experimental study in the rhesus monkey." Brain **83**: 161-184.

Kuypers, H. G. (1982). "A new look at the organization of the motor system." Prog Brain Res **57**: 381-403.

Kuypers, H. G., W. R. Fleming and J. W. Farinholt (1962). "Subcorticospinal projections in the rhesus monkey." J Comp Neurol **118**: 107-137.

Kuypers, H. G. and D. G. Lawrence (1967). "Cortical projections to the red nucleus and the brain stem in the Rhesus monkey." Brain Res **4**(2): 151-188.

Lacroix, S., L. A. Havton, H. McKay, H. Yang, A. Brant, J. Roberts and M. H. Tuszynski (2004). "Bilateral corticospinal projections arise from each motor cortex in the macaque monkey: a quantitative study." J Comp Neurol **473**(2): 147-161.

Landry, E. S., N. P. Lapointe, C. Rouillard, D. Levesque, P. B. Hedlund and P. A. Guertin (2006). "Contribution of spinal 5-HT1A and 5-HT7 receptors to locomotor-like movement induced by 8-OH-DPAT in spinal cord-transected mice." Eur J Neurosci **24**(2): 535-546.

Laubach, M., J. Wessberg and M. A. Nicolelis (2000). "Cortical ensemble activity increasingly predicts behaviour outcomes during learning of a motor task." Nature **405**(6786): 567-571.

Lawrence, D. G. and H. G. Kuypers (1968). "The functional organization of the motor system in the monkey. I. The effects of bilateral pyramidal lesions." Brain **91**(1): 1-14.

Lee, J. K., C. G. Geoffroy, A. F. Chan, K. E. Tolentino, M. J. Crawford, M. A. Leal, B. Kang and B. Zheng (2010). "Assessing spinal axon regeneration and sprouting in Nogo-, MAG-, and OMgp-deficient mice." Neuron **66**(5): 663-670.

Lemon, R. N. (2008). "Descending pathways in motor control." Annu Rev Neurosci **31**: 195-218.

Lemon, R. N. and J. Griffiths (2005). "Comparing the function of the corticospinal system in different species: organizational differences for motor specialization?" Muscle Nerve **32**(3): 261-279.

Li, C. X. and R. S. Waters (1991). "Organization of the mouse motor cortex studied by retrograde tracing and intracortical microstimulation (ICMS) mapping." Can J Neurol Sci **18**(1): 28-38.

Li, N., T. W. Chen, Z. V. Guo, C. R. Gerfen and K. Svoboda (2015). "A motor cortex circuit for motor planning and movement." Nature **519**(7541): 51-56.

Li, Q., H. Ko, Z.-M. Qian, L. Y. C. Yan, D. C. W. Chan, G. Arbuthnott, Y. Ke and W.-H. Yung (2017). "Refinement of learned skilled movement representation in motor cortex deep output layer." Nature Communications **8**: 15834.

Liang, F. Y., V. Moret, M. Wiesendanger and E. M. Rouiller (1991). "Corticomotoneuronal connections in the rat: evidence from double-labeling of motoneurons and corticospinal axon arborizations." J Comp Neurol **311**(3): 356-366.

Lovely, R. G., R. J. Gregor, R. R. Roy and V. R. Edgerton (1986). "Effects of training on the recovery of full-weight-bearing stepping in the adult spinal cat." Exp Neurol **92**(2): 421-435.

Lovely, R. G., R. J. Gregor, R. R. Roy and V. R. Edgerton (1990). "Weight-bearing hindlimb stepping in treadmill-exercised adult spinal cats." Brain Res **514**(2): 206-218.

Lu, P., A. Blesch and M. H. Tuszynski (2001). "Neurotrophism without neurotropism: BDNF promotes survival but not growth of lesioned corticospinal neurons." J Comp Neurol **436**(4): 456-470.

Lu, P., Y. Wang, L. Graham, K. McHale, M. Gao, D. Wu, J. Brock, A. Blesch, E. S. Rosenzweig, L. A. Havton, B. Zheng, J. M. Conner, M. Marsala and M. H. Tuszynski (2012). "Long-distance growth and connectivity of neural stem cells after severe spinal cord injury." Cell **150**(6): 1264-1273.

Luccarini, P., Y. Gahery and O. Pompeiano (1990). "Cholinoceptive pontine reticular structures modify the postural adjustments during the limb movements induced by cortical stimulation." Arch Ital Biol **128**(1): 19-45.

M Piecharka, D., J. Kleim and I. Whishaw (2005). "Limits on recovery in the corticospinal tract of the rat: Partial lesions impair skilled reaching and the topographic representation of the forelimb in motor cortex." Brain research bulletin **66**: 203-211.

Mao, T., D. Kusefoglu, B. M. Hooks, D. Huber, L. Petreanu and K. Svoboda (2011). "Long-range neuronal circuits underlying the interaction between sensory and motor cortex." Neuron **72**(1): 111-123.

Margolis, D. J., H. Lutcke, K. Schulz, F. Haiss, B. Weber, S. Kugler, M. T. Hasan and F. Helmchen (2012). "Reorganization of cortical population activity imaged throughout long-term sensory deprivation." Nat Neurosci **15**(11): 1539-1546.

Martinez, M., M. Delcour, M. Russier, Y. Zennou-Azogui, C. Xerri, J. O. Coq and J. M. Brezun (2010). "Differential tactile and motor recovery and cortical map alteration after C4-C5 spinal hemisection." Exp Neurol **221**(1): 186-197.

Matsuyama, K., F. Mori, K. Nakajima, T. Drew, M. Aoki and S. Mori (2004). "Locomotor role of the corticoreticular-reticulospinal-spinal interneuronal system." Prog Brain Res **143**: 239-249.

McKinley, W., S. McNamee, M. Meade, K. Kandra and N. Abdul (2006). "Incidence, Etiology, and Risk Factors for Fever Following Acute Spinal Cord Injury." The Journal of Spinal Cord Medicine **29**(5): 501-506.

Mignardot, J.-B., C. G. Le Goff, R. van den Brand, M. Capogrosso, N. Fumeaux, H. Vallery, S. Anil, J. Lanini, I. Fodor, G. Eberle, A. Ijspeert, B. Schurch, A. Curt, S. Carda, J. Bloch, J. von Zitzewitz and G. Courtine (2017). "A multidirectional gravity-assist algorithm that enhances locomotor control in patients with stroke or spinal cord injury." Science Translational Medicine **9**(399): eaah3621.

Minassian, K., B. Jilge, F. Rattay, M. M. Pinter, H. Binder, F. Gerstenbrand and M. R. Dimitrijevic (2004). "Stepping-like movements in humans with complete spinal cord injury induced by epidural stimulation of the lumbar cord: electromyographic study of compound muscle action potentials." Spinal Cord **42**(7): 401-416.

Miri, A., C. L. Warriner, J. S. Seely, G. F. Elsayed, J. P. Cunningham, M. M. Churchland and T. M. Jessell (2017). "Behaviorally Selective Engagement of Short-Latency Effector Pathways by Motor Cortex." Neuron **95**(3): 683-696 e611.

Moraud, E. M., M. Capogrosso, E. Formento, N. Wenger, J. DiGiovanna, G. Courtine and S. Micera (2016). "Mechanisms Underlying the Neuromodulation of Spinal Circuits for Correcting Gait and Balance Deficits after Spinal Cord Injury." Neuron **89**(4): 814-828.

Muir, G. D. and I. Q. Whishaw (1999). "Complete locomotor recovery following corticospinal tract lesions: measurement of ground reaction forces during overground locomotion in rats." Behav Brain Res **103**(1): 45-53.

Mushahwar, V. K., P. L. Jacobs, R. A. Normann, R. J. Triolo and N. Kleitman (2007). "New functional electrical stimulation approaches to standing and walking." J Neural Eng **4**(3): S181-197.

Musienko, P., R. van den Brand, O. Maerzendorfer, A. Larmagnac and G. Courtine (2009). "Combinatory electrical and pharmacological neuroprosthetic interfaces to regain motor function after spinal cord injury." IEEE Trans Biomed Eng **56**(11 Pt 2): 2707-2711.

Musienko, P., R. van den Brand, O. Marzendorfer, R. R. Roy, Y. Gerasimenko, V. R. Edgerton and G. Courtine (2011). "Controlling specific locomotor behaviors through multidimensional monoaminergic modulation of spinal circuitries." J Neurosci **31**(25): 9264-9278.

Nardone, R., Y. Holler, F. Brigo, M. Seidl, M. Christova, J. Bergmann, S. Golaszewski and E. Trinka (2013). "Functional brain reorganization after spinal cord injury: systematic review of animal and human studies." Brain Res **1504**: 58-73.

Nathan, P. W. (1994). "Effects on movement of surgical incisions into the human spinal cord." Brain **117 (Pt 2)**: 337-346.

Nathan, P. W., M. Smith and P. Deacon (1996). "Vestibulospinal, reticulospinal and descending propriospinal nerve fibres in man." Brain **119 (Pt 6)**: 1809-1833.

Nathan, P. W. and M. C. Smith (1973). "Effects of two unilateral cordotomies on the motility of the lower limbs." Brain **96**(3): 471-494.

National.Spinal.Cord.Injury.Statistical.Center (2014). "Spinal Cord Injury Facts and Figures at a Glance." J Spinal Cord Med. **37(1)**: 117–118.

Ni, Y., H. Nawabi, X. Liu, L. Yang, K. Miyamichi, A. Tedeschi, B. Xu, N. R. Wall, E. M. Callaway and Z. He (2014). "Characterization of long descending premotor propriospinal neurons in the spinal cord." J Neurosci **34**(28): 9404-9417.

Nielson, J. L., M. K. Strong and O. Steward (2011). "A reassessment of whether cortical motor neurons die following spinal cord injury." The Journal of comparative neurology **519**(14): 2852-2869.

Nudo, R. J. and R. B. Masterton (1988). "Descending pathways to the spinal cord: a comparative study of 22 mammals." J Comp Neurol **277**(1): 53-79.

Nudo, R. J., G. W. Milliken, W. M. Jenkins and M. M. Merzenich (1996). "Use-dependent alterations of movement representations in primary motor cortex of adult squirrel monkeys." J Neurosci **16**(2): 785-807.

Otchy, T. M., S. B. E. Wolff, J. Y. Rhee, C. Pehlevan, R. Kawai, A. Kempf, S. M. H. Gobes and B. P. Ölveczky (2015). "Acute off-target effects of neural circuit manipulations." Nature **528**: 358.

Oza, C. S. and S. F. Giszter (2014). "Plasticity and alterations of trunk motor cortex following spinal cord injury and non-stepping robot and treadmill training." Exp Neurol **256**: 57-69.

Pascual-Leone, A., D. Nguyet, L. G. Cohen, J. P. Brasil-Neto, A. Cammarota and M. Hallett (1995). "Modulation of muscle responses evoked by transcranial magnetic stimulation during the acquisition of new fine motor skills." J Neurophysiol **74**(3): 1037-1045.

Peron, S. P., J. Freeman, V. Iyer, C. Guo and K. Svoboda (2015). "A Cellular Resolution Map of Barrel Cortex Activity during Tactile Behavior." Neuron **86**(3): 783-799.

Peters, A. J., S. X. Chen and T. Komiyama (2014). "Emergence of reproducible spatiotemporal activity during motor learning." Nature **510**(7504): 263-267.

Peters, A. J., J. Lee, N. G. Hedrick, K. O'Neil and T. Komiyama (2017). "Reorganization of corticospinal output during motor learning." Nat Neurosci **20**(8): 1133-1141.

Petersen, J. A., B. J. Wilm, J. von Meyenburg, M. Schubert, B. Seifert, Y. Najafi, V. Dietz and S. Kollias (2012). "Chronic cervical spinal cord injury: DTI correlates with clinical and electrophysiological measures." J Neurotrauma **29**(8): 1556-1566.

Philippson, M. (1905). L'autonomie et la centralisation dans le système nerveux des animaux: étude de physiologie expérimentale et comparée, Falk.

Pivetta, C., M. S. Esposito, M. Sigrist and S. Arber (2014). "Motor-circuit communication matrix from spinal cord to brainstem neurons revealed by developmental origin." Cell **156**(3): 537-548.

Plautz, E. J., G. W. Milliken and R. J. Nudo (2000). "Effects of repetitive motor training on movement representations in adult squirrel monkeys: role of use versus learning." Neurobiol Learn Mem **74**(1): 27-55.

Radhakrishna, M., I. Steuer, F. Prince, M. Roberts, D. Mongeon, M. Kia, S. Dyck, G. Matte, M. Vaillancourt and P. A. Guertin (2017). "Double-Blind, Placebo-Controlled, Randomized Phase I/IIa Study (Safety and Efficacy) with Buspirone/Levodopa/Carbidopa (SpinalonTM) in Subjects with Complete AIS A or Motor-Complete AIS B Spinal Cord Injury." Curr Pharm Des **23**(12): 1789-1804.

Raineteau, O. and M. E. Schwab (2001). "Plasticity of motor systems after incomplete spinal cord injury." Nat Rev Neurosci **2**(4): 263-273.

Ravassard, P., A. Kees, B. Willers, D. Ho, D. A. Aharoni, J. Cushman, Z. M. Aghajan and M. R. Mehta (2013). "Multisensory control of hippocampal spatiotemporal selectivity." Science **340**(6138): 1342-1346.

Resendez, S. L., J. H. Jennings, R. L. Ung, V. M. Namboodiri, Z. C. Zhou, J. M. Otis, H. Nomura, J. A. McHenry, O. Kosyk and G. D. Stuber (2016). "Visualization of cortical, subcortical and deep brain neural circuit dynamics during naturalistic mammalian behavior with head-mounted microscopes and chronically implanted lenses." Nat Protoc **11**(3): 566-597.

Riddle, C. N., S. A. Edgley and S. N. Baker (2009). "Direct and indirect connections with upper limb motoneurons from the primate reticulospinal tract." J Neurosci **29**(15): 4993-4999.

Rioult-Pedotti, M. S., F. D. Fau, G. Hess, H. G. Fau, J. P. Donoghue and J. P. Donoghue "Strengthening of horizontal cortical connections following skill learning." (1097-6256 (Print)).

Rosenzweig, E. S., J. H. Brock, M. D. Culbertson, P. Lu, R. Moseanko, V. R. Edgerton, L. A. Havton and M. H. Tuszynski (2009). "Extensive spinal decussation and bilateral termination of cervical corticospinal projections in rhesus monkeys." J Comp Neurol **513**(2): 151-163.

Rosenzweig, E. S., J. H. Brock, P. Lu, H. Kumamaru, E. A. Salegio, K. Kadoya, J. L. Weber, J. J. Liang, R. Moseanko, S. Hawbecker, J. R. Huie, L. A. Havton, Y. S. Nout-Lomas, A. R. Ferguson, M. S. Beattie, J. C. Bresnahan and M. H. Tuszynski (2018). "Restorative effects of human neural stem cell grafts on the primate spinal cord." Nat Med.

Rosenzweig, E. S., G. Courtine, D. L. Jindrich, J. H. Brock, A. R. Ferguson, S. C. Strand, Y. S. Nout, R. R. Roy, D. M. Miller, M. S. Beattie, L. A. Havton, J. C. Bresnahan, V. R. Edgerton and M. H. Tuszynski (2010). "Extensive spontaneous plasticity of corticospinal projections after primate spinal cord injury." Nat Neurosci **13**(12): 1505-1510.

Rossignol, S., N. Giroux, C. Chau, J. Marcoux, E. Brustein and T. A. Reader (2001). "Pharmacological aids to locomotor training after spinal injury in the cat." The Journal of physiology **533**(Pt 1): 65-74.

Roth, Bryan L. (2016). "DREADDs for Neuroscientists." Neuron **89**(4): 683-694.

Roy, F. D., E. T. Zewdie and M. A. Gorassini (2011). "Short-interval intracortical inhibition with incomplete spinal cord injury." Clin Neurophysiol **122**(7): 1387-1395.

Ryczko, D. and R. Dubuc (2013). "The multifunctional mesencephalic locomotor region." Curr Pharm Des **19**(24): 4448-4470.

Schepens, B. and T. Drew (2004). "Independent and convergent signals from the pontomedullary reticular formation contribute to the control of posture and movement during reaching in the cat." J Neurophysiol **92**(4): 2217-2238.

Sengul, G. and C. Watson (2012). Chapter 13 - Spinal Cord. The Mouse Nervous System. C. Watson, G. Paxinos and L. Puelles. San Diego, Academic Press**:** 424-458.

Serradj, N., S. F. Agger and E. R. Hollis, 2nd (2017). "Corticospinal circuit plasticity in motor rehabilitation from spinal cord injury." Neurosci Lett **652**: 94-104.

Serradj, N., S. Paixao, T. Sobocki, M. Feinberg, R. Klein, K. Kullander and J. H. Martin (2014). "EphA4-mediated ipsilateral corticospinal tract misprojections are necessary for bilateral voluntary movements but not bilateral stereotypic locomotion." J Neurosci **34**(15): 5211-5221.

Sheintuch, L., A. Rubin, N. Brande-Eilat, N. Geva, N. Sadeh, O. Pinchasof and Y. Ziv (2017). "Tracking the Same Neurons across Multiple Days in Ca^{2+} Imaging Data." Cell Reports **21**(4): 1102-1115.

Sherrington, C. S. (1910). "Flexion-reflex of the limb, crossed extension-reflex, and reflex stepping and standing." The Journal of Physiology **40**(1-2): 28-121.

Siegel, C. S., K. L. Fink, S. M. Strittmatter and W. B. J. Cafferty (2015). "Plasticity of intact rubral projections mediates spontaneous recovery of function after corticospinal tract injury." The Journal of neuroscience : the official journal of the Society for Neuroscience **35**(4): 1443-1457.

Silver, J., M. E. Schwab and P. G. Popovich (2014). "Central nervous system regenerative failure: role of oligodendrocytes, astrocytes, and microglia." Cold Spring Harb Perspect Biol **7**(3): a020602.

Slawinska, U., S. Rossignol, D. J. Bennett, B. J. Schmidt, A. Frigon, K. Fouad and L. M. Jordan (2012). "Comment on "Restoring voluntary control of locomotion after paralyzing spinal cord injury"." Science **338**(6105): 328; author reply 328.

Smith, H. C., G. Savic, H. L. Frankel, P. H. Ellaway, D. W. Maskill, M. A. Jamous and N. J. Davey (2000). "Corticospinal function studied over time following incomplete spinal cord injury." Spinal Cord **38**(5): 292-300.

Steward, O., B. Zheng, C. Ho, K. Anderson and M. Tessier-Lavigne (2004). "The dorsolateral corticospinal tract in mice: an alternative route for corticospinal input to caudal segments following dorsal column lesions." J Comp Neurol **472**(4): 463-477.

Takeoka, A., I. Vollenweider, G. Courtine and S. Arber (2014). "Muscle spindle feedback directs locomotor recovery and circuit reorganization after spinal cord injury." Cell **159**(7): 1626-1639.

Tank, D. W., M. Sugimori, J. A. Connor and R. R. Llinas (1988). "Spatially resolved calcium dynamics of mammalian Purkinje cells in cerebellar slice." Science **242**(4879): 773-777.

Tator, C. H., K. Minassian and V. K. Mushahwar (2012). "Spinal cord stimulation: therapeutic benefits and movement generation after spinal cord injury." Handb Clin Neurol **109**: 283-296.

Thevenaz, P., U. E. Ruttimann and M. Unser (1998). "A pyramid approach to subpixel registration based on intensity." IEEE Trans Image Process **7**(1): 27-41.

Tian, L., S. A. Hires, T. Mao, D. Huber, M. E. Chiappe, S. H. Chalasani, L. Petreanu, J. Akerboom, S. A. McKinney, E. R. Schreiter, C. I. Bargmann, V. Jayaraman, K. Svoboda and L. L. Looger (2009). "Imaging neural activity in worms, flies and mice with improved GCaMP calcium indicators." Nat Methods **6**(12): 875-881.

Tomer, R., L. Ye, B. Hsueh and K. Deisseroth (2014). "Advanced CLARITY for rapid and high-resolution imaging of intact tissues." Nat Protoc **9**(7): 1682-1697.

Topka, H., L. G. Cohen, R. A. Cole and M. Hallett (1991). "Reorganization of corticospinal pathways following spinal cord injury." Neurology **41**(8): 1276-1283.

Trautmann, E. M., D. J. O'Shea, X. Sun, J. H. Marshel, A. Crow, B. Hsueh, S. Vesuna, L. Cofer, G. Bohner, W. Allen, I. Kauvar, S. Quirin, M. MacDougall, Y. Chen, M. P. Whitmire, C. Ramakrishnan, M. Sahani, E. Seidemann, S. I. Ryu, K. Deisseroth and K. V. Shenoy (2019). "Dendritic calcium signals in rhesus macaque motor cortex drive an optical brain-computer interface." bioRxiv: 780486.

Tseng, G. F. and D. A. Prince (1996). "Structural and functional alterations in rat corticospinal neurons after axotomy." J Neurophysiol **75**(1): 248-267.

van den Brand, R., J. Heutschi, Q. Barraud, J. DiGiovanna, K. Bartholdi, M. Huerlimann, L. Friedli, I. Vollenweider, E. M. Moraud, S. Duis, N. Dominici, S. Micera, P. Musienko and G. Courtine (2012). "Restoring voluntary control of locomotion after paralyzing spinal cord injury." Science **336**(6085): 1182-1185.

Vilensky, J. A. (1987). "Locomotor behavior and control in human and non-human primates: comparisons with cats and dogs." Neurosci Biobehav Rev **11**(3): 263-274.

Vilensky, J. A. and B. L. O'Connor (1998). "Stepping in nonhuman primates with a complete spinal cord transection: old and new data, and implications for humans." Ann N Y Acad Sci **860**: 528-530.

von Zitzewitz, J., L. Asboth, N. Fumeaux, A. Hasse, L. Baud, H. Vallery and G. Courtine (2016). "A neurorobotic platform for locomotor prosthetic development in rats and mice." Journal of Neural Engineering **13**(2): 026007.

Wagner, F. B., J.-B. Mignardot, C. G. Le Goff-Mignardot, R. Demesmaeker, S. Komi, M. Capogrosso, A. Rowald, I. Seáñez, M. Caban, E. Pirondini, M. Vat, L. A. McCracken, R. Heimgartner, I. Fodor, A. Watrin, P. Seguin, E. Paoles, K. Van Den Keybus, G. Eberle, B. Schurch, E. Pralong, F. Becce, J. Prior, N. Buse, R. Buschman, E. Neufeld, N. Kuster, S. Carda, J. von Zitzewitz, V. Delattre, T. Denison, H. Lambert, K. Minassian, J. Bloch and G. Courtine (2018). "Targeted neurotechnology restores walking in humans with spinal cord injury." Nature **563**(7729): 65-71.

Wahl, A. S., W. Omlor, J. C. Rubio, J. L. Chen, H. Zheng, A. Schroter, M. Gullo, O. Weinmann, K. Kobayashi, F. Helmchen, B. Ommer and M. E. Schwab (2014). "Neuronal repair. Asynchronous therapy restores motor control by rewiring of the rat corticospinal tract after stroke." Science **344**(6189): 1250-1255.

Wang, H., J. Peca, M. Matsuzaki, K. Matsuzaki, J. Noguchi, L. Qiu, D. Wang, F. Zhang, E. Boyden, K. Deisseroth, H. Kasai, W. C. Hall, G. Feng and G. J. Augustine (2007). "High-speed mapping of synaptic connectivity using photostimulation in Channelrhodopsin-2 transgenic mice." Proc Natl Acad Sci U S A **104**(19): 8143-8148.

Wang, L., J. M. Conner, J. Rickert and M. H. Tuszynski (2011). "Structural plasticity within highly specific neuronal populations identifies a unique parcellation of motor learning in the adult brain." Proceedings of the National Academy of Sciences **108**(6): 2545-2550.

Wannier, T., E. Schmidlin, J. Bloch and E. M. Rouiller (2005). "A unilateral section of the corticospinal tract at cervical level in primate does not lead to measurable cell loss in motor cortex." J Neurotrauma **22**(6): 703-717.

Weidner, N., A. Ner, N. Salimi and M. H. Tuszynski (2001). "Spontaneous corticospinal axonal plasticity and functional recovery after adult central nervous system injury." Proc Natl Acad Sci U S A **98**(6): 3513-3518.

Weiler, N., L. Wood, J. Yu, S. A. Solla and G. M. Shepherd (2008). "Top-down laminar organization of the excitatory network in motor cortex." Nat Neurosci **11**(3): 360-366.

Weishaupt, N., S. Li, A. Di Pardo, S. Sipione and K. Fouad (2013). "Synergistic effects of BDNF and rehabilitative training on recovery after cervical spinal cord injury." Behav Brain Res **239**: 31-42.

Wenger, N., E. M. Moraud, J. Gandar, P. Musienko, M. Capogrosso, L. Baud, C. G. Le Goff, Q. Barraud, N. Pavlova, N. Dominici, I. R. Minev, L. Asboth, A. Hirsch, S. Duis, J. Kreider, A. Mortera, O. Haverbeck, S. Kraus, F. Schmitz, J. DiGiovanna, R. van den Brand, J. Bloch, P. Detemple, S. P. Lacour, E. Bezard, S. Micera and G. Courtine (2016). "Spatiotemporal neuromodulation therapies engaging muscle synergies improve motor control after spinal cord injury." Nat Med.

Wernig, A. (2014). "No dawn yet of a new age in spinal cord rehabilitation." Brain **138**(7): e362-e362.

Whishaw, I. Q., B. Gorny and J. Sarna (1998). "Paw and limb use in skilled and spontaneous reaching after pyramidal tract, red nucleus and combined lesions in the rat: behavioral and anatomical dissociations." Behav Brain Res **93**(1-2): 167-183.

Wise, S. P. and J. P. Donoghue (1986). "Motor Cortex of Rodents " Jones E.G., Peters A. (eds) Sensory-Motor Areas and Aspects of Cortical Connectivity. Cerebral Cortex, vol. 5. Springer, Boston, MA.

Withers, G. S. and W. T. Greenough (1989). "Reach training selectively alters dendritic branching in subpopulations of layer II-III pyramids in rat motor-somatosensory forelimb cortex." Neuropsychologia **27**(1): 61-69.

Wolpert, D. M., J. Diedrichsen and J. R. Flanagan (2011). "Principles of sensorimotor learning." Nat Rev Neurosci **12**(12): 739-751.

Wrigley, P. J., S. R. Press, S. M. Gustin, V. G. Macefield, S. C. Gandevia, M. J. Cousins, J. W. Middleton, L. A. Henderson and P. J. Siddall (2009). "Neuropathic pain and primary somatosensory cortex reorganization following spinal cord injury." PAIN® **141**(1): 52-59.

Xu, T., X. Yu, A. J. Perlik, W. F. Tobin, J. A. Zweig, K. Tennant, T. Jones and Y. Zuo (2009). "Rapid formation and selective stabilization of synapses for enduring motor memories." Nature **462**(7275): 915-919.

Yang, H. W. and R. N. Lemon (2003). "An electron microscopic examination of the corticospinal projection to the cervical spinal cord in the rat: lack of evidence for cortico-motoneuronal synapses." Exp Brain Res **149**(4): 458-469.

Ying, Z., R. R. Roy, H. Zhong, S. Zdunowski, V. R. Edgerton and F. Gomez-Pinilla (2008). "BDNF-exercise interactions in the recovery of symmetrical stepping after a cervical hemisection in rats." Neuroscience **155**(4): 1070-1078.

Zaaimi, B., S. A. Edgley, D. S. Soteropoulos and S. N. Baker (2012). "Changes in descending motor pathway connectivity after corticospinal tract lesion in macaque monkey." Brain **135**(Pt 7): 2277-2289.

Zariwala, H. A., B. G. Borghuis, T. M. Hoogland, L. Madisen, L. Tian, C. I. De Zeeuw, H. Zeng, L. L. Looger, K. Svoboda and T. W. Chen (2012). "A Cre-dependent GCaMP3 reporter mouse for neuronal imaging in vivo." J Neurosci **32**(9): 3131-3141.

Zhou, P., S. L. Resendez, J. Rodriguez-Romaguera, J. C. Jimenez, S. Q. Neufeld, A. Giovannucci, J. Friedrich, E. A. Pnevmatikakis, G. D. Stuber, R. Hen, M. A. Kheirbek, B. L. Sabatini, R. E. Kass and L. Paninski (2018). "Efficient and accurate extraction of in vivo calcium signals from microendoscopic video data." eLife **7**: e28728.

Ziv, Y., L. D. Burns, E. D. Cocker, E. O. Hamel, K. K. Ghosh, L. J. Kitch, A. E. Gamal and M. J. Schnitzer (2013). "Long-term dynamics of CA1 hippocampal place codes." **16**(3): 264-266.

Ziv, Y. and K. K. Ghosh (2015). "Miniature microscopes for large-scale imaging of neuronal activity in freely behaving rodents." Curr Opin Neurobiol **32**: 141-147.

Zörner, B., L. C. Bachmann, L. Filli, S. Kapitza, M. Gullo, M. Bolliger, M. L. Starkey, M. Rothlisberger, R. R. Gonzenbach and M. E. Schwab (2014). "Chasing central nervous system

plasticity: the brainstem's contribution to locomotor recovery in rats with spinal cord injury." <u>Brain</u> **137**(Pt 6): 1716-1732.

Curriculum Vitae

Selin Anil

✉ Rue de Lyon 29, 1201 Geneva, Switzerland

@ selin.anil@polytechnique.org

☎ +41787906667

RESEARCH EXPERIENCE

2014-present	PhD training in Neuroscience, Prof. Courtine, EPFL, Geneva, Switzerland **Corticolumbar dynamics during recovery after spinal cord injury** *- Leadership, communication and organizational skills for team and long-term project management* *- Strong time-management skills developed in a high-pressure environment* *- Biology: establishment of a technical platform for chronic calcium recordings in freely-moving rats, surgical implantations and stereotaxic injections in rodents, behavioral training, histology, clarity, wide field and confocal microscopy, molecular biology* *- Computer skills: Matlab, Fiji macro, Adobe Illustrator* *- Scientific writing: Grant (ERC) and scientific publications* *- Class and slide preparation for high-level international conferences* *- Student supervision: B.Sc., M.Sc., PhD fellows, scientific outreach*
2014	Master's thesis, Center for Neural Repair, Prof. Tuzsynski, UCSD, San Diego, USA **Early growth and topographical organization of neural stem cells-graft-derived neurons projecting to the host spinal cord in a model of neuronal relay after severe injury**
2013	Research internship, IRP chair in spinal cord repair, Prof. Courtine, EPFL, Lausanne, Switzerland **Decoding the voluntary cortical control of locomotion in healthy and spinal cord injured rats**
2012	Research internship, IRP chair in spinal cord repair, Prof. Courtine, EPFL, Lausanne, Switzerland **Histological analysis and 3D-reconstruction to investigate the extent of spinal cord injuries in rats with a traumatic contusion**
2012	Bachelor's thesis, Neural circuit development, Prof. Kania, IRCM, Montréal, Canada **Molecular characterization of the spinothalamic tract in mice**

EDUCATION

2014-present	**Ecole Polytechnique Fédérale de Lausanne**, Geneva, Switzerland PhD training in Neuroscience
2012-2014	**Ecole Polytechnique Fédérale de Lausanne**, Lausanne, Switzerland Master in Bioengineering, minor in Neuroprosthetics
2009-2012	**Ecole Polytechnique**, Paris, France France's leading university for high-level scientific training Master and engineering degrees in general and Bio-engineering

2007-2009   **Lycée Sainte Geneviève**, Versailles, France
Intensive program in Advanced Physics and Chemistry in preparation for the nationwide competitive exams to enter French engineering schools

LANGUAGES

- French: mother tongue
- Turkish: good, native language
- English: fluent

- German: fluent
- Spanish: basic knowledge
- Italian: basic knowledge

PUBLICATIONS & PRESENTATIONS

- J.-B. Mignardot, C. G. Le Goff, R. van den Brand, M. Capogrosso, N. Fumeaux, H. Vallery, S. Anil, J. Lanini, I. Fodor, G. Eberle, A. Ijspeert, B. Schurch, A. Curt, S. Carda, J. Bloch, J. von Zitzewitz, G. Courtine, "A multidirectional gravity-assist algorithm that enhances locomotor control in patients with stroke or spinal cord injury". Sci. Transl. Med. 9, eaah3621 (2017)

- L. Asboth, L. Friedli, J. Beauparlant, C Martinez-Gonzalez, S. Anil, E. Rey, L. Baud, G. Pydpruzhnykova, M.A. Anderson, P. Shkorbatova, L. Batti, S. Pagès, J. Kreider, B .L. Schneider, Q. Barraud, G. Courtine, "Cortico-reticulo-spinal circuit reorganization enables functional recovery after severe spinal cord contusion". Nat. Neuroscience 21 (2018)

- Presentation: "Dynamics of corticolumbar neurons in rats throughout recovery after spinal cord injury" Inscopix European user meeting (September 2019), Paris, France

DISTINCTIONS & ACADEMIC HONORS

2014	Prize of EPFL best master's thesis in Neuroprosthetics
2014	EPFL-WISH foundation master's thesis abroad scholarship
2012-2014	EPFL excellence scholarship for the master program

EXTRA-CURRICULAR ACTIVITIES

- Argentine tango: travelling, participating in marathons and festivals
- Trekking, road and trail running
- Self-published writing
- Psychology